Performance of Receiver Autonomous Integrity Monitoring (RAIM) for Maritime Operations

Zur Erlangung des akademischen Grades eines

DOKTOR-INGENIEURS

von der Fakultät für

Bauingenieur-, Geo- und Umweltwissenschaften

des Karlsruher Instituts für Technologie (KIT)

genehmigte

DISSERTATION

von

Dipl.-Ing. Michael Mink

aus Rottweil

Tag der mündlichen Prüfung: 27.07.2016

Hauptreferent: Prof. Dr.-Ing. Dr. h. c. Bernhard Heck

Geodätisches Institut

Karlsruher Institut für Technologie

Korreferent: PD Dr.-Ing. habil. Jan Wendel

Institut für Theoretische Elektrotechnik und Systemoptimierung

Karlsruher Institut für Technologie

Karlsruhe 2016

Kurzfassung

Die Anwendung von Globalen Satellitengestützten Navigationssystemen (GNSS) hat sich in der heutigen Zeit auf dem Gebiet der maritimen Navigation durchgesetzt und kommt dabei weltweit zur Anwendung. Hierbei gibt es Anwendungen, die als sicherheitskritisch eingestuft und für die entsprechende Anforderungen an das GNSS gestellt werden. Die International Maritime Organisation (IMO) hat für verschiedenste Anwendungsbereiche Anforderungen hinsichtlich verschiedener Parameter definiert und veröffentlicht. Eine entscheidende Rolle spielt hierbei die Integrität einer GNSS-gestützten Positionslösung: die Integrität stellt ein Maß für die Vertrauenswürdigkeit einer Positionslösung dar. Zudem beinhaltet der Begriff der Integrität die Fähigkeit den Nutzer rechtzeitig zu warnen, falls das System nicht den jeweiligen Anforderungen genügt. Als weiterer Performance-relevanter Parameter ist die Kontinuität zu nennen: die Kontinuität gibt an, mit welcher Wahrscheinlichkeit das System – für die Dauer der jeweiligen Operation – innerhalb der Spezifikation agiert.

Den bedeutendsten Anwenderkreis im Zusammenhang mit der GNSS-Integrität bildet jedoch die Luftfahrt. Deren sicherheitskritische Anwendungen, die sehr stark auf GNSS angewiesen sind, waren in der Vergangenheit und sind bis heute die Treiber für sämtliche Entwicklungen auf dem Gebiet der GNSS-Integrität. Diese Aussage wird unterstützt durch die Tatsache, dass beispielsweise das Integritätskonzept des europäischen satelliten-basierten Augmentierungssystem EGNOS im Jahre 2011 von der Internationalen zivilen Luftfahrtbehörde (ICAO) zertifiziert wurde. Eine Erweiterung der Fähigkeiten von EGNOS ist zeitnah zu erwarten, wenn das System für LPV-200 Operationen – mit erhöhten Anforderungen – freigegeben wird. Vergleichbare Anstrengungen werden zurzeit nicht von der maritimen Anwenderseite unternommen. Der starke Fokus auf sicherheitskritische Luftfahrtanwendungen spiegelt sich auch sehr deutlich in der aktuellen Literatur wider. Daraus ergibt sich die Tatsache, dass Bedingungen, die für die Luftfahrt relevant sind, besser verstanden sind als für die Schifffahrt. Diese Bedingungen beinhalten vor allem die Fehlermodelle für die einzelnen Fehlerbeiträge, die sich auf die Positionsgenauigkeit auswirken. Außerdem ist das Verständnis der Gefahren, die aus einer Fehlfunktion des GNSS resultieren, viel weiter ausgereift. Diese Gefahren müssen in den Simulationen mit einkalkuliert werden, um der Realität Rechnung zu tragen.

In dieser Arbeit werden zwei Nutzergruppen betrachtet, die zusammen einen Großteil der maritimen Anwendungen abdecken. Die „Ocean" und „Coastal" Operationen heben sich gegenüber den Anwendungen „Port Approach and Restricted Waters" insofern ab, als dass keine Anforderungen für die Kontinuität spezifiziert sind. Die Kontinuität für letztere Anwendung ist über einen Zeitraum

von 3 Stunden definiert, was sich deutlich im Vergleich zur Luftfahrt unterscheidet. Diese genannte Zeitdauer wird auch als Expositionsdauer bezeichnet. Auch gibt es aktuelle Anregungen aus diversen Veröffentlichungen die stringenten Kontinuitätsanforderungen zu vereinfachen, indem die Expositionsdauer von 3 Stunden auf 15 Minuten reduziert wird. Um dieser Entwicklung Rechnung zu tragen und zu antizipieren, werden in der vorliegenden Arbeit beide Expositionszeiten berücksichtigt. Für beide Nutzergruppen gibt es keine Anforderung bezüglich der vertikalen Positionskomponente.

Somit zeigen sich signifikante Unterschiede zwischen maritimen und aeronautischen Nutzern in den für die jeweiligen an das GNSS gestellten Anforderungen. Daraus lässt sich die Notwendigkeit einer Überprüfung und gegebenenfalls einer Anpassung der Algorithmen und der damit verbundenen Annahmen ableiten. Eine Anstrengung, die sich durch die ganze Arbeit zieht, ist die Überprüfung der Annahmen, die für die Luftfahrt getroffen werden, hinsichtlich der Übertragbarkeit auf den maritimen Nutzer. Dabei wird unter anderem der Schluss gezogen, dass nicht alle Fehlermodelle übernommen werden können. Außerdem ergeben sich aufgrund der verschiedenen Anforderungen neue Gefahren für den maritimen Nutzer, die für die Luftfahrt nicht relevant sind. Diese werden ausführlich dargelegt und diskutiert.

Eine intensive Literaturrecherche zeigt bereits existierende Integritätsalgorithmen auf. Es wird ein Vorschlag dahingehend gemacht, diese hinsichtlich geeigneter Kriterien zu klassifizieren. Die Algorithmen werden im Wesentlichen in drei Kategorien eingeteilt, die sich hauptsächlich in der Allokation der Verantwortung für die Integritätsaussage unterscheiden: bei vollständig autonomen Integritätsalgorithmen liegt die Bürde ausschließlich auf Nutzerseite, wohingegen bei den sogenannten Advanced RAIM-Algorithmen die Bürde zwischen Nutzer und System aufgeteilt wird. Beispielsweise Satelliten-basierte Augmentierungssysteme (SBAS) allokieren die Integritätsbürde fast ausschließlich auf Systemseite. Das Tragen der Bürde für die Integrität geht, entsprechend mit den jeweiligen Anforderungen, in der Regel mit einer erhöhten Komplexität für die Auswertestrategien und die Ausrüstung einher.

Im Rahmen dieser Arbeit wurde ein neuer RAIM-Algorithmus entwickelt, der auf die Rahmenbedingungen eines maritimen Nutzers eingeht. Es wird im Wesentlichen die Tatsache ausgenutzt, dass die Höhenkomponente sich kurzfristig nur marginal ändert und demnach eine geeignete Höhenreferenz darstellt. Zudem wird hier die Tatsache ausgenutzt, dass die Meeresoberfläche zum großen Teil mit dem Geoid zusammenfällt, womit eine zusätzliche und GNSS-unabhängige Höhenschätzung eingeführt werden kann. Dies erlaubt bis zu einem gewissen Grad die Überprüfung der Konsistenz mit den GNSS-Beobachtungen. Dieser neue Ansatz stellt eine Erweiterung des konventionellen Least-Squares Residual (LSR) RAIM dahingehend dar, als dass das finale Ergebnis sich aus dem Optimum beider beteiligten Ansätze definiert. Somit ist per Definition eine Verbesserung der Leistungsfähigkeit zu erwarten, die in den entsprechenden Auswertungen bestätigt werden kann.

Ein zentraler Aspekt dieser Arbeit ist die Evaluierung der Leistungsfähigkeit der ausgewählten Ansätze hinsichtlich Genauigkeit, Integrität und Kontinuität auf Nutzerseite. Ein entscheidender Parameter ist hierbei die Verfügbarkeit der Integrität und Kontinuität über alle Nutzerpositionen über den gesamten Auswertezeitraum. Dabei werden drei Szenarien unter Berücksichtigung der Navigationssysteme GPS, Galileo und GLONASS definiert. Hierbei werden im Wesentlichen drei ausgesuchte Algorithmen betrachtet: den LSR RAIM-Ansatz, der als klassischer RAIM-Ansatz häufig in der Literatur auftaucht. Der Novel RAIM-Ansatz stellt – wie oben beschrieben – eine Erweiterung des LSR RAIM dar. Als Vertreter der Advanced RAIM-Algorithmen ist der „Multiple Hypothesis Solution Separation" (MHSS) RAIM zu nennen. Diese ausgesuchten Algorithmen werden detailliert beschrieben und diskutiert.

Als Ergebnis der Evaluierung der Leistungsfähigkeit der oben genannten Ansätze zeigt sich unter Berücksichtigung einer Konstellation (GPS) eine Nicht-Konformität gegenüber den Verfügbarkeitsanforderungen. Dies ist im Wesentlichen mit der Geometrieabhängigkeit gegenüber den RAIM-Algorithmen zu erklären, da anzunehmen ist, dass die jeweils schlechteste Geometrie einen Treiber für die Leistungsfähigkeit darstellt. Unter der Annahme von zwei (GPS und Galileo) Konstellationen ist zu beobachten, dass alle drei untersuchten Ansätze konform mit den Anforderungen sind, mit der Ausnahme der Kontinuität über die Dauer von 3 Stunden bei dem LSR- und Novel RAIM Ansatz.

Hingegen zeigt sich bei drei Konstellationen (GPS, Galileo und GLONASS) eine Limitation des LSR und Novel RAIM. Beide Ansätze basieren auf der Ein-Fehler-Annahme, die bei der hohen Anzahl von verfügbaren Satelliten nicht mehr gültig ist, da die Wahrscheinlichkeit von mehreren simultan ausfallenden Satelliten nicht mehr vernachlässigbar ist. Aus diesem Grund kann unter diesen Rahmenbedingungen keine sinnvolle Aussage über deren Leistungsfähigkeit gemacht werden. Generell zeigt sich, dass der MHSS RAIM den anderen RAIM-Ansätzen hinsichtlich Leistungsfähigkeit überlegen ist und volle Konformität gegenüber den Anforderungen unter Verwendung von mindestens zwei Konstellationen aufzeigt.

Über die Evaluierung der Leistungsfähigkeit der ausgewählten Algorithmen hinaus wird verstärkt auf das Advanced RAIM-Konzept eingegangen, das die Verwendung des MHSS RAIM vorsieht. Dieses Konzept nutzt ein zusätzliches und unabhängiges Referenz-Netzwerk, das die Aufgabe hat den Nutzer mit entsprechenden Information zu versorgen, so dass dieser mithilfe dieser Daten in der Lage ist, eine geeignete Aussage über die Integrität seiner Positionslösung treffen zu können. Die Entwicklungen für das Konzept, das primär für den Luftfahrtbereich Anwendung finden soll, stehen noch in der Anfangsphase. Diese Aussage stützt sich auf der Tatsache, dass entsprechende Beschreibungen und Überlegungen ausschließlich die Rahmenbedingungen, wie sie in der Luftfahrt vorkommen, geltend machen. Es werden in dieser Arbeit diverse Aspekte dieses Konzepts angesprochen und hinsichtlich der Verwendbarkeit für den maritimen Nutzer diskutiert. Empfehlungen werden ausgesprochen, die in aktuelle Entwicklungen Eingang finden sollen.

Sogenannte „Overbounding"-Konzepte werden vorgestellt: ein „Overbound" ist eine konservative Repräsentation einer zugrunde liegenden Fehlerverteilung, die - unter anderem aufgrund eines reduzierten Stichprobenumfangs - nicht zwingend einer bekannten Charakteristik entsprechen muss. Die Notwendigkeit eines „Overbounds" ergibt sich aus der Tatsache, dass sämtliche Integritätskonzepte auf der Annahme der Normalverteilung basieren. Es wird eine Übersicht über vorhandene Konzepte gegeben, auf deren Basis eine Empfehlung für den maritimen Nutzer ausgesprochen wird.

Desweiteren werden Analysen durchgeführt, die die Toleranz in der Fehlermodellierung bezüglich den aus der Luftfahrt übertragenen Fehlermodellen aufzeigen sollen. Dabei wurde die Bedingung der Konformität gegenüber den Anforderungen zugrunde gelegt. Der Fokus liegt hierbei unter anderem auf den lokalen Fehlereinflüssen wie Mehrwege-Effekten und Signal-Interferenzen. Mehrwege-Effekte und beispielsweise nominale Signaldeformationen werden hier als zusätzlicher Bias auf den Beobachtungen zu den jeweiligen Satelliten modelliert. Die Biases werden in zwei unterschiedlichen Analysen jeweils auf einen Satelliten und auf allen Satellitenbeobachtungen simultan modelliert. Das Ergebnis ist eine deutlich erhöhte Toleranz des Bias auf einer Satellitenbeobachtung gegenüber dem zweiten Fall. Hierbei ist zu beachten, dass der gemeinsame Bias nicht in die Schätzung der Empfängeruhr eingeht, sondern von dem RAIM absolut in die Positionskomponente übertragen wird. Dem gegenüberzustellen sind Fehlereinflüsse wie beispielsweise Jamming oder Signalinterferenzen, die eine Inflation der Fehlerverteilung auf den Satellitenbeobachtungen verursachen können. Die gezeigte Analyse geht davon aus, dass alle Satellitenbeobachtungen simultan davon betroffen sind. Es zeigt sich eine Toleranz im Dezimeter-Bereich, wobei anzumerken ist, dass die Verwendung von drei Konstellationen eine um etwa Faktor drei erhöhte Toleranz gegenüber der Verwendung von zwei Konstellationen ergibt.

Für die Simulationen wurde eine frei verfügbare, Matlab-basierte Plattform ausgewählt, die für globale Systemevaluierungen hinsichtlich Genauigkeit und Integrität ausgelegt ist (MAAST). Dieses Tool wurde dahingehend erweitert, dass es die Evaluierung der Leistungsfähigkeit eines maritimen GNSS-Nutzers erlaubt. Dies beinhaltet die Anpassung des bereits implementierten MHSS RAIM-Algorithmus und die Implementierung neuer Algorithmen in diese Simulationsumgebung. Außerdem wurde dieses Tool auch adaptiert um die Durchführung auxiliarer Analysen zu unterstützen.

Abstract

The use of Global Navigation Satellite Systems (GNSS) in the context of maritime applications has evolved during the recent past. Some applications are classified safety critical that claim specific demands towards a GNSS. The International Maritime Organization (IMO) has defined and published requirements for those applications. A key parameter is the integrity of a position solution. Integrity is a measure of trust that can be placed in the correctness of the information that the system is providing to the user. Besides, integrity includes also the ability to warn a user within a specified time interval. In this context, also continuity is a relevant parameter: continuity is the ability of a system to provide continuous conformity to the needs during an operation given that the system is available at the beginning of the operation.

The aviation user community has always been the major driver for developments in the field of GNSS integrity. In fact, for example the European Geostationary Navigation Overlay Service (EGNOS) has been certified by the International Civil Aviation Organization (ICAO) in 2011. This leads to the conclusion that the conditions are better understood compared to maritime applications - especially in terms of error modelling. But also threat scenarios are defined that need to be considered in order to account for real situations.

Comparing the requirements on the one hand specified by ICAO and on the other hand by IMO, significant differences get obvious such as no demands being defined for the vertical position component and continuity is specified over a much longer exposure period for maritime applications. This implies the need to review and if necessary adapt the algorithms and the corresponding assumptions. For integrity, a possible extension of the integrity exposure period does not result in a higher or different number of events to be considered and their probability is assumed to grow linearly with the specific interval. Instead, for continuity the number or type of events to be considered is different depending on the exposure period. The consequences on the threat modelling are discussed in detail.

An extensive literature survey shows existing integrity algorithms. A way to classify the algorithms is proposed: three main categories are identified. First, fully autonomous integrity algorithms do not require input from an external source. In contrast, so-called Advanced Receiver Autonomous Integrity Monitoring (ARAIM) implies the usage of an independent reference network that provides the user with relevant input. The other extreme certainly constitute augmentation systems such as Satellite Based Augmentation Systems (SBAS) that allocate the full integrity burden on system side.

A Novel RAIM scheme has been derived in the frame of this thesis that copes with the condition of a maritime user. The fact that a maritime user moves along the sea surface which is approximated by the geoid model brings in an opportunity of using additional height information. The idea is to use the additional height information in order to perform a cross-check with the GNSS-derived height.

A major focus is on the evaluation of the performance of the integrity algorithms at user level. For this, three algorithms have been selected: the Least-Squares Residual (LSR) RAIM, the Novel RAIM scheme and the Multiple Hypothesis Solution Separation (MHSS) RAIM representing the so-called Advanced RAIM schemes. A further effort consists in highlighting the concept of Advanced RAIM that relies on an external independent reference network that is in charge of computing relevant integrity parameters on ground and sending them to the user via an Integrity Support Message (ISM). The ISM parameters contain information about current error characterization and failure probability that is used to state about its integrity. Concept drivers are discussed and supported via dedicated analyses.

Table of Contents

Acronyms

AIS	Automatic Identification System
AMRS	VHF Aeronautical Mobile Route Services
ASF	Additional Secondary Factors
CDF	Cumulative Distribution Function
CNMP	Code Noise and Multipath
CTI	Continuity Time Interval
DOP	Dilution of Precision
ECD	Envelope to Cycle Difference
eLORAN	Enhanced Low Range Navigation
EPIRB	Emergency Position Indication Radio Beacon
FD	Fault Detection
FDE	Fault Detection and Exclusion
FE	Feared Event
FOC	Full Operational Capability
GBAS	Ground Based Augmentation System
GEAS	GNSS Evolutionary Architecture Study
GEO	Geostationary
GIVE	Grid Ionosphere Vertical Error
GNSS	Global Navigation Satellite Systems
GPS	Global Positioning System
GRI	Group Repletion Interval
GSA	European GNSS Agency
GSAT	Galileo Satellite
GSS	Galileo Sensor Station
GUI	Graphical User Interface

HAL	Horizontal Alert Limit
HPL	Horizontal Protection Level
IALA	International Association of Lighthouse Authorities
ICAO	International Civil Aviation Organization
ICD	Interface Control Document
IF	Interference
IGSO	Inclined Geosynchronous Orbit
IMO	International Maritime Organization
INS	Inertial Navigation Sensors
IR	Integrity Risk
IRN	Independent Reference Network
ISM	Integrity Support Message
IWW	Inland Waterways
LAAS	Local Area Augmentation System
LOP	Lines of Position
LORAN	Long Range Navigation
LRIT	Long-Range Identification and Tracking
LSR	Least-Squares Residual
MAAST	Matlab Algorithm Availability Simulation Tool
Max	Maximum
MDE	Minimum Detectable Error
MEO	Medium Earth Orbit
MERR	Minimum Detectable Error in Range Domain
MGEX	Multi-GNSS Experiment
MHSS	Multiple Hypothesis Solution Separation
Min	Minimum
MOPS	Minimum Operational Performance Standard
MP	Multipath

MSI	Misleading Signal-in-Space Information
NNSS	Navy Navigation Satellite System
NTE	not-to-exceed
OCS	Operational Control Segment
ODTS	Orbit Determination and Timing Synchronization
PCO	Phase Center Offset
PCV	Phase Center Variation
PDF	Power Density Function
P_E	Position Error
PF	Primary Factors
P_{fa}	Probability of false alert
PHMI	Probability of Hazardous Misleading Information
PLB	Personal Location Beacon
P_{md}	Probability of missed detection
PS	Parity Space
PVT	Position Velocity Time
RAIM	Receiver Autonomous Integrity Monitoring
RANCO	Range Consensus
RNSS	Radio Navigation Satellite System
RTCA	Radio Technical Commission for Aeronautics
SAM	System Area Monitors
SBAS	Satellite Based Augmentation System
SF	Secondary Factors
SIS	Signal In Space
SIS ICD	Signal In Space Interface Control Document
SOC	Statement of Compliance
SOLAS	Safety of Life at Sea
SPS	Standard Positioning Service

SS   Solution Separation

SV   Satellite Vehicle

SVS   System Volume Simulator

TDOA   Time Difference of Arrival

TH   Threshold

TOA   Time of Arrival

TTIA   Time To ISM Alert

UDRE   User Differential Range Error

UERE   User Equivalent Range Error

ULS   Uplink Station

UMSI   Unalerted Misleading Signal-in-Space Information

URA   User Range Accuracy

URE   User Range Error

VAL   Vertical Alert Limit

VHF   Very High Frequency

VPL   Vertical Protection Level

WAAS   Wide Area Augmentation System

WADGPS   Wide Area Differential GPS

WRS   WAAS Reference Stations

WSSR   Weighted Sum Squared Residuals

WWRNS   World Wide Radio Navigation System

1   Introduction

In the last decades satellite based navigation became one of the most essential infrastructures of the daily life which evolved out of a GPS-based niche technology for military and professional users to a multi-provider technology for a wide variety of users. Nowadays, a plethora of applications make use and rely on Global Navigation Satellite Systems (GNSS) which has therefore become an indispensable technology for navigation, positioning and timing. Moreover, GNSS is used for safety critical applications – in particular the aviation community strongly depends on GNSS in various life critical phases such as landing approaches where a non-sight landing of an aeroplane shall be possible in an extreme case. It is obvious that such applications require a high level of trust in the GNSS navigation solution that is called integrity. The International Civil Aviation Organization (ICAO) defines integrity as a measure of the trust that can be placed in the correctness of the information supplied by a navigation system. Integrity includes the ability of the system to provide timely warnings to users when the system should not be used for its intended operation. Furthermore, an important aspect for safety critical applications is continuity. The continuity of a system is the ability of the total system to perform its function without interruption during the intended operation. More specifically, continuity is the probability that the specified system performance will be maintained for the duration of a phase of operation, presuming that the system was available at the beginning of that phase of operation.

In the past, aviation was and still is the main driver for developments in the field of GNSS integrity and continuity. However, a further user group emerges more and more to a greater extent into awareness in the field of GNSS integrity and continuity. Analogously to the aviation, GNSS has become the main navigation means for maritime navigation in the recent past. Today, the maritime section is a worldwide commercial mass transport means. Also maritime navigation is deemed safety critical and relies on GNSS. The International Maritime Organization (IMO) defined requirements for integrity and continuity. Those requirements differ significantly from those defined by the ICAO. IMO requirements have barely been considered in recent and current integrity algorithms and concept developments. These requirements constitute a massive challenge to adapting the existing integrity schemes in order to satisfy the needs of maritime users. This fact actually prepares the ground of this thesis.

The permanent enhancements in existing GNSS and the advent of new GNSS are reflected in this thesis by characterizing the maritime user as a GNSS multi-frequency and multi-constellation user. Even IMO requirement specifications act on the assumption that dual frequency observations are applied. Various schemes verifying integrity and continuity requirements are available: one major group of representatives are Receiver Autonomous Integrity Monitoring (RAIM). RAIM is a fully

receiver autonomous approach that exploits the residuals of pseudorange measurements in order to perform a consistency check and to identify the presence of a potential faulty measurement. With the dual-frequency services and the large number of satellites available the Least-Squares Residuals (LSR) RAIM will have its renaissance. While the concept is known already quite for some time, it was mainly limited by the low accuracy of single-frequency ranging signals and the limited number of satellites of a single constellation which led to an integrity performance being far beyond the expectations of the aviation user community. However, the potential of this scheme is undoubted and promising. In the context of this thesis a Novel RAIM scheme has been developed. This novel RAIM scheme is based on assumptions that are exclusively valid for maritime users. Namely the fact that a maritime user moves along the sea surface allows for deriving additional height information based on the geoid that coincides mainly with the global sea surface. Current developments in the field of integrity algorithms reveal a new group of algorithms called Advanced RAIM. The most promising hereof is the Multiple Hypothesis Solution Separation (MHSS) RAIM scheme which will be treated in more detail within this thesis. This concept relies on an external independent network of reference stations whose task is to estimate an Integrity Support Message (ISM) broadcast to the user. Needless to mention, this requires an additional infrastructure on top of the GNSS ground segment whose design aspects will be treated in detail within this thesis.

A key objective of this thesis is to provide an understanding of the needs of a maritime user and work out the differences in the requirements of ICAO on the one hand and IMO on the other hand and highlight the implications on the designs of algorithms. Extensive performance evaluations based on different RAIM concepts are conducted in order to clearly make a statement whether current GNSS are able to satisfy the need of the maritime user based on RAIM techniques. A major part of this thesis is dedicated to highlighting the implications to Advanced RAIM design employing MHSS RAIM. Based on extensive analyses, clear recommendations are given to support current development efforts enabling integrity and continuity also to the maritime user group. The thesis is intended to contribute to long term evolutions of integrity concepts by evaluating promising algorithms and to identify and refine potential system architecture, to deeply assess the performance and the drivers of the different algorithms and to identify a clear way forward in terms of investigation and realization steps.

Outline of the Thesis

Chapter 2 - Overview of Modern Techniques for Maritime Navigation

Before the advent of aviation, maritime applications in general were one of the main trigger for developments in the field of navigation. However, to give a full overview of maritime navigation means is not the intention of this chapter, rather to provide a meaningful overview over the main

navigation techniques that have been used and/or are still in use since the middle of the 20th century. Although the focus in this thesis is with no doubts on GNSS solely, this chapter aims at putting GNSS as such into the context of other navigation means and thus provides a full picture in which GNSS plays a major role these days. Also, this chapter is used to provide an introduction into GNSS.

Chapter 3 – General Aspects on Integrity Algorithms

After having given an introduction to GNSS in general, this chapter aims at further pointing towards the content of this thesis by providing details on relevant aspects for integrity algorithms in particular. This comprises an understanding of the service performance parameters – namely accuracy, integrity, continuity and availability. Their relationships together with their definitions are provided. Algorithms are designed to detect vulnerable faults with sufficient probability to ensure their integrity. Thus, some details on integrity algorithms are provided regarding their capability of fault detection and fault exclusion. Finally, in order to provide a solid understanding of an integrity algorithm, a unified approach for protection level computation is depicted. It will be shown later on in this thesis that other algorithms can be related to the logic presented in this last subsection.

Chapter 4 – Understanding of Performance Requirements

After having provided a basic understanding of RAIM algorithms, their design and functionalities, this chapter aims at summarizing the minimum required performance level. Hereby, the different sets of requirements – on the one hand from the aeronautics and on the other hand from the maritime users – are worked out. The International Civil Aviation Organisation (ICAO) defines the needs for the aeronautics whereas the International Maritime Organization (IMO) defines those for the maritime user.

It is important to understand that the design parameters in every RAIM algorithm are derived from the applicable set of requirements for each GNSS operation respectively. The different sets are compared and discussed in detail. The main goal of this chapter is to present the baseline set of requirements that will be used throughout this thesis.

Chapter 5 – Integrity Algorithms

At this point, the basis for an understanding of integrity algorithms is provided. This chapter gives an overview of existing algorithms and proposes a classification of these algorithms into three main groups: the first group comprises the fully autonomous integrity algorithms, also known as RAIM. The second group is formed by the so-called Advanced RAIM techniques. The third main group covers the augmentation systems in general such as SBAS and GBAS. Their characteristics and relationship to each other is described in detail in this chapter.

From the set of these algorithms, three candidates have been selected to be further studied within this thesis. The algorithms together with their characteristics, advantages and disadvantages are presented and discussed in detail within this chapter.

Chapter 6 – Fault-Free Error Model

In order to assess the performance of an integrity algorithm by simulation, the conditions in which the algorithm is conducted have to be defined. Hereby, the fault-free error models define the assumed nominal performance level of a GNSS. It has to be distinguished between error contributions which are under control of the GNSS itself such as ephemeris and clock error and error contributions such as atmospheric and local errors (i.e. multipath) that depend on the user environment. The fault-free error model gives conservative assumptions about the error characteristics. These are empirical error models derived from long-term measurement campaigns. The respective error distributions are conservatively overbounded in a sense that the real underlying performance level can be assured.

Chapter 7 – Threat Space

The threat space is a consistent set of assumptions under which the integrity and continuity performance is assessed. It defines basically the satellite failure probabilities and the probability of a constellation to fail. Another major aspect of this chapter is the discussion for the need of a maritime dedicated threat space. In contrast to the aeronautics being the main driver for standardization and development activities, the maritime user lacks of a maritime dedicated threat space. This point is discussed extensively. In addition, this investigation bears some novel aspects to be considered in a maritime dedicated threat space.

Chapter 8 – Performance Results

This chapter summarizes the performance evaluation results related to the set of selected algorithms. The results are derived via simulation and depicted with respect to accuracy, integrity, continuity and availability. For the performance evaluation, three different scenarios have been assumed: single, dual and triple GNSS constellation. The intention is to also cover near future developments where multiple constellations will be available for usage. All performance results will be summarized and discussed in this chapter.

Chapter 9 – Advanced RAIM Related Considerations

As will turn out from the latter chapter, the MHSS RAIM as representative of Advanced RAIM shows the most promising results in terms of performance. This chapter shall focus exclusively on aspects relevant for Advanced RAIM and works out the implications on its architecture and design if

amended for maritime GNSS users. In general, the main drivers of the Advanced RAIM concept are worked out and discussed taking into account maritime user requirements.

Chapter 10 – Conclusion and Outlook

Finally, an extensive discussion on the findings and final conclusions is provided. This chapter shall also summarize recommendations for future developments in the frame of maritime integrity. In addition, an outlook on potential further investigations and a proposed way forward is depicted.

2 Overview of Modern Techniques for Maritime Navigation

Maritime navigation is a broad field with a long history. In the beginning, navigation was mostly based on astronomical observations by looking to constant objects like the sun, the moon and the stars and using them to estimate a position. For example the sextant was becoming one of the main navigation tools in the 18th century allowing for positioning with accuracy much better than ever before.

A selection of various techniques that arose during the last century and those with the biggest impact on ship navigation will be introduced. With the advent of GPS and further GNSS, satellite navigation became more and more the most commonly used aid. But before satellite navigation was available, so-called hyperbolic terrestrial systems constituted the status quo.

Enhanced LORAN (eLORAN) is about to attain new attention in the near future as the descendant of LORAN-C which was a ground-based navigation system operated by the U.S. Coast Guard. In May 2009, the system was declared obsolete and plans have been announced to terminate it [GPS 2016]. The Coast Guard began shutting it down in February 2010. A strong lobby pushes currently for reanimation of the system under the acronym eLORAN. According to the "Enhanced Loran Definition Document" [International Loran Association 2007], the LORAN-C infrastructure is planned to be retained and upgraded to become eLORAN. The main motivation for this development is the fact that eLORAN perfectly suits as backup solution for GNSS that is vulnerable to jamming and spoofing. Actually, eLORAN is more robust to those kinds of threats and hence might serve as a complementary navigation means [Divis 2015].

For complementary reasons also the OMEGA and Decca system are marked out. Omega has been developed in the 1960s in the USA and is fully deployed in 1982. As opposed to LORAN-C (or eLORAN) and Decca, OMEGA has global coverage. The fact that the system operates on very low frequencies increases the complexity at the user receiver level. A typical accuracy is in the order of 1 NM. Omega has been taken out of service in 1997 [Kayton et al 1997]. Decca was also a hyperbolic based navigation system that has been originally developed during World War II for maritime navigation purposes. The system was shut down in the year 2000.

Nowadays and in the future, satellite systems play a key role in maritime navigation. The major GNSS are introduced in this chapter. Additionally, the integration and combination of GNSS with other navigation aids such as inertial sensors is shortly introduced to provide the full overview.

The aim of this chapter is to provide an overview of maritime navigation and to identify the role of GNSS as a component in modern maritime navigation that becomes more and more important in the future. In order to put GNSS in a maritime context where also other navigation techniques are commonly in use an overview of those systems is provided in this chapter.

2.1 Hyperbolic Terrestrial Systems

Hyperbolic terrestrial navigation is based on the difference in timing between the receptions of signals from two stations on ground. The basic idea behind is the intersection of the hyperbolic lines resulting from the measured delays between the user's position and the reference stations. The first hyperbolic navigation systems have been developed during the beginning of the 20th century. Since then, different systems have been developed and established.

2.1.1 LORAN-C

The principle of Long Range Navigation (LORAN) navigation is based on curve cutting using distance differences between the user and several static stations. The LORAN signal is emitted using the 100 kHz frequency band that can be received up to 1000 kilometres away from the emitting station [Forssell 2008], [Weblink 2014d]. The version of LORAN-C is based on a network of stations that are distributed with a distance of several 100 kilometres. Figure 2-1 shows the global distribution of LORAN-C stations. LORAN-C covers wide areas such as the North Pacific, North Atlantic, the Mediterranean, North- and Eastern Sea, the Red Sea and the Persian Gulf [Weblink 2014d].
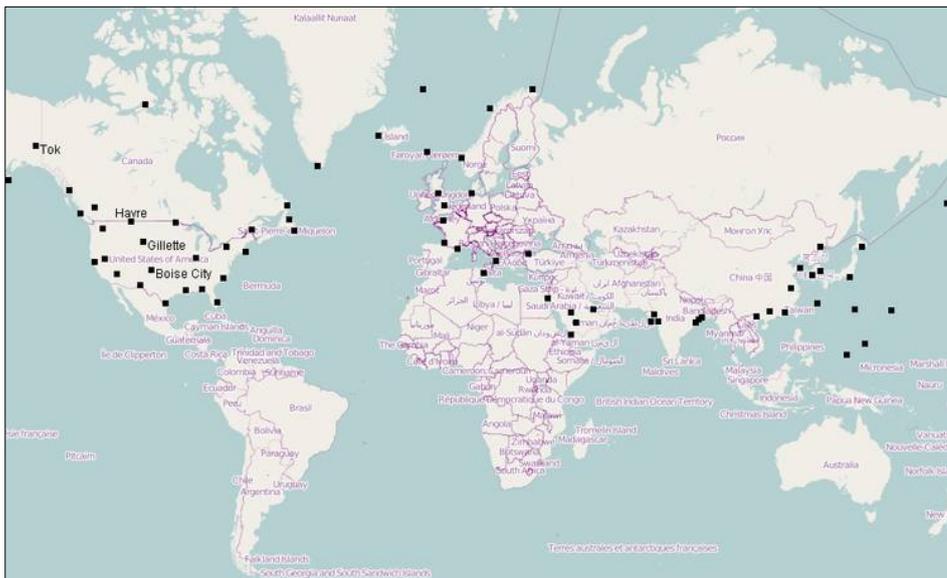

Figure 2-1: Global Distribution of LORAN Stations [Weblink 2014d]

Each LORAN-C system realization comprises transmitters, control stations and System Area Monitors (SAM). LORAN stations are grouped together into chains and basic navigation relies on using a specific chain. In each chain, there is a master station and several secondary stations.
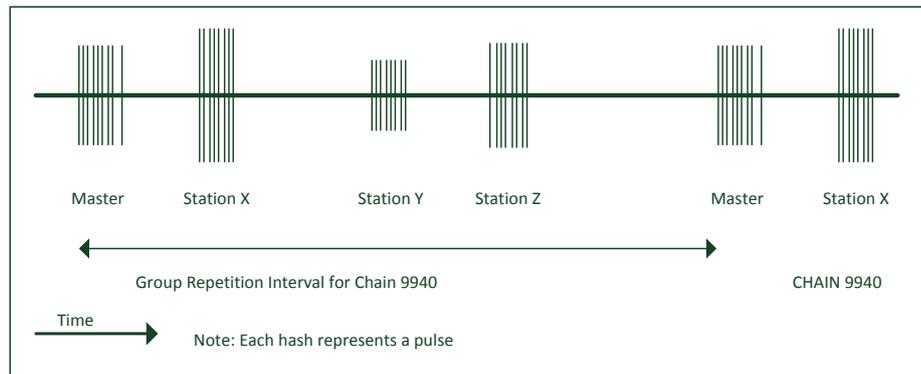
Figure 2-2: LORAN Chain Signals [Sherman 2003]

In LORAN-C, each station transmits a group of eight pulses (nine for the master station) at a specified interval. The amount of time between transmissions of the pulse groups, known as the group repetition interval (GRI), is unique to each chain. Hence chains are designated by their GRI. Some stations transmit signals for two different chains. These are termed dual rated stations [Forssell 2008], [Sherman 2003]. The GRI is usually expressed as a multiple of ten microseconds, i.e. GRI 7960 = 79600 microseconds. Figure 2-2 illustrates the 9940 chain transmissions. Each hash mark represents one LORAN pulse (which is 250 microseconds in length). The pulse has a specified shape or envelope that aids in tracking the correct cycle. Typically the tracking point is set around 30 microseconds (or the sixth zero crossing) after the start of the pulse. As the signal propagates, the envelope may shift relative to the underlying carrier (and hence the tracking point). This shift is termed the envelope to cycle difference (ECD).

The power of LORAN transmissions allows users at distances of 800 km or more to receive these signals. The transmitters emit a set of LORAN pulses at precise time instances. Within a chain, the transmission time of each secondary station is specified as an offset from the transmission of the master station. The SAMs regulate the transmission offset. Traditionally, position determination is based on measuring the distance difference of arrival (TDOA) of pulses from the master and a secondary station in a chain to create lines of position (LOPs). A minimum of two LOPs are required to determine a position. Newer technology has resulted in LORAN receivers capable of operating without requiring a master station signal. They also can determine positions using signals from

stations in different chains (all stations in view) to improve the LORAN performance. These receivers are known as "all-in-view" (AIV) receivers. Processing permits the calculation of a range measurement using the signal time of arrival (TOA) provided that the receiver has rough knowledge of the current time and station identification. Using TOA is akin to using GNSS pseudoranges [Forssell 2008], [Sherman 2003].

There are two ways of LORAN signal propagation. The signals propagate as a groundwave along the Earth's surface. They also propagate as a skywave by reflecting from the ionosphere. TDOAs are calculated using the groundwaves since they are more reliable and their phase is more stable. Skywave reflections can interfere with the desired groundwave signals much like multipath in GNSS. Typical skywaves arrive as early as 32-35 microseconds and as late as 1000 microseconds after the reception of the groundwave [Forssell 2008]. The groundwave from a station can interfere with the groundwave of another station if they are not in the same chain. This type of interference is called cross rate interference since it is due to stations transmitting at different rates.

The propagation speed of the LORAN groundwave is dependent on factors such as ground conductivity. These properties change the signal propagation speed from the speed of light in vacuum. For navigation only the groundwave part is used. The primary (PF), secondary (SF) and additional secondary factors (ASF) influence the groundwave velocity from the transmitter to the user. The first term is the propagation speed in space. On top of that, the signal experiences some extra delay if it travels over a seawater path, called the secondary factor. Finally, signals traveling over a land path will experience an additional delay over an all seawater path, called ASF. These three factors are only effective at the part of the total trajectory where the propagation mechanism has a far-field character. PF is solely dependent on distance while ASF need to be measured or modelled. On its trip to the receiver, a blend of interferences adds to the LORAN-C signal. This blend consists of continuous wave interference, interference from other LORAN-C stations and atmospheric noise. When the signals arrive at the receiver antenna, locally generated noise from engines or receiver electronics will further dilute the LORAN-C signal. Depending on the application and the local signal conditions, either an electric-field or a magnetic-field type antenna may actually receive the electromagnetic signal [Forssell 2008].

2.1.2   eLORAN

LORAN systems are designated to a series of radio based navigation systems that are used for positioning and navigation. Among this series, eLORAN is the latest in the longstanding and proven series of LORAN systems but still about to being deployed. LORAN-A is the first LORAN system and developed during World War II, initiated by the US Navy. LORAN-C is the further development of the previous versions LORAN-A and LORAN-B which is described in a dedicated section.

It needs to be pointed out that the following description of the eLORAN system is based on the Enhanced LORAN Definition Document [International Loran Association 2007] which does not fully define the system but is a first out of several documents. It is planned to tighten requirements in the system design in order to serve new applications. The basis of the eLORAN signal is the LORAN-C signal and the possibility of the continuation of using existing LORAN-C receivers is foreseen. However, in that case the benefits of eLORAN are excluded [International Loran Association 2007].
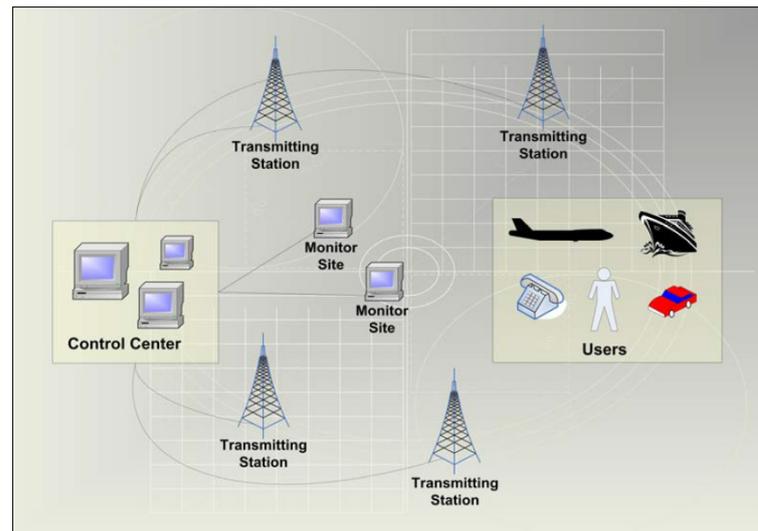
Figure 2-3: eLORAN System Concept [International Loran Association 2007]

Figure 2-3 highlights a rough sketch of the eLORAN system concept that comprises of transmitting stations and monitor sites connected to a control centre. The measured propagation delays at the monitor sites are used to compute corrections at the control centre for the user. The major improvement compared to LORAN-C is the usage of an additional data channel to provide differential corrections to the user. This additional feature allows eLORAN to reach a new level of perfomance and thus the possibility to serve applications with more stringent demands. For further details, it is referred to [International Loran Association 2007].

2.1.3   Omega

The Omega navigation system is a long-range radio system developed by the U.S. Navy and no more available since 1997 [Kayton et al 1997]. It provides full-time worldwide coverage from eight strategically located terrestrial very-low frequency transmitting stations. Omega is a hyperbolic navigation system using phase comparison of very-low frequency (10 to 14 KHz) continuous-wave radio signals and can be used by aircraft, ships, land vehicles and also by submarine at moderate antenna depth of about 12 to 15 meters [Forssell 2008], [Van Etten 1976].

Table 2-1: Omega transmitter stations [Forssell 2008]

Station	Location	Transmitter Antenna	Administered by
A	Bratland, Norway	Suspended wires across a fjord	Norwegian Telecommunications Administrations
B	Monrovia, Liberia	Grounded tower with radial top elements	Ministry of Industry and Commerce
C	Haiku, Hawaii	As A	US Coast Guard
D	La Moure, North Dakota	Bottom-isolated monopole	As C
E	Reunion in the Indian Ocean (France)	As B	French Navy
F	Golfo Nuevo, Argentina	As D	Argentine Navy
G	Woodside, Victoria, Australia	As B	Department of Transport
H	Tsushima, Korean Strait, Japan	As D	Japanese Coast Guard

All Omega transmitters (see Table 2-1) are synchronized in phase and transmit on each of 3 common navigation frequencies: 10.2, 11.33, and 13.6 kHz. Synchronization is maintained by synchronized atomic clocks. Each transmitter A to H respectively has a unique frequency that is used for identification. The signal format of the system is such that each station transmits signal segments that are separated by a time interval of 0.2 seconds. The repetition frequency of the signals is 0.1 Hz. Further information about signal format is found in [Forssell 2008].

Phase differences between signals received from a pair of transmitters determine a set of hyperbolic lines of position separated one from another by a phase difference of 2π radians, corresponding to a distance difference of one wavelength λ. On the baseline between stations, the lane width is approximately 15 km if only the 10.2 kHz transmissions are used; the lanes can be resolved to approximately 45 km by employing the difference frequency of 3.4 kHz with respect to 13.6 kHz frequency for phase measurements. Similarly, if the 11.33 kHz frequency is also used, the resolution is around 133 km. Dead-reckoning or redundant Omega phase measurement can be used to resolve this 133 km ambiguity. However, it became necessary to enlarge the non-ambiguity area further, and a fourth transmitter frequency, 11.05 kHz, was introduced. The difference frequency between this one and 11.33 kHz gives a lane width of about 529 km.

Transforming from Omega phase coordinates into a terrestrial reference frame (latitude and longitude) would be relatively easy if the velocity of propagation of the very-low-frequency signals was constant. Unfortunately, it is not constant but is a function of several parameters, such as time of day, season, direction of propagation, solar activity, earth conductivity, etc. First, there is a natural random fluctuation that cannot be reduced by any known method. Second, there is a systematic variation mainly due to the above factors and systematic errors will persist even after these factors have been corrected because of deficiencies in the propagation model. Estimates of Omega position accuracy vary from 0.9 to 1.5 km in the day-time, and double that value at night. Thus, Omega is a low accuracy system [Van Etten 1976]. A technique known as differential Omega may be employed to improve the accuracy of the Omega system: an Omega monitoring at a known location establishes real-time Omega phase values. The difference between a set of fixed reference values for that location and these real-time values are called differential corrections and are transmitted to mobile users in the area. The mobile user applies the same real-time differential corrections to his observed phase values. The technique is based upon the principle that phase changes at the monitor station and at the user's receiver due to propagation are well correlated [Forssell 2008], [Van Etten 1976].

2.1.4 Decca

Decca is a low-frequency hyperbolic navigation system using continuous-wave phase comparison. This system is out of service since 2000. The transmitting stations are arranged in so-called chains consisting of a main station (master) with control functions and several slaves whose signals are phase locked to those of the main station. The master station transmits at a frequency of 6 f (f being the fundamental frequency of about 14 kHz) and 3 slave stations transmit at frequencies of 5 f, 8 f and 9 f, respectively. These coherent frequency transmissions are received by the mobile receiver and frequency-multiplied to a common frequency. Phase measurements are then made between the master and slave signals at these comparison frequencies. Each phase-difference measurement represents a hyperbolic line of position and 2 or more define a position fix. However, there are multiple lines of position that represent the same phase difference and, on the base line between the master and slave stations, identical phase differences are spaced at a distance $c/2f_c$, where c is the velocity of light and f_c is the comparison frequency at which the phase difference is measured. The main limitation of the Decca system is sky wave contamination of the ground wave signal. This seriously degrades phase accuracy and the lane identification may be unacceptable beyond a distance of about 400 km in the daytime and 160 km at night between transmitter and receiver [Forssell 2008], [Van Etten 1976].

The system is British and was introduced during World War II. It has been used mainly in Europe where most of the coastal waters are covered, but also in Japan, India, Pakistan, the Persian Gulf,

South Africa and parts of Australia and Canada (although some of these regions are no longer covered). Consequently, it is a very widespread area radio navigational system, and in 1987 there were 140 stations in 42 chains in 17 countries [Beattie 1988]. In Norway there are six chains, Skagerak, Vestlandet, Trondelag, Helgeland, Lofoten and Finnmark. Decca is mainly used by ships and, to some extent, by aircraft as well, especially helicopters. Trials on land have also shown fairly good results, both in the United Kingdom [Powell 1982] and Norway [Forssell 2008]. The accuracy of the Decca system is, to a large extent, dependent on the position of the user with regard to the transmitting stations, the time of year and the time of day. Even if the distances from the receiver to the transmitters are well within the stated range of the system, the accuracy varies because of propagation condition changes. The standard deviation of Decca position errors is often counted in hundredths of an average lanewidth (called a centilane), this unit being defined to be 5 m [DECCA 1979]. Thus, this corresponds to position accuracy in the order of a few hundred meters to several kilometres.

2.2   Satellite Systems

With the use of artificial satellites, new approaches for navigation have become possible. First satellite based systems were based on Doppler counts. The US Marine developed the Navy Navigation Satellite System (NNSS) also known as Transit in the 1950s and 1960s as being the predecessor of the GPS [Geodesy, Trends and Prospects 1978]. In this context also the Russian system called Cicada which is similar to the Transit system is to be mentioned. However, those systems are not in use anymore nowadays. Present-day GNSS are based on the ranging principle and are comprised of three segments [Bauer 2003], [Forssell 2008]:

- The space segment containing the satellites in orbit that provide the ranging signals and data messages transmitted to the user equipment.
- The ground segment tracks the satellites in their positions and monitors the health and status of the satellite subsystems. Furthermore, the ground segment collects pseudorange and carrier phase measurements at the remote monitor stations to determine almanac, ephemeris and satellite clock corrections.
- The user segment consists of the equipment to perform navigation, timing and other user related functions.

2.2.1   Navstar GPS

In the early 1960s, several US government organizations, including Department of Defence (DoD) were interested in developing a global satellite system for three-dimensional positioning meaning latitude, longitude and altitude. The requirement was to continuously operate on a global basis

under all weather conditions, serving high-dynamic platform ability and high accuracy. For the past several years, 31 operational GPS satellites have been in orbit plus 3-4 decommissioned satellites that can be reactivated if needed. GPS satellites fly in Medium Earth Orbit (MEO) at an altitude of approximately 20200 km. The satellites in the GPS constellation are placed in six Earth-centred orbital planes with a minimum of four satellites in each plane. The ground segment of GPS consists of three different components: the Master control station located near Colorado Springs in US, several monitor stations and the ground antennas.

GPS signals are based on the Code Division Multiple Access (CDMA) principle to distinguish signals coming from different satellites [Parkinson et al 1996]. The legacy GPS satellites broadcast ranging code and navigation data on two carrier frequencies. These two frequencies are referred to L1 centred at 1575.42 MHz and L2 centred at 1227.60 MHz. Each GPS satellite transmits two different codes: Coarse/Acquisition (C/A) code at L1 and the encrypted Precision signal (P(Y)) at both L1 and L2. The L1 and L2 carrier signals are currently modulated by pseudorandom noise (PRN) sequences using Binary Phase Shift Keying (BPSK) modulation [Hofmann-Wellenhof et al 2001]. Since each satellite uses the same carrier frequencies, the signals are separated with a unique PRN sequence associated with each satellite.

With the upcoming of other GNSS, the GPS system is in competition. Hence the pressure on the existing system to improve performance was growing which led to efforts to modernize the GPS system. In the late 1990s, a modernization program was initiated by the US government including an upgrade of the space and ground segment. A major focus in this program is adding new navigation signals to the satellites. These new signals are designed for civilian use: L2C, L5 and L1C. A more detailed description of GPS can be found in the following references [Parkinson et al 1996], [Hofmann-Wellenhof et al 2001], [Bauer 2003], [Seeber 1989].

2.2.2   Galileo

Galileo is the European GNSS that is currently in its deployment phase towards Full Operational Capability (FOC). The In-Orbit Validation (IOV) phase has recently been carried out successfully. The next step in the program is towards Initial Services. The FOC is expected to be achieved around 2020.

The FOC constellation consists of 30 satellites (27 operational plus 3 spares) which fly in 3 orbital planes at an inclination of 56° to the equator. The satellites are equally distributed over each plane at a height of approximately 23222 km. The first two experimental navigation satellites, Galileo In-Orbit Validation Element GIOVE-A and GIOVE-B were launched in 2005 and 2008 for testing purposes. The Galileo satellites transmit navigation signals at four different frequency bands, namely E5a, E5b, E6 and E1.

The ground segment is responsible for maintaining proper operations of the system. Galileo Sensor Stations (GSS) are globally distributed to collect amongst others code and carrier phase measurements and send them to the Galileo Control Centres (GCC). There are two GCC for redundancy reasons: one located in Fucino, Italy and one in Oberpfaffenhofen, Germany. The purpose of the GCC is to compute ephemeris and clock predictions and generate a navigation message which is up-linked to the satellites. System time scale is also generated at the GCC: Galileo System Time (GST). Communication links between the GCC and different UTC laboratories exist in order to steer GST towards UTC.

Currently the following services are planned: Open Service (OS) gives basic level services, dedicated to usual consumer applications. The service provides positioning, velocity and timing information that can be accessed free of charge by mass-market receivers. The OS performance is expected to be competitive with the existing GNSS in terms of both accuracy and availability. Commercial Service (CS) is a restricted-access service level for commercial and professional applications where higher accuracy is required. The CS is based on adding to the OS signals two additional signals, which are protected through commercial encryption. Within CS, the users will be offered high data rate throughput, high accurate positioning and several value-added applications, such as provision of ionosphere delay models. Public Regulated Service (PRS) is intended for authorities such as police and customs. It is encrypted and operational at all time and circumstances. A major advantage of PRS is that it is designed to be robust against jamming and spoofing. A more detailed description of Galileo can be found in the following references [Parkinson et al 1996], [Hofmann-Wellenhof et al 2001], [Bauer 2003], [Seeber 1989], [European Union 2015], [European Union 2016].

2.2.3 GLONASS

When GPS was under development in the 1970s, the former Union of Soviet Socialist Republics (USSR) developed a similar system called GLONASS. Similar to GPS, the system was initially designed for military purposes. The first satellite was launched in 1982 and the system was declared fully operational 1996. However, with the collapse of the Russian economy, the system was not sufficiently maintained leading to a decay of the system. Satellites that have exceeded their lifetime were taken out of service and have not been replaced. Recently, it was decided in Russia to take the effort to restore the system. Since 2010, GLONASS reached full coverage over Russian territory and since December 2011, it has been fully operational, providing global coverage and acceptable accuracy for most users. The space segment consists of 21 satellites plus 3 spare satellites. The constellation operates at an altitude of approximately 19100 km and is uniformly located in three orbital planes 120° apart in right ascension. Each satellite transmits navigation signals in two frequency bands, L1 (1598.0625 - 1609.3125 MHz) and L2 (1242.9375 - 1251.6875 MHz). Unlike all other GNSS, GLONASS employs the frequency division multiple access (FDMA) technique in

order to identify the satellites. In order to provide more robust signals and interoperability capabilities the modern GLONASS-K satellites also transmit CDMA signals in addition to the FDMA signals. A more detailed description of GLONASS can be found in the following references [Parkinson et al 1996], [Hofmann-Wellenhof et al 2001], [Bauer 2003], [Seeber 1989].

2.2.4   BeiDou

BeiDou, also referred to as Compass, is a Chinese satellite based navigation system. For the deployment of the system, an incremental approach is followed. In the beginning of its development it was meant to be a regional navigation system. In 2011, the BeiDou system announced officially its Initial Operational Service including navigation and timing services for the whole Asia-Pacific region with a constellation of 10 satellites (5 geostationary (GEO) satellites and 5 Inclined Geosynchronous Orbit (IGSO) satellites)[Weblink 2016a], [China Daily Europe 2011]. However, since the end of the nineties of the past century, the system evolved its capabilities towards a global navigation system. This final capability is stepwise put in place by launching further satellites (1 GEO satellite and 4 MEO satellites) during 2012. The final configuration of BeiDou is planned to be achieved in 2020 when the system shall evolve towards global navigation capability with a constellation of 35 satellites (5 GEO satellites, 27 in Medium Earth Orbit (MEO) and 3 in IGSO) [GMV 2011]. The BeiDou-2 is Chinas's second-generation satellite navigation system providing global positioning and timing capabilities [Shen 2009]. The BeiDou satellites are transmitting open and authorized signals at B1 (1561.098 MHz) and B2 (1207.14 MHz) and an authorized service at B3 (1268.52 MHz).

BeiDou supports both global and regional services: for the global services two different services are identified, namely the Open Service on the one hand and the Authorized Service on the other hand. The Open Service is available to all civilian users worldwide. Position accuracy is provided in the order of 10 meters, a timing accuracy of 50 ns and a velocity accuracy of 0.2 meters per second [BeiDou System 2013]. For the regional services, differential corrections are broadcast through the GEOs that allow for higher positioning accuracy. For more information on the wide area differential services, it is referred to [Chen 2011].

2.2.5   Usage of GNSS

From the GNSS Market Report published by the European GNSS Agency (GSA) in March 2015 [GSA 2015] a significant increasing use of GNSS emerges. According to the distinction provided by IMO Resolution A.915(22) [IMO 2002], maritime GNSS applications can be split into navigation and positioning:

- Navigation
  - Sea
    - Safety of Life at Sea (SOLAS) vessels: all passenger ships and cargo ships larger than 500 gross tonnages (300 tons for international voyages) are regulated and rely heavily on GNSS for navigation. At least three devices are typically fitted on vessels for redundancy reasons
    - Non-SOLAS vessels: GNSS systems for maritime navigation are widespread across commercial and recreational vessels, both overseas and in high traffic areas.
  - Inland Waterways (IWW): GNSS is also used to ensure safe navigation in inland waterways (rivers, canals, lakes and estuaries)
- Positioning
  - Traffic management and surveillance: these activities are supported by GNSS-based systems including Automatic Identification System (AIS) and Long-Range Identification and Tracking (LRIT)
  - Search and Rescue is the search for and provision of aid to people in distress or danger. Different types of devices can make use of GNSS positioning:
    - In the frame of the Cospas-Sarsat programme [Weblink 2015b], ship and person-registered beacons (i.e. Emergency Position Indicating Radio Beacons s5 (EPIRBs5) and Personal Location Beacons s6 (PLBs6)) transmit, once activated, the necessary information for rescue to authorities via satellite communication.
    - When activated, AIS Search and Rescue Transmitter (AIS-SART7) devices continuously transmit an alert message that includes GNSS-based location which triggers an alarm on all AIS equipped vessels within Very High Frequency 8 (VHF8) range.
  - Fishing vessel control: GNSS positioning enables Vessel Monitoring Systems to check the position of fishing vessels, as well as the time spent in international and foreign waters, protected marine areas, etc.
  - Port operations: transit progress, docking and loading-unloading operations are monitored through GNSS-based technologies.
  - Marine engineering: GNSS is used to support marine construction activities (e.g. cable and pipeline laying).

The key market trends (status 2015) are that GNSS-enabled solutions are increasingly used to monitor the operations of fishing vessels. The market demand for positioning and navigation supports a wide range of GNSS applications, improving safety and productivity of maritime opera-

tions. GNSS is the preferred positioning technology for maritime Search and Rescue solutions [GSA 2015].

A large user group can be identified among the different operations as summarized in Figure 2-4. It is obvious that the use of positioning is widespread, with different categories of vessels, beacons and ports using GNSS for different purposes.

Vessels	Merchant vessels 81,500 vessels	Fishing vessels 2.7 million vessels	Recreational vessels 29.2 million vessels	IWW vessels 529,000 vessels
Beacons	EPIRBs 648 k beacons		PLBs 580 k beacons	
Ports	Sea Ports 8,289 sea ports		Recreational marinas 23,380 marinas (in 20 countries)	

Figure 2-4: Global number of vessels, beacons and ports [GSA 2015]

The end users in maritime applications are ship masters, pilots and port authorities. The beneficiaries are a much wider category, including passengers, companies served by the maritime supply chain and through logistic applications and consumers of sea products.

The user needs and performance requirements of GNSS solutions depend heavily on the applications, designed to satisfy needs of improved safety and productivity. In this sense, accuracy and integrity are key elements for navigating in restricted waters (e.g. port approach, inland waterways) as well as for positioning applications (e.g. manoeuvring, traffic management, Search and Rescue operations, marine engineering), as stated in IMO resolution A.915 [IMO 2002].
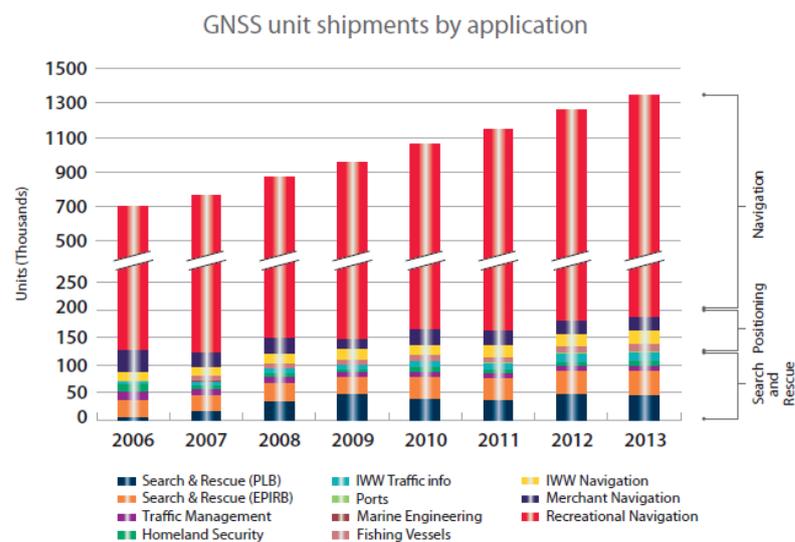

Figure 2-5: GNSS unit shipments by application [GSA 2015]

The GNSS unit shipments by application are shown in Figure 2-5. It has to be highlighted that a strong increasing trend of the GNSS units can be observed which leads to an even stronger exploitation of GNSS for all maritime operations in the future. This gives an overview of the proportion of the maritime operations for which GNSS is used. Navigation is the main application while Positioning and Search and Rescue are smaller application areas but nevertheless both with a significant amount of users and increasing trends for the future.

2.2.6   GNSS and Inertial Navigation Systems

An inertial navigation system (INS) is typically composed of different types of sensors measuring acceleration and rotation velocities (or velocity and angle increments). The main challenges are the double integration of the acceleration measurements and the single integration of the rotation velocity measurements. The introduction of the derived latter information from the respective previous time interval is used to derive a navigation solution for the current time interval. This approach is described in a so-called strapdown-algorithm. The advantage and at the same time a disadvantage of an INS is the ability of navigating without an absolute reference. Depending on the type and quality, the sensors are affected by significant sensor drifts allowing for short term navigation only. To compensate for this, an INS can be used for integration with GNSS. In general, the combination of the two independent navigation systems allows for bringing together their complementary features.

Different strategies of integrating INS and GNSS are pointed out in [Wendel 2011]: typically, a distinction is made between a loosely, tightly and ultra-tight integration strategy. Each strategy has its advantages as well as disadvantages depending on the user application and complexity. Kalman filter algorithms for such integration usually incorporate a fairly high number of variables or states, e.g. position, velocity in the three coordinates, clock bias and drift, accelerometer errors, gyro drift parameters, etc., often twelve to twenty parameters [Hansen 1989]. [Wendel 2011] derives a navigation filter for the combination of GNSS and INS sensor data. This approach is based on a so-called error-state-space-Kalman-Filter.

INS can be used for example to bridge outages of the GNSS positioning due to obstruction or high acceleration. In such a case, on a short term basis, INS provides aiding data such as velocity that can be used by the receiver to keep track or to speed up re-acquisition of the GNSS signal. Another advantage of the integration of INS with GNSS is that INS support can also be used for maintaining relatively low tracking bandwidths, thus enabling the receiver to withstand high noise levels, e.g. jamming [Forssell 2008].

For the interested reader the following references are recommended: [Wendel 2011], [Forssell 2008].

3   General Aspects on Integrity Algorithms

Since the beginning of the civil use of GPS, the satellite system provides basic integrity information. This GPS integrity information consists only of a "flag" of the navigation message, which allows the trust in operation of the corresponding satellite. This form of integrity information alone does not fulfil the user requirements of trustfulness in positioning. Therefore, in the nineties of last century the Receiver Autonomous Integrity Monitoring (RAIM) method was put forward as a consistency check to protect the user against incorrect position estimation in terms of vertical and horizontal dimension. The performance of this monitoring is highly dependent on how conservative the user requirements are and on the assumptions for the GNSS satellite and constellation faults which may occur with certain probabilities during the processing time. RAIM originated with the publication of RTCA/DO-208 in 1991. Since that time the recommendations of RTCA Special Committee 159 for using GPS as a supplementary navigation aid in U.S. civil aviation were used as a strong design driver for most of present developed algorithms. Nowadays, RAIM applications range from avionics to consumer grade receivers, with different requirements concerning its reliability being met. Its two functions are:

- Detection and exclusion of large measurement faults leading to large position offsets,
- Computation of an upper bound on the position error.

This chapter aims at the provision of a basic understanding on the service performance parameters. More details are provided on the before mentioned capabilities on failure detection and the computation of a protection level. Also the calculation of the so-called k-factor is depicted as well as a unified approach for the protection level computation. The analogy of the theory for RAIM to geodetic applications is highlighted in the last sub-section.

3.1   Service Performance Parameters

Safety critical GNSS based operations distinguish from typical mass market applications. For this kind of applications stringent requirements are clearly defined in terms of availability, continuity, integrity and accuracy. These performance related terms are closely linked to each other and form together a set of user requirements that need to be satisfied allowing for successful accomplishment of a user's operation.

The mentioned service performance parameters are arranged in a certain hierarchy which somehow attaches different values to the parameters. Basically, the objective is to achieve availability yielding the requirements to be fulfilled. As already mentioned, there exist different classes of GNSS

related applications which all come along with different requirements. The performance related terms together with their hierarchy and dependency are highlighted in a pyramid (see Figure 3-1).

The accuracy requirement is crucial for any GNSS application. For safety critical applications for which integrity is required, accuracy is a prerequisite. Thus, the service performance parameters are closely related to each other such that one depends on one another. In a next step continuity is declared available if integrity is ensured at the beginning and throughout the period of an operation. This implies the fulfilment of accuracy requirement as well. Availability is given if integrity, continuity and accuracy are available.
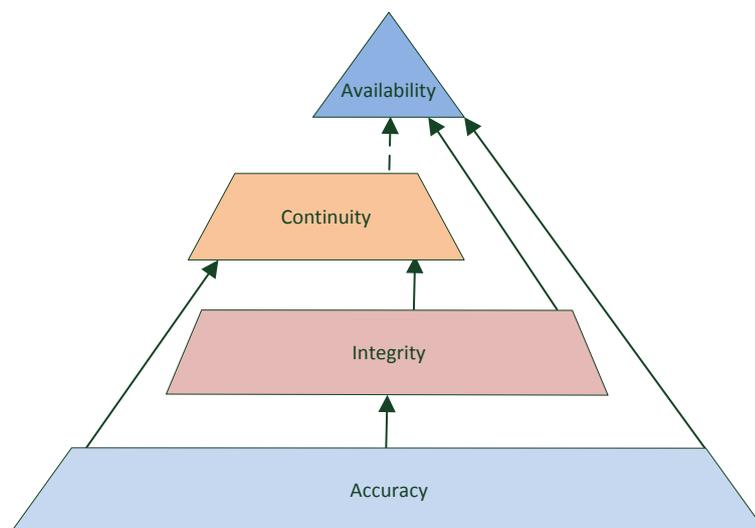
Figure 3-1: Dependency and hierarchy of service performance parameters

In the following, the service performance parameters are introduced in more detail together with their definitions. In addition, some further terms in the respective context are introduced.

3.1.1 Accuracy and Pseudorange Accuracy

Generally, accuracy is a measurement of the degree of closeness of the provided quantity (for example a position measured by the receiver) to its actual (true) value [RTCA 2006]. "The measurement values for GNSS are either measurements associated with one satellite (e.g., pseudorange and carrier phase) or measurements computed from information from more than one satellite which provide a 'Position, Velocity or Time (PVT) solution)" [EC 2008].

Pseudorange accuracy relates to the noise on the pseudorange measurements which is usually elevation dependent and described in a User-Equivalent Range Error (UERE) budget. Thus, a UERE budget is a statistical description of the pseudorange accuracies one can expect to see when track-

ing the GNSS satellites. Hereby, a (rough) distinction is made between system induced errors such as Signal-In-Space Error (SISE), atmospheric and local effects.

The SISE is an error bound of the remaining error in the pseudorange domain at user level mainly caused by the satellite ephemeris errors and the satellite clock errors [EC 2008]. The SIS error due to system contribution in the frame of Galileo is denoted as SISE whereas for GPS the term User-Range Error (URE) is more common. The SISE/URE originates directly from the GNS system itself as opposed to local and atmospheric effects. Local effects are understood mainly to be receiver noise, interference and multipath whereas atmospheric effects take into account the ionosphere and troposphere.

In the context of Galileo, the Signal-In-Space Accuracy (SISA) corresponds to the estimation of the SISE. Therefore, it is an estimation of the bound of the SISE. Note that every user may have a different SISE, and therefore the SISA may depend on the user position. In order to solve this problem, the SISA shall bind the SISE for the worst user in the coverage area. The worst user refers to the user with the highest projection of the SISE in a respective coverage area. SISA can also be referred to by Estimated User Range Error (EURE) [EC 2008]. The SIS accuracy in the frame of Galileo is denoted as SISA whereas for GPS the term User-Range Accuracy (URA) is used.

Positioning accuracy relates to the uncertainty of an estimated position at user level with respect to its true position.

3.1.2   Integrity

A definition of integrity exists from the International Civil Aviation Organization (ICAO) which is as follows: „Integrity is a measure of trust which can be placed in the correctness of the information supplied by the total system. Integrity includes the ability of a system to provide valid and timely warnings to the user (alerts) when the system must not be used for the intended operation (or phase of flight) [RTCA 2006]". In [IMO 2002] the following definition can be found: "The ability to provide users with warnings within a specified time when the system should not be used for navigation."

The Time-To-Alert (TTA) is the maximum allowable elapsed time from the onset of a positioning failure until the equipment announces the alert. In [IMO 2002] the following definition can be found: "The time elapsed between the occurrence of a failure in the system and its presentation on the bridge". The TTA is understood to be a system relevant requirement and that the system has the ability to provide timely warnings within that specified TTA. However, this requirement also applies in principle at user level if a user tries to detect and exclude failures originating from the system.

The so-called Alert Limit (AL) is the maximum allowable error in the user position solution before an alarm is to be raised within the specific TTA [EC 2008]. Depending on the requirements of the operation respectively, AL are specified for the two position domains: Horizontal Alarm Limit (HAL) and Vertical Alarm Limit (VAL).

The Horizontal resp. Vertical Protection Level is the statistical limit of the horizontal resp. vertical position error. The probability of the absolute horizontal and vertical position error exceeding the Protection Level shall be smaller than or equal to the integrity risk.
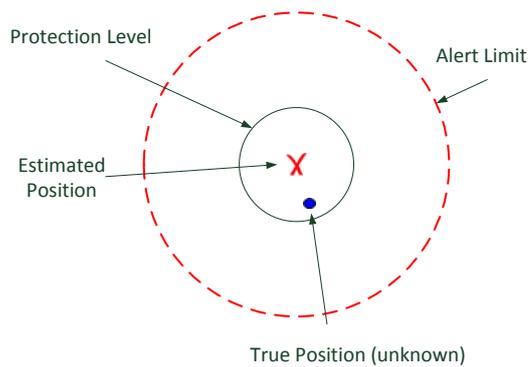

Figure 3-2: Definition of a Protection Level

Figure 3-2 depicts the situation where the PL is smaller than the AL. The PL bounds the true position around the estimated position. The relationship of the position error, PL and AL is crucial for declaring a position solution available or not.
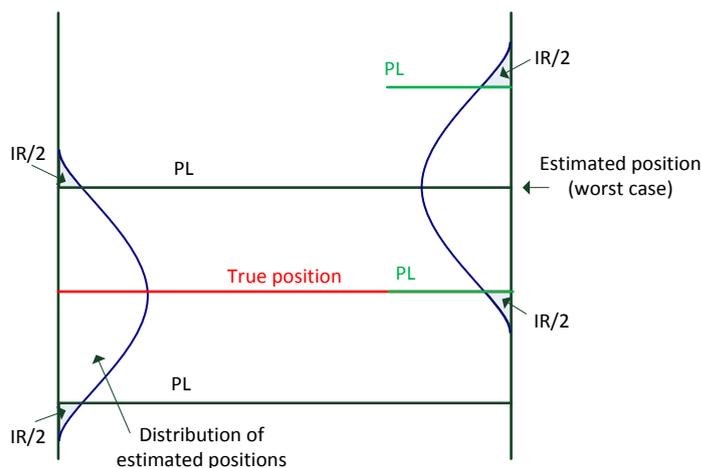

Figure 3-3: Relationship of Protection Level centered around True and Estimated Position

An important aspect is the understanding and the justification that a PL can be computed around the estimated position. Figure 3-3 gives a simplified overview of the relationship of a protection level that is computed either around the true position and an estimated position. Under fault-free conditions, the estimated positions will normally distribute around the true position. In fact, the true position is un-known and considered as a theoretic reference. In this case, the protection levels are given with respect to the true position (left side). The integrity risk is being allocated above the PL respectively considering both tails of the error distribution. Analogously, the protection level can be interpreted as being centered around the estimated position. This is justified by looking at the worst case position estimate by shifting the error distribution on the right side such that the worst case equals the PL from the left error distribution. According to the definition of a PL, it should contain the true position with the integrity risk probability. This implies both tails being symmetric with respect to the mean of the error distribution. Not having the knowledge about the true position relative to the estimated position, the worst case position estimate is assumed which still fulfills the need of having the true position inside the PL limits with required probability. In the end, this results in the same value for the PL for both interpretations.

The integrity risk (IR) is the probability that the position error exceeds the protection level in the presence of an undetected failure event. "The probability that a user will experience a position error larger than the threshold value without an alarm being raised within the specified time to alarm at any instant of time at any location in the coverage area" [IMO 2002].

An integrity event occurs if an occurring failure has not been detected and at the same time causing the position error PE to exceed its PL. So in general the resulting "conditioned" integrity risk is a product of three probabilities and is given by:

$$IR_{cond} = P_{occ} \cdot P_{md} \cdot P(P_E > PL)$$

3.1

P_{occ}: probability of occurrence

P_{md}: probability of missed detection

$P(P_E > PL)$: probability of the Position Error (PE) exceeding its PL

The allocation of the total integrity risk to the different probabilities is of course a task of the specific algorithm and system designs. It depends also on the assumptions that are made about the threats that are to be considered together with their likelihood respectively. This will be discussed further in the following chapters of this thesis.

3.1.3   Continuity

The following definitions are provided by the RTCA and IMO:

„The continuity of a system is the ability of the total system (...) to perform its function without interruption during the intended operation. More specifically, continuity is the probability that the specified system performance will be maintained for the duration of a phase of operation, presuming that the system was available at the beginning of that phase of operation and was predicted to operate throughout the operation" [RTCA 2006].

"The probability that, assuming a fault-free receiver, a user will be able to determine position with specified accuracy and is able to monitor the integrity of the determined position over the (short) time interval applicable for a particular operation within a limited part of the coverage area" [IMO 2002].

The continuity risk is the probability that the system will not provide guidance information with the accuracy and the integrity required for the intended operation [EC 2008].

3.1.4   Availability

Availability of GNSS is characterized by the portion of time the system is to be used for navigation during which reliable navigation information is present. The service will be declared available when accuracy and integrity requirements are met at the beginning of an operation and are estimated to be met during the operation period (continuity requirement).

The IMO defines availability as "the percentage of time that an aid, or system of aids, is performing a required function under stated conditions. Non-availability can be caused by scheduled and/or unscheduled interruptions [IMO 2002]". Hereby, the following distinction is made:

- Signal availability: the availability of a radio signal in a specified coverage area.
- System availability: the availability of a system to a user, including signal availability and the performance of the user's receiver [IMO 2002].

It is impossible to give an absolute guarantee on the position error; in contrast, it can only be guaranteed that the actual position error can exceed the Protection Level at the IR. The IR is the sum of the Probability of Misleading Information (MI) and Probability of Hazardous Misleading Information (HMI). The AL is the maximum tolerable position error. If the position error exceeds the AL, the system becomes unavailable and the user must be warned. In case of MI, the position error exceeds the PL, but not the Alert Limit (AL). In case of HMI, the position error exceeds the PL and the AL, but the PL is below the AL. In summary, four cases need to be distinguished (see Table 3-1).

Table 3-1: System States w.r.t. Integrity

System States w.r.t. integrity	
Position Error < PL Position Error < AL PL < AL	Integrity available
Position Error > PL Position Error < AL PL < AL	Misleading Information (MI)
Position Error > PL Position Error > AL PL < AL	Hazardous Misleading Information (HMI)
PL > AL	System unavailable

3.2 Fault Detection and Fault Exclusion

Beside the ability of computing a protection level, some integrity algorithms come along with a further important characteristic. The detection of the presence of an inconsistent set of data that is used to compute a position estimate can be supportive. One step further would be the identification and exclusion of potential failed measurements. Thus in the presence of a failure a distinction needs to be done between the following two cases:

- Fault Detection (FD)
- Fault Detection and Exclusion (FDE)

RAIM is based on measurement redundancy and is closely connected to the navigation solution in the receiver. Under the assumption of a single GNSS constellation being available, four range measurements are required to solve the navigation equation and estimate the four unknowns: latitude, longitude, height and a local user clock offset. In that case, a minimum of five pseudoranges is needed to perform FD by analysing the possible position subset solutions based on a number of pseudoranges that is less than the total available number respectively. Outlying position subset solutions might indicate the presence of an inconsistent measurement. This approach is also referred to as solution separation (see section 5.5). Another approach is based on a least-squares approach that is used to calculate a position estimate where in addition to the position estimate a

set of pseudorange residuals becomes available. Here, large residuals suggest that a measurement error or measurement bias is present. This approach is further detailed in section 5.3.

Basically, FD is done via a consistency check of the available set of measurements in order to decide if one measurement diverges from the others and hence can be declared as failure. In that case however, the user needs to withdraw the whole set of measurements and thus cannot declare its position solution available from the integrity point of view. Generally, to perform fault detection there must be at least one redundant observation available for positioning. Considering one constellation, four satellites in view are needed to compute a position and time solution, five satellites are needed to detect a failure (FD) and six (or more) satellites are needed to detect and exclude the failure (FDE). These numbers are changing accordingly if more satellite failures are considered and if more constellations are used, because one inter-system clock bias for each additional constellation has to be computed, too.

3.3 Calculation of the k-factor

This section derives a way to compute the multiple of the standard deviation which is related to a certain probability. This value is also known as k-factor and is used for scaling the standard deviation of a Gaussian random variable in order to retrieve a percentile value corresponding to a certain probability. The cumulative distribution function $F(x, \mu, \sigma^2)$ of a Gaussian random variable x with mean μ and variance σ^2 is given by [Abramowitz and Stegun 1972]:

$$F(x, \mu, \sigma^2) = \frac{1}{2}\left(1 + erf\left(\frac{x - \mu}{\sigma\sqrt{2}}\right)\right) = \{erf(-x) = -erf(x)\} = \frac{1}{2}\left(1 - erf\left(\frac{\mu - x}{\sigma\sqrt{2}}\right)\right)$$

$$= \{erf(x) = 1 - erfc(x)\} = \frac{1}{2}\left(1 - \left(1 - erfc\left(\frac{\mu - x}{\sigma\sqrt{2}}\right)\right)\right) = \frac{1}{2}erfc\left(\frac{\mu - x}{\sigma\sqrt{2}}\right)$$

3.2

where $erf(\ )$ refers to the error function which is defined as follows [Abramowitz and Stegun 1972]:

$$erf(x) = \frac{2}{\sqrt{\pi}}\int_0^x e^{-t^2}dt.$$

3.3

The complementary error function $erfc(\ )$ is denoted as [Abramowitz and Stegun 1972]

$$erfc(x) = 1 - erf(x) = \frac{2}{\sqrt{\pi}} \int_{x}^{\infty} e^{-t^2} dt.$$

3.4

Therefore, the k-factor refers to the multiple of standard deviations corresponding to a specific probability P for a zero-mean normalized Gaussian error distribution. It can be determined by solving:

$$F(k, 0,1) = P = \frac{1}{2} erfc\left(\frac{k}{\sqrt{2}}\right)$$

3.5

which leads to:

$$k = \sqrt{2} \cdot erfcinv(2 \cdot P)$$

3.6

where $erfcinv(\ )$ being the inverse of the complementary error function and defined as

$$erfcinv\big(erfc(x)\big) = x.$$

3.7

Hereby, it is important to note that it is assumed that only the right tail of the Gaussian distribution contributes to P, not both tails. This case is illustrated in Figure 3-4 on the left.
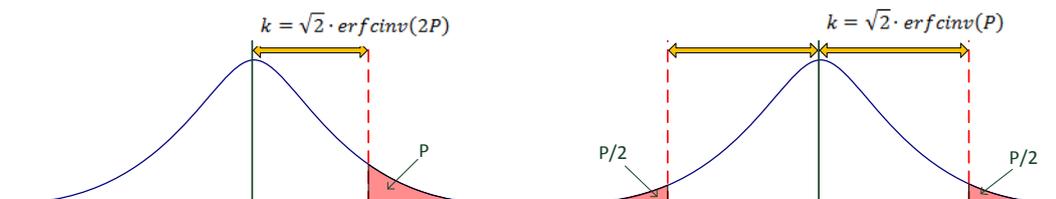

Figure 3-4: k-factor based on one (left) or two (right) tails contributing to probability P

However, considering both tails of the error distribution while assuming symmetry for the error distribution leads to the following equation for the k-factor:

$$k = \sqrt{2} \cdot erfcinv(P)$$

3.8

This case is highlighted in Figure 3-4 on the right. If both tails of the Gaussian distribution contribute to P, e.g. if a position error can be positive and negative, then the k-factor is calculated accordingly.

3.4 Unified Approach for Protection Level Computation

This section introduces a generalized approach for the computation of a protection level. It unifies the theory given in this overall section and puts it in a clear context. This approach given here is leaned on the protection level computation for the least-squares residual (LSR) RAIM as detailed in section 5.3. A general approach is introduced whose idea behind can be adopted to various integrity algorithms and provides a solid understanding for those which will be introduced in the next chapter 5.

In any integrity algorithm with FD capability, a metric or test statistic for example related to pseudorange observations is compared to a threshold. Assuming for the moment that a fault causes a deterministic bias in the test statistic, the test statistic has two components: this bias, and the noise that is also present in the fault-free case. A mapping function describes how the test statistic value maps to an error in the position domain. This mapping function is a function of the geometry of the satellites usually taking into account the most critical satellite. The most critical satellite is the one with the highest sensitivity to the position domain. For the sake of simplicity, it is assumed that an unambiguous mapping between test statistic and position domain exists. Two cases have to be distinguished:

1. The test statistic is formed from pseudoranges. In this case, the noise corrupting the pseudoranges enters the test statistic and a mapping of this noise into position domain can be calculated. In other words, the distribution of the noise corrupting the position solution can be obtained from the distribution of the test statistic via the mapping function into position domain.

2. If the test statistic is not formed from pseudoranges, it is not obvious that the distribution of the position error can be obtained from a mapping of the distribution of the test statistic into the position domain. In this case, the relation between the test statistic and the position error might be not straight forward and would need to be assessed carefully.

The generalized method for protection level calculation covers both cases and is illustrated schematically in Figure 3-5. In this figure, the metric or test statistic value is shown on the abscissa, the position error probability density is shown on the ordinate. The orange line illustrates the mapping function which describes how a bias of the test statistic is mapped into position domain. For the sake of simplicity a linear mapping function was assumed here, but this approach works with any reasonable mapping function. The distribution of the test statistic is plotted over the abscissa, green

indicates the fault free case, and red the faulty case. Now the protection level calculation works as follows:

1. The first step is to specify the probability of false alarm, P_{fa}. From this P_{fa}, the threshold T is calculated with which the test statistic is compared in order to detect a fault. The area under the test statistic distribution in fault-free case corresponding to P_{fa} is found right from the threshold value T.

2. The next step is to specify the probability of missed detection, P_{md}. It is assumed that a fault causes a bias in the test statistic which is the case for any reasonable test statistic. The specification of P_{md} determines the value of the minimum detectable bias which is indicated as Pbias: the bias shifts the test statistic distribution in faulty case along the abscissa. P_{md} corresponds to the area left of the threshold T under the test statistic distribution in faulty case. In other words, by specifying the P_{md} and knowing the test statistic distribution, it is basically specified how far the test statistic distribution has to be shifted along the abscissa to the right in the faulty case. It is noted that the test statistic is not only shifted but is usually changes its shape considerably.

3. In general, the mapping of the test statistic into the position domain using the mapping function can be done differently. In dediacted literature there is no clear recommendation how to perform this step. Different strategies are to be found: for example [Walter et al 1995] suggests using the threshold T for projection. Other strategies are possible using Pbias for projection into the position domain. Section 5.3.5 discusses the different approaches. Furthermore, a recommendation is given based on a comparison of those. However, in any case, this leads to a corresponding bias in position domain, shown by a red arrow. The position error distribution in the fault-free case is shown by the Gaussian-like distribution plotted along the ordinate, and the position error distribution in presence of a fault is shown in red.

4. Finally, the probability that the actual position error, P_E, exceeds the protection level, PL, $P(P_E > PL)$, is specified. The protection level is now chosen such that the area under the position error distribution in the faulty case for errors larger than the protection level corresponds to $P(P_E > PL)$. Obviously, it is not important whether or not the distributions of test statistic and position error are the same in fault-free case and in faulty case. As already stated, it is assumed that a fault causes a bias in the test statistic. For certain types of faults, it might be possible that a fault just causes a change of the distribution function of the position error, without shifting it along the ordinate. For example, a decrease in C/N0 as test statistic can indicate an increase in the noise of the position solution. In this case, the protection level can be calculated in exactly the same way, using the position error distribution in the faulty case caused by a fault that causes a bias in the test statistic.
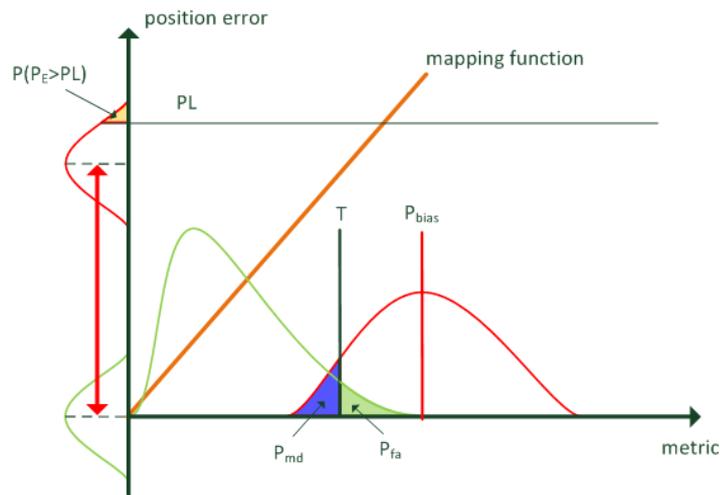
Figure 3-5: Unified Approach for Protection Level Computation

This general formalism allows calculating protection levels for horizontal and vertical position errors and receiver clock estimate errors in a straight forward way. Furthermore, in the special case of Signal Quality Monitoring (SQM), alternative designations such as Minimum Detectable Error in Range Domain (MERR), k-factor under fault-free missed detection (Kffmd) and k-factor for Protection Level (Kpl) as can be found for example in [Soualle et al 2015] are deemed special cases of the general formalism presented here.

3.5 Analogy to Geodetic Network Analysis

The theory which RAIM is based upon is also equivalent to the field of the analysis of geodetic networks. A geodetic network is a system of survey points arranged together. In general, different kinds of geodetic network exist according to the application (global or local survey, position components to be considered) and form as such the basis for further surveying. Its theory of adjustment is generally used for many years. Also the estimation of the surveying position is based on distance or angle measurements between the stations, for example. An important task is the detection of gross errors that occur not only due to an outlier in the measurements but also under certain conditions due to fault-free measurement noise. The quality of a geodetic network is measured in terms of accuracy of the results, but also of their reliability. The following references are given for the interested reader: [Baarda 1968], [Pelzer 1980], [Heck 1981], [Heck 1983], [Niemeier 2008].

In the following, some techniques will be pointed out allowing for interpretation and ensuring reliability.

- Data Snooping according to Baarda:

    This approach is commonly used in dedicated software realizations [Lehmann et al 2006] for the detection of gross errors in the set of measurement. It is based on normalized residuals for each measurement which are tested against a given threshold. In case of an excess of that threshold, this particular measurement is identified as a potential outlier. However, a disadvantage of this approach is the strong dependency on the a-priori assumptions regarding the accuracy of the measurements. Further, outliers can also impact other measurements which might lead to difficulties in identifying the ouliers. This approach is based on the assumption that only a single failure is present in the set of measurement [Wicki 1989].

- Reliability
    - Internal reliability
        The internal reliability indicates the minimum detectable measurement errors in a geodetic network. This is analogeous to the minium detectable bias in the test statistic domain in RAIM (see section 5.3). However, based on that, the impact on the results is to be assessed which is of more importance. By this, the outer reliability is meant [Wicki 1989].
    - External reliability
        This parameter indicates the impact on the final results based on the minimum detectable errors in the measurements. The reliability of the resulting coordinates for example can be optimized by analyzing these quantities in a geodetic network and adapting the configuration respectively [Wicki 1989].

    The common assumption for all these approaches is based on the single failure assumption. Other approaches are available allowing for ensuring reliability in a geodetic network and are outlined in [Wicki 1989]. Nevertheless, for further studies, it is referred to [Baarda 1968], [De Heus 1982] and [Lehmann et al 2006].

4 Understanding of Performance Requirements

Most integrity providing systems and integrity algorithms have been developed and designed in the past for the needs of the aeronautical users as they are the primary user community. However, other user communities exist, e.g. the maritime user who has different demands in contrast to the aviation community. This chapter derives and compares the performance requirements both for the aviation and the maritime users.

4.1 IMO

The International Maritime Organization (IMO), known as the Inter-Governmental Maritime Consultative Organization (IMCO) until 1982, was established in Geneva in 1948 and came into force ten years later, meeting for the first time in 1959 [Weblink 2015c].

Headquartered in London, United Kingdom, the IMO is a specialized agency of the United Nations with 171 Member States and three Associate Members. The IMO's primary purpose is to develop and maintain a comprehensive regulatory framework for shipping, and its remit today includes safety, environmental concerns, legal matters, technical co-operation, maritime security and the efficiency of shipping. IMO is governed by an assembly of members and is financially administered by a council of members elected from the assembly. The work of IMO is conducted through five committees and these are supported by technical subcommittees. Member organizations of the UN organizational family may observe the proceedings of the IMO. Observer status is granted to qualified non-governmental organizations.

IMO is supported by a permanent secretariate of employees who are representative of the organization's members. The secretariate is composed of a Secretary-General who is periodically elected by the assembly, and various divisions such as those for marine safety, environmental protection and a conference section [Weblink 2015c].

This section derives and defines a requirement baseline based on publications from the IMO. The IMO ran through a development of their operational requirements since 1983. Since then, IMO initiated a study into a world-wide satellite position-fixing system for safety of navigation and a report – Study of a world-wide radio navigation system – was adopted by the IMO Assembly in 1989. IMO resolutions have been published by the IMO since then. It is noted that there are obviously two independent developments (here also called "families") for the operational requirements within the IMO – on the one hand for worldwide radio navigation systems and on the other hand for

a future GNSS. Both points of view are deemed relevant and will therefore be discussed. According to the understanding of the author the link between these two "families" is missing.

First, accuracy standards for navigation are described and assessed "for position-fixing systems, in particular radio navigation systems, including satellite systems" in the IMO Resolution A.529(13) [IMO 1983]. The IMO Resolution A.577(14) [IMO 1985] stated some basic recommendations on the operational status of electronic position-fixing systems such as "the authorities or companies responsible for the operation of a selected system, or of any of its constituent parts, should at all times make available to navigators appropriate information on the operational status of such systems or parts thereof".

The diagram in Figure 4-1 depicts the chronicle evolution of the respective IMO resolutions on navigation related issues ("Family 1"). The upper layers revoke the latter layer respectively which means that resolution A.1046(27) [IMO 2011] contains the actual operational requirements.
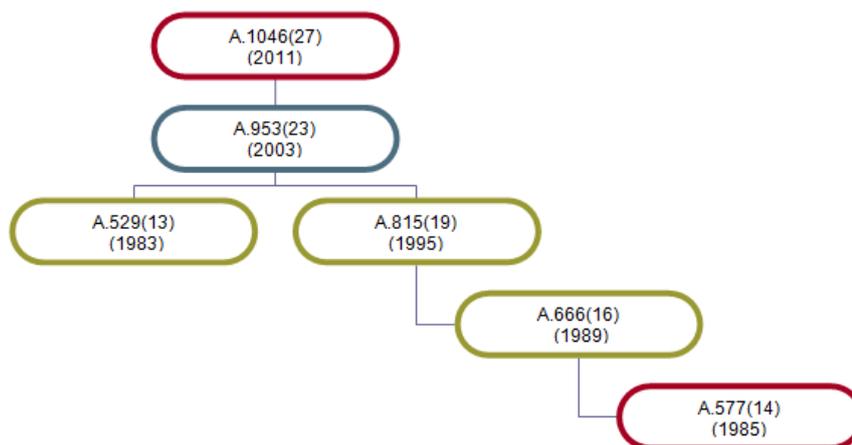
Figure 4-1: Chronicle evolution of respective IMO resolutions on navigation related issues („Family 1")

The IMO resolution A.666(16) from 1989 [IMO 1989] for the first time expresses the "need for a world-wide radio navigation system to provide ships with navigational position-fixing throughout the world". Different relevant systems (GPS, Differential Omega, Loran-C, etc.) are listed and detailed with respect to their technical and operational aspects. It is also noted that "GPS would be suitable for use as it is expected to be operational in the early 1990s". Resolution A.815(19) [IMO 1995] recalls and revokes Resolution A.666(16) [IMO 1989] by which it adopted some studies of a world-wide radio navigation system. Operational requirements for a world-wide radio navigation system are expressed here for different phases of operation.

Resolution A.953(23) [IMO 2003] updates resolution A.815(19) [IMO 1995] by which it adopted the report on the study of a world-wide radio navigation system which is annexed to that resolution. The resolution A.1046(27) [IMO 2011] recollects and revokes resolution A.953(23) [IMO 2003] and expresses the actual operational requirements on worldwide radio navigation systems that are summarized in Table 4-1.

Table 4-1: Summary of operational requirements for a worldwide radionavigation system according to resolution A.1046(27) published by the IMO [IMO 2011]

	Horizontal 95%	Update Rate of Computed/Displayed Position Data	Integrity	Time-To-Alarm [sec]	Continuity	Availability
Ocean Waters	100m	<2s	N/A	ASAP	N/A	0.998 over 30d *
Harbour Entrances, Harbour Approaches and Coastal Waters	10m	<2s	N/A	10s	≥0.9997 over a period of 15min	0.998 over 30d *

*: the period of time of 30d is taken from the previous resolution A.953 as there is no actual value in the resolution A.1046(27) [IMO 2011].

It is noted that the operational requirements expressed in Table 4-1 do not consider a need for integrity. The operational requirements according to the IMO resolutions which are associated to "family 2" differ from those derived from the resolutions of "family 1". The relation between the IMO resolutions of "family 2" is depicted in Figure 4-2 showing the chronicle evolution of the respective IMO resolutions on navigation related issues ("Family 2"). The upper layers revoke the latter layer respectively which means that resolution A.915(22) [IMO 2002] contains the actual operational demands.
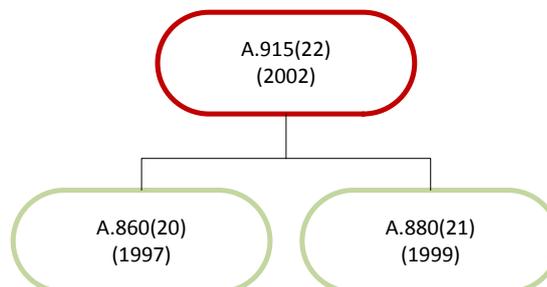

Figure 4-2: Chronicle evolution of respective IMO resolutions on navigation related issues („Family 2")

The actual resolution A.915(22) [IMO 2002] revokes resolution A.860(20) [IMO 1997] and recognizes "the need for a future civil and internationally-controlled global navigation satellite system

(GNSS) to contribute to the provision of navigational position-fixing for maritime purposes throughout the world for general navigation, including navigation in harbour entrances and approaches and other waters in which navigation is restricted" [IMO 2002]. The maritime requirements for a future GNSS are described in the resolution and are depicted in Table 4-2. Resolution A.880(20) [IMO 1999] does not contain any operational requirements for GNSS but deals with the implementation of the International Safety Management (ISM) Code.

Table 4-2: Summary of operational requirements for a worldwide radionavigation system according to resolution A.915(22) published by the IMO

Operation	System Level Parameters		Service Level Parameters			
	Abs. Accuracy	Alert Limit	Integrity			
	Hor. [m]	Hor. [m]	TTA [sec]	Integrity Risk (per 3 hours)	Availability [%] per 30 days	Continuity [%] over 3 hours
Ocean*	10	25	10	1.E-05	99.8	N/A
Coastal*	10	25	10	1.E-05	99.8	N/A
Port approach and restricted waters**	10	25	10	1.E-05	99.8	99.97
Port***	1	2.5	10	1.E-05	99.8	99.97
Inland waterways*	10	25	10	1.E-05	99.8	99.97

*: global coverage; **: regional; ***: local

It is noted that no specifications are defined for the vertical component. The fix interval is required to be 1s for all phases of operation. More stringent demands may be necessary for ships operating above 30 knots.

Currently the IMO resolutions A.1046(27) and A.915(22) form the backbone of IMO's requirements for maritime radio navigation systems. The first "family" with A.1046(27) depicts operational needs for a worldwide radio navigation system including systems other than GNSS as well. It does not claim any need for integrity but for coarse positioning accuracy. The second "family" represented by A.915(22) exclusively focuses on GNSS. At first sight, these requirements seem to be very challenging as there are specifications for integrity and continuity defined over a period of time of 3 hours.

Comparing both "families", it turns out that the demands from the first "family" are quite lax compared to the second "family". Basically, both sets of operational requirements derived in this section could be associated to GNSS as it is a worldwide radio navigation system. As mentioned earlier, the first "family" is not only related to GNSS but also to other systems such as LORAN-C, for example. The specifications from the second "family" are specified for a GNSS exclusively. A.915(22) must be

viewed as a 'positioning' document related to requirements for future developments of GNSS to be considered within the framework of A.1046(27).

Because continuity over an exposure period of 3 hours seems to be very demanding with respect to compliance of the system design, an exposure period of 15 minutes (according to the requirement from A.1046(27)) shall be assumed in parallel to the analysis performed in this document. In doing so, the impact on performance shall be assessed considering the two different exposure periods.

4.2 ICAO

The International Civil Aviation Organization (ICAO) is a specialized agency of the United Nations. It codifies the principles and techniques of international air navigation and fosters the planning and development of international air transport to ensure safe and orderly growth. Its headquarters are located in the Quartier International of Montreal, Quebec, Canada [ICAO 2015].

The ICAO Council adopts standards and recommends practices concerning air navigation, its infrastructure, flight inspection, prevention of unlawful interference, and facilitation of border-crossing procedures for international civil aviation. ICAO defines the protocols for air accident investigation followed by transport safety authorities in countries signatory to the Convention on International Civil Aviation (Chicago Convention).

ICAO is distinct from the International Air Transport Association (IATA), a trade association representing 240 of the world's airlines, also headquartered in Montreal, or with the Civil Air Navigation Services Organization (CANSO), an organization for Air Navigation Service Providers (ANSPs) with its headquarters at Amsterdam Airport Schiphol in the Netherlands. These are trade associations representing specific aviation interests, whereas ICAO is a body of the United Nations [ICAO 2015].

Figure 4-3 gives an overview of the classifications of approaches. It needs to be understood that depending on the severity of the operation a different set of requirements becomes applicable. In this context different phases of flight are distinguished which are described in [ICAO 2006a] and are listed in the following for convenience:

- Take-Off: "From the application of takeoff power, through rotation and to an altitude of 35 feet above runway elevation or until gear-up selection, whichever comes first"
- Departure: "From the end of the Takeoff sub-phase to the first prescribed power reduction, or until reaching 1000 feet above runway elevation or the VFR pattern (Visual Flight Rules), whichever comes first"
- Cruise: "Any level flight segment after arrival at initial cruise altitude until the start of descent to the destination."

- Descent:
  - o Instrument Flight Rules (IFR): descent from cruise to either Initial Approach Fix (IAF) or VFR pattern entry).
  - o Visual Flight Rules (VFR): descent from cruise to the VFR pattern entry or 1000 feet above the runway elevation, whichever comes first.
- Final Approach: "From the FAF (Final Approach Fix) to the beginning of the landing flare."
- Landing: "Transition from nose-low to nose-up attitude just before landing until touchdown."

Three classes of approaches and landing operation have been defined by the ICAO [RTCA 2006] and are classified as follows:

- Non-precision approaches and landing operations: an instrument approach and landing which utilizes lateral guidance but does not utilize vertical guidance.
- Approaches and landing operations with vertical guidance: an instrument approach and landing which utilizes lateral and vertical guidance but does not meet the requirements established for precision approach and landing operation.
- Precision approaches and landing operation: an instrument approach and landing using precision lateral and vertical guidance with minima as determined by the category of operation.
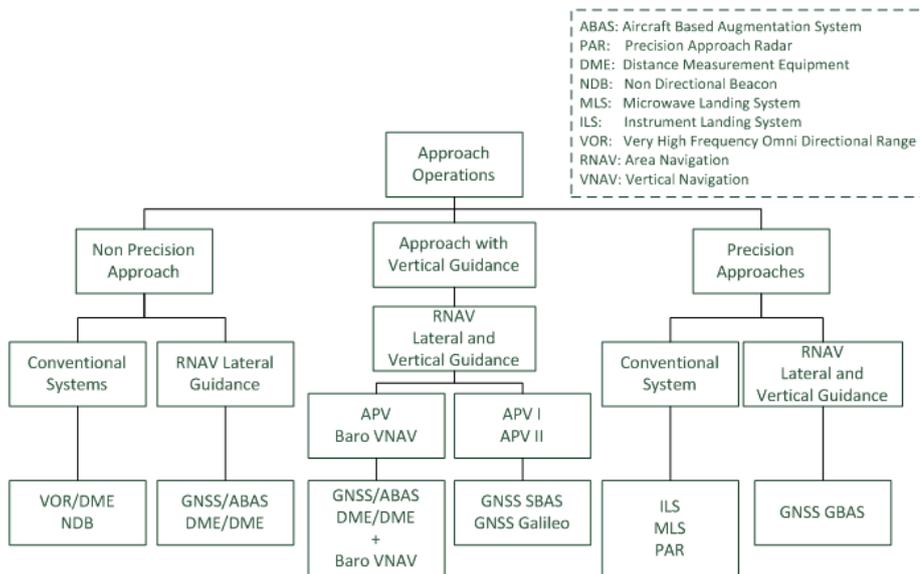
Figure 4-3: ICAO Classification of Approaches [Rotourier 2004]

Figure 4-4 indicates how the different classes of requirements are connected. For an approaching aircraft the demands in terms of accuracy, integrity and continuity get more stringent with decreas-

ing decision height (DH). The DH is specified as the critical point in the approach path which is the minimum height above the runway threshold at which a missed approach procedure must be executed if the minimum visual reference is not established [ICAO 2005]. It is noted that in Figure 4-4, the DH is given in feet whereas the VAL are given in meters.
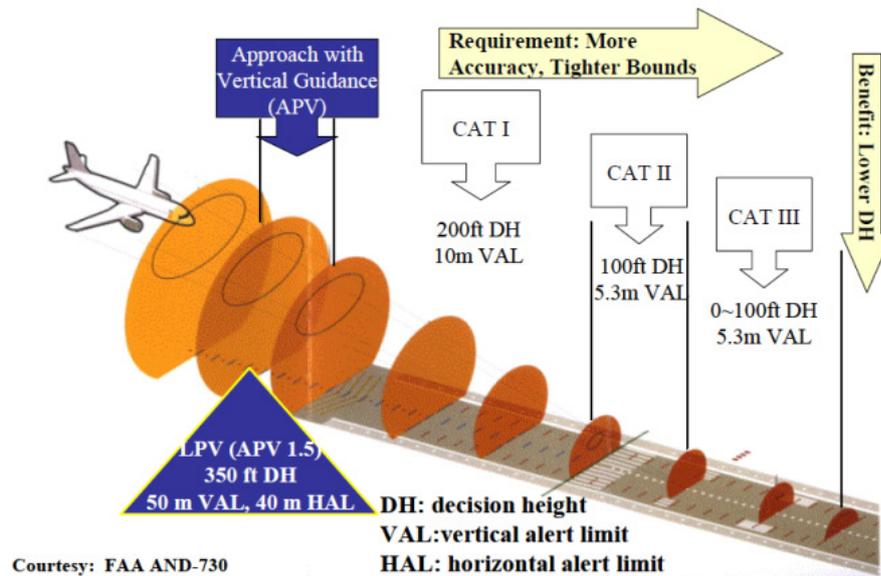
Figure 4-4: Alert Limit Evolution for Aircraft Precision Approaches [ICAO 2006b], [Pullen et al 2002]

Table 4-3 summarizes the requirements in terms of various parameters (amongst others accuracy, integrity risk) [RTCA 2006].

Table 4-3: Signal-in-space Performance Requirements

| Typical Operation	Accuracy Horizontal 95%	Accuracy Vertical 95%	Integrity risk	Time To Alert	Horizontal Alert limit	Vertical Alert limit	Continuity	Availability
En-route	3.7 km (2.0 NM)	N/A	$1 - 1 \times 10^{-7}/h$	5 min	7.4 km	N/A	$1 - 1 \times 10^{-4}/h$ to $1 - 1 \times 10^{-8}/h$	0.99 to 0.99999
En-route, Terminal	0.74 km (0.4 NM)	N/A	$1 - 1 \times 10^{-7}/h$	15 s	3.7 km	N/A	$1 - 1 \times 10^{-4}/h$ to $1 - 1 \times 10^{-8}/h$	0.99 to 0.99999
Initial approach, Intermediate approach, Non precision approach, Departure	220 m (720 ft)	N/A	$1 - 1 \times 10^{-7}/h$	10 s	556 m	N/A	$1 - 1 \times 10^{-4}/h$ to $1 - 1 \times 10^{-8}/h$	0.99 to 0.99999
Approach Operations with vertical Guidance APV I	16 m (52 ft)	20 m (66 ft)	$1 - 2 \times 10^{-7}$ per approach	10 s	40 m	50 m	$1 - 8 \times 10^{-6}/h$ in any 15 s	0.99 to 0.99999
Approach Operations with vertical Guidance APV II	16 m (52 ft)	8 m (26 ft)	$1 - 2 \times 10^{-7}$ per approach	6 s	40 m	20 m	$1 - 8 \times 10^{-6}/h$ in any 15 s	0.99 to 0.99999
Category I precision approach	16 m (52 ft)	6 m to 4m (20 ft to 13ft)	$1 - 2 \times 10^{-7}$ per approach	6 s	40 m	15.0 m to 10 m	$1 - 8 \times 10^{-6}/h$ in any 15 s	0.99 to 0.99999

More details on the requirements specified by ICAO can be found in [Pullen et al 2002], [Laurel 1999], [DeCleene 2001] and [Pullen et al 1998].

4.3   Conclusion

Different specifications by ICAO and IMO are highlighted that exist for a plethora of different GNSS based operations. However, a representative selection for the maritime user is to be found that will be used as a baseline throughout this thesis. The needs are expressed in terms of system level parameters covering accuracy and AL for both the horizontal and vertical position component. Further, the service level parameters cover the integrity and continuity aspects including TTA, integrity risk, availability and continuity risk each specified over a certain period. Basically, three different sets of requirements have been identified for which two of them are used as baseline. The first baseline is related to Ocean and Coastal operations which are assumed being applicable on a global basis (Table 4-4).

Table 4-4: System and Service Level Requirements (Ocean and Coastal)

Operation	System Level Parameters				Service Level Parameters			
	Accuracy		Alert Limit		Integrity			
	Hor. [m]	Vert. [m]	Hor. [m]	Vert. [m]	TTA [s]	Integrity Risk (per 3 hours)	Availability [%] per 30 days	Continuity [%] over 3 hours
Ocean	10	N/A	25	N/A	10	1.E-05	99.8	N/A
Coastal	10	N/A	25	N/A	10	1.E-05	99.8	N/A

The second baseline set applies for port approach and restricted waters and inland waterways operations and has thus set an additional demand for continuity (Table 4-5), in contrast to the first baseline.

Table 4-5: System and Service Level Requirements (Port Approach and restricted waters, Inland Waterways)

| Operation | System Level Parameters | | | | Service Level Parameters | | | | considered for update |
| | Accuracy | | Alert Limit | | Integrity | | | | |
	Hor. [m]	Vert. [m]	Hor. [m]	Vert. [m]	TTA [s]	Integrity Risk (per 3 hours)	Availability [%] per 30 days	Continuity [%] over 3 hours	Continuity [%] over 15 min
Port Approach and restricted waters	10	N/A	25	N/A	10	1.E-05	99.8	99.97	99.97
Inland Waterways	10	N/A	25	N/A	10	1.E-05	99.8	99.97	99.97

For the second baseline set of requirements actually two different continuity exposure periods are introduced leading to the consideration of two different sets. As investigated in this section, continuity is originally specified over a 3 hours exposure period. However, strong indications become apparent from the recent past that the exposure period for continuity might be relaxed down to 15 minutes. This trend is supported for example in [Klepsvik et al 2007] and especially in the frame of modernization of SBAS where the maritime user more and more attracts notice by current design considerations. Thus, to account and even support these current developments and to anticipate possible adaptations in the requirements, this option is considered as well.

Actually, what the latter introduced sets of requirements have in common is the fact that there are no needs for the vertical position component. This fact certainly constitutes a major aspect that actually distinguishes from the aeronautics. As will be explained later, this fact will have an impact on the design of the integrity algorithms.

Another major difference between IMO and ICAO gets obvious when comparing the exposure periods over which integrity and continuity are specified. While comparable sets of requirements for aviation based operations (for example LPV-200) are defined over an exposure period of 150 seconds for integrity and 15 seconds for continuity, the IMO defines its exposure periods consistently over 3 hours. This will have implications on the threat modelling for the maritime user: for integrity, a possible extension of the integrity exposure period does not result in a higher or different number of events to be considered and their probability is assumed to grow linearly with the specified interval. Instead, for continuity the number or type of events to be considered in 15 seconds or in a 3 hours (and 15 minutes) period is different.

The need for availability is specified as percentage of time over a period of 30 days for which the GNS system is supporting the user in its intended operation. In this thesis, the assessment of performance in terms of availability is based on simulations relying on assumptions for the GNSS (see Annex A.2). This implies fixed constellation cycle periods for example ~1 day for GPS and GLONASS and ~10 days for Galileo.

5 Integrity Algorithms

The field of GNSS integrity comprises a plethora of integrity related algorithms, each featured with different characteristics. This field constitutes a huge area of research and developments driven by the various needs for different applications. In the past, the aviation needs have been the main driver for developments of any kind to reach compliance to various sets of requirements. However, recent developments show that many more user groups demand the need of GNSS integrity. Apart from the aviation, also maritime and other various GNSS based applications have requirements with respect to integrity (and continuity). Furthermore, many new GNSS related applications evolve not only due to further developments in existing GNSS but due to the rise of new GNSS.

This chapter provides a survey of integrity algorithms while aiming at categorizing them for their specific characteristics. A selection of algorithms is presented that will be focused on in this thesis. The selected algorithms are pointed out in detail including the relevant computation steps amongst others. It concludes with a comparison of the selected algorithms and provides a justification in a dedicated discussion.

5.1 Survey of Integrity Algorithms

This section provides an adequate overview of the main groups in which the various GNSS integrity algorithms can be allocated. The algorithms can be distinguished with respect to the fact whether they work on a fully autonomous basis or not. Some integrity algorithms make use of an independent reference network which is in charge of computing respective parameters that are sent to the user. Based on this set of parameters the user is able to provide a statement of its integrity. Usually, the augmented systems in which those integrity algorithms are used provide higher performance to the user simply by the fact that the parameters represent the current environment more realistically. Fully receiver-autonomous algorithms need to make very conservative assumptions about their environment. These conservative assumptions decrease performance.

Conventional RAIM algorithms are fully autonomous whereas the Advanced RAIM algorithms are supported by an independent reference monitoring network providing the algorithms with the needed information. Also augmentation systems like SBAS for instance are based on a reference network of surveying stations. An overview is provided in Figure 5-1. It has to be noted that this distinction reflects the author's view. Due to the massive number of different algorithms, there is no mandatory need for completeness.
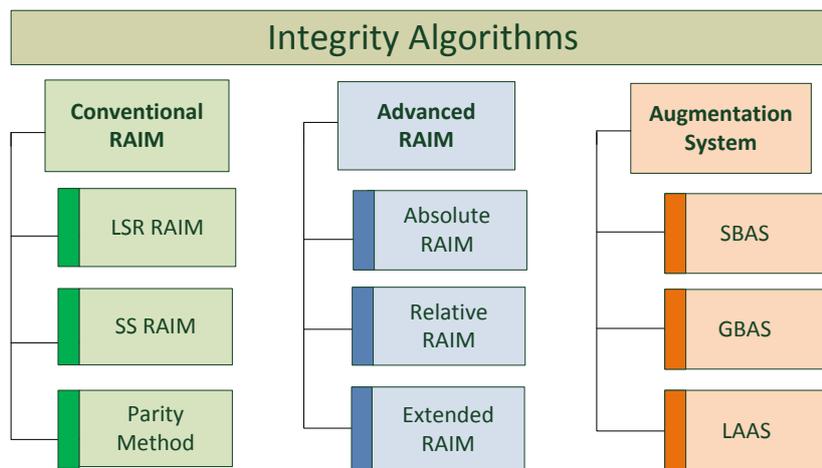
Figure 5-1: Overview of Integrity Algorithms

Conventional RAIM algorithms do have the characteristic of being fully receiver-autonomous. The principle of such RAIM is to perform a consistency check of measurements and then to decide whether to withdraw the positioning results or not. The required input parameters (such as error model parameters for example) usually are hard coded in the receivers. Due to the impossibility of updating these parameters they are usually set in a conservative manner. In this field various approaches with different characteristics exist. As outlined in Figure 5-1, the Least-Squares Residu-al (LSR) RAIM, the Parity-Space method together with the Range Comparison method are found to be equivalent [Brown 1992]. The Solution Separation (SS) RAIM approach will be outlined in this chapter. An additional method is for example the Range Consensus (RANCO) algorithm which is a RAIM with adapted failure detection mechanism allowing for multiple failure detection capabilities under certain conditions [Schroth et al 2008]. New RAIM methods were coming up using a weighting concept [Walter et al 1995]. A published method called NIORAIM likewise applies nu-merically derived weights to the range measurements [Hwang 2005]. To name and describe all of them would certainly not fit in the frame of this thesis. Therefore for the interested reader the following references are given: [Roberts et al], [Murphy et al 2008], [Miaoyan 2008], [Martineau et al 2009], [Isshiki 2008], [Hewitson 2003], [Blanch et al 2009], [Brown 1988].

Advanced RAIM is a general term that stands for a new class of integrity algorithms taking into account actual and modern developments in the field of GNSS. Advanced RAIM algorithms account for the modernization of GNSS – namely multi-constellation and multi-frequency scenarios. Multi-frequencies allow reducing the error contribution coming from the ionosphere and hence to achieve smaller protection levels. The use of more than a single constellation will have a positive impact on positioning performance. However, with an increased number of satellites, for which the user needs to deal with, the number of faults that need to be considered increases as well. The

assumption of having a single failure does not hold true anymore using more than one constellation. Nevertheless, the use of more constellations allows for detecting failures that affect a whole constellation – so-called constellation wide failures.

The GNSS Evolutionary Architecture Study (GEAS) Panel supports the development of Advanced RAIM algorithms. Three different approaches have been identified:

- Absolute RAIM [Blanch et al 2007], [Blanch et al 2010a], [Blanch et al 2010b], [Blanch et al 2010c], [Ene et al 2008]. This approach is also referred to as MHSS RAIM.
- Relative RAIM [Gratton et al 2009], [Lee 2008], [GEAS 2010]
- Extended RAIM [GEAS 2010]

These approaches are based on using an independent reference ground network which computes respective data that is sent to the user.

Augmentation Systems such as Local Area Augmentation Systems (LAAS), Ground Based Augmentation System (GBAS) and Satellite Based Augmentation System (SBAS) are featured with an external ground monitoring network. In contrast to Advanced RAIM, where a reference ground network is foreseen as well, the integrity burden is allocated much more to the network. That means that the system is in charge of detecting anomalies and to warn a user if the system must not be used for its intended operation within the specified time period. Thus, the user is provided with integrity related data (such as the information whether a satellite can be used or not) in order to state about its integrity. Although following the same principle, SBAS distinguishes mainly from GBAS/LAAS in terms of available stations of reference network spacing. SBAS covers huge continental land regions; GBAS/LAAS are limited to very specific areas (usually airports). Sometimes, a further distinction is made where it is argued that a GBAS system is limited to small areas in airports and LAAS covers wider areas. For further studies of GBAS/LAAS systems the following references are given: [Rife et al 2008], [Shively 1999], [Zaugg 2002].

Yet, other RAIM classes of integrity algorithms exist, e.g.

- **Carrier Phase based RAIM (CRAIM)**

Pseudorange-based integrity monitoring such as Receiver Autonomous Integrity Monitoring and its variations has been studied extensively over recent decades. This has primarily been driven by the safety critical nature of aviation and the important link to the integrity of the positioning and navigation solution required. However, for higher accuracy requirements, the more precise carrier phase measurements are used. The applications include positioning both in static and dynamic modes, with the latter employing Real Time Kinematic (RTK) positioning techniques. A reference to such kind of algorithms is [Milner et al 2011].

- **RAIM with INS (ERAIM)**

In principle, the benefit of integrating INS with GNSS is with respect to continuity performance due to relative support of INS in order to bridge phases where GNSS is weak. Furthermore, INS can be used to identify measurements from satellites that are consistent with others and thus enhance fault detection probabilities, especially under limited satellite availability conditions and under severe conditions such as spoofing [Wendel et al 2008]. For further details, it is pointed to [Brenner 1996], [Brenner 1990].

5.2   Selected Algorithms

A plethora of integrity algorithms have been identified in the previous section. These algorithms can be distinguished according to different aspects such as field of application, infrastructure, and performance just to name a few. Hence for every application only a specific selection of algorithms is reasonable. This limits the selection for adequate integrity algorithms significantly. Maritime applications require global coverage and high performance. For this reason, the following algorithms have been selected in the frame of this thesis:

- Least-Squares Residual RAIM (LSR RAIM)
- Novel Maritime RAIM
- Multiple Hypothesis Solution Separation (MHSS)

The **LSR RAIM** is a classical RAIM scheme in the context of GPS. In principle three RAIM schemes are to be distinguished within the group of classical RAIMs: LSR RAIM [Parkinson et al 1988a], Range Comparison method [Lee 1986] and Parity method [Brown 1992], [Brown 1997]. All three methods are snapshot schemes meaning that they assume that at any instance in time range measurements are available. These methods have been shown to be equivalent [Brown 1992], therefore the focus will only be put on the LSR RAIM. The LSR RAIM is an autonomous algorithm which means that its performance is independent of external input data coming from a ground segment on a regular time basis. Hence, it is a simple and yet powerful approach which is used solely in the aviation domain. Its flexibility and ability to adapt to another set of requirements will be evaluated in the next sections. The fact that no external ground infrastructure is required allows usage on a global basis with no restriction with respect to the user location. Due to the autonomous nature of this algorithm the integrity burden is clearly on the user side. That means that FD and/or FDE must be performed at user side. A constraint of the LSR RAIM is that it generally relies upon a single failure assumption. This constraint needs to be taken into account in a multi-constellation scenario. A promising development in the near future is the already ongoing modernization of current GNSS and the rise of new GNSS which will undoubtedly lead to higher performance in terms of availabil-

ity, reliability and accuracy. This development moves the classical RAIM algorithms such as LSR RAIM into the spotlight because higher performance can be expected.

In the frame of this thesis a **Novel Maritime RAIM** algorithm has been developed which is specifically adapted to the environment of the maritime user. It is obvious that a maritime user (i.e. a ship) moves along the sea surface and its height changes slowly. As the geoid approximates the sea surface it is possible to derive additional height information which is independent from the one based on GNSS. The idea of the novel approach is to make use of the fact that independent height information is available in order to perform FD and derive HPL. It has to be noted that this approach is combined with the LSR RAIM. The theory is described in section 5.4. The Novel Maritime RAIM approach is hence fully autonomous and has no restriction with respect to the user location. It is an experimental approach based on several assumptions which will be depicted later. However, an improvement compared to the LSR RAIM is to be expected.

Another group of integrity algorithms is known under the term of Advanced RAIM. The group of Advanced RAIM means in principle three different methods called Absolute RAIM also known as **Multiple Hypothesis Solution Separation RAIM**, Relative RAIM [GEAS 2010] and Extended RAIM [GEAS 2010]. The focus in this thesis will be on the MHSS RAIM as it is a promising method. MHSS RAIM, based on the so-called Solution Separation approach, is a very straight forward way to derive a PL. The idea is that one or more satellites are assumed to be faulty and are eliminated from the position equation subsequently. Hence, each of the obtained subset position solutions is based only on the remaining satellites respectively. The final PL interval is defined such that all subset solutions are contained within that final PL. Hence, the correct position solution will be included in the range of positions that constitute the final PL interval. The MHSS RAIM is a further development of the Solution Separation method. But it is not a fully autonomous approach and requires a GNSS independent ground infrastructure to provide the required input to the user. The external input consists of information about pseudorange errors and failure probabilities. Thus, it is obvious to choose this MHSS RAIM method in order to consider current developments in the field of GNSS integrity.

This selection of RAIM algorithms is snapshot-based – that means the integrity is computed for each time step independently. In contrast to the snapshot-based approach, filter-based approaches provide integrity and continuity results that are correlated over a certain period corresponding to the filter length. Filter-based algorithms are advantageous in environments with high short-term variations in the satellite availability, for example in urban canyons. In such periods, in which one or more satellites are obstructed for example by buildings, such a filter-based approach can support to maintain the level of performance before the decrease of satellite availability. Snapshot-based approaches would instantly experience an impact on performance if the satellite geometry significantly changes (due to loss of one or more satellites simultaneously). However, this selection is

justified by the fact that a maritime user will not observe any loss of satellites due to obstructions (besides in harbor regions).

Furthermore, this selection covers a broad band of available classes of integrity-related algorithms. This allows for identifying potential advantages and drawbacks and to gain experience of these classes, in particular in the focus of maritime operations. In summary, the aim is to cover a broad variation of potential possibilities and not just to limit to a single approach.

The following sub-sections depict detailed insights to the selected algorithms and provide an understanding of those.

5.3 Least Squares Residuals RAIM

The consistency can be checked in the position- and in the range domain. There are three concepts for Conventional RAIM methods:

- Least-Squares-Residuals (LSR) method
- Parity-Space (PS) method
- Range Comparison (RC) method

These methods have been shown to be equivalent [Brown 1992]. The LSR method obtains the test statistics by taking the root-square-sum of the range residuals, which are the differences between the predicted and the measured pseudoranges. The PS method obtains the test statistics from the so-called parity vector magnitude. The RC method is based on the comparison of predicted and actual measured pseudoranges in order to check the consistency of measurements. In the following, the LSR RAIM is described in more detail.

5.3.1 Test Statistics

In the calculation of user position and clock error, the following linearized measurement equation is solved to estimate corrections of the current estimate of user position and clock error:

$$\boldsymbol{y} = \boldsymbol{H}\boldsymbol{x} + \boldsymbol{v}$$

5.1

Hereby, $\boldsymbol{y}$ is a vector containing the differences of measured and predicted pseudoranges, where the pseudorange prediction is based on the current estimate of user position and clock error. Furthermore, $\boldsymbol{H}$ is the design matrix, $\boldsymbol{x}$ is the state vector containing the corrections for the current total state estimates and $\boldsymbol{v}$ is a vector of zero-mean residuals with Gaussian measurement noise

with covariance $E[\boldsymbol{v}\boldsymbol{v}^T] = \boldsymbol{R}$. This covariance matrix is assumed to be diagonal (i.e. correlations are neglected); its inverse is given by the weight matrix:

$$\boldsymbol{W} = \boldsymbol{R}^{-1} = \begin{pmatrix} \dfrac{1}{\sigma_1^2} & 0 & \dots \\ 0 & \ddots & \ddots \\ \vdots & \ddots & \dfrac{1}{\sigma_n^2} \end{pmatrix}$$

5.2

The σ_i are the known standard deviations of the range measurements which are composed of the different error contributions. The variance is denoted as σ_i^2 which is the distribution that over-bounds the real error distribution in the range domain. The weighted least squares solution for **x** results from minimizing $\boldsymbol{v}^T\boldsymbol{W}\boldsymbol{v}$ and is given by

$$\hat{\boldsymbol{x}} = (\boldsymbol{H}^T\boldsymbol{W}\boldsymbol{H})^{-1}\boldsymbol{H}^T\boldsymbol{W} \cdot \boldsymbol{y} = \boldsymbol{S} \cdot \boldsymbol{y}$$

5.3

The covariance of the estimation error is given by

$$E[\hat{\boldsymbol{x}}\hat{\boldsymbol{x}}^T] = E[\boldsymbol{S}\boldsymbol{y}\boldsymbol{y}^T\boldsymbol{S}^T] = \boldsymbol{S}\boldsymbol{W}^{-1}\boldsymbol{S}^T = (\boldsymbol{H}^T\boldsymbol{W}\boldsymbol{H})^{-1}\boldsymbol{H}^T\boldsymbol{W}\boldsymbol{W}^{-1}\boldsymbol{W}^T\boldsymbol{H}(\boldsymbol{H}^T\boldsymbol{W}\boldsymbol{H})^{-1,T}$$
$$= (\boldsymbol{H}^T\boldsymbol{W}\boldsymbol{H})^{-1}\boldsymbol{H}^T\boldsymbol{W}\boldsymbol{H}(\boldsymbol{H}^T\boldsymbol{W}\boldsymbol{H})^{-1,T} = (\boldsymbol{H}^T\boldsymbol{W}\boldsymbol{H})^{-1} = \boldsymbol{C}_{xx},$$

5.4

as both $(\boldsymbol{H}^T\boldsymbol{W}\boldsymbol{H})^{-1}$ and $\boldsymbol{W}$ are symmetric. From $\boldsymbol{C}_{xx}$, the so-called dilution of precision (DOP) values are derived. For more information, it is referred to [Seeber 1989].

The least squares residuals are obtained as follows:

$$\boldsymbol{v} = \boldsymbol{y} - \boldsymbol{H}\hat{\boldsymbol{x}} = \boldsymbol{y} - \boldsymbol{H}(\boldsymbol{H}^T\boldsymbol{W}\boldsymbol{H})^{-1}\boldsymbol{H}^T\boldsymbol{W}\boldsymbol{y} = (\boldsymbol{I} - \boldsymbol{H}(\boldsymbol{H}^T\boldsymbol{W}\boldsymbol{H})^{-1}\boldsymbol{H}^T\boldsymbol{W})\boldsymbol{y} = (\boldsymbol{I} - \boldsymbol{P})\boldsymbol{y}$$

5.5

In order to detect a fault, a test statistic is formed from the Weighted Sum of Squared Residuals ($WSSR$). This $WSSR$ is given by

$$WSSR = \boldsymbol{v}^T \boldsymbol{W} \boldsymbol{v} = \sum_{i=1}^{n} \frac{v_i^2}{\sigma_i^2} = \boldsymbol{y}^T (\boldsymbol{I} - \boldsymbol{P}^T) \boldsymbol{W} (\boldsymbol{I} - \boldsymbol{P}) \boldsymbol{y}$$

$$= \boldsymbol{y}^T (\boldsymbol{I} - \boldsymbol{W}^T \boldsymbol{H} (\boldsymbol{H}^T \boldsymbol{W} \boldsymbol{H})^{-1,T} \boldsymbol{H}^T) \boldsymbol{W} (\boldsymbol{I} - \boldsymbol{H} (\boldsymbol{H}^T \boldsymbol{W} \boldsymbol{H})^{-1} \boldsymbol{H}^T \boldsymbol{W}) \boldsymbol{y}$$

$$= \boldsymbol{y}^T (\boldsymbol{W} - \boldsymbol{W}^T \boldsymbol{H} (\boldsymbol{H}^T \boldsymbol{W} \boldsymbol{H})^{-1,T} \boldsymbol{H}^T \boldsymbol{W} - \boldsymbol{W} \boldsymbol{H} (\boldsymbol{H}^T \boldsymbol{W} \boldsymbol{H})^{-1} \boldsymbol{H}^T \boldsymbol{W}$$

$$+ \boldsymbol{W}^T \boldsymbol{H} (\boldsymbol{H}^T \boldsymbol{W} \boldsymbol{H})^{-1,T} \boldsymbol{H}^T \boldsymbol{W} \boldsymbol{H} (\boldsymbol{H}^T \boldsymbol{W} \boldsymbol{H})^{-1} \boldsymbol{H}^T \boldsymbol{W}) \boldsymbol{y}$$

$$= \boldsymbol{y}^T (\boldsymbol{W} - \boldsymbol{W}^T \boldsymbol{H} (\boldsymbol{H}^T \boldsymbol{W} \boldsymbol{H})^{-1,T} \boldsymbol{H}^T \boldsymbol{W} - \boldsymbol{W} \boldsymbol{H} (\boldsymbol{H}^T \boldsymbol{W} \boldsymbol{H})^{-1} \boldsymbol{H}^T \boldsymbol{W}$$

$$+ \boldsymbol{W} \boldsymbol{H} (\boldsymbol{H}^T \boldsymbol{W} \boldsymbol{H})^{-1,T} \boldsymbol{H}^T \boldsymbol{W}) \boldsymbol{y} = \boldsymbol{y}^T (\boldsymbol{W} - \boldsymbol{W}^T \boldsymbol{H} (\boldsymbol{H}^T \boldsymbol{W} \boldsymbol{H})^{-1,T} \boldsymbol{H}^T \boldsymbol{W}) \boldsymbol{y} = \boldsymbol{y}^T \boldsymbol{W} (\boldsymbol{I} - \boldsymbol{P}) \boldsymbol{y}$$

5.6

which is following a normalized χ^2- distribution with N-4 degrees of freedom (DOF), where N is the number of pseudorange measurements that are available. This can be understood in a simplified view as follows: in case that only four satellites would be available, solving for $\boldsymbol{x}$ provides a state vector that when multiplied with the measurement matrix $\boldsymbol{H}$ exactly matches $\boldsymbol{y}$, consequently the vector $\boldsymbol{v}$ has to be seen as zero and so is the $WSSR$. In case of five satellites, four satellites can be seen as to determine $\boldsymbol{x}$ and one satellite is left to contribute to the error, which explains the 1 degree of freedom for this case. A formal proof is found in [Parkinson et al 1988b]. The theory on least-squares adjustment is provided in [Niemeier 2008] and [Helmert 2006].

The test statistic formed from the $WSSR$ is given by

$$TestStatistic = \sqrt{\frac{WSSR}{N-4}} = \sqrt{\frac{\hat{\sigma}^2}{\sigma^2}}$$

5.7

In order to highlight the anaolgy to geodetic network analyses (see section 3.5), the square-root of the ratio of the a posteriori variance factor $\hat{\sigma}^2$ and the a priori variance factor σ^2 is provided. The statistical distribution of the test statistic follows a Fisher distribution $\sqrt{F_{N-4,\infty}}$ with N-4 degrees of freedom [Heck 1983], [De Heus 1982].

The derivation of the LSR RAIM is based on a weighted position, velocity and time (PVT) solution [Bauer 2003] by introducing a weighting matrix $\boldsymbol{W}$. By doing so, the test statistic $WSSR$ gets normalized with the pseudorange variance σ^2 (see equation 5.6). However, this derived approach is deemed universally valid: in case of computing a PVT solution where all pseudorange variances have the same weight (i.e. un-weighted PVT) which means that the test statistic gets not normalized by the pseudorange variance σ^2. As will be explained later, this will have an impact on the mapping function as σ^2 has not to be considered.

5.3.2 Threshold Determination

A fault is detected, if the test statistic exceeds a threshold. Usually, this threshold is chosen from the maximum tolerable probability of false alarm, P_{fa}. For a probability distribution, the quantile α defines the point below which the α fraction of the probability mass is found, i.e. where the cumulative distribution function (CDF) has reached the value α. The CDF is obtained by integration of the probability density function (PDF). Denoting the threshold corresponding to a specific P_{fa} with T, the following relationship holds:

$$P_{fa} = 1 - \alpha = 1 - \int_0^T f_{\chi^2_{WSSR}}(\chi, \sigma^2, N - 4)dx$$

5.8

where the PDF of a χ^2-distribution with N degrees of freedom is given by:

$$f_{\chi^2}(x) = \left(2^{\frac{N}{2}} I\left(\frac{N}{2}\right)\right)^{-1} \int_0^{\chi^2} (t)^{\frac{N}{2}-1} e^{-\frac{t}{2}} dt \, ; \, 0 \leq \chi^2 < \infty$$

5.9

and where $I(\quad)$ denotes the modified Bessel function of first kind [Abramowitz and Stegun 1972].

Typically, for the desired P_{fa}, a lookup table is established which contains for normalized χ^2-distributions, i.e. with variance 1, the threshold as a function of the degrees of freedom. Obviously, the pseudorange measurements do not have variance 1, but this is irrelevant because in the calculation of the $WSSR$, an implicit normalization is performed by introducing the weighting matrix $\boldsymbol{W}$. In other words, the $WSSR$ would have the same distribution, if no weighting would be performed and, $E[\boldsymbol{vv}^T] = \boldsymbol{R} = \boldsymbol{I}$ so the threshold can be determined from the normalized χ^2-distribution.

Therefore, the threshold T_{WSSR} is determined for a given P_{fa} from the normalized χ^2-distribution with N-4 degrees of freedom by solving

$$P_{fa} = 1 - \alpha = 1 - \int_0^{T_{WSSR}} f_{\chi^2_{WSSR}}(x, 1, N - 4)dx$$

5.10

the threshold for the test statistic for a given α is consequently given by

$$T = \sqrt{\frac{T_{WSSR}}{N - 4}}$$

5.11

5.3.3 Detectable Bias in Test Statistic

An important characteristic of a RAIM algorithm is the size of a bias in the test statistic domain, usually called *Pbias*, that can exist for the derived threshold T without being detected with probability P_{md}, the probability of missed detection. In the presence of a bias in one of the pseudorange measurements, the $WSSR$ is still following a χ^2-distribution with N-4 degrees of freedom, but now with a non-centrality parameter λ. In general, λ is given by

$$\lambda = \sum_i \frac{\mu_i^2}{\sigma_i^2}$$

5.12

where μ_i is the mean of the i-th Gaussian random variable which is squared and normalized contributing to the χ^2-distribution. A bias on a single pseudorange translates into non-centralized residual estimations for all satellites leading to a non-centralized test statistic (i.e. $WSSR$). However, a non-central χ^2-distribution of the sum of n squared normally distributed random variables with mean μ_i and standard deviation of unity is distributed as the sum of (n – 1) random variables with zero mean and one random variable with $\mu = \sqrt{\lambda}$. Finally, this simplifies to

$$\lambda = \frac{\mu_i^2}{\sigma_i^2}$$

5.13

where μ_i refers to a single projection into the test statistic domain replacing all the projections caused by the pseudorange bias b_i.

From this, two different possibilities arise of how Pbias is represented:

The pseudorange bias μ leading to a shift of the non-centrality parameter λ can be normalized by the pseudorange variance σ^2. This leads to the following expression for $Pbias_{norm}^2$:

$$\lambda = WSSE = \frac{\mu^2}{\sigma^2} = Pbias_{norm}^2$$

5.14

Alternatively, *Pbias* can be expressed as follows:

$$\lambda \sigma^2 = \mu^2 = Pbias^2$$

5.15

Depending on weighted or un-weighted PVT is used, the test statistic $WSSR$ gets normalized by the pseudorange variances σ^2 or not. This directly impacts the choice of the corresponding mapping function. In case of weighted PVT, the normalized $Pbias^2_{norm}$ is used, then the pseudorange variance σ^2 needs to be considered in the mapping function respectively. And analogously in case of un-weighted PVT, $Pbias^2$ is used as minimum detectable bias in test statistic domain, then the pseudorange variance σ^2 does not need to be considered in the mapping function. In the following, it will be proceeded using $Pbias^2_{norm}$. Therefore, λ is derived for a given P_{md} and threshold from a non-central χ^2-distribution f'_{χ^2}

$$P_{md} = \int\limits_0^{T_{WSSR}} f'_{\chi^2}(x, 1, N-4, \lambda)dx$$

5.16

and from λ the desired $Pbias_{norm}$ is derived. The normalized non-central χ^2-distribution f'_{χ^2} is given by

$$f'_{\chi^2}(x, \lambda) = \frac{1}{2}\left(\frac{x}{\lambda}\right)^{\frac{N}{4}-\frac{1}{2}} e^{\frac{-(x+\lambda)}{2}} I_{\frac{N}{2}-1}\left(\sqrt{\lambda x}\right)$$

5.17

where $I_v(\ )$ denotes the modified Bessel function of first kind.

As an example, Figure 5-2 highlights the relationship between a normalized χ^2-distribution and the threshold T being a function of P_{fa} corresponding to a certain quantile. Based on the requirement for P_{md}, the non-centrality parameter λ is derived and consequently the parameter $Pbias_{norm}$. The corresponding central χ^2-distribution for the fault-free case, the non-central χ^2-distribution for the faulty case, the threshold, the P_{fa} and P_{md} are illustrated in Figure 5-2.
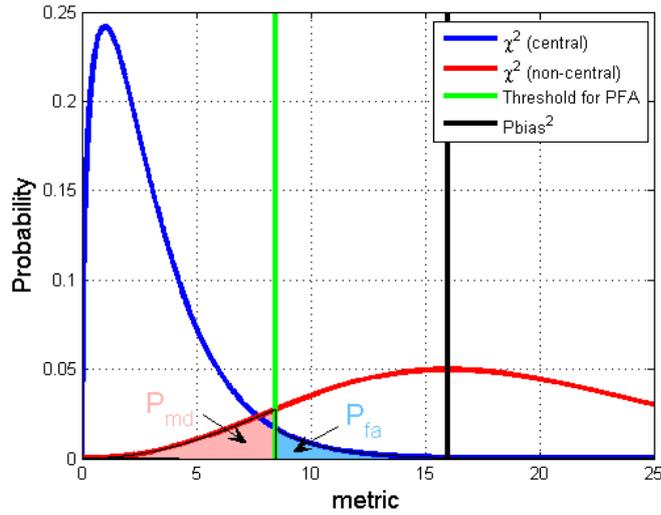
Figure 5-2: Normalized χ^2-distribution with 4 degrees of freedom

It has to be noted that in Figure 5-2 the chosen P_{fa} and P_{md} are highly unrealistic for a RAIM application; these values have been selected in order to allow for a meaningful visualisation only.

5.3.4   Mapping function derivation

A bias in a pseudorange measurement leads to a position error. Hereby, the size of the position error is depending on which satellite is faulty. Therefore, the projection of a bias into position domain has to be investigated. As shown previously, the weighted least squares position solution is calculated as follows:

$$\hat{x} = (H^T W H)^{-1} H^T W \cdot y = S \cdot y$$

5.18

Given that the i-th satellite is faulty with a bias b_i, the resulting position errors and the receiver clock error are obtained from

$$\begin{pmatrix} \delta x_E \\ \delta x_N \\ \delta x_U \\ \delta x_T \end{pmatrix} = \begin{pmatrix} S_{11} & S_{12} & \cdots & S_{1N} \\ S_{21} & S_{22} & \cdots & S_{2N} \\ S_{31} & S_{32} & \cdots & S_{3N} \\ S_{41} & S_{42} & \cdots & S_{4N} \end{pmatrix} \begin{pmatrix} 0 \\ \vdots \\ 0 \\ b_i \\ 0 \\ \vdots \\ 0 \end{pmatrix}$$

5.19

as follows

$$\delta x_E = S_{1i} \cdot b_i$$
$$\delta x_N = S_{2i} \cdot b_i$$
$$\delta x_U = S_{3i} \cdot b_i$$
$$\delta x_T = S_{4i} \cdot b_i$$

5.20

The horizontal and vertical position errors as functions of the bias b_i are now introduced as follows:

$$R_H = \sqrt{\delta x_N^2 + \delta x_E^2} = b_i \sqrt{S_{1i}^2 + S_{2i}^2}$$

$$R_V = |\delta x_D| = b_i |S_{3i}|$$

5.21

Next, the impact of the bias b_i on the test statistic has to be assessed. Starting from

$$WSSR = \boldsymbol{y'}^T \boldsymbol{W}(\boldsymbol{I} - \boldsymbol{P})\boldsymbol{y'}$$

5.22

and considering that

$$\boldsymbol{W} = \begin{pmatrix} w_{11} & 0 & \cdots \\ 0 & \ddots & \ddots \\ \vdots & \ddots & w_{nn} \end{pmatrix}, \boldsymbol{y'} = (0 \cdots \quad b_i \quad \cdots 0)^T$$

5.23

with $\boldsymbol{y'}$ as vector containing bias b_i on the pseudorange for satellite i (as opposed to $\boldsymbol{y}$ being the measurement vector).

Evaluating $WSSR$ that is now based on $\boldsymbol{y'}$ leads to

$$WSSR = \lambda = b_i^2 w_{ii}(1 - P_{ii}) = \frac{b_i^2}{\sigma_i^2}(1 - P_{ii})$$

5.24

and consequently to the test statistic value

$$teststatistic(b_i) = \sqrt{\frac{WSSR}{N - 4}} = \frac{b_i}{\sigma_i}\sqrt{\frac{1 - P_{ii}}{N - 4}}$$

5.25

Now, the slope is derived which defines the linear mapping function between the test statistic and the position error (see section 3.4):

$$SLOPE_{H,i} = \frac{R_H(b_i)}{teststatistic(b_i)} = \frac{b_i\sqrt{S_{1i}^2 + S_{2i}^2}}{\frac{b_i}{\sigma_i}\sqrt{\frac{1 - P_{ii}}{N - 4}}} = \sigma_i\sqrt{\frac{(S_{1i}^2 + S_{2i}^2)(N - 4)}{1 - P_{ii}}}$$

5.26

$$SLOPE_{V,i} = \frac{R_V(b_i)}{teststatistic(b_i)} = \frac{|S_{3i}|b_i}{\frac{b_i}{\sigma_i}\sqrt{\frac{1 - P_{ii}}{N - 4}}} = \sigma_i\frac{|S_{3i}|\sqrt{N - 4}}{\sqrt{1 - P_{ii}}}$$

5.27

5.3.5 Protection Level Calculation

The Protection Level (PL) is a limit for the position error, which is exceeded with a certain probability called integrity risk (IR). A bias in a pseudorange measurement leads to an offset in the position estimate. Hereby, the size of the position error is depending on which satellite is faulty. In principle, different approaches can be found in dedicated literature: either the threshold T or the parameter *Pbias* derived from the test statistic domain is mapped into position domain. Both approaches are deemed specific cases with each different allocation of the integrity risk probability to P_{md} and $P(P_E > PL)$. Therefore, in order to cover all cases, the summary section evaluates performance as function of possible values for P_{md} and $P(P_E > PL)$ between 0 and 1 based on a given value for IR.

5.3.5.1 Mapping of Threshold

This approach abandons the computation of *Pbias* by mapping directly the derived threshold T from the test statistic domain into the position domain. Therefore, the protection levels are obtained by adding $k(P(P_E > PL))$-times the standard deviation of the horizontal or vertical position error, respectively, leading to

$$HPL = max_i(SLOPE_{H,i}) \cdot T + k(P(P_E > PL))\sqrt{C_{xx,11} + C_{xx,22}}$$

5.28

$$VPL = max_i(SLOPE_{V,i}) \cdot T + k(P(P_E > PL))\sqrt{C_{xx,33}}$$

5.29

where the maximum slope determined among all available satellites is used to cover the worst case and $\boldsymbol{C_{xx}}$ being the covariance matrix of the estimation error. The protection level calculation is illustrated in Figure 5-3.
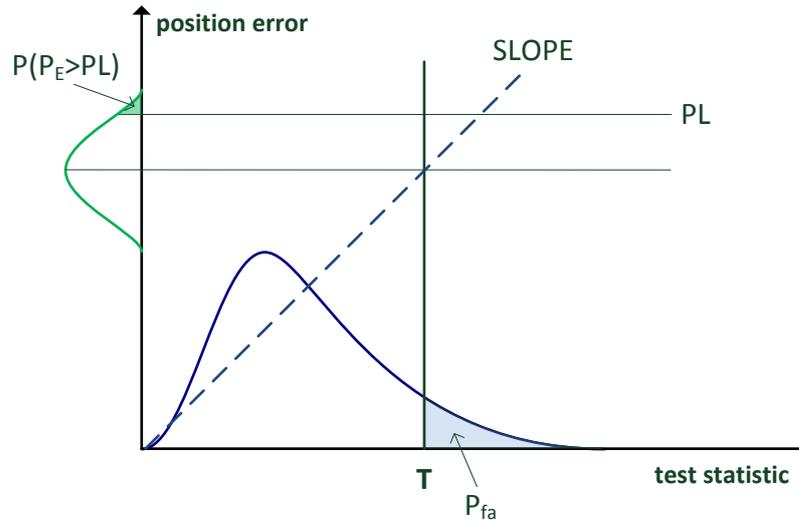
Figure 5-3: Illustration of Protection Level Calculation based on Mapping of T

This approach can be interpreted such that the threshold T equals the minimum detectable error *Pbias* in the test statistic domain. The RAIM approach introduced in [Walter et al 1995] is based on a weighted PVT solution and is basically following the approach analgouos to the threshold mapping approach. After mapping the threshold T, the vertical (resp. horizontal) position error is scaled by a factor of $k(P_{md})$. For the computation of the k-factor, it is referred to section 3.3. At first sight, this approach seems contradictory to the understanding that is derived in this thesis. However, [Walter et al 1995] gives an example for the considered probability for P_{md} accounting for the overall integrity risk which is therefore deemed to be a conservative approach.

5.3.5.2   Mapping of Pbias

Another approach consists in mapping the minimum detectable bias *Pbias* from the test statistic domain into the position domain. Choosing the probability $P(P_E > PL)$ being equal to 0.5 allows for neglecting the contribution of the position error. Thus, the following equations apply for computing the HPL and VPL respectively:

$$HPL = max_i\big(SLOPE_{H,i}\big) \cdot Pbias(T, P_{md})$$

5.30

$$VPL = max_i\big(SLOPE_{V,i}\big) \cdot Pbias(T, P_{md})$$

5.31

where the maximum slope determined among all available satellites is used to cover the worst case. This case is illustrated in Figure 5-4.
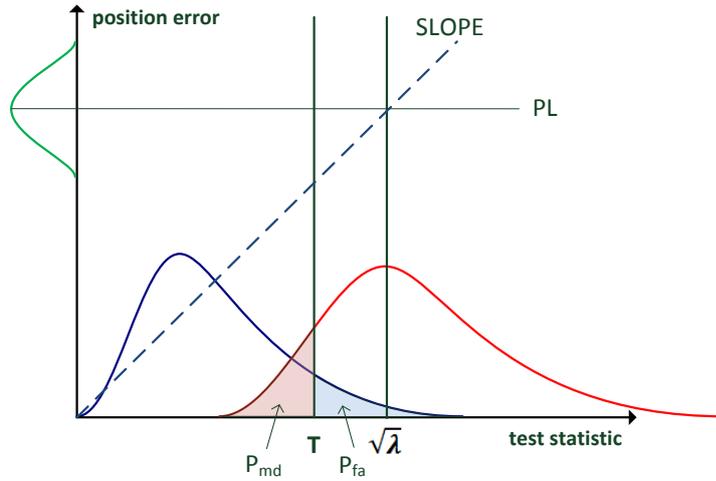
Figure 5-4: Illustration of Protection Level Calculation based on Mapping of Pbias

5.3.5.3   Summary

The previous approaches are specific ones that form a possibility to derive a protection level. However, a generalized approach allows variable allocation of the probabilities P_{md} and $P(P_E > PL)$ and thus implementing different designs of the algorithm. A generalized expression for the HPL and VPL equations is given as follows:

$$HPL = max_i\big(SLOPE_{H,i}\big) \cdot Pbias(T, P_{md}) + k\big(P(P_E > PL)\big)\sqrt{C_{xx,11} + C_{xx,22}}$$

5.32

$$VPL = max_i\big(SLOPE_{V,i}\big) \cdot Pbias(T, P_{md}) + k\big(P(P_E > PL)\big)\sqrt{C_{xx,33}}$$

5.33

These equations contain both probabilities P_{md} and $P(P_E > PL)$. The following results are based on an example with given satellite coordinates from a total number of 6 satellites and a given user position. All possible values for P_{md} and $P(P_E > PL)$ between 0 and 1 are covered.
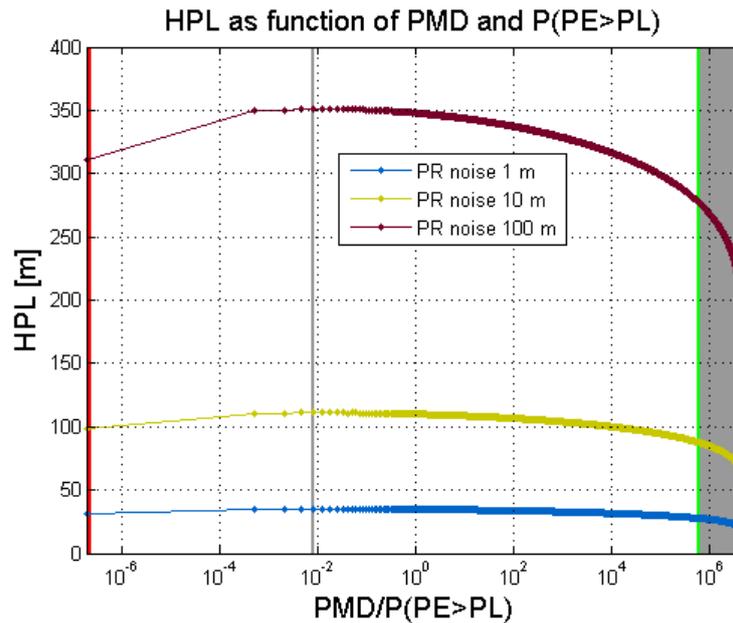
Figure 5-5: HPL as Function of PMD and P(PE>PL)

The underlying integrity risk is 2E-7. Figure 5-5 shows the sensitivity of the results for HPL as function of the ratio between P_{md} and $P(P_E > PL)$. Hereby, three different scenarios are depicted based on different assumptions regarding pseudorange variances for the satellites (1 m, 10 m, 100 m). The red line represents the approach of "mapping of *Pbias*" based on $P(P_E > PL)$=1. Green line gives the ratio corresponding to a P_{md} of 0.35 that refers to the "mapping of threshold" approach based on P_{fa} of 0.01 and a number of 6 satellites. The grey vertical line at the value of 8.08E-3 indicates the worst performance with the largest HPL which is identical for all three scenarios based on different pseudorange variances. The grey area indicates a not allowed range of values that is constrained through the P_{fa} requirement: the threshold T in the test statistic domain is the minimum allowable bias still satisfying the P_{fa} requirement. Thus, *Pbias* must not get below T. This defines a maximum value for P_{md} by setting *Pbias* equal to T. It is obvious that HPL performance depend on the allocation of the probabilities where the differences in the HPL results themselves strongly depend on the pseudorange variances. Based on this example, the conclusion can be drawn that the optimum results can be achieved when the threshold T is directly used to derive a PL in the position domain.

5.3.6   Extension to Account for Nominal Range Biases

The PL computation formulas shown in the previous section are correct under the assumption that the noise on the pseudoranges is zero-mean distributed and uncorrelated. However, the presence

of nominal pseudorange biases must not be neglected in an adequate fault-free error model. Nominal biases are assumed to exist even under nominal conditions due to antenna phase center variations, multipath or signal deformations for example.

In the following, it will be assumed that the nominal biases on the pseudoranges are bounded by b_{nom} and are assumed to be present on all satellite measurements respectively. For further details, it is referred to section 6.7. The theory is orientated to [Martineau 2008].

A common (additive) bias on all pseudoranges would directly translate into the user receiver clock estimate and no impact on the position solution will be observed. However, biases could be present with different signs and magnitudes on the pseudoranges. Thus, the approach that is followed here is such that the worst case impact on the position solution is considered by using the norm of the corresponding elements of the projection matrix S. Thus, the impact on the position can be expressed as:

$$b_E = b_{nom} \cdot \sum_{i=1}^{N} |S_{1i}| \; ; \;\; b_N = b_{nom} \cdot \sum_{i=1}^{N} |S_{2i}| \; ; \;\; b_V = b_{nom} \cdot \sum_{i=1}^{N} |S_{3i}|$$

$$5.34$$

The presence of nominal biases on the pseudorange measurements will cause the fault-free χ^2-distribution to be non-central (as opposed to the case where no nominal biases are considered). Analogously to the RAIM approach without considering nominal biases, the non-centrality parameter is derived in the following.

From equation 5.24, the minimum bias that can be detected in the test statistic domain λ (with a given P_{md}) can be expressed by the $WSSR$ and the relation between the bias on every pseudorange b_i normalized by the pseudorange variance σ_i:

$$WSSR = \lambda = \frac{b_i^2}{\sigma_i^2}(1 - P_{ii})$$

$$5.35$$

$(1 - P_{ii})$ is the projection of satellite i into detection space. It is assumed that the magnitude of the nominal biases b_{nom} is identical for all pseudoranges N. Now, assuming a nominal bias on all pseudoranges with random sign leads to the following expression:

$$b_{nom,detection\ space,no\ correlation}^2 = b_{nom}^2 \cdot \sum_{i=1}^{N}(1 - P_{ii})$$

$$5.36$$

This expression takes into account the projection of the nominal biases of each satellite into detection space but without considering correlations between the satellites ($b_{nom,detection\ space,no\ correlation}$). The nominal biases on the satellites might influence each other. Therefore, the following expression will be used to derive $b_{nom,detection\ space}$ which describes the projection of the nominal biases into detection space taking into account their correlations:

$$b_{nom,detection\ space}{}^2 = b_{nom}{}^2 \cdot \sum_{i=1}^{N} \sum_{j=1}^{N} \left(\left| 1 - P_{ij} \right| \right)$$

5.37

For the projection, the absolute values $\left(\left| 1 - P_{ij} \right| \right)$ are used to represent the worst case respectively. The fault-free non-centrality parameter $\lambda(b)$ of the χ^2-distribution is then derived as follows:

$$\lambda(b) = \frac{b_{nom,detection\ space}{}^2}{max(\sigma_i{}^2)}$$

5.38

Consequently, the threshold $T_{WSSR'}$ is derived based on a normalized non-central χ^2-distribution with non-centrality parameter $\lambda(b)$:

$$P_{fa} = 1 - \alpha = 1 - \int_{0}^{T_{WSSR}} f_{\chi^2{}_{WSSR}}(x, 1, N - 4, \lambda(b)) dx$$

5.39

This leads to the threshold T'

$$T' = \sqrt{\frac{T_{WSSR} \cdot max(\sigma_i^2)}{N - 4}}$$

5.40

For the derivation of the minimal detectable bias *Pbias'* in the test statistic domain taking into account a requirement for P_{md} and the presence of nominal biases, an additional bias on a single pseudorange is assumed (analogously to the bias-free RAIM approach). The non-centrality parameter $\lambda(bb)$ is derived by solving the following equation:

$$P_{md} = \int_{0}^{T_{WSSR}} f'_{\chi^2}(x, 1, N - 4, \lambda(bb)) dx$$

5.41

Figure 5-6 highlights the LSR RAIM approach taking into account nominal biases on the pseudo-ranges: the presence of nominal biases leads to a fault-free non-central χ^2-distribution (shown in blue). Analogously to the "bias-free" LSR RAIM, the decision threshold T is set according to the P_{fa} requirement. The faulty non-central χ^2-distribution (shown in red) is set according to a respective P_{md}.
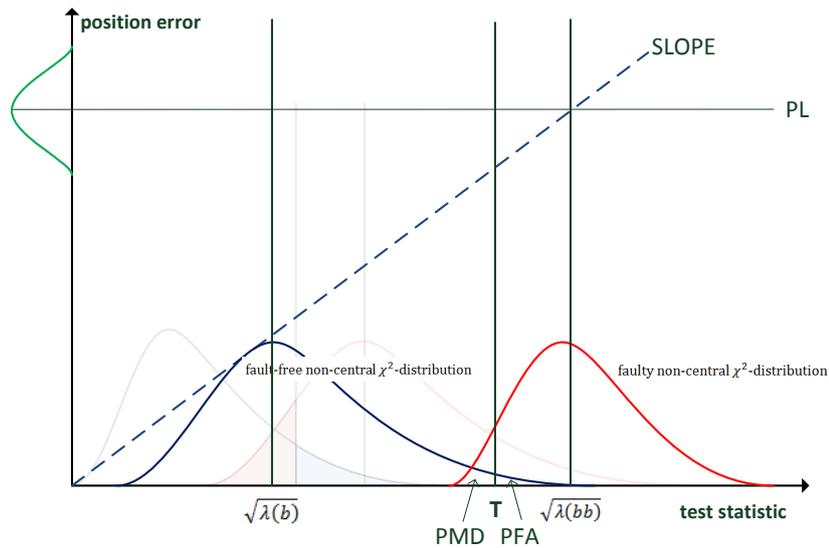

Figure 5-6: LSR RAIM (accounting for nominal biases on pseudoranges)

Figure 5-7 shows the non-centrality parameter $\sqrt{\lambda(b)}$ and $\sqrt{\lambda(bb)}$ of the χ^2-distribution as function of b_{nom}. The example is based on a snapshot geometry based on 6 satellites assuming a pseudo-range noise of 1 m. The probabilities are set to $P_{md} = 1E - 3$ and $P_{fa} = 1E - 2$. The horizontal line in blue indicates the level for the $\sqrt{\lambda(bb)}$ without assuming nominal biases and therefore corresponds to $\sqrt{\lambda}$ in the LSR RAIM approach previously described. Based on this example, in can be seen for example that assuming nominal biases on the pseudoranges in the order of 1m would lead to an increase in the $\sqrt{\lambda(bb)}$ parameter in the test statistic domain from 6 m to 8 m.
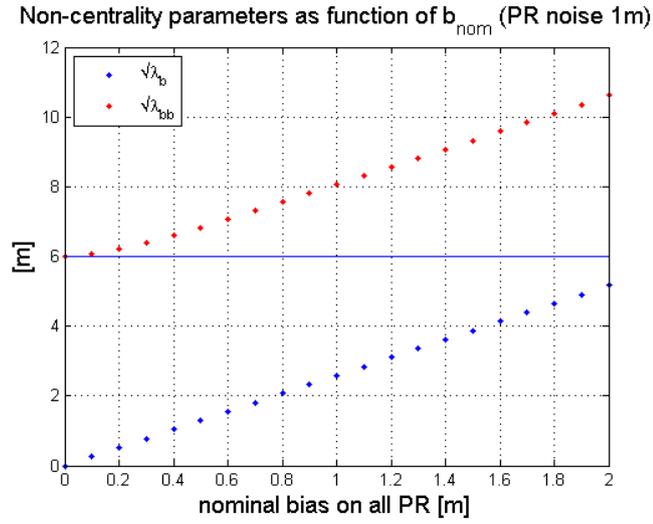
Figure 5-7: Non-centrality parameters $\lambda(b)$ and $\lambda(bb)$ as function of b_{nom}

In order to derive the PL equation, equation 5.35 is solved for the parameter b_i leading to the minimum pseudorange bias that can be detected with at least the specified P_{md} in the "bias-free" case:

$$b_i = \sigma_i \frac{\sqrt{\lambda}}{\sqrt{1 - P_{ii}}}$$

5.42

The smallest detectable bias on the pseudorange b needs to be expressed as the sum of the nominal bias b_{nom} (with different signs) and an additive unknown bias part b_i. Now, equation 5.42 is adapted in order to account for nominal biases leading to the following equation:

$$(b_i \pm b_{nom}) = \sigma_i \frac{\sqrt{\lambda(bb)}}{\sqrt{1 - P_{ii}}}$$

5.43

In the worst case, the nominal bias b_{nom} is assumed being additive to the smallest detectable bias b_i (leading to the most conservative PLs):

$$b_i = \sigma_i \frac{\sqrt{\lambda(bb)}}{\sqrt{1 - P_{ii}}} + b_{nom}$$

5.44

In the following, the derivation is done for the horizontal case. However, it can be analogously derived also for the vertical position component. The HPL is computed by deriving the impact of the minimum bias b_i in the position domain using the following equation:

$$HPL_i = \sqrt{S_{E,i}^2 + S_{N,i}^2} \cdot b_i$$

5.45

Combining equation 5.44 and 5.45 leads to

$$HPL_i = \sqrt{S_{E,i}^2 + S_{N,i}^2} \cdot \left(\sigma_i \frac{\sqrt{\lambda(bb)}}{\sqrt{1 - P_{ii}}} + b_{nom} \right)$$

5.46

Previous equation can also be written as:

$$HPL_i = \frac{\sqrt{S_{E,i}^2 + S_{N,i}^2}}{\sqrt{1 - P_{ii}}} \sqrt{\lambda(bb)} \cdot \sigma_i + \frac{\sqrt{S_{E,i}^2 + S_{N,i}^2}}{\sqrt{1 - P_{ii}}} \cdot \sqrt{1 - P_{ii}} \cdot b_{nom}$$

5.47

Further arrangements lead to the following to equations:

$$HPL_i = \sqrt{\frac{S_{E,i}^2 + S_{N,i}^2}{1 - P_{ii}}} \cdot \left(\sqrt{\lambda(bb)} \cdot \sigma_i + \sqrt{1 - P_{ii}} \cdot b_{nom} \right)$$

5.48

The first term from equation 5.48 is denoted as $SLOPE_{H,i}$ hereafter to highlight the analogies of the slope factor derived in section 5.3.4. This is used to perform the mapping between the test statistic and the horizontal position domain:

$$HPL_i = SLOPE_{H,i} \cdot \left(\sqrt{\lambda(bb)} \cdot \sigma_i + \sqrt{1 - P_{ii}} \cdot b_{nom} \right)$$

5.49

The final HPL (and VPL respectively) is derived by taking the maximum out of the HPL_i:

$$HPL = max_i \left(SLOPE_{H,i} \cdot \left(\sigma_i \sqrt{\lambda(bb)} + \sqrt{1 - P_{ii}} \cdot b_{nom} \right) \right)$$

5.50

$$VPL = max_i \left(SLOPE_{V,i} \cdot \left(\sigma_i \sqrt{\lambda(bb)} + \sqrt{1 - P_{ii}} \cdot b_{nom} \right) \right)$$

5.51

5.3.7   Conclusion

The steps of the RAIM algorithm described in the previous sections can be summarized as follows:

- The $WSSR$ is computed using all satellites in view.
- The $WSSR$ is compared to the pre-defined threshold taken from a look-up table, which was calculated for the desired P_{fa}. If the $WSSR$ does not exceed the threshold, the integrity check is completed.
- If the $WSSR$ exceeds the threshold, steps 1 (computation of test statistic) and 2 (threshold determination) are repeated for the N subsets of N-1 satellites. If for one subset the $WSSR$ does not exceed the corresponding threshold, the satellite excluded from this subset is assumed to be the faulty satellite. Excluding this satellite from the further processing in this epoch completes the integrity check. In case all subsets exceed the thresholds, the fault cannot be excluded and it has to be recognized that the position accuracy is degraded with unknown bounds.
- In case the integrity check after step 2 for all satellites or after step 3 for a subset of satellites was completed successfully, the horizontal and vertical protection levels are calculated. Unless these protection levels do not exceed the alert limits, integrity is available. Otherwise, this positioning has to be considered a continuity event.

Based on the description of the Conventional RAIM algorithms the following assumptions are valid for these algorithms:

- Errors are independently Gaussian distributed
- Fixed (conservative) assumptions for standard deviations of pseudorange measurements
- Single constellation
    - only single fault scenarios are considered
    - probability of two or more faults is negligible

5.4   Novel Maritime RAIM

This section derives a novel integrity algorithm in order to provide statistical bounds of the position error for maritime users. The fact that maritime users move exclusively along the sea surface which is approximated by the geoid brings in an opportunity of using additional height information. The idea is to use the additional height information in order to perform a cross-check with the GNSS

derived height. In reality, the geoid does not coincide with the sea surface as there are many effects such as sea surface topography, tides and waves which need to be accounted for in an adequate way. This section discusses the main effects and their correction. However, an assumption about the residual deviation between the sea surface and the geoid height needs to be made. Assuming that the height coming from the geoid, bounds the true height with a certain probability, allows for fault detection (FD) to some extent. The possibility of performing FD based on a test statistic, expressed as the difference between the height derived from the geoid and the one based on GNSS, is assessed. Furthermore, a scheme is proposed in order to derive a horizontal protection level (HPL) based on this test statistic.

This section develops the Novel RAIM approach: some background information regarding height definitions and effects that a maritime user has to deal with, is provided. During the development of this Novel RAIM approach the aspects regarding FD and HPL computation will be covered.

5.4.1 Background

This section provides an overview of the basic fundamentals which the Novel RAIM approach is based on, such as the height definitions and an overview of the effects on a GNSS sensor mounted on a ship. The aim of this overview is to provide an understanding on how ellipsoidal heights from the geoidal heights can be derived.

The geoid is the shape that the surface of the oceans would take under the influence of Earth's gravity and rotation alone, in the absence of any other influences such as winds, currents and tides. Specifically, the geoid is the equipotential surface that would coincide with the mean ocean surface of the Earth if the oceans and atmosphere were in equilibrium and at rest relative to the rotating Earth. According to Gauß, who first described it, it is the "mathematical figure of the Earth", a smooth but irregular surface that does not correspond to the actual surface of the Earth's crust, but to a surface which can only be known through extensive world-wide gravity measurements and calculations. An overview of various geo potential models is provided for example by the International Centre for Global Earth Models (ICGEM) [ICGEM 2016].
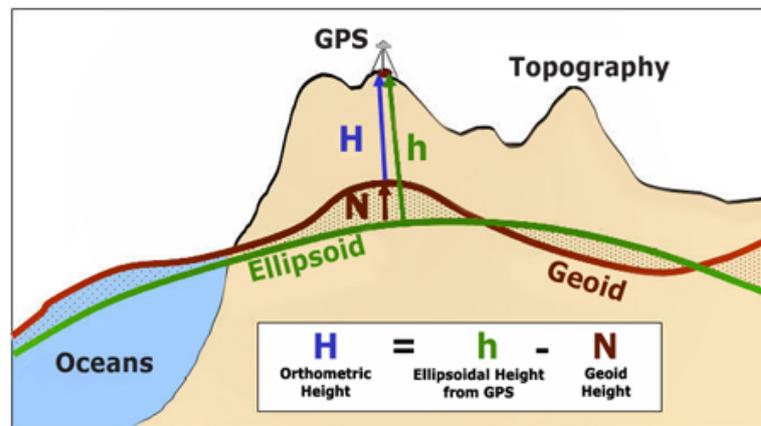
Figure 5-8: Relation between geoid and ellipsoid [Wonnacott 2010]

GNSS uses an ellipsoid as global reference surface. Hence, the geoidal height N is needed to translate ellipsoidal heights from GNSS h to orthometric heights H and vice versa (see Figure 5-8). The relationship between the geoid and the ellipsoid is illustrated in Figure 5-8. As already indicated, several effects cause the ocean surface to deviate from the geoid that need to be considered in order to derive an adequate reference height from the geoid. Some major effects are pointed out in the following together with respective mitigation actions to reduce their impact on the final height estimation:

- Hydrostatic effects,
- Hydrodynamic effects,
- Geodynamic processes.

The fact that a ship with a certain shape and weight moves on water introduces hydrostatic effects. Triming describes the rotation about the lateral axis whereas it is distinguished between static and dynamic trimming. Static trimming depends on load (and its centre of mass), shape of the ship and the lifting power of the water. Dynamic trimming is caused by hydrodynamics of the ship [Weblink 2014a]. Analogously, heeling describes the same effects but for the along direction [Weblink 2014b]. Also hydrodynamic effects need to be considered. The diving of a ship in its own wave system is called squat effect [Weblink 2014c]. The water runs with higher velocity around the ship's body. This results in a change of water pressure. Hence, the increase of velocity of the ship comes along with a drop of the ship. Geodynamic processes affect the total ocean surface and can be structured in high (waves) and low frequent (tides) effects. Waves are a function of the position and time and cause vertical movements of the ship. In order to reduce or mitigate the impact on height due to wave motions, a three axis gyro can be applied to correct position and height of the GNSS antenna for this effect. Ocean tides cause periodic variations of the sea surface due to tidal forces.

The time period between tidal high water and tidal low water is designated as low tide and analogously inverse for high tide. The magnitude of the impact can well be modelled over time and mitigated respectively.

It needs to be pointed out that the list of effects identified here is neither complete nor discussed in the very details. The scope of this thesis is not to focus on the discussion of these effects but wants to raise awareness of the presence of them. Figure 5-9 gives an overview of the relationship between the different height definitions:
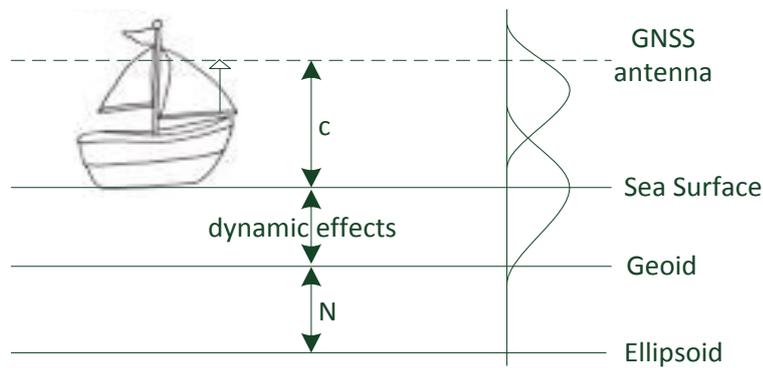

Figure 5-9: Height Definitions

A ship moving along the sea surface with a GNSS antenna on board derives h_{GNSS} based on respective pseudorange measurements. Because the GNSS antenna is mounted somewhere on the ship, a constant offset c needs to be applied to directly refer to the height of the sea surface ($h_{sea\ surface}=h_{GNSS}-c$). This offset c is assumed to be known. Variations of the offset c due to changes of weight and inclination of the ship for example are neglected.

The ellipsoid is the reference surface on which the GNSS height (h_{GNSS}) is referenced to. The ellipsoidal height ($h_{ellipsoid}$) can be converted to an orthometric height ($h_{orthometric}$) by applying the offset N which is known as the geoid undulation (see Figure 5-8). N is assumed to be known and error-free, although its accuracy at ocean level is typically below 1 m [Rapp 1993]. Under theoretical conditions, as described above, the geoid equals the sea surface; however, due to the presence of various effects, this is not exactly the case. So the set of contributions accounting for the variations between the sea surface and the geoid will be called "dynamic effects". In addition, because of the uncertainty due to the effects $h_{sea\ surface}$ is assumed to have an "inflated" error variance following Gaussianity.

In summary, a height for the sea surface ($h_{sea\ surface}$) whose error variance is accounting for the additional effects (called "dynamic effects") is derived for which it is assumed to cover the ortho-

metric height from the geoid as a reference. The idea is now to state about the presence of a fault in the GNSS measurements if the height of the sea surface differs significantly enough from its reference. The difference is compared to a threshold TH. The orthometric height is assumed to be bounded by $\sigma_{\text{sea surface}}$ with a certain probability.

5.4.2   Fault Detection

It is assumed that the error distribution of $h_{\text{sea surface}}$ contains the orthometric height with the probability P_1 (Figure 5-10). The condition that the distribution of $h_{\text{sea surface}}$ does not contain the orthometric height with a given probability might lead to an integrity issue and hence must be taken into account in the integrity risk allocation. The probability P_1 that a realisation of the orthometric height is further away from the mean than a defined maximum value (orthometric height) is defined as follows:

$$P_1 = 1 - \int_{\text{orthometric height}}^{\infty} f_{N(x, h_{sea\ surface}, \sigma_{sea\ surface})} dx$$

5.52

Based on $h_{\text{sea surface}}$ and its error variance, the detection threshold TH is set according to the requirement for P_{fa} (Figure 5-10). Taking into account the orthometric height and $h_{\text{sea surface}}$ the detection threshold is defined as follows:

$$TH = [k(P_1) + k(P_{fa})] \cdot \sigma_{\text{sea surface}}$$

5.53

The relation of the height of the sea surface ($h_{\text{sea surface}}$) and the orthometric height depends clearly on the assumed error distribution ($\sigma_{sea\ surface}$) reflecting the dynamic effects as described above. These parameters define the accuracy of the reference which defines the orthometric height and finally the threshold TH. The factor k describes the multiple of the standard deviation which is related to a certain probability (see section 3.3). The test statistic is defined as the difference between h_{GNSS} and $h_{\text{sea surface}}$:

$$TestStatistic = |h_{\text{GNSS}} - h_{\text{sea surface}}|$$

5.54

Now, a failure is assumed to be detected if the test statistic exceeds the threshold TH.

In the case of a fault detection basically two options are identified:

- The set of measurements will be excluded.

- Trying to identify faulty measurements and exclude them by composing and analysing subsets of measurements [Isshiki 2008].
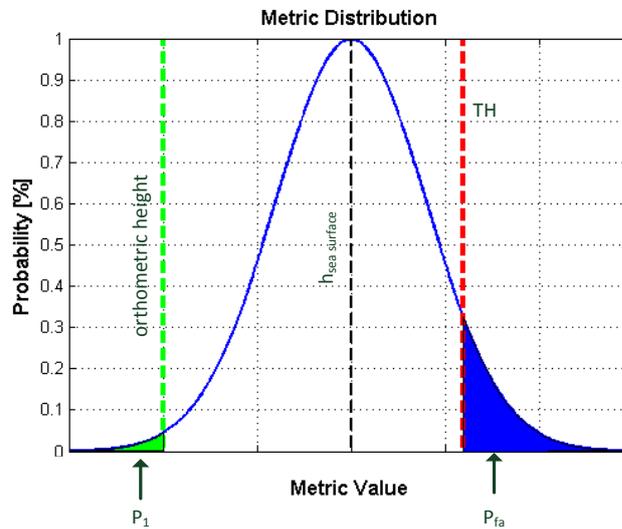

Figure 5-10: Definition of TH

For the maritime user, requirements are solely specified for the horizontal position component and hence faults impacting the vertical component are not of priority. Faulty measurements might cause the vertical position component to deviate much stronger from its expectations than it could be the case for the horizontal position component (and vice versa). That means, if a faulty measurement is detected in the vertical component, this needs to be mapped into the horizontal component to verify its impact. It is clear that ranging errors are only detected for satellites that sufficiently contribute to the vertical component. This signifies that although an error occurs, it may not be detected as the error is not sensitive enough to be detected in the vertical component. As a consequence, in a first iteration, only satellites whose contribution to the vertical component is higher than to the horizontal component can be considered for FD. For those satellites i the following condition is valid:

$$\frac{S_{3i}}{\sqrt{S_{1i}^2 + S_{2i}^2}} \geq 1$$

5.55

The preliminary conclusion on the FD capability of the Novel RAIM approach is that the prior condition is not always met. In order to validate this conclusion, an analysis based on a single constellation (GPS only) with 24 satellites has been performed to assess the percentage of time during which this condition is met. For each user location at a specific instance in time the projec-

tion matrix $\boldsymbol{S}$ reveals the factors for every satellite for projection from the pseudorange domain into the position domain. The performed analysis considers only the most critical satellite at each user location. The most critical satellite is defined as the satellite whose vertical contribution is the most sensitive for the horizontal position domain and for which the following condition is met:

$$\min_i \left(\frac{S_{3i}}{\sqrt{S_{1i}^2 + S_{2i}^2}} \right) \geq 1$$

5.56
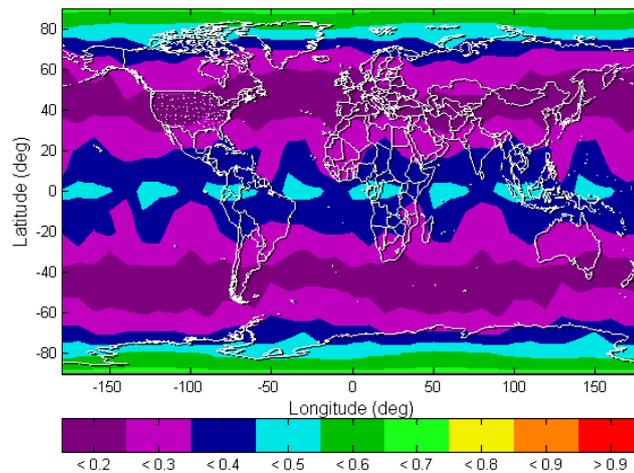
Figure 5-11: Availability of FD pre-condition based on GPS only (masking angle 20°)

Figure 5-11 shows the availability of the FD pre-condition (see equation 5.56) based on GPS only. The results reveal a clear dependency on the latitude: at the poles (latitude >70° and <-70°), the above condition is met around 70% of the time because more satellites are at lower elevations leading to higher sensisivity for the vertical position component. Under this condition, the enumerator from equation 5.56 is larger than the denominator respectively. This behaviour of course is different at lower latitudes: in the latitudes from ~20° to ~70° and from -20° to -70°, the condition from equation 5.56 is met only around 20-30% of the time. It is clear that the ability to perform FD is dependent on the user location and that in regions where the majority of the ship traffic is assumed (namely in the mid-latitudes), the user observes lower FD capabilities compared to other regions.

The simulation is based on GPS only (see Annex A.2) over a period of 1 day with a sampling rate of 60 seconds. The global grid is based on a 10° sampling for longitude and latitude. The results provided in Table 5-1 summarize the availability of the FD pre-condition as the average over all time steps and user locations.

Table 5-1: Availability of pre-condition to perform FD

Global Availability of FD Pre-condition [%]		
Masking angle	20°	10°
GPS only	31.10	5.15

The results shown in Figure 5-11 are based on GPS only with an elevation mask of 20°. The mapping factor is strongly dependent on the applied elevation mask where the optimum results could be achieved at an elevation mask of 20°. The analysis is depicted in section 8.4.

As already stated, it can be concluded that FD capability is dependent on the user location. However, averaging the results on a global basis, it can be noted that ∼31% of the time the above condition is fulfilled meaning that during this period a FD can be performed. In the absence of the required FD pre-condition, the probability of missed detection (P_{md}) would be 1 which means that in the presence of a failure no FD can be performed. As a consequence, P_{md} can be tuned according to the obtained results.

5.4.3   HPL Computation

The computation of a HPL is divided into three consecutive steps: the first step identifies the minimum error that can be detected in the vertical component (MDE) based on the requirements for P_{md} and P_{fa}. In a second step, MDE is projected into the horizontal position domain by using the satellite with the minimum contribution to the vertical component. Choosing the satellites whose sensitivity to the vertical component is the lowest ensures that the MDE mapped into the horizontal component bounds the errors in the range domain. In a last step the final HPL is computed taking into account the corresponding position error distribution.

The minimum detectable error in the vertical component $MDE_{vertical}$ is defined by the difference of the orthometric height and TH as well as taking into account the overbounding uncertainty P_1 to bound the orthometric height. The probability of missed detection P_{md} related to the error distribution for the GNSS derived height $\sigma_{h_{GNSS}}$ needs to be considered as well. Therefore, the Minimum Detectable Error in Vertical component ($MDE_{vertical}$) is given by

$$MDE_{vertical} = [k(P_1) + k(P_{fa})] \cdot \sigma_{h_{sea\ surface}} + k(P_{md}) \cdot \sigma_{h_{GNSS}}$$

5.57

The mapping factor slope$_I$ is denoted as follows:

$$\text{slope}_i = \frac{\sqrt{S_{1i}^2 + S_{2i}^2}}{|S_{3i}|}$$

5.58

It has to be noted that this is a conservative approach as always the satellite whose ratio between the contribution to the horizontal and the vertical position domain is the highest is assumed to be the faulty one and thus considered for the mapping. Mapping $\text{MDE}_{\text{vertical}}$ with the projection of the most critical satellite leads to HPL_0:

$$\text{HPL}_0 = \max(\text{slope}_i) \cdot \text{MDE}_{\text{vertical}}$$

5.59

The final HPL is computed taking into account the probability that the horizontal position error P_E with its error variance σ_{hor} exceeds the PL ($P(P_E > PL)$).

$$\text{HPL} = \text{HPL}_0 + k(P_E > PL) \cdot \sigma_{\text{hor}} + B_H$$

5.60

Here, a bias term B_H is added in order to account for the nominal biases on the pseudoranges. It is derived by mapping the respective biases into the horizontal position domain. Figure 5-12 illustrates the computation of a HPL derived from the minimum detectable error in the vertical component ($\text{MDE}_{\text{vertical}}$) which is then mapped to the horizontal position component respectively, considering the most critical satellite as described above, resulting in the worst case position error in the horizontal component.
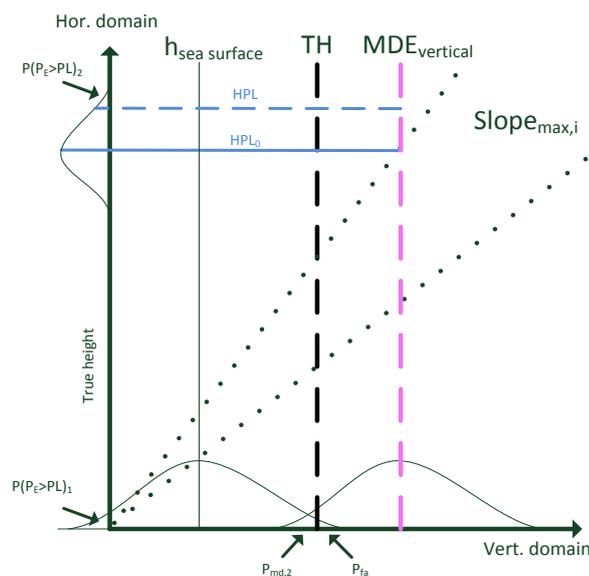

Figure 5-12: Computation of HPL

Most likely, the integrity risk is the probability that the position error exceeds the protection level. However, in general this is not equal to $P(P_E > PL)$, because different types of faults have to be considered. The total integrity risk IR_{total} is allocated to the two failure modes I ($i\epsilon1,2$). A failure mode considers one of the different fault scenarios. With each hypothesis I there will be an associated contribution to the total integrity risk, this contribution is denoted by $IR_{cond,i}$. The probability for that particular fault mode to occur is denoted by $P_{occ,I}$ and under each hypothesis there will exist a separate probability for an integrity fault to occur, denoted as $P(P_E > PL)_i$. Also a probability of missed detection $P_{md,I}$ will be associated to each failure mode i. Thus, for failure mode I, the contribution to the integrity risk IR is given by

$$IR_{total} = \sum_{i=1,2} IR_{cond,i} = \sum_{i=1,2} P_{occ,i} \cdot P_{md,i} \cdot P(P_E > PL)_i$$

5.61

For the Novel RAIM, two failure modes have been identified along which the IR_{total} needs to be allocated:

- The orthometric height is not bounded by the error variance $\sigma_{h_{sea\,surface}}$. More specifically, that means in case the following condition is met:

$$|\text{orthometric height} - h_{sea\,surface}| > k(IR_{cond,1}) \cdot \sigma_{h_{seasurface}}$$

5.62

- $MDE_{vertical}$ is not detected when exceeding its detection threshold while at the same time its projection into the horizontal component exceeds its PL ($P(P_E > PL)$).

IR_{total} is equally allocated to both failure modes. However, both failure modes are coupled to each other: the contribution from failure mode 1 is an additive part to the MDE from failure mode 2. In case of the failure mode that the orthometric height is not bounded by $\sigma_{sea\,surface}$ this causes directly the position error to exceed the PL.

It needs to be pointed out that the Novel RAIM constitutes an extension of the LSR RAIM. That means that for every instance in time two HPLs are computed, on the one hand for the LSR RAIM and on the other hand for the novel approach. This is illustrated in Figure 5-13. The final HPL is defined as the optimum of the two resulting HPLs.
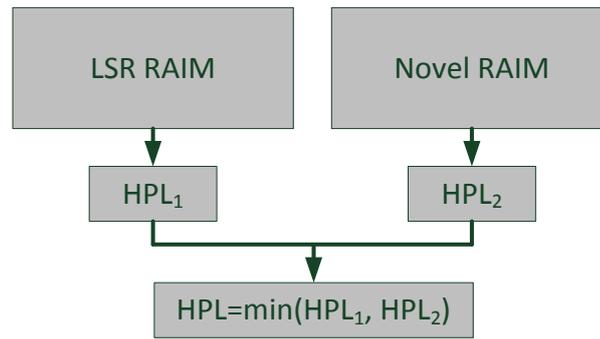
Figure 5-13: Combination of LSR RAIM and Novel RAIM

Comparing the Novel RAIM approach to the LSR RAIM it is obvious that the approaches work in different detection domains. The detection statistic of the LSR RAIM approach is the scalar product of the pseudorange residuals while the novel RAIM performs FD in the vertical component. This yields limited FD capabilities for the Novel RAIM approach as only faults contributing sufficiently to the vertical component can be detected. Both approaches are based on the single failure assumption. Under the condition of a single constellation the common assumption is a single failure to occur at a time. The probability of multiple simultaneous failures cannot be neglected in the case of two constellations and need thus to be reflected in the integrity risk allocation.

5.4.4   Conclusion

The Novel RAIM is an approach which has been developed in the frame of this thesis and is clearly adapted to the environment of a maritime user. Like the LSR RAIM, the Novel RAIM approach does not depend on external input during operation which makes it applicable at all global locations.

For the Novel RAIM the main driver for the HPL is the mapping factor from the vertical to the horizontal component. This mapping factor is dependent on the elevation mask that is used because low satellites drive the S_{3i} factor which is the factor used to map the range error into the vertical component for the satellite I respectively.

The assumptions that are underlying are summarized in the following:

- The height of the sea surface which is derived from the orthometric height and takes into account the effects that cause the sea level to deviate from the geoid is called $h_{sea\ surface}$. The standard deviation ($\sigma_{h_{sea\ surface}}$) is assumed to be 1 m in the performance analyses.
- It is assumed that the orthometric height is bounded by the error distribution of $h_{sea\ surface}$ with a certain probability which is considered in the integrity risk allocation.

This Novel RAIM approach has been already made publicly available in advance of the publication of this thesis [Mink et al 2015].

5.5 Multiple Hypothesis Solution Separation RAIM

Advanced RAIM (ARAIM) is represented through the Multiple Hypothesis Solution Separation algorithm (MHSS). MHSS is a further development of the classical Solution Separation (SS) RAIM technique. The name SS RAIM is used to identify the RAIM algorithm which combines position solutions from different subsets of the satellites in view to derive a Protection Level (PL). In the following, the basic principle of SS RAIM is highlighted together with the MHSS algorithm that is explained in more detail.

5.5.1 Solution Separation

The Solution Separation approach is a very straightforward way to derive a PL. The idea is that one or more satellites are assumed to be faulty and are eliminated from the position equation subsequently. Hence, each of the obtained subset position solutions is based only on the remaining satellites respectively. Among all the subsets of satellites, there exists at least one fault-free subset given the respective integrity risk probability. For example, assuming a single satellite being faulty, there is one position subset among all possible subsets (each subset excluding one satellite respectively) that does not contain the faulty satellite. But still, the presence of faulty satellites is accepted with a given integrity risk probability. The final PL interval is defined such that all subset solutions are within that final PL. The correct position solution will be included in the range of positions that constitutes the final PL interval. The principle is illustrated in Figure 5-14 comprising the all-in-view solution as well as the corresponding position subset solutions.
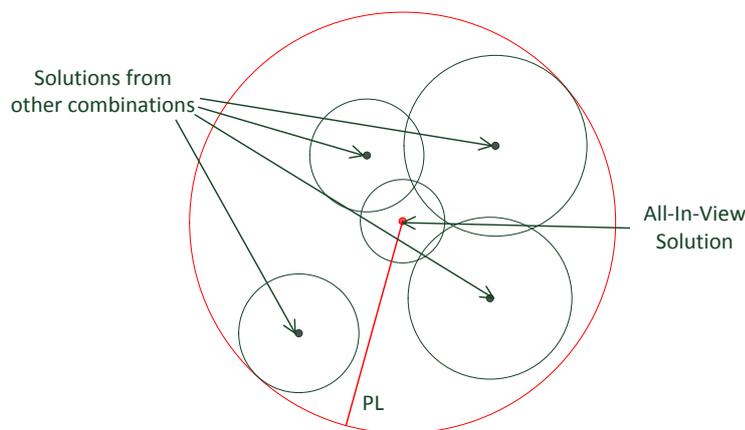

Figure 5-14: The concept of Protection Level computation for the Solution Separation approach

This approach can be used either as FDE or as a PL computation algorithm. The all-in-view position solution is computed as well as other subset solutions. The number of subsets depends on the number of satellites and the assumption on how many satellites potentially could fail. Typically, for one constellation there will be one satellite failure assumed and the respective subsets are computed. The subset solutions distribute around the all-in-view solution each with a certain distance to it. The distance can be used as test statistic. If it exceeds a certain threshold value, the satellites not contained in the respective subset solution are assumed to be faulty and hence excluded. A protection level is computed around the all-in-view solution in such a way that it takes into account all subset solutions and their failure distributions. Certain allocation of the allowable integrity risk differently to the subset solutions allows for optimizing the protection level. This approach is described in [Brown 1988].

5.5.2   Overview

MHSS constitutes a further development of the SS RAIM approach as it addresses integrity by analysing each threat case probabilistically meaning that it weighs threat cases based on their probability. This algorithm can account in principle for all threats as long as it is possible to provide a definition and a corresponding probability. In particular, multiple satellite failures can easily be accounted for. Another aspect is that is has a straight forward proof of safety as the total allowable integrity risk is allocated to each possible threat case. The original MHSS algorithm has been developed during the last years and is described in detail in [Blanch et al 2014], [Blanch et al 2007], [Blanch et al 2010b], [Blanch et al 2012].

With each hypothesis I there will be an associated contribution to the total integrity risk, this contribution is denoted with $IR_{cond,i}$. The probability for that particular threat case to occur is denoted with $P_{occ,i}$ and under each hypothesis there will exist a separate probability for an integrity fault to occur, denoted as $P(P_E > PL)_i$. Also a probability of missed detection $P_{md,i}$ will be associated to each threat case i. So for threat case I, the contribution to the integrity risk is given by

$$IR_{cond,i} = P_{occ,i} \cdot P_{md,i} \cdot P(P_E > PL)_i$$

5.63

The total integrity risk IR_{total} is the sum of the contributions of all considered threat cases i:

$$IR_{total} = \sum_{all\ i} IR_{cond,i} = \sum_{all\ i} P_{occ,i} \cdot P_{md,i} \cdot P(P_E > PL)_i$$

5.64

Based on a defined threat space with its respective threat cases I plus their according conditional integrity risks $IR_{cond,i}$, the partial PL_i can be computed based on the following simplified equation:

$$PL_i = \Delta_i + \sum_{all\ sats} |S_i \cdot b_{max,i}| + k(IR_{cond,i}) \cdot \sigma_i$$

5.65

In this equation, σ_i is the standard deviation of the position solution used for threat case i. The term $k(IR_{cond,i})$ constitutes the number of standard deviations k that correspond to $IR_{cond,i}$ in that sense that probability mass outside k standard deviations from the mean equals $IR_{cond,i}$. Also for every threat case respective biases coming from the pseudoranges can be considered with this equation. The maximum bias is mapped via the according projection matrix S into the position domain. For every position of the threat cases I, a so-called "Solution Separation Term" is computed:

$$\Delta_i = |x_i - x_0|$$

5.66

As it can be noticed, the magnitude of this term is zero for the fault-free mode since its purpose is only to align all other partial PL_i around a common position solution, which was taken here to correspond to the all-in-view solution. This is done since the user is interested in a PL which bounds its position.

Once error bounds have been computed for all partial modes, the overall PL value will be the one which protects every single threat case against integrity failures with a specific probability. The protection level that is finally communicated to the user the largest protection level of all threat case i.

$$PL = max(PL_i)$$

5.67

For each threat case, a protection level PL$_i$ has been calculated based on a given $P(P_E > PL)_i$.
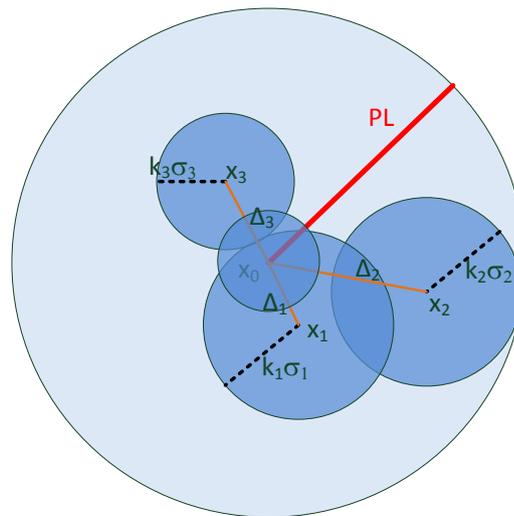
Figure 5-15: Protection Level Calculation using MHSS Algorithm

This approach is illustrated in Figure 5-15. The position communicated to the user based on the full set of satellites is denoted with x_0, the positions x_1 to x_3 are position solutions based on a subset of satellites excluding satellite 1, 2 and 3, respectively. The individual solution separation terms are shown in red denoted with Δ_1, Δ_2 and Δ_3 respectively. Around each subset solution, the $k \cdot \sigma_I$ radii are shown in blue. The final protection level is given by the largest sum of Δ_i and $k \cdot \sigma_I$ term, shown in green and denoted with PL.

The plus that the MHSS brings to the pre-existing SS RAIM algorithms is a reduction in conservatism. Instead of examining each pseudorange separately in establishing a PL, the classical LS and SS algorithms assume the worst possible combined error along all satellites and then proceed to protect the user against that hypothetical case or attempt to eliminate a faulty satellite. Particularly, the SS algorithm considers the maximum position solution separation between any of the evaluated measurement subsets and the all-in-view case as a test statistic, regardless of what the actual likelihood is for a failure to reduce the set of all satellites in view of that particular subset.

The processing steps are described in more detail in the following. The convention is aligned to [Blanch et al 2012].

5.5.3 Computation of Subset Solutions

For all satellites of one constellation, the same satellite fault probability will be assumed. The decision whether to consider single faults only or two simultaneous faults depends on the satellite fault probability itself and the threshold ($P_{TH,sat}$, $P_{TH,const}$). The probability of having more satellite failures than the considered number is deemed very low (and therefore not monitored), however

needs to be accounted for. This probability is called $P_{not_{monitored}}$ and is the sum of the not moni-tored satellite failures ($P_{not_{monitored,sat}}$) and the not monitored constellation failures ($P_{not_{monitored,const}}$) [Blanch et al 2012]:

$$P_{not\ monitored} = P_{not\ monitored,sat} + P_{not\ monitored,const}$$

5.68

The probability $P_{not\ monitored,sat}$ (respective $P_{not\ monitored,const}$) takes into account the number of satellite (respective constellation) failures whose probabilities are below a pre-defined threshold $P_{TH,sat}$ (respective $P_{TH,const}$ for the constellation failures)

$$P_{not\ monitored,sat} = \left(1 - P_{no\ fault} - \sum_{i=1}^{t_{sat}} \left(P_{i\ sat\ failures} \right) \right) < P_{TH,sat}$$

5.69

$$P_{not\ monitored,const} = \left(1 - P_{no\ fault} - \sum_{i=1}^{t_{const}} \left(P_{i\ const\ failures} \right) \right) < P_{TH,const}$$

5.70

where t is the number of satellites (resp. constellations) simultaneously assumed being faulty. The above inequalities highlight basically that the probability of not monitored threat cases – either for the satellites or constellations – must stay below a certain threshold. If that's not the case further threat cases need to be taken into account until the inequalities are fulfilled. Therefore the higher the number of considered threat cases the smaller $P_{not\ monitored}$ will get. The final IR* which needs to be allocated to the different threat cases is now given by the difference of IR as defined from the requirements and $P_{not\ monitored}$:

$$IR^* = IR - P_{not\ monitored}$$

5.71

The position solution for the all-in-view solution $\Delta \hat{x}_0$ together with all threat cases I to be consid-ered is computed. The all-in-view position solution is given by the following formula:

$$\Delta \hat{x}_0 = (G^T W G)^{-1} G^T W \Delta PR$$

5.72

The design matrix G is an N_{sat} by 3+N_{const} matrix, where N_{const} is the number of independent constellations. ΔPR is the vector of pseudorange measurements minus the expected ranging values

based on the location of the satellites and the position solution given by the previous iteration. When the position solution has converged, the last ΔPR is the vector **y** as defined above. The weighting matrix **W** for integrity is defined as:

$$\boldsymbol{W} = \boldsymbol{C}^{-1} \; ; C(k,k) = \sigma_{URA}^2 + \sigma_{tropo}^2 + \sigma_{user}^2$$

5.73

Only the diagonal elements k are considered meaning that no correlations between the satellites are taken into account. For each threat case, **W** needs to be adapted in a way that it contains only the satellites to be considered for that particular threat case i, meaning for example that if a satellite s is left out this leads to $\text{W}^{(i)}(\text{s},\text{s}) = 0$. As a consequence, the projection matrix **S** is given by

$$\boldsymbol{S}^{(i)} = \left(\boldsymbol{G}^T\boldsymbol{W}^{(i)}\boldsymbol{G}\right)^{-1}\boldsymbol{G}^T\boldsymbol{W}^{(i)}$$

5.74

Each position solution dedicated to threat case i is referenced to the all-in-view position solution. The distance between the all-in-view position and the subset i is given by:

$$\Delta\widehat{\boldsymbol{x}}^{(i)} = \widehat{\boldsymbol{x}}^{(i)} - \widehat{\boldsymbol{x}}^{(0)} = \left(\boldsymbol{S}^{(i)} - \boldsymbol{S}^{(0)}\right)\boldsymbol{y}$$

5.75

Denoting the three position components east, north and up with q = 1,2 and 3, the variances of the difference $\Delta\widehat{\text{x}}_q^{(i)}$ between the all-in-view and the fault tolerant position solutions is given by

$$\sigma_{ss,q}^{(i)^2} = \boldsymbol{e}_q^T\left(\boldsymbol{S}^{(i)} - \boldsymbol{S}^{(0)}\right)\boldsymbol{C}'\left(\boldsymbol{S}^{(i)} - \boldsymbol{S}^{(0)}\right)^T\boldsymbol{e}_q$$

5.76

in which $\boldsymbol{e}_q$ denotes a column vector whose q^{th} entry is one and all others are zero. For the accuracy of the subset solutions the following weighting matrix $\boldsymbol{W}'$ is used (now based on URE instead of URA to account for continuity):

$$\boldsymbol{W}' = \boldsymbol{C}'^{-1} \; ; C'(k,k) = \sigma_{URE}^2 + \sigma_{tropo}^2 + \sigma_{user}^2$$

5.77

The parameter $\sigma_{ss,q}^{(i)^2}$ will be used to derive the test thresholds $T_{i,q}$ for each dimension q and subset i. The test threshold considers the accuracy of the position solution and therefore the URE is used instead of the URA in the weighting matrix $\boldsymbol{W}'$ to account for continuity.

5.5.4 Fault Detection

In order to support the FD, a so-called Solution Separation Test is carried out. The purpose of this test is to identify the presence of potential faulty satellites in a constellation. Therefore, each satellite subset corresponding to a threat case respectively is tested. The test statistic is the difference of the distance between the all-in-view and the subset position solution in the dimension q. Furthermore the test threshold $T_{i,q}$ is computed which is a function of the allocated continuity budget (P_{fa}) and $\sigma_{ss,q}^2$:

$$T_{i,q} = k \left(0.25 \cdot P_{fa,hor} \Big/ nr_{fault\ modes} \right) \cdot \sigma_{ss,q}^{(i)}$$

5.78

where k gives the k-factor of the (1-p)-quantile of a zero-mean unit-variance Gaussian distribution. The total false alert probability for the horizontal position component $P_{fa,hor}$ (continuity risk) is divided by the number of dimensions (east and north), both tails of the error distribution and the number of fault modes to equally allocate the probability. It is necessary to consider the threshold $T_{i,q}$ as this represents the potential distance between the all-in-view and the solution separation solution satisfying the continuity requirement (P_{fa}) that is due to the noise of both position solutions. This test statistic is then compared to the test threshold $T_{i,q}$:

$$\left| \hat{x}_q^{(i)} - \hat{x}_q^{(0)} \right| \leq T_{i,q}$$

5.79

If this test is passed the subset is considered non-faulty, otherwise exclusion must be attempted. The budget of probability of false alarm (P_{fa}) is assumed to be equally split among all considered threat cases i. Also a hypothesis test is being performed based on the error distribution of the pseudorange residuals which follow a χ^2-distribution as depicted in section 5.3.

5.5.5 HPL Computation

In order to derive a PL for the horizontal position component, for each of the two dimensions (q=1,2), an individual PL is computed and later on combined to a final PL. In order to compute a PL the following equation needs to be solved [Blanch et al 2012]:

$$2Q\left(\frac{HPL_q - b_q^{(0)}}{\sigma_q^{(0)}}\right) + \sum_{k=1}^{N_{fault\,modes}} p_{fault,i} Q\left(\frac{HPL_q - T_{i,q} - b_q^{(i)}}{\sigma_q^{(i)}}\right)$$

$$= \frac{1}{2} IR_{hor}\left(1 - \frac{P_{sat,not\,monitored} + P_{const,not\,monitored}}{IR_{vert} + IR_{hor}}\right)$$

5.80

Q gives the k-factor of a Gaussian distribution at given mean value and sigma. The first term is related to the all-in-view solution with bias $b_q^{(0)}$ and variance $\sigma_q^{(0)}$. The second term is related to the threat cases i each with bias $b_q^{(i)}$ and variance $\sigma_q^{(i)}$ as previously derived. In addition, the test threshold $T_{i,q}$ is considered accounting for continuity. Each threat case i is weighted by its probability $p_{fault,i}$. The final HPL_q must be chosen such that it satisfies the allowable horizontal integrity risk IR_{hor} which is equally split among the two position components. As mentioned above, the sum of the residual probabilities that are not covered by the threat cases $\left(P_{sat,not\,monitored} + P_{const,not\,monitored}\right)$ are considered in the total allowable IR ($IR_{vert} + IR_{hor}$) respectively.

This equation needs to be solved by HPL_q. This can be done for example by using a half interval search as depicted in [Blanch et al 2012]. The final PL is then a combination of the PL_j:

$$HPL = \sqrt{\sum_{j=1}^{2} PL_j^2}$$

5.81

This computation is performed at every time instance. The required external input is then a dedicated set of parameters consisting of characterization of the system errors such as URE, URA, nominal biases as well as the failure probabilities P_{sat} and P_{const}.

5.6   Conclusion

One strong disadvantage of RAIM algorithms is that they do not provide reliable multiple-faults detection capabilities [Miaoyan 2008]. Faults on more than one pseudorange tend to cancel out each other. This makes it very hard to detect multiple faults occurring at the same time. Outliers need to be very significant for detecting them. In LSR RAIM (and Novel RAIM), only single faults are assumed. The mapping function from observation domain to position domain is linear and the slope of this linear function indicates how a severe bias in the metrics maps to a position error. This slope is different, depending on which satellite is faulty. In order to be conservative, the maximum slope over all satellite faults is used. The resulting protection level is the largest protection level of all the

protection levels for each individual satellite to be faulty. The LSR and Novel RAIM have been extended to account for biases in the pseudoranges.

As opposed to the latter RAIM approaches, simple Solution Separation and MHSS RAIM have the ability of accounting for multiple failures. This property makes these approaches very flexible in terms of threat modelling. Although MHSS RAIM can also act fully autonomously, its idea is to exploit an independent infrastructure in charge of providing the user with integrity related information such as current ephemeris and clock error or probability of satellite and constellation wide failures. Based on this input, the user algorithm is able to account for the various threat cases by weighting them probabilistically.

The Novel RAIM approach can be seen as an extension of the LSR RAIM in the sense that two independent RAIM approaches are combined. The expectation is an improvement in the HPL computation (e.g. smaller HPLs) compared to LSR RAIM solely. A logical next step would be the combination of the principle behind Novel RAIM with the MHSS RAIM approach. For example, the additionally derived orthometric height information could be added as an independent observation into the HPL computation. However, this step is not performed in the frame of this thesis but is clearly identified as a potential topic for future work beyond this thesis.

6   Fault-free Error Model

The performance in general of integrity algorithms is based on assumptions about the error contributions amongst which it is distinguished between two states: the condition that is assumed under nominal or fault-free conditions and as opposed to that the conditions under which the GNS system exceeds its nominal expectations (or specification). The latter will be discussed in detail in a dedicated chapter dealing with the threat space. This chapter introduces the fault-free error model that upon which the performance of a maritime GNSS user will be assessed. The fault-free error models present assumptions that are made in order to derive adequate performance results. The aim is to derive a User Equivalent Range Error (UERE) Budget that characterizes all relevant and nominal error contributions on a pseudorange measurement. A UERE budget is a statistical description of the pseudorange accuracies one can expect. Therefore, various effects which deteriorate the performance of a GNSS and specially its receivers in terms of wave propagation effects are depicted and discussed. The sum of these effects describes the error characteristic a user can expect under fault-free conditions. However, it has to be noted that based on these models integrity performance evaluations will be performed. Therefore, it is mandatory that the models are conservative.

The maritime user is assumed to be a multi-constellation and multi-frequency user. Hence, the user has signals available at two different frequencies allowing for cancelling out the ionospheric contribution. The use of the so-called iono-free measurements increases noise contribution. Besides, it is assumed that the user is using carrier phase smoothed code measurements to obtain its navigation solution. The process of smoothing code measurements is described.

Major efforts have been undertaken to define adequate fault-free error assumptions for the aviation user. The Minimum Operational Performance Standard (MOPS) [RTCA 2006] that are published by the Radio Technical Commission for Aeronautics (RTCA), acting as certification authority, presents and describes well defined error models for the aeronautical user. They are empirically derived based on long-term measurement campaigns to characterize the error contributions respectively. It is to be mentioned that the quantitative user error performance characterization is meant for RAIM simulation purposes only and may not necessarily be fully representative of the performance of the future systems. Also most of the fault-free error models are assumed being Gaussian with a known variance and a zero mean.

However, as will be discussed later in more detail, there is no guarantee that these assumptions are also valid for the maritime user. It is rather assumed that at least some error models will probably be different for the maritime user. In contrast to the aeronautical user, there is no published description of error models dedicated to the maritime user group. Thus, the lack of such maritime

related schemes drives the investigation on how the assumptions for the aeronautics are also valid for the maritime user. Nevertheless, an adequate UERE budget for a maritime user is derived that will be used for the performance analyses.

Satellite- and station specific error contributions are briefly summarized and discussed. A detailed description of the error contributions within a GNSS is not provided in this thesis – instead, only a short introduction per error contributor is given. References are provided allowing for further information respectively.

6.1   Satellite Clock and Ephemeris Error

User positioning performance using GNSS is based on the knowledge of the accurate position of the GNSS satellites. Furthermore, the satellite clock performance is crucial for the measurements of the distance between satellite and user. Therefore, the knowledge of the accuracy of the satellite position and clock is one of the key drivers for user positioning performance.

GNSS infrastructure consists amongst others of a global network of reference stations equipped with GNSS receivers collecting observation data coming from the satellites respectively. These observations are centrally collected in a dedicated processing facility that is in charge of solving for orbits, clocks and other model parameters using a priori estimates and a weighted least squares estimation by a differential correction to the receiver observations [Gonzalez 2013]. In a last step, predictions of the approximated orbit and clock are computed and uplinked to the satellites. For further information on Orbit Determination and Time Synchronization (ODTS), the following references are recommended: [Montenbruck et al 2000], [Seeber 1989].

The User Range Accuracy (URA) and the Signal in Space Accuracy (SISA) for Galileo are defined as the standard deviation of the range component of clock and ephemeris error. Ephemeris errors result from the mismatch between the actual and its predicted satellite position as broadcasted in the navigation message respectively. Clock errors are due to a satellite clock offset with respect to the system time [Gonzalez 2013]. Both URA and SISA are expressed as zero mean Gaussian distributions that overbound the User Range Error (URE) for GPS and analogously the Signal in Space Error (SISE) for Galileo. URE and SISE that do not have to be necessarily Gaussian are provided for each satellite as part of the broadcast navigation message. Under nominal conditions the values for URA (resp. SISA) as shown in Table 6-1 will be assumed [WG-C ARAIM 2015].

Table 6-1: Assumed User Range Accuracy for each GNSS

GNSS	User Range Accuracy [m]
GPS	1.0
Galileo	1.0
GLONASS	1.0

The values from Table 6-1 correspond to assumptions that have been made for aviation related integrity analyses in the frame of Advanced RAIM (ARAIM) [WG-C ARAIM 2015]. Nevertheless, these values are also assumed in this thesis for the maritime user.

6.2   Ionospheric Error

The ionosphere is a part of the atmosphere that contains a sufficient amount of free electrons in order to significantly impact the radiation of radiofrequency signals. The height of the ionosphere cannot be defined exactly due to its variable character. However, in order to provide a magnitude of order the upper bound is estimated around 1000-1500 km above the ground while the lower bound is around 50-100 km above the ground [Davies 1990].

The propagation of GNSS signals through the ionosphere is characterized through its dispersive characteristics. The ionospheric delay on GNSS signals depends on the frequency and thus impacts the signals, sent on different frequencies, differently. This can be used in order to account for the ionospheric delay. Creating the respective linear combination of pseudorange or carrier phase observations on the different frequencies allows eliminating the major part of this delay. However, inhomogeneous plasma distribution causes higher order nonlinear effects which are not removed in this linear approach. Mainly the second and third order ionospheric terms and errors due to bending of the signal remain uncorrected. They can amount to several tens of centimetres of range error at low elevation angles and during high solar activity conditions [Hoque et al 2012].

As the maritime user is assumed to be a multi-frequency user the ionospheric delay can easily be accounted for to a minimal extent. For simplification reasons, the iono error is assumed to be zero:

$$\sigma_{iono,DF} = 0$$

6.1

Although not relevant for this thesis it has to be noted that also deterministic models are available to account for the ionospheric delay. These models are used by single-frequency users. For example the Klobuchar model is commonly used by single frequency users. This is an azimuth invariant and elevation dependent model [Parkinson et al 1996]. Another model is called NeQuick Ionospheric

Model that is used by the Galileo single frequency receiver to compute ionospheric corrections [EC 2015].

6.3 Tropospheric Error

The troposphere is the lowest layer of the earth's atmosphere and is characterized by the fact that all weather phenomena develop and happen there. The upper bound of the troposphere is estimated to be approximately 8-10 km at the poles of the earth and around 17 km at the equator [Parkinson et al 1996], [Mayer 2006]. The state of the troposphere is characterized basically through three parameters:

- Temperature,
- Atmospheric pressure,
- Relative humidity.

It is obvious that these three parameters are highly temporarily and spatially uncorrelated. Additionally, it is very complex to approximate the actual conditions of the troposphere (for example using weather balloons). Different models that account for the tropospheric delay are based on assumptions about a standard atmosphere. Due to the non-dispersity of the troposphere, the tropospheric delays are approximated based on deterministic models. Two models shall be named here, together with its references for further studies: Saastamoinen [Saastamoinen 1972], [Saastamoinen 1973] and Hopfield [Hopfield 1969], [Hopfield 1978].

The RTCA proposes a model for the residual tropospheric delay [RTCA 2006]:

$$\sigma_{i,tropo} = 0.12m \cdot \frac{1.001}{\sqrt{0.002001 + (\sin(elev_i))^2}}$$

6.2

This model is elevation dependent and was adopted for GPS L1 C/A. In this thesis, it will be assumed that this model is valid for the other GNSS respectively.

6.4 Frequency Dependent Contributions

The option of using multi-frequencies gives the opportunity of cancelling out the ionospheric contribution to an extent where it can be neglected. The derivation of the iono-free measurements is explained in the following. As already mentioned the user is assumed using carrier phase smoothed code measurements. The theory of code smoothing is depicted in this section. Based on

this fundamental theory, the contributions of the ionosphere, multipath, receiver noise and antenna calibration are discussed.

6.4.1 Iono-Free Combination

Due to the dispersive characteristics of the ionosphere, the signal delay caused by the medium is frequency-dependent. The first order ionospheric effects on code PR and carrier-phase Φ measurements depend (99.9%) on the inverse of squared signal frequency f [ESA 2014]. By this, a dual-frequency receiver is able to eliminate the ionospheric effect by means of a linear combination of code or carrier measurements:

$$\Phi_{iono-free} = \frac{f_i^2 \Phi_{f_i}}{f_i^2 - f_j^2} - \frac{f_j^2 \Phi_{f_j}}{f_i^2 - f_j^2}$$

6.3

$$PR_{iono-free} = \frac{f_i^2 PR_{f_i}}{f_i^2 - f_j^2} - \frac{f_j^2 PR_{f_j}}{f_i^2 - f_j^2}$$

6.4

This combination is called ionosphere-free. For further information on the ionospheric-free combination, it is referred to [Bauer 2003]. The standard deviation of the ionospheric combinations is depicted. Two new notions will be introduced:

$$a(f_i, f_j) = \frac{f_i^2}{f_i^2 - f_j^2}$$

6.5

$$b(f_i, f_j) = \frac{f_j^2}{f_i^2 - f_j^2}$$

6.6

The standard deviation of the ionospheric-free combination for both the carrier phase and the pseudorange measurements can be simplified according to the following formula:

$$\sigma_{\Phi_{iono-free}} = \sqrt{\left(a(f_i, f_j) \cdot \sigma_{\Phi, f_i}\right)^2 + \left(b(f_i, f_j) \cdot \sigma_{\Phi, f_j}\right)^2}$$

6.7

$$\sigma_{PR_{iono-free}} = \sqrt{\left(a(f_i, f_j) \cdot \sigma_{PR, f_i}\right)^2 + \left(b(f_i, f_j) \cdot \sigma_{PR, f_j}\right)^2}$$

<div align="right">**6.8**</div>

Table 6-2 summarizes the frequency-dependent values for a and b. The computation of the code delay tracking error variance is described in [Julien 2005] and [Betz et al 2000]. Typical values for σ_{PR,f_i} and σ_{PR,f_j} are in the order of 0.86 m for Galileo E1 and 0.59 m for E5b [Eurocae 2006].

<div align="center">Table 6-2: Frequency-dependent parameters of the iono-free combination</div>

iono-free combi- nation	f_I [MHz]	f_j [MHz]	$a(f_I, f_j)$	$b(f_I, f_j)$
GPS L1-L5	$f_{L1} \approx 1575.42$	$f_{L5} \approx 1176.45$	2.261	1.261
Galileo E1-E5b	$f_{E1} \approx 1575.42$	$f_{E5b} \approx 1207.14$	2.422	1.422

6.4.2   Carrier Smoothed Code

The code measurements are noisy (in the order of 1-2m [Kaplan 2006]) while the carrier phase measurements provide a relatively noise-free but biased (ambiguous) measurement of the pseudorange. Carrier smoothing is one approach to achieve an unbiased and smooth pseudorange estimate. The iono-free measurements are then smoothed in order to reduce the influence of noise and multipath [Hegarty 1996]. Typical time smoothing constants are in the order of 100 – 200 seconds [Petovello 2006]. The respective error variance of the smoothed code pseudorange is approximated by

$$\sigma_{\tilde{p}}^2 \approx \frac{\sigma_P^2}{2T_{smooth}}$$

<div align="right">**6.9**</div>

with

$2T_{smooth}$: time smoothing constant,

σ_P^2: raw code pseudorange measurement error variance,

$\sigma_{\tilde{p}}^2$: smoothed code pseudorange measurement error variance.

6.4.3   Multipath

This section addresses the multipath error which is strongly dependent on the direct vicinity of the user receiver. Multipath effects occur if a GNSS signal that is received on its direct way from the transponder to the receiver is superposed by the same signal that is received on an indirect way. Hereby a distinction is made between the following effects:

- Reflection: the GNSS signal is reflected on smooth surfaces (Figure 6-1)

- Diffraction: the GNSS signal gets deflected on borders of objects
- Diffusion: the GNSS signal gets dispersed on rough surfaces
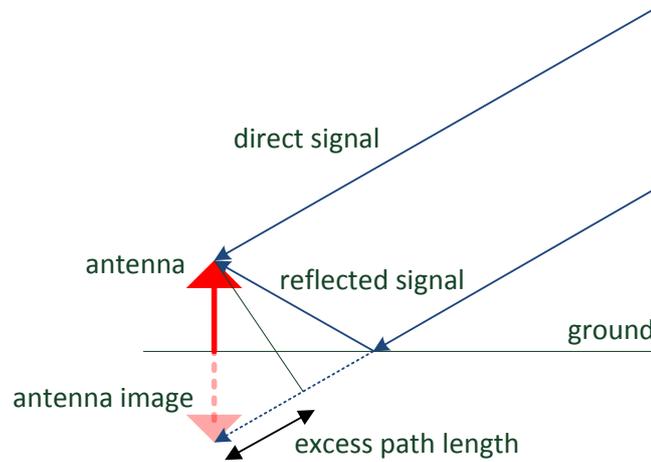
Figure 6-1: Multipath (Source: [ESA 2014])

The maximum pseudorange measurement error due to multipath interference from a reflected signal of the same amplitude as the direct signal is half of a ranging code chip (e.g., 150 meters for GPS C/A code). However, most receivers are designed to produce smaller errors [Petovello 2013]. Multipath interference also affects the carrier-phase measurements. The maximum carrier-phase tracking error due to multipath interference from a reflected signal of the same amplitude as the direct signal is a quarter of a wavelength (e.g., 4.76 centimeters for GPS L1) [Petovello 2013]. Further information on multipath can be found in [Hofmann-Wellenhof et al 2008].

The RTCA investigated a model describing the standard deviation of the multipath error for GPS L1/CA code users. This elevation dependent model has been adopted in the ICAO SARPs. The smoothed multipath error for the airborne equipment is described by [RTCA 2006]:

$$\sigma_{multipath,i} = 0.13 + 0.53 e^{\left(-\frac{elev_i[°]_\circ}{10}\right)} (m)$$

6.10

This model was validated and adopted for GPS L1 C/A thanks to efforts made by the FAA, Boing and Honeywell, mainly using data collected during normal production flight testing [Murphy et al 1999], [Liu 1998]. Their studies demonstrated that even if the distribution of airframe multipath errors depends on the specific airframe, these distributions are similar enough that a single model may adequately cover all airframes. This model will be assumed for all GNSS and their respective frequencies.

No significant correlation can be expected for the multipath error affecting measurements on different frequencies. This allows for combining the different frequencies. The smoothed multipath errors of each available signal are affected by the iono free combination:

$$\sigma_{mp\ L1-L5} = \sqrt{2.261^2\sigma_{mp,L1}^2 + 1.261^2\sigma_{mp,L5}^2}$$

6.11

$$\sigma_{mp\ E1-E5b} = \sqrt{2.422^2\sigma_{mp,E1}^2 + 1.422^2\sigma_{mp,E5b}^2}$$

6.12

It needs to be pointed out that the multipath environment for the maritime user differs significantly to the one assumed for the aviation user. Due to the surrounding water, it is very likely that the multipath contribution is increased. Extensive literature survey has not revealed a reliable error model for multipath on or near a water surface. At this stage the multipath model published in [RTCA 2006] and used for aviation related simulations will be also used in the simulations in this thesis. It will be assumed that the user takes care of his multipath environment and needs to ensure that he protects himself sufficiently. This can be achieved by paying attention to the location of the GNSS antenna. The GNSS antenna needs to be located high enough so that the reflected multipath signals will enter the antenna from below its elevation plane. Further a respective hardware (for example choke ring) needs to be used to prevent signals to enter the antenna below its elevation plane. Hence, the responsibility to prevent an excessive influence of multipath is assumed to be at user side. A respective requirement for the maritime user is to be specified. With this assumption, the proposed multipath error model can be used. A sensitivity analysis has been conducted within this thesis that aims at assessing the sensitivity of multipath to user performance. The order of magnitude of the multipath contribution that can be tolerated to still achieve the user requirement is to be assessed and compared to the multipath error model that is used.

6.4.4   Antenna Calibration

High positioning accuracy demands require attention to heterogenous (receiver-) antennas. This station specific error potentially gains importance as other error contributors such as atmosphere and orbit for example are modelled with better accuracy. The impact of incorrect modeling of the antenna pattern on positioning accuracy can be up to the level of a few centimeters [El-Hattab 2013].

The total antenna phase center correction for an individual phase measurement is composed of the influence by the (constant) phase center offset (PCO) and direction (elevation and azimuth) de-

pendent phase center variatios (PCV) [Hofmann-Wellenhof et al 2008]. The mechanic phase center corresponds to a theoretical (i.e. caused by production) required position. However, the electric phase centers of the various carriers do not coincide (frequency dependency). The PCO is a mean position of the electrical phase center that is usually provided per frequency, whereas PCV are elevation and azimuth dependent and frequency dependent as well. For further information, it is referred to [Hofmann-Wellenhof et al 2008].

Various calibration methods exist allowing for accurate modelling of the antenna pattern for example in [Zeimetz and Kuhlmann 2001] and [Bilich et al 2012]. For this reason, the error contribution due to an incorrect antenna pattern is neglected.

6.5 Receiver Noise

The receiver noise is a white-noise-like error that affects both the code and the carrier phase measurements, but with different magnitude. The accuracy of the measured pseudorange is about 1% of the wavelength ("chip") or better. This means, for instance, a noise with a maximum value of 3 m for the GPS civil C1-code (i.e. C/A-code). However, a significant reduction of the pseudorange noise can be achieved down to a level of 0.50 m when smoothing the code with the carrier phase (see section 6.4.2). The carrier phase noise is at the level of a few millimetres (about 1% of carrier phase wavelength) [ESA 2014]. Therefore, in the following the receiver noise contribution is represented by the receiver noise residual variance of carrier-phase smoothed iono-free measurements. It corresponds to the receiver noise, inter channel bias and processing error:

$$\sigma_{noise,i} = 0.15 - 0.43 \cdot \frac{(-E_i[°])}{6.9}(m)$$

6.13

6.6 UERE Budget

The UERE budget unifies all error contributors affecting pseudorange accuracy into an elevation dependent scalar. The main error contributors considered in the UERE budget are the following:

- Satellite Clock and Ephemeris Error
- Ionospheric Error
- Tropospheric Error
- Multipath
- Receiver Noise

The sum of the squared contributors finally depicts the UERE which is denoted as follows:

$$\sigma^2_{UERE} = \sigma^2_{SatClk,Ephemeris} + \sigma^2_{iono,DF} + \sigma^2_{tropo} + \sigma^2_{mp,DF} + \sigma^2_{receiver\ noise,DF}$$

6.14

In this equation the L1-L5 and E1-E5b combination respectively is denoted as dual frequency (DF). This notation will be kept from now on. Based on the latter discussion on the individual error contributions, the following UERE budget in Figure 6-2 is derived that will be used consistently for all GNSS:
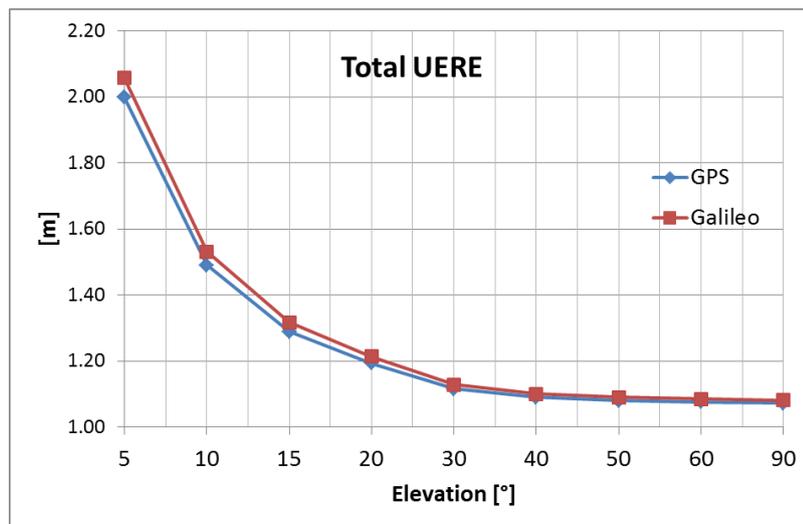

Figure 6-2: Fault-Free UERE Budgets (DF)

It is obvious that the UERE budget for GPS and Galileo shows differences due to the use of different frequencies. However, the use of the worst case values for all GNSS represents an adequate conservative case and accounts also for the uncertainties in the maritime dedicated error models. The quantitative UERE characterization is meant for performance simulation purposes only and may not necessarily be fully representative of the performance of the future system.

6.7 Nominal Biases

A main characteristic of the latter models is that the error contributions to the UERE budget follow a Gaussian and zero mean behavior. This presumption does not necessarily mirror the realistic environmental conditions. Nominal biases are assumed to exist even under nominal conditions. The following list summarizes some effects that could potentially cause a mean offset in the error distribution.

- Antenna phase centre:

  Look-angle dependent biases in the code phase and carrier phases are present on GNSS antennas. These biases are quasi-periodic as the satellite position and its attitude relative to a "fixed" user repeats according to the repetition period of the GNSS respectively. This systematic bias is assumed to be covered within the maximum nominal bias. These biases depend on the look angle of the signal with respect to the antenna and may be different for each frequency and for code and carrier.

- Multipath:

  Depending on the user environment, multipath can severely impact the user performance. However, it is accepted, that the influence of multipath is covered within the bias assumption.

- Signal deformation:

  The amount of nominal signal deformation that is situated within the equipment design specs will cause small errors at the user level. Additionally, faulted signal distortions may occur in any signals. These faulted distortions also lead to biases that depend upon the correlator spacing and bandwidth of the observing receivers. Signal deformation may occur independently on any of the code measurements. It does not affect all receivers identically [WG-C ARAIM 2012].

- Inter-Frequency Bias (IFB):

  The IFB is defined as the difference of the delay with respect to the signal paths and the signal modulation type. The IFB can change due to a failure on the satellite itself. IFBs are effectively timing differences between one frequency and another. Unlike signal deformation, all receivers are affected identically and it only comes into play when comparing one frequency (or frequency combination) to another [WG-C ARAIM 2012].

The following adoption about the biases for integrity and continuity respectively will be assumed [WG-C ARAIM 2015]:

$$b_{integrity} = 0.75 \, m$$

6.15

$$b_{continuity} = 0 \, m$$

6.16

The values are typically used in current literature for integrity (resp. accuracy and continuity) simulations [WG-C ARAIM 2012], [WG-C ARAIM 2015]. The quantitative characterization of the nominal bias is meant for performance simulation purposes only and may not necessarily be fully representative of the performance of the future system.

7   Threat Space

A threat space is a consistent and complete set of assumptions about the environment in which an integrity algorithm is applied. A threat space is usually represented by a tree in which the total allowable integrity (resp. continuity) risk probability is split among the various threat cases. In this context, a threat is defined similarly to the definition (of misleading information) given in the SARPS MOPS [RTCA 2006], namely: a threat is defined to be "any data that is output to other equipment or displayed to the user that has an error larger than the alert limit (AL) or current protection level (PL), without any indication of the error within the time-to-alert (TTA) for the applicable operation. It is assumed that the kind of operation and its set of applicable requirements are known to the user. Therefore, a threat is defined relative to the AL."

In general, different requirements result in different threat spaces to adapt the allocation of the total risks. For integrity, a possible extension of the integrity exposure period does not result in a higher or different number of events to be considered and their probability is assumed to grow linearly with the specified interval. Instead, for continuity the number or type of events to be considered in 15 seconds or in a 3 hours (and 15 minutes) period is different. What needs to be considered is that some faults have a small contribution in the avionic allocation tree due to the small probability of occurrence during a time span of 15 seconds. These faults will have a higher contribution in the maritime allocation tree due to a higher probability of occurrence during a time span of 3 hours.

Due to the latter reasoning, potential new contributions to continuity allocation trees are investigated that are relevant for maritime operations compared to aviation assumptions. Therefore, the aim is to revise the threat space for a maritime user taking into account in particular the integrity and continuity requirement which is specified over a period of 3 hours (resp. 15 minutes). A discussion is provided on this issue resulting in the need of adapting the threat space for maritime users.

This chapter is structured in a way that different relevant points are highlighted and discussed with respect to the threat space for the aviation and maritime user. First, the integrity triad – reflecting the relationship between simulation, data analysis and theoretical analysis – is highlighted. A brief summary of the feared events follows, leading to the derivation and justification of the satellite failure probabilities. Analyses of the impact of the continuity requirement for maritime users are carried out. The aim of this chapter is to derive both an integrity and continuity tree that reflects the conditions of a maritime user.

7.1   Integrity Triad

The validation of integrity/continuity requirements in the order of 1E-5 requires an active proof [Walter et al 2005]. In order to verify such numbers, data sets over several decades would be required which are simply currently not available. However, a large amount of data is essential for verifying performance (under many different conditions). Besides the option of evaluating real data sets, validation of performance can be done by analysis and simulation. To somehow overcome this latter constraint, the three approaches – analysis, simulation and data – must support each other. In order to validate probabilities at such magnitudes of order none of the latter is sufficient by itself.

The integrity triad describes the relationship between data, theory and simulation (see Figure 7-1). Data cannot prove 1E-5, simulation only tests specific scenarios and theory may miss "real-world" effects. Hence, data support theory, theory extends data and simulation validates implementation [Walter et al 2005]. In order to prove 1E-5 all three methods must be accounted together. Simulation is basically the first step in performance validation also allowing shaping some system aspects (for example risk allocations).
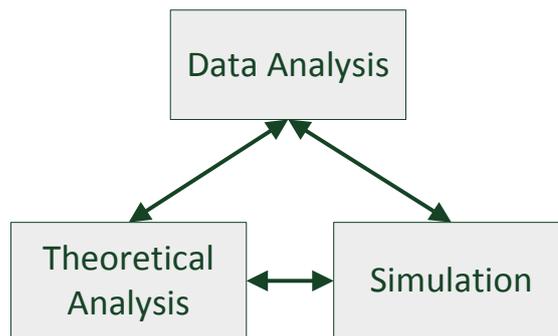
Figure 7-1: Integrity Triad

The demand for the proof of a GNSS being safe drives the need for a threat space model that is required to judge system performance and safety. A general statement about system performance is required because the integrity requirement of 1E-5 applies to each and every operation. A threat space model is essential for validating the implementation of the system.

The aim of a threat space model is to limit the extent of threats by providing a description and an according occurrence probability figure. Therefore, it is needed to cover all threats – also referred to as feared events – that induce an integrity or continuity event. The sum of all threats must meet the total risk requirement respectively. The allocation of the total available risk budget is usually done via an integrity/continuity tree where the different threats are shown together with their

probabilities. Usually, three branches are distinguished: fault-free, single failures (dominating branch) and multiple simultaneous failures.

7.2   Feared Events

The system behavior in front of an external system such as Advanced RAIM is characterized by the nominal behavior of feared events (FE) which a GNSS user has to be protected against. As such, the definition of FE is a design driver for an Advanced RAIM system. Those FE are defined through a probability of occurrence of the FE and a FE magnitude. In the context of Advanced RAIM various FE for the aviation have been identified [Blanch et al 2013]. These FE are categorized using the following nomenclature:

- Nominal Errors correspond to the errors when all operational capabilities are nominal (ground segment, satellites, and user) including
    - o   Nominal Clock and Ephemeris Errors
    - o   Nominal Signal Deformation Errors
    - o   Antenna Biases
    - o   Tropospheric Errors
    - o   Code and Multipath
- Narrow failure errors corresponds to errors induced by ground segment or satellite faults which affect the navigation signals or/and the navigation message of just one satellite including
    - o   Clock and Ephemeris Estimation Errors
    - o   Signal Deformations
    - o   Code-Carrier Incoherency
- Wide failure errors correspond to errors induced by ground segment or satellite faults which affect simultaneously the navigation signals or/and the navigation messages of multiple satellites including
    - o   Inadequate Manned Operations
    - o   Ground Segment Inherent Failures
    - o   Externally Induced Faults

For a more detailed description of the FE, it is pointed to [Blanch et al 2013]. A complete threat space model should include the nature of the FE, its magnitude, duration and likelihood [Blanch et al 2013]. The errors due to ionosphere are not mentioned because it is assumed that the maritime user makes use of dual-frequency GNSS measurements and that the first order ionospheric delay cancels out (second order effects have been shown to be well below a meter in the worst case [Datta-Barua et al 2006]).

It can be concluded at this stage that the FE applicable in the aviation domain can be transferred to the maritime domain without a change of the definitions. However, the continuity requirement over the period of 3 hours (resp. 15 minutes) leads mandatorily to the consideration of additional threats which will be assessed in the following sections.

7.3   Satellite Failure Probabilities

Integrity and continuity performance analyses are based upon probabilities of satellite failures to occur. The number of satellite failures to be considered for a specific user location and over a specified time interval is a function of the number of available satellites together with their specific failure probabilities. The more satellites are available and used for positioning, the higher the probability of single or simultaneous satellite failures to occur.

In the case of GPS, the probability of a major service failure is defined as "the probability of a major service failure to be the probability that the signal-in-space (SIS) instantaneous URE exceeds the SIS URE not-to-exceed (NTE) tolerance (i.e. misleading signal-in-space information (MSI)) without a timely alert being issued (i.e. unalerted MSI (UMSI)). Alerts generically include both alarms and warnings" [GPS Navstar 2008]. Also, it is stated that the standard is based on 3 service failures per year, lasting no more than 6 hours each (across GPS constellation) for a maximum constellation of 24 satellites. A service failure is a SV failure leading to a standard positioning service (SPS) user range error > 4.42 URA without timely Operational Control System (OCS) warning or alert. This leads to the following assumption for the onset probability of a satellite to fail ($P_{sat,onset}$):

$$P_{sat,onset_{SV,h}} = \frac{3 events}{(365 \cdot 24)h \cdot 24 SV} \approx 8.56 \cdot 10^{-5} \frac{events}{h \cdot SV}$$

7.1

The occurrence of a major service failure is interpreted as 3 events with each 6 hours period which leads to a total period of 18 hours. This value is linearly scaled and given per hour. Because such values are exclusively available for GPS only, the same probability will be assumed within this thesis for Galileo and Glonass. The author is confident that the full operational Galileo system and Glonass will achieve similar performance.

The scaled probabilities of satellite failure with respect to the 15 minutes and the 3 hours requirement are:

$$P_{sat_{SV,15min}} = \frac{3 events \cdot 6h}{365 \cdot 4 \cdot 24h \cdot 24 SV} \approx 2.14 \cdot 10^{-5} \frac{events}{SV}$$

7.2

$$P_{sat_{SV,3h}} = \frac{3 events \cdot 3 \cdot 6h}{365 \cdot 24h \cdot 24 SV} \approx 2.57 \cdot 10^{-4} \frac{events}{SV}$$

7.3

Based on the satellite failure probability P_{sat}, the probability of one or more simultaneous satellite failures $p_{failure}$ as function of a given amount of satellites in view of the user can be derived. It can be calculated with the help of the following formula assuming equal failure probabilities for the satellites involved:

$$p_{failure} = \sum_{j=0}^{m} \binom{n}{j} (P_{sat})^j (1 - P_{sat})^{n-j}$$

7.4

with the binomial coefficient $\binom{n}{j} = \frac{n!}{j! \cdot (n-j)!}$,

and m being the number of satellites or signals that fail independently and n being the number of satellites in view.

From the satellite visibility analysis, the global average number of visible satellites is 8 per constellation. Based on that situation, it is assumed that 8 satellites correspond to a single-, 16 satellites to a dual- and 24 satellites to a triple constellation. The following two figures (Figure 7-2 and Figure 7-3) show the probability of k satellite failures as function of the number of satellites. This assessment is based on the assumptions derived above about satellite failure probability and based on an exposure period over 3 hours and 15 minutes respectively. The decision threshold (dashed lines) above which a probability is deemed being relevant for consideration is assumed to be 10% of the overall integrity (resp. continuity) risk requirement (continuous lines).
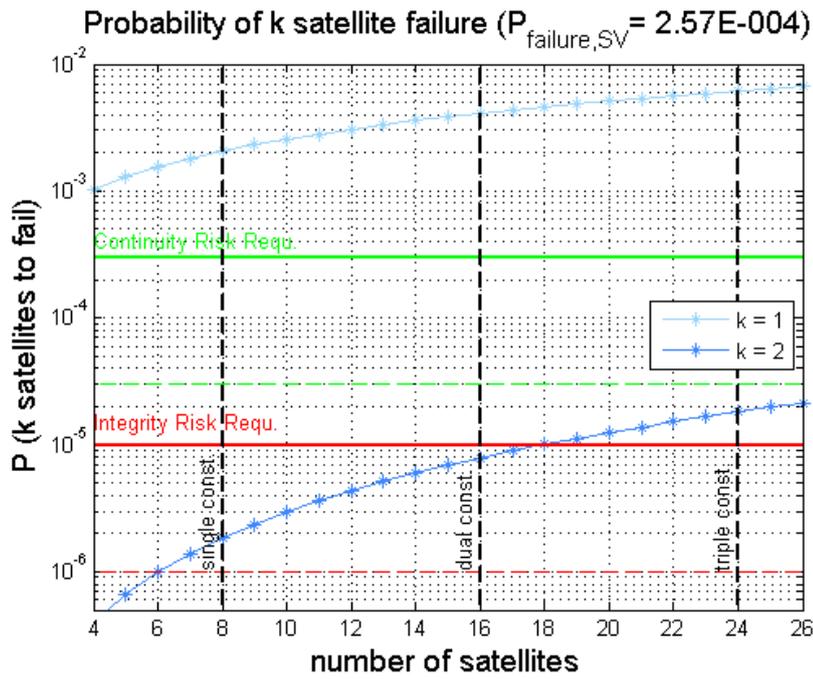
Figure 7-2: Probability of k satellite failures (exposure period over 3 hours)
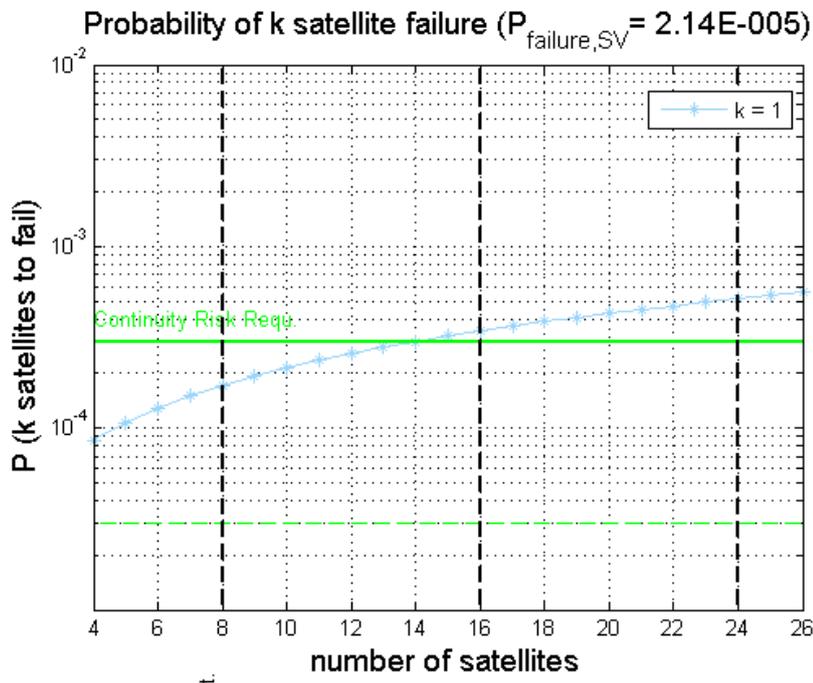
Figure 7-3: Probability of k satellite failures (exposure period over 15 minutes)

The assessment based on the 15 minutes exposure period is done against the continuity require-ment only as the exposure period assumed for integrity is consistently at 3 hours. For the three cases (3 hours integrity/continuity- and 15 minutes continuity exposure period) the number of satellites failures k is plotted in different colours for which they have to be taken into account in case of an excess of the threshold. Table 7-1 summarizes the number of satellite failures to be considered given the satellite configuration and exposure period. It is shown for integrity, up to 2 satellite failures are to be considered. For continuity, basically a single satellite failure needs to be considered regardless of the exposure period being 3 hours or 15 minutes.

Table 7-1: Number of simultaneous satellite failures

	Integrity Risk over 3 h	Continuity Risk over 3 h	Continuity Risk over 15 min
Single Constellation (8 satellites)	2	1	1
Dual Constellation (16 satellites)	2	1	1
Triple Constellation (24 satellites)	2	1	1

In that case, satellite failures (as well as outages) have to be accounted when assessing the continui-ty requirement for the considered exposure periods. This perception is in contrast to the assump-tions used for the aviation where a continuity exposure period over 15 minutes is specified. For example, a satellite fault with an onset probability of 1E-5 per hour will have an impact on a conti-nuity requirement of 1E-6 per 15 seconds. In the case of vertical guidance, if the satellite failure probabilities are below 1E-5 per hour, then satellite failures do not need to be taken into account (their impact on continuity is negligible). This is why aeronautics does not account for faults when assessing the continuity requirement [Blanch et al 2013].

In the framework of this thesis, the prior satellite failure probability is intentionally assumed conservative to account for the limited experience of the maritime user (for example more severe multipath environment) compared to the aeronautics case where much more dedicated long term assessments are available.

7.4 Wide Failure Probabilities

Wide failures correspond to errors induced by ground segment or satellite faults which affect simultaneously the navigation signals or/and the navigation messages of multiple satellites [Blanch et al 2013]. Wide failures also include failures that affect the whole constellation itself.

The potential physical causes are briefly summarized. Basically, three groups have been identified. **Inadequate Manned Operations** may for example occur during software or hardware updates in the ground segment or by erroneous tele-commands to the satellites. **Ground Segment Inherent Failures** correspond for example to cases regarding the generation of the navigation message or its uplink to the satellites. **Externally Induced Faults** have their origin completely outside the system. A typical example of such failures is the Earth Orientation Parameters (EOP) that are used in the Orbit and Time Synchronization (ODTS) processing. For example, it might happen that at the time of a navigation message upload, their validity has already expired due to change of earth rotation possibly due to atmospheric effects. For further details, it is referred to [Blanch et al 2013]. The probability of wide failure to occur will be assumed being 1E-4 per hour for all GNSS consistently. This value corresponds to approximately 1 constellation-wide fault per year with several hours time to flag the fault. The value is typically used in current literature for integrity (resp. accuracy and continuity) simulations [WG-C ARAIM 2012], [WG-C ARAIM 2015]. Of course, more consolidated values will be available in the future as the GNSS mature. The quantitative characterization is deemed conservative and for performance simulation purposes only and may not necessarily be fully representative of the performance of the future system.

7.5 Revision of Integrity and Continuity

There is no commonly accepted and published threat space for maritime operations. Most assumptions are taken from aviation where the threat space is well defined. In order to properly state about maritime integrity and continuity performance, there is urgent need for a threat space that complies with maritime conditions.

The logic followed here is to assess whether the assumptions made for aviation can be adopted for maritime operations. The ICAO and IMO requirements for both continuity and integrity are compared in Table 7-2. For each requirement, both 15 minutes and 3 hours exposure period, are considered. The probabilities are linearly scaled to the respective exposure period and then directly compared to the IMO requirement. A negative margin means that the respective ICAO requirement is below its corresponding IMO requirement and vice versa.

For reasons of comparison the corresponding set of requirements for the LPV-200 operation that originate from the ICAO requirements is listed as well. For the MHSS RAIM, the LPV-200 operation is the baseline [Blanch et al 2013]. In fact, the LPV-200 operation is deemed to be the most comparable operation in terms of requirements given in Table 7-2 between aviation and maritime users. Due to the fact that no requirements for the vertical position component exist for maritime operations, both, the ICAO continuity and integrity risks are equally split among the two position compo-

nents horizontal and vertical (division by factor of 2) in order to align to the maritime allocation logic.

Table 7-2: Comparison of ICAO and IMO Requirements

		Continuity		Integrity	
		LPV-200	allocation to	LPV-200	allocation to
	ICAO Req.	8E-6/15s	hor. only (/2)	2E-7/150s	hor. only (/2)
15min	scaled	4.80E-04	2.40E-04	1.20E-06	6.00E-07
	IMO Req	3.00E-04	3.00E-04	1.00E-05	1.00E-05
	margin	1.80E-04	-6.00E-05	-8.80E-06	-9.40E-06
3hours	scaled	5.80E-03	2.90E-03	1.44E-05	7.20E-06
	IMO Req	3.00E-04	3.00E-04	1.00E-05	1.00E-05
	margin	5.50E-03	2.60E-03	4.40E-06	-2.80E-06

For integrity, the LPV-200 requirement (2E-7/150s) is linearly scaled to the respective exposure periods (15 minutes and 3 hours). Under the assumption of an equal split among the two position components (horizontal and vertical), those values are divided by the factor of 2. This is done for comparison reasons because maritime requirements are only available for the horizontal position component. The same logic is followed for the continuity requirement for LPV-200 (8E-6/15s).

For integrity, it is obvious that there is a margin when comparing both sets of requirements (2.80E-6 considering 3 hours exposure period and 9.40E-6 considering 15 minutes exposure period) which leads to the conclusion that the integrity requirement for maritime operations is slightly relaxed compared to the requirements for LPV200. For continuity, assuming 15 minutes exposure period, the IMO continuity requirement is slightly relaxed compared to its corresponding ICAO requirement. However, it can be shown that the IMO continuity requirement is more stringent compared to its corresponding ICAO requirement if a 3 hours exposure period is assumed.

From a system design point of view, this perception means that the likelihood of an integrity (resp. continuity) event must comply with the requirement respectively. This requires a review of the feared events: for integrity, a relaxation is tolerable. For continuity, the system must ensure that the likelihood of all feared events causing a continuity event is equal or below its requirement.

Threats that have not been considered for aviation or even novel threats might have to be considered when assessing the continuity requirement for longer exposure periods compared to the one used for LPV-200. In the following, it will be shown that novel threats might become relevant. Their probability would need to be considered on top on the continuity risk budget. Also from the fact that the scaled continuity risk from a comparable aviation operation (LPV-200) to the 3 hours exposure period exceeds the IMO continuity requirement, it can be concluded that a revision of the

continuity tree needs to be performed (for example by tuning of various continuity risk contributors).

7.5.1 Integrity

An integrity tree defines the allocation of the total allowable integrity risk among all the considered threat cases. Each fraction of the total allowable integrity risk is a function of probability of occurrence, missed detection probability and the probability of leading to an integrity event. All these parameters are based on the design of the elements on ground as well as on user level (i.e. potential mitigation mechanisms) in charge of providing integrity to the user.

The integrity tree that is proposed by the GNSS Evolutionary Architecture Study (GEAS) panel in the context of Advanced RAIM for aviation needs is depicted [GEAS 2010]. A review of this integrity tree is presented followed by an assessment related to the need for adapting this integrity tree to the maritime users' needs.

The Phase 2 of the GNSS Evolutionary Architecture Study (GEAS) panel provides an evolutionary path to support seamless air navigation worldwide based on GNSS [GEAS 2010]. This GNSS based plan would provide – amongst others – support for various aviation based operation modes. Figure 7-4 depicts the integrity tree as proposed by the GEAS panel. The total allowable integrity risk is split equally among the two position dimensions vertical and horizontal. As can be seen the following threat cases are considered:

- Fault-Free Case: it covers the causes of integrity events that are due to large random errors that can occur with small probability in the normal operation of the system such as those caused by receiver noise, multipath and inaccurate tropospheric delay estimation along with an unfortunate combination of bias errors [GEAS 2010].
- Single Satellite Failure: in this case, the integrity risk is the product of the assumed prior probability of a single fault and the conditional probability that it is not detected and thus leads to an integrity event [GEAS 2010].
- Simultaneous Multiple Satellite Faults: this probability is assumed to be $1.3E{-}8$ per approach. In Advanced RAIM no attempt is made to detect an integrity event explicitly caused by multiple satellite failures. Instead, this probability is subtracted from the total allowable integrity risk so that – even if the probability of detecting an integrity failure caused by multiple faults is zero – the total allowable integrity risk requirement is still met.

The remaining integrity risk requirement ($8.7E{-}8$ per approach) is allocated to the fault-free and individual satellite failure cases [GEAS 2010]. The probability of having Hazardous Misleading Information (Pr{HMI}) is synonymously used for the integrity risk in Figure 7-4.
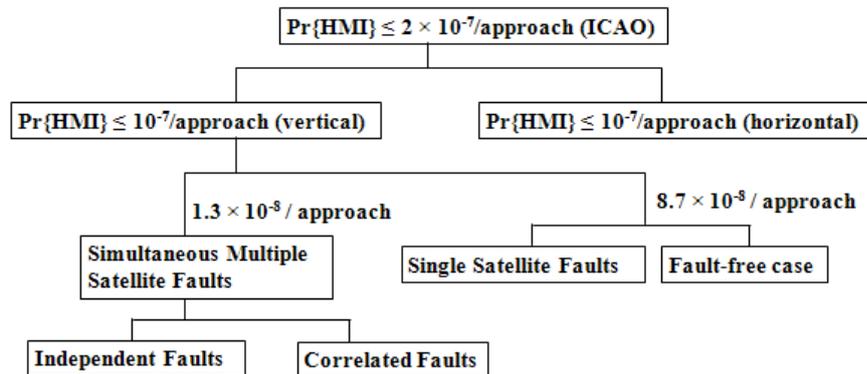
Figure 7-4: Allocation of Integrity Risk for Advanced RAIM [GEAS 2010]

There is no need considering additional threat cases for the maritime user compared to the aviation. Based on the assumed satellite failure probabilities, the according probabilities of having one or more simultaneous satellite failures are considered as function of the number of satellites. In contrast to the aviation, the IMO specifies only requirements for the horizontal position domain. As such, the integrity tree in Figure 7-5 has been adapted in the way that it allocates the total available integrity risk to the horizontal position exclusively.

The allocated integrity risk per threat case needs to be defined and justified. It depends on the user's need (overall integrity risk budget) and the technical realisability and performance of potential mitigation mechanisms. The integrity tree shown in Figure 7-5 is proposed for maritime operations. As opposed to the integrity tree schown in Figure 7-4, no static allocation of the overall integrity risk to the threat cases is done and therefore intentionally left as "$xE - y$". The probabilities (for fault-free, single and multiple simultaneous faults) are a function of P_{sat} and the number of available satellites respectively. Both parameters can vary over time. It is understood that having fixed allocation in an integrity tree gives more weight to the definition of P_{md} and $P(P_E > PL)$ (see equation 5.62). The approach followed here is to keep the partial integrity risks (over the threat cases) dynamic in order to allow for more flexibility in the definition of the latter parameters (P_{md} and $P(P_E > PL)$).
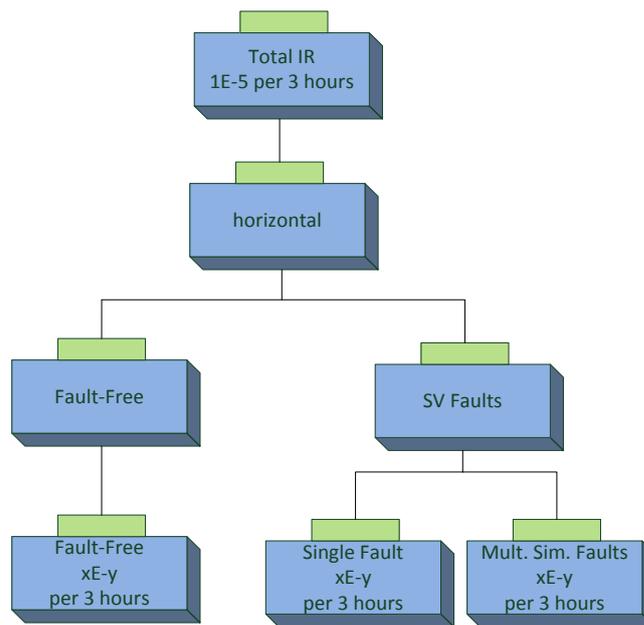
Figure 7-5: Integrity Tree for Maritime Operations

Local effects such as multipath or interference are not explicitly considered in this integrity tree. However, in the framework of this thesis a sensitivity analysis is to be performed evaluating the maximum allowable bias (for example caused by multipath effects) and the maximum allowable spread of the fault-free distribution (for example caused by interference) to still satisfy the requirements for the user (see section 9.3).

7.5.2   Continuity

Potential discontinuities may occur in the position accuracy and/or integrity when:

- A new satellite is included in the navigation solution over a period up to 3 hours. This may lead to signal acquisition issues affecting user performance and to discontinuities.
- Navigation data is updated at user level. The update rate of the parameters broadcasted in the navigation message (independently of which GNSS is considered) is certainly below the exposure period of 3 hours. If the update is not considered in the continuity allocation, the result is a complete unavailability of the service.

7.5.2.1   Impact of Dynamic Constellation

The satellite constellation is varying within a few minutes just in the range of some degrees and thus the performance will not change significantly. Thus, for very short exposure periods like in aviation, a static constellation can safely be assumed. In case of hours, satellites are changing their

positions in the order of some ten degrees and the performance changes significantly since start of operation. It is obvious that during such a period of 3 hours, satellites will ascend above the user's horizontal plane. Ascending satellites may be potentially the cause for signal acquisition problems and failures and hence might affect the positioning performance. Therefore, a possible discontinuity coming from the acquisition of new signals should be considered. Moreover, the user does not know whether the satellites would be flagged as usable or not as they are probably not monitored by the system.

The number of ascending satellites that are in view of a user above its horizontal plane over the exposure period is assessed. This analysis is based on dual constellation assumption and on a user masking angle of 5 degrees. Globally distributed user locations with a sampling for latitude and longitude of 10 degrees have been assumed. A period of 10 days to cover all possible geometries of the satellites is used. Figure 7-6 and Figure 7-7 show the average number of satellites ascending above the user's horizontal plane over the exposure period of 3 hours (left) and 15 minutes (right) based on single constellation (GPS only) and dual constellation (GPS+Gal). For the simulation, the GNSS constellations as described in the Annex have been used.
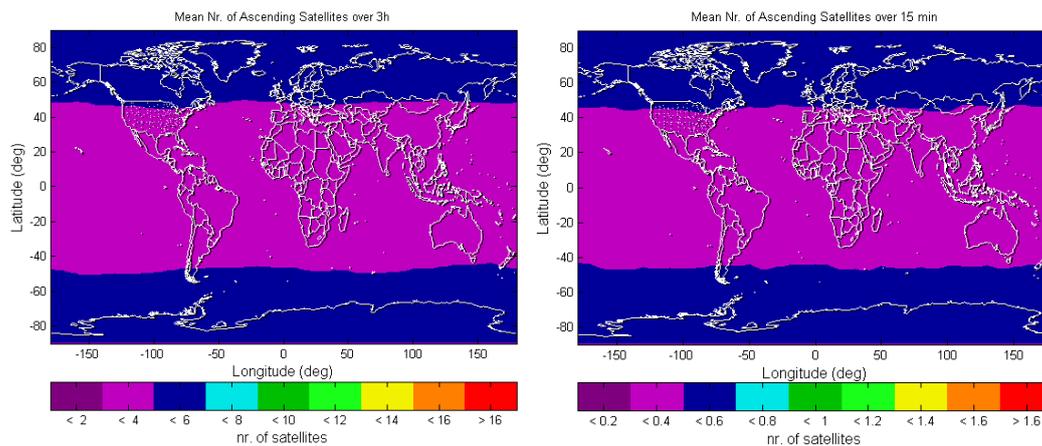

Figure 7-6: Average number of ascending satellites (GPS only) at user locations over a period of 3 hours (left) and 15 minutes (right)
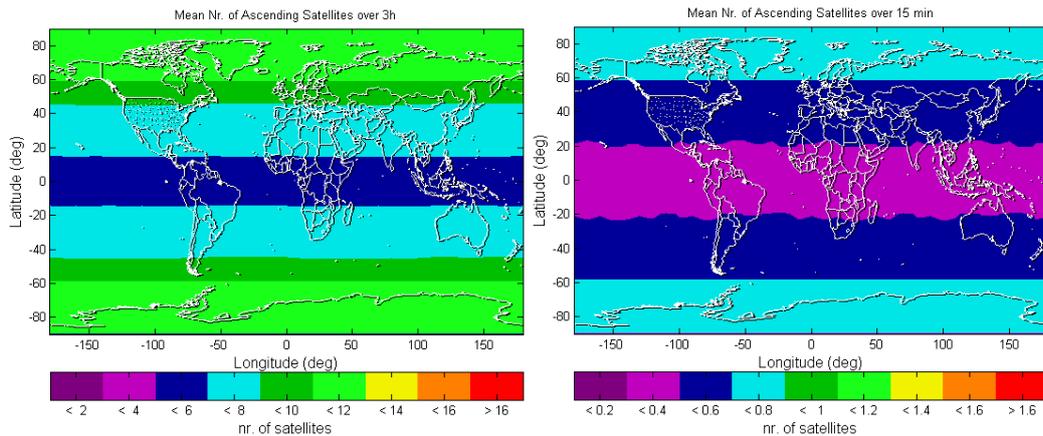
Figure 7-7: Average number of ascending satellites (GPS+Gal) at user locations over a period of 3 hours (left) and 15 minutes (right).

A clear dependency on the latitude can be observed: less ascending satellites can be observed for lower latitudes whereas for higher latitudes a higher number of new satellites appear in view of the user over time. Furthermore, the statistics are depicted in Table 7-3 taking into account all considered global user locations. The analysis has been performed for both GPS only and GPS+Gal cases.

Table 7-3: Number of ascending satellites

	min	max	mean
GPS only (3 h)	0	9	4.07
GPS+Gal (3 h)	0	15	7.43
GPS only (15 min)	0	4	0.40
GPS+Gal (15 min)	0	5	0.73

It is obvious that the number of satellites ascending above the user's plane over a period of 15 minutes is much lower than for a period of 3 hours. It is shown that for both exposure periods, satellites that ascend above the user's plane are observed and thus need to be taken into account. As a consequence, the probability of having an erroneous ascending satellite (P_{asc}) needs to be taken into account as an additional contributor to the overall continuity risk P_{cont}:

$$P_{cont} = \sum_{i=1}^{N_{cont.events}} \left(P_{cont_i} \right) + P_{asc}$$

7.5

P_{cont} is the sum over all conditioned probabilities P_{cont_I} over N events causing a continuity event together with P_{asc}.

The impact of P_{asc} on the probability of having satellite failures and thus on the final performance of the user is not quite intuitive. Therefore, the following sensitivity analysis depicts the probability of having a single satellite failure as function of the number of ascending satellites. A maximum number of 15 available satellites (GPS+Gal) in view will be assumed. Each available satellite is assumed with a negligible probability of failure (P_{sat}=0). This allows to focus on the probability contributions exclusively coming from P_{asc}. The ascending satellites are afflicted with the according P_{asc} independently.
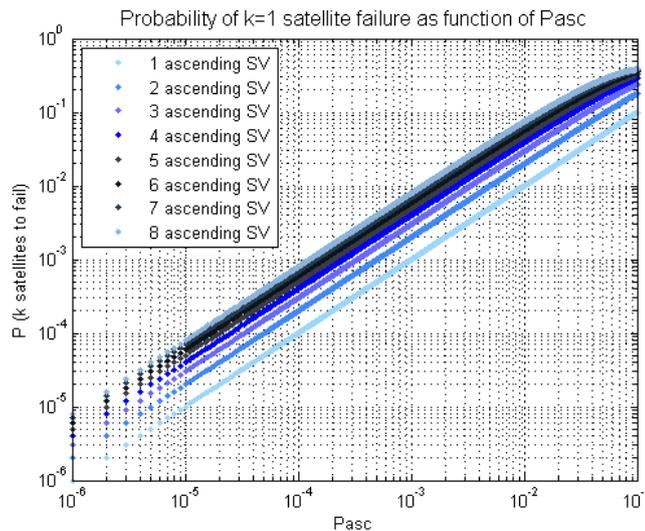

Figure 7-8: Probability of having a single satellite failure as function of P_{asc} (15 satellites)

It can be observed that the probability of having a single satellite failure (k=1) increases with the probability of failure of an ascending satellite (P_{asc}) taking into account a number up to 8 ascending satellites. If a single ascending satellite is assumed, the failure probability is proportional to the probability of having a single satellite failure. The reason is the fact that all failure probabilities of the satellites (P_{sat}) are assumed being zero. The probabilities of having k=1 satellite failures out of a set of 15 satellites shown in Figure 7-8 are exclusively based on P_{asc}. The number of ascending satellites of course influences the probability of satellite fault (P_{sat}) – however, this is deemed being not a main driver.

The probability of a continuity event due to signal acquisition of ascending satellites during the exposure period needs to be sufficiently low to not exceed the overall continuity risk budget. This need can be directly translated into a requirement for the false alert probability (P_{fa}). The overall continuity budget is allocated to disruptions due to false alert. The acquisition of a signal is hence deemed more complex and more sensitive to failures than the tracking of a signal. The continuity event due to signal acquisition is deemed relevant for maritime users and its probability is assumed

to be covered within the overall continuity budget. This assumption is supported by the fact that the continuity budget is allocated to the horizontal component and thus allows for compensating this additional demand. For the tracking of signals, the failure probability is assumed to be negligible.

7.5.2.2   Update of Erroneous Navigation Data

Considering a continuity exposure period of 15 seconds like in the aviation case (for example LPV-200), it is assumed that the user is using the currently available navigation parameters and does not need to take into account any updates of the navigation message. However, given the continuity requirements for the maritime user, this assumption needs to be revised.

The current Galileo system design presumes a more frequent update of the navigation message certainly well below the exposure period for maritime users [EC 2010]. While in the case of GPS the update rate of the navigation message is in the order of hours [Navstar GPS 2012], GNSS users in general use the youngest available (most up-to-date) navigation message respectively. This implies frequent navigation message updates during the continuity exposure period specified for maritime services.

The validity of navigation parameters is constrained to a certain period. Navigation message validity is the period in which the parameters that are contained in the navigation message are valid and are permitted for usage at user level. In order to avoid any updates of the navigation message during the applicable continuity exposure period, a very pragmatic approach would consist in using the particular set of navigation parameters throughout an operation phase without considering any updates. However, predicted performance decreases in accuracy with time and the user positioning performance would significantly suffer. This approach would require a more conservative characterization of the system errors such as orbits and clocks in order to cope for longer prediction times. This option is not further discussed in this thesis.

Regarding navigation message update rate at user level, the following is assumed: navigation messages are updated every 10 minutes at user level. The navigation message update rate is the time between two consecutive received messages at user level. The maritime user receiver – in contrast to the aviation case – will experience several updates of the navigation message used for positioning and navigation throughout an operation period. In fact, considering the latter presumptions, this would lead to a maximum number of updates u=17 during a period of 3 hours (analogously u=2 over an exposure period of 15 minutes). The principle is illustrated in Figure 7-9 where periodic navigation message updates are indicated with vertical green bars as well as the end of the validity of ISM parameters in blue respectively. It is noted that the indicated ends of validity time of ISM parameters are set arbitrarily in Figure 7-9 and are indicated to show a potential update of ISM parameters during the exposure period.
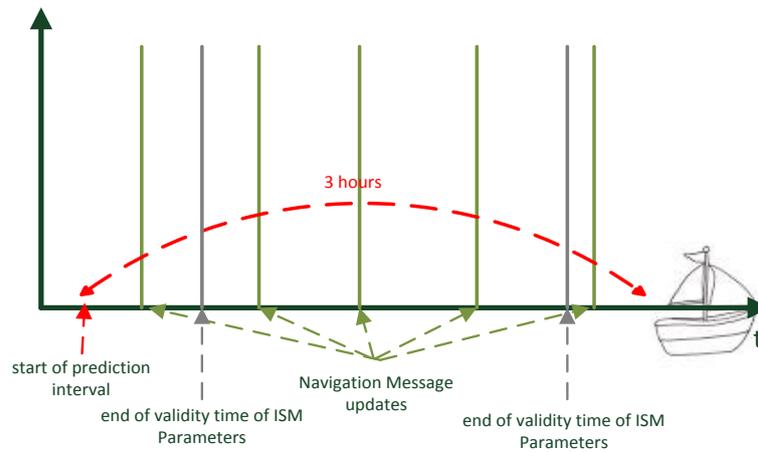
Figure 7-9: Navigation message updates versus exposure period

The probability of experiencing a continuity event due to an update of the user receiver with an erroneous navigation message is denoted as $P_{erroneous\ navmsg\ update}$ and scales with factor u representing the message update rate. The event that a navigation message has not been received or was no longer valid at reception or contains an erroneous content might lead to severe impacts on positioning and navigation performance of the user – if undetected. Thus, this threat scenario is deemed being an additive contributor to the overall continuity risk:

$$P_{cont} = \sum_{i=1}^{N_{cont.events}} \left(P_{cont_i} \right) + P_{erroneous\ navmsg\ update} \cdot u$$

7.6

P_{cont} is the sum over all conditioned probabilities P_{cont_I} over N events causing a continuity event together with $P_{erroneous\ navmsg\ update}$ (multiplied with factor u). It has to be noted that each continuity contributor is the product of occurrence, missed detection probability and the likelihood that the event causes the position error exceeding its protection level.

A sensitivity analysis has been performed aiming at assessing the sensitivity of the probability of having a single satellite failure (k=1) over time assuming a navigation message update every 10 minutes with a given failure probability ($P_{erroneous\ navmsg\ update}$). Figure 7-10 depicts the contribution to the satellite failure probability over time with a sampling rate of 10 minutes reflecting the assumption with respect to the update rate. The considered exposure period is 3 hours. A total number of 15 available satellites is used.
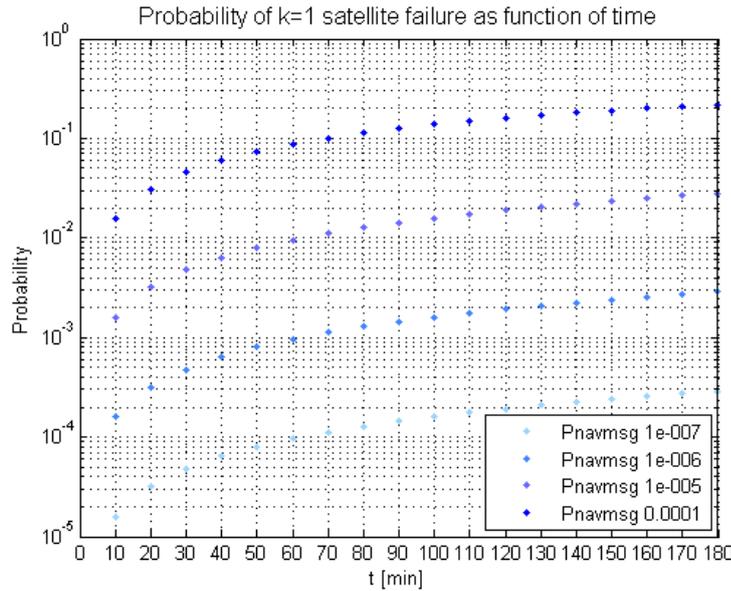
Figure 7-10: Probability of a single satellite failure as function of probability of failure of navigation message update $P_{erroneous\ navmsg\ update}$ (based on 3 hours requirement, GPS+Gal)

An expected increase of the probability of having a single satellite failure can be observed with time as function of the likelihood of having an erroneous update ($P_{erroneous\ navmsg\ update} = P_{navmsg}$ =1E-7 – 1E-4). As expected, the probability of having an erroneous update accumulates over time. All failure probabilities of the satellites (P_{sat}) are assumed to be zero at time t=0. The probabilities of having k=1 satellite failures out of a set of 15 satellites is shown assuming accumulation of failure satellite probability for each satellite independently due to increasing probability of having an erroneous update with time.

Another aspect is the validity time of the ISM. Over a period of 3 hours, it is very likely that also an update of the ISM needs to be considered. This is depending on the ISM concept that is selected [WG-C ARAIM 2015]. Potential unavailability due to update of erroneous ISM parameters is neglected.

7.5.2.3   Continuity Tree

In [Blanch et al 2013] the continuity requirement (for LPV-200) is formulated that the receiver must be able to compute and predict a Vertical Protection Level (VPL_{pred}) and a Horizontal Protection Level (HPL_{pred}) such that the false alert probability requirement (P_{fa}) is fulfilled:

$$P\big(VPL > VPL_{pred}\ or\ HPL > HPL_{pred}\big) \leq P_{fa}$$

7.7

In the current implementation of the MHSS RAIM algorithm, this requirement is met by adjusting the monitor threshold adequately. This implies that xPL_{pred} (x being horizontal or vertical) takes into account a Solution Separation Threshold T which is a function of P_{fa}. This threshold is denoted as $T(P_{fa})$ in Figure 7-11. Details on the computation of T have been depicted in section 5.5. This is understood to be a corresponding uncertainty interval that is defined for the measurement errors around each partial position solution, inside which the continuity risk is lower than a specified value (P_{fa}).

This approach is based on the fact that the geometry does not change significantly over the exposure period which in the case of LPV-200 is 15 seconds. Over the period of 15 seconds this can safely be accepted. However, this assumption is not true anymore if the exposure period is extended to a period where significant changes in the geometry need to be considered. In this case the above approach cannot be followed anymore.
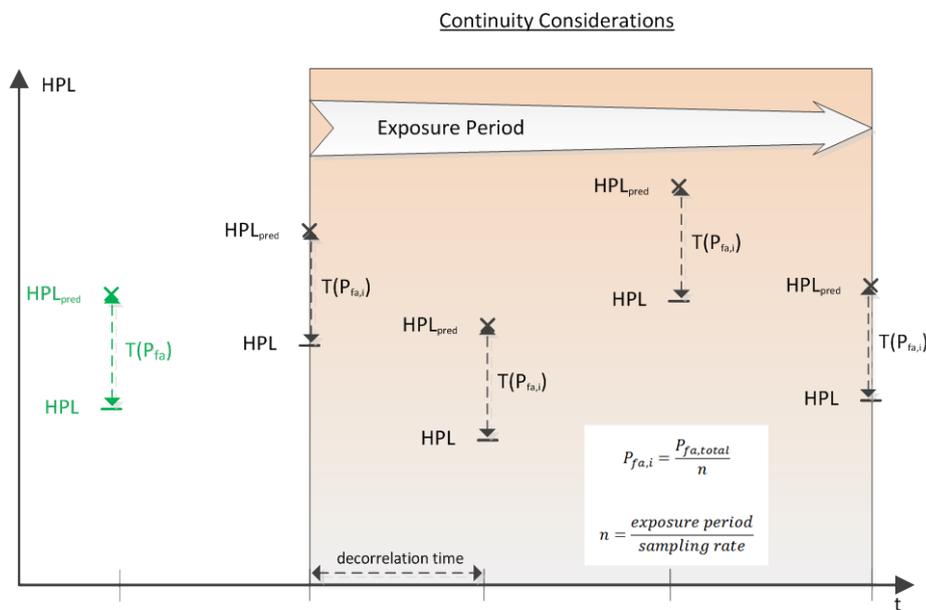
Figure 7-11: Continuity Considerations

Figure 7-11 highlights the implications if the continuity exposure period is extended. In case of LPV-200 that is shown in green, the total P_{fa} is allocated to a single time step. For longer exposure periods, the continuity requirement needs to be translated to a shorter period. For this, it is necessary to characterize the time decorrelation between tests. This time decorrelation depends on both the time decorrelation of the errors and the geometry. It is assumed that after a period of 600 seconds the errors and geometry are decorrelated for a multi-constellation scenario considering GPS and Galileo (and 60 seconds for GPS only). The factor of 10 corresponds to the respective

longer constellation repetition period for Galileo compared to GPS. The decorrelation times are assumptions and are driven by computational resources of the simulation environment MAAST (see Annex).

The underlying assumption is that the number of continuity events is equally distributed over the total evaluation period. This leads to the computation of the mean time between failures (MTBF). MTBF is computed as total time divided by the number of failure events and decorrelation time. The continuity time interval (CTI) corresponds to the total exposure period specified for the continuity requirement. Consequently, the continuity in the evaluation period is computed as:

$$continuity = 1 - \frac{CTI}{MTBF}$$

7.8

$$MTBF = \frac{total\ time}{nr.\ of\ failure\ events \cdot decorrelation\ time}$$

7.9

This methodology is deemed conservative as it presumes continuity events being uniformly distributed over time.

The continuity tree presented in Figure 7-12 is proposed for maritime operations. It takes into account the identified continuity events. The continuity risk budget is exclusively allocated to the horizontal component. Two high level threat cases are identified: the fault-free case and the case where a minimum of one satellite fault is to be considered. The latter threat case divides into a branch in which only a single satellite fault is considered and in a second branch in which multiple simultaneous satellite faults are considered. Both branches take into account the new identified threats in addition to potential threats as summarized in section 7.2.

No static allocation of the overall continuity risk to the threat cases is done and therefore intentionally left as "$xE - y$". The probabilities (for fault-free, single and multiple simultaneous faults) are a function of P_{sat} and the number of available satellites respectively. Both parameters can vary over time. The implementation and tuning of dedicated failure detection mechanism are decisive drivers for the required false alert probabilities (P_{fa}).
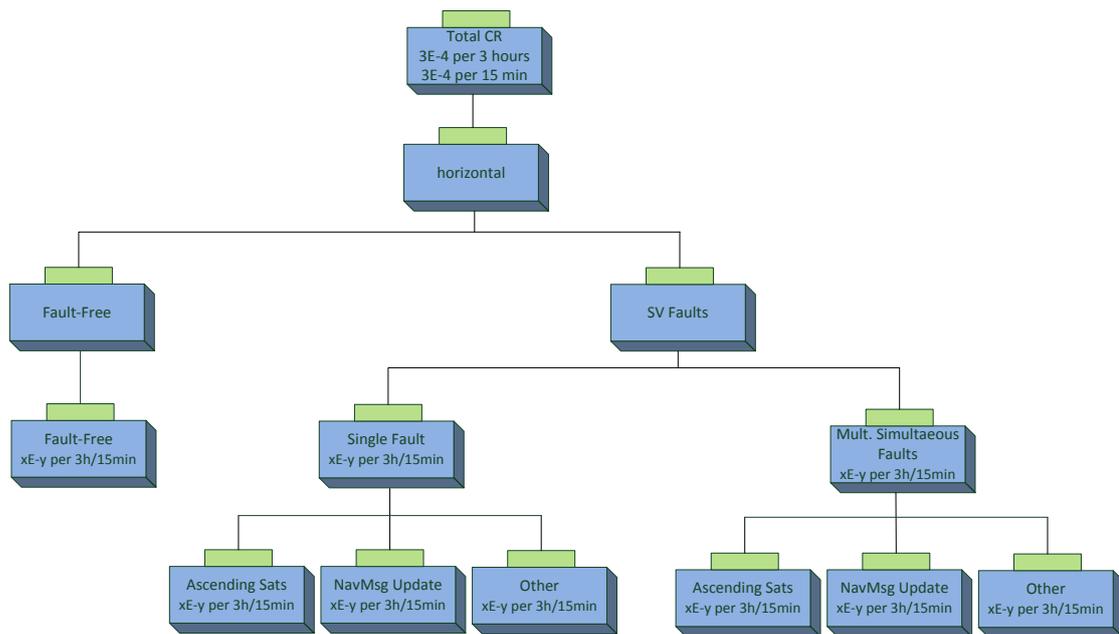
Figure 7-12: Continuity Tree for Maritime Operations

For maritime operations, continuity is the critical aspect. This becomes obvious by the sheer fact that the continuity required for a comparable flight operation (LPV-200) with a probability of a discontinuity event of 8E-6 in any 15 seconds falls short of the required continuity for maritime operations (see previous section). That means for example that efficient failure detection mechanisms and more stringent barriers need to be introduced either on the user or on the system side. The following major options have been identified as continuity performance drivers:

- Computation of integrity parameters from independent Advanced RAIM processing: too optimistic URA/SISA values will reduce the probability of having discontinuity events (P_{fa}). However, tuning the values too conservative will increase the probability of having an integrity event (P_{md}). This trade-off is not further elaborated within this thesis and therefore identified as a potential future work.
- Receiver acquisition of new GNSS signals needs to be such that it satisfies continuity needs.
- Failure rates on navigation message updates need to be sufficiently low.

The task of allocating specific probabilities to each threat case identified in the above tree shall not be further pursued in this thesis. For that task, extensive performance characterizations over long periods are required in order to derive consolidated probability values for each identified threat case. Especially the characterization of the new identified threat cases with respect to the probability of occurrence has not been performed to the knowledge of the author and would go beyond the scope of this thesis. In addition, the performance characterization of the younger GNSS (e.g. Galileo)

is not possible to the required extent. Another aspect is the implementation and characterization of dedicated failure detection mechanisms in order to define and tune the required false alert probabilities. This is deemed a long-term task as all GNSS mature with time. In the end, in order to comply with IMO continuity requirement, it is required that the sum of all probabilities for all considered threat cases satisfies the requirement for the maximum allowable continuity risk.

7.6   Conclusion

Based on reasonable assumptions about the probabilities of a satellite failure, it is demonstrated that for integrity the probability of having two simultaneous satellite failures is not negligible in case of multiple GNSS constellations. Also for continuity, the probability of having a single satellite failure is significant enough regardless of the exposure period being 3 hours or 15 minutes. Based on a summary regarding the feared events to be considered, the conclusion has been derived that this list of feared events is applicable not only for the aviation but also for the maritime user. For continuity in particular, it has been found that new threat cases need to be taken into account due to the significantly increased exposure period up to 3 hours as opposed to the aviation (15 seconds). The following two potential events causing discontinuities in the position accuracy and/or integrity have been identified:

- During a 3 hours period the satellite geometry changes significantly. A possible discontinuity coming from the acquisition of new signals (ascending satellites) is to be considered.
- Frequent updates of the navigation message at user level. The validity of the navigation message is well below the exposure period of 3 hours.

Omitting these events in the continuity allocation, the result would lead to a complete unavailability of the service. A comparison has been performed between the integrity and continuity risk requirements specified for LPV200 – which is deemed to be the baseline for current Advanced RAIM architecture developments – and the IMO. The result is that for integrity the IMO requirements are slightly relaxed compared to LPV200. However, for continuity, it can be concluded that the specifications from IMO are more stringent which leads to the conclusion that in terms of continuity the Advanced RAIM system – as it is currently planned – does not comply with IMO requirements. This perception is based on a direct comparison of both the IMO and LPV200 requirements in terms of continuity where it turns out that the IMO requirements are more stringent (see Table 7-2). Therefore, it is required that both the independent ground segment and the maritime user would need to take dedicated responsibility in order to reduce the risk of a feared event. This can be done by applying failure detection mechanisms with sufficient probability of missed detection rate. Using the independent ground segment an appropriate latency of the ISM notifying the user would need

to be defined. The longer the ISM latency the more conservative the satellite failure probability must be set because the user is notified with the respective latency.

8   Performance Results

RAIM algorithms have originally been developed with the focus on aeronautical applications. Due to different demands for a maritime user, also the algorithms are required to be adapted. The major differences in the requirements are the restriction to the horizontal position component only and a higher demand for continuity. That is why maritime operations are carefully to be distinguished from the aeronautics.

The following questions need to be answered: first, what is the level of performance that can be achieved with the selected RAIM algorithms? Second, under which conditions compliance can be achieved? This question is related to geometry aspects answering which and how many independent GNSS constellations are required. Also, it will be interesting to see the performance enhancement considering continuity exposure periods of 3 hours towards 15 minutes. Third, what are the expectations and can they be met? Certainly, availability will increase with a higher number of satellites as geometry is usually identified being one of the major performance drivers. Further expectations are that the Novel RAIM brings better performance compared to the LSR RAIM as well as the fact that MHSS RAIM leads to best results within the selection of algorithms, as being a representative for a new RAIM generation.

The selected RAIM algorithms (LSR RAIM, Novel RAIM and MHSS RAIM) are individually assessed in terms of accuracy, integrity, continuity and availability. Horizontal positioning accuracy evaluation is independent of the integrity algorithm and is driven by the satellite geometry and the fault-free error model. The use of up to three GNSS constellations (GPS only, GPS+Galileo, GPS+Galileo+GLONASS) is considered. For GPS and Galileo, a 24 satellite based constellation is assumed while for GLONASS a 23 satellite constellation is assumed (see Annex A.2). For the position accuracy also a comparison of – on the one hand considering nominal biases and the other hand not considering nominal biases on the pseudoranges – is done. For integrity, continuity and availability analyses, the presence of nominal biases on the pseudoranges is assumed. The LSR RAIM and the Novel RAIM are evaluated using GPS only and GPS+Galileo while the MHSS RAIM uses also triple constellations. The reason of not considering triple constellations for LSR RAIM and Novel RAIM is the non-compatibility regarding the multiple-failure assumption.

GPS-only scenarios are simulated over one day with a sampling rate of 60 seconds while the multi-constellation scenarios (GPS+Galileo and GPS+Galileo+GLONASS) are based on a total simulation time of 10 days with a sampling rate of 600 seconds. A global grid within the parameters of [90°S 90°N] for the latitude and [180°W 180°E] for the longitude is used with a 10° sampling for latitude and longitude. All collected samples per grid point are used to derive representative statistics per

grid point in the global figures. An elevation mask angle of 5° has been consistently used through-out the simulations except for the Novel RAIM which applies an elevation mask angle of 20° due to performance optimization reasons (see section 8.4). For the analyses, the elevation dependent fault-free error model (UERE) as described in chapter 6 and the threat space defined in chapter 7 have been used consistently for all constellations. The threat space is considered in the sense that the respective failure probabilities are considered in the algorithms. However, it is noted that no artificial threats (e.g. MIs or HMIs) are simluated in the performance evaluations.

Basically, these form the overall frame and describe the conditions in which the RAIM algorithms apply and for which the resulting performance is referring to. The demand of maritime services is to achieve a global coverage for the required performance level. The performance results therefore follow a global representation as well as the given statistics which correspond to the global average (average over all grid points and time steps). In addition, a sensitivity analysis is presented sup-porting the optimization of Novel RAIM performance. All analyses are performed based on the MAAST tool (see Annex A.1).

This chapter is structured in such a way that every performance aspect is covered in a separate subsection. This allows for a detailed assessment and a direct comparison of the results between the individual RAIM algorithms which are discussed and compared in a conclusive section. A final discussion clarifies the performance of the RAIM algorithms and provides feedback for usage for a maritime GNSS user.

8.1 Position Accuracy

The compliance to position accuracy is a prerequisite for availability. Position accuracy is derived based on the fault-free error model using the GNSS constellation parameters respectively (see Annex A.2). The vertical position performance has been neglected as no requirements for it exist. Three different cases are distinguished: a single constellation (GPS only), a dual constellation (GPS+Gal) and a triple constellation (GPS+Gal+GLO) have been taken into account for the evalua-tion. For GPS and Galileo, a 24 satellite based constellation is assumed while for GLONASS a 23 satellite constellation is assumed (see Annex A.2). Furthermore, for reasons of investigation on the impact of the presence of nominal biases, for each case, the horizontal position accuracy is charac-terized on the one hand considering the presence of nominal biases and on the other hand neglect-ing them. The fault-free error model as described in chapter 6 is assumed. The horizontal position-ing accuracy evaluation is independent of the RAIM algorithm in use and is based on the all in view satellites available at the respective user location. The bias-free horizontal position accuracy is derived from the respective diagonal elements from the covariance matrix of the estimation error (see equation 5.4). In the case where the nominal range biases (see section 6.7) are considered,

they have been mapped into the horizontal position domain by their absolute values in all dimensions such as to yield the worst case.

The performance results with respect to the horizontal position accuracy are illustrated for each case (single, dual and triple constellation) respectively. The histograms presented below (on the left) take into account all horizontal position accuracy values at every grid point and at every time instance. The histograms (on the left) are presented in a way that different groups of user locations are presented. It is distinguished between three global areas: the poles (latitude >70°N and <70°S), the mid-latitudes (latitude >20°N-<70°N and <20°S->70°S) and the equator region (latitude >20°S-<20°N). The number of samples per bin (with a bin size of 1 cm) is composed of the sum over the samples from the three different global areas. Also the results visualize horizontal position accuracy on a global map (on the right). For each grid point the 99-percentile values over the whole evaluation period are shown. A clear latitude dependency can be seen in the results. Basically, the global map divides into different latitude dependent regions with different performance. This characteristic can be observed for all cases.

Horizontal Position Error (GPS only)
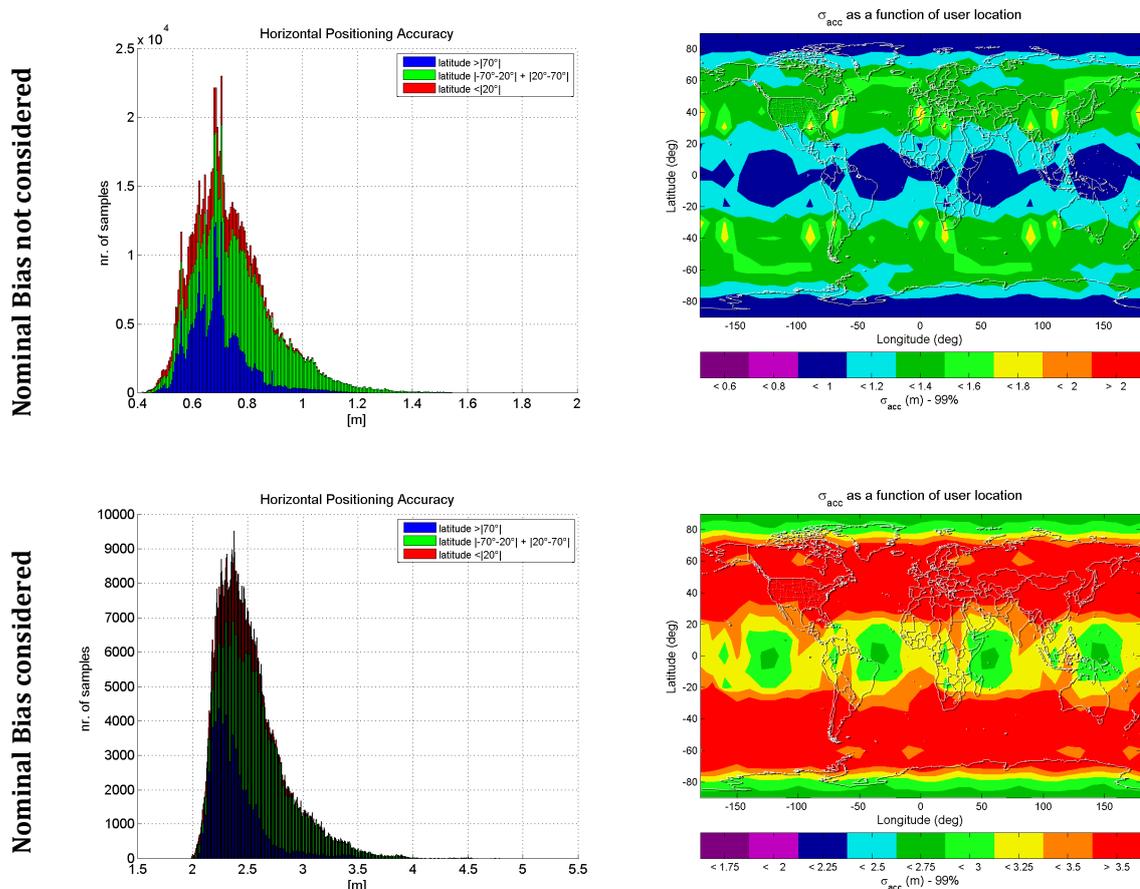
Figure 8-1: Horizontal Position Accuracy (left: PDF over all grid points and epochs; right: Position Accuracy as function of User Location) – GPS only

125

The results for the horizontal position accuracy based on a single constellation (GPS only) are depicted in Figure 8-1. The power density functions on the left are based on all samples from all grid points and over all time steps. The characteristic of the error distribution is explained by the fact that geometry depends on user location and thus every user location derives its own error statistics. The fault-free error model as introduced in chaper 6 introduces nominal biases on the pseudoranges (see section 6.7). The impact of considering nominal biases (0.75 m) on pseudorange measurements is basically a shift of the mean value of the power density function in the order of approximately 2 m. The global accuracy figures showing 99-percentile values per user location reveal a strong dependence on latitude as expected. Equatorial areas together with areas above 70°N and below 70°S, approximately, show better accuracy performance (~<1.20 m without considering nominal biases on the pseudorange measurements) compared to mid-latitude regions (~<1.60 m without considering nominal biases on the pseudorange measurements).

Horizontal Position Error (GPS+Gal)
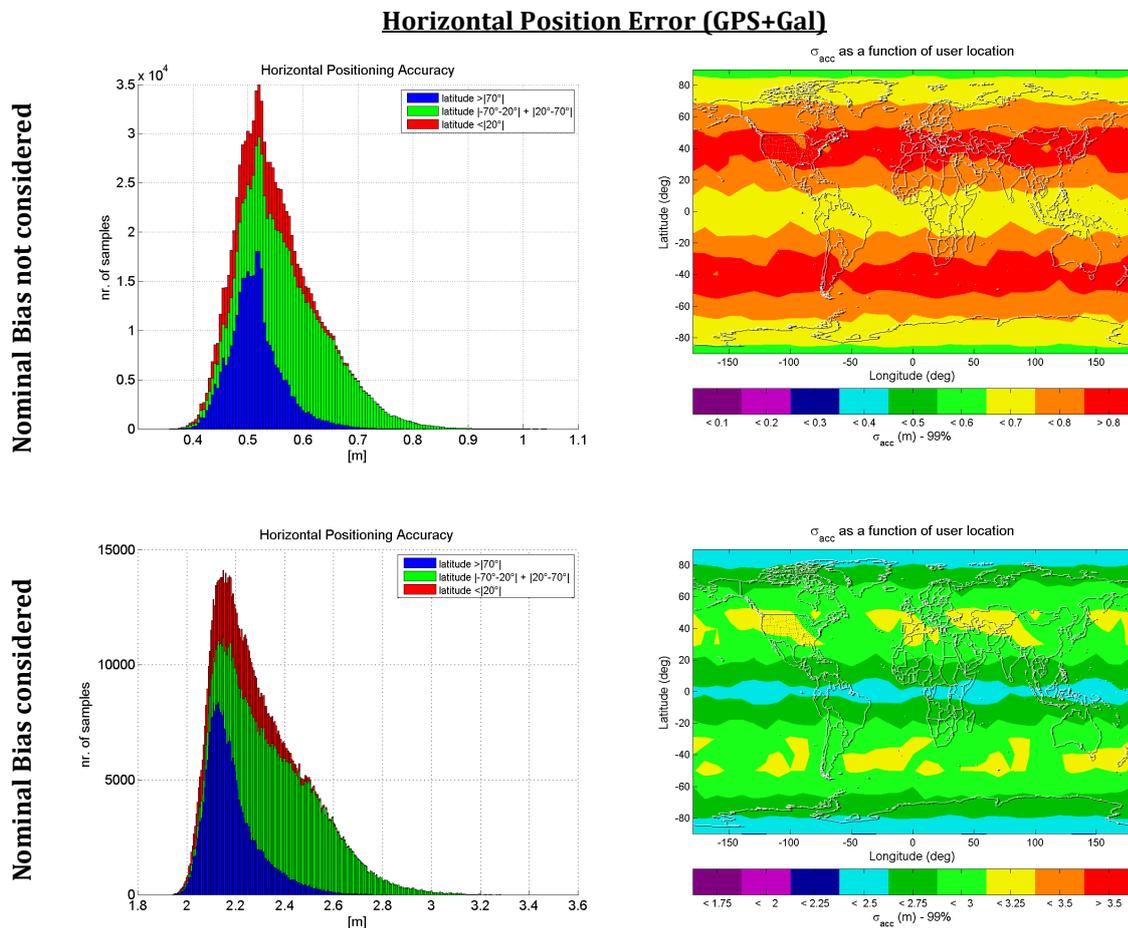
Figure 8-2: Horizontal Position Accuracy (left: PDF over all grid points and epochs; right: Position Accuracy as function of User Location) – GPS+Gal

The horizontal position accuracy based on dual constellations (GPS+Gal) is shown in Figure 8-2. The impact of considering nominal biases (0.75 m) on pseudorange measurements is basically a shift of the mean value of the power density function in the order of 2 m. The global accuracy figures showing 99-percentile values per user location reveal a strong dependence on latitude as expected. Equatorial areas together with areas above 70°N and below 70°S, approximately, show better accuracy performance (~<0.70 m without considering nominal biases on the pseudorange measurements) compared to mid-latitude regions (~<0.80 m without considering nominal biases on the pseudorange measurements). Already, a clear improvement in the results for the dual constellation case (mean ~0.55 m) can be observed compared to the single constellation case (mean ~0.74 m) if the presence of nominal biases on the pseudoranges are neglected. For further statistics, it is referred to Table 8-1.

**Horizontal Position Error (GPS+Gal+GLO)**
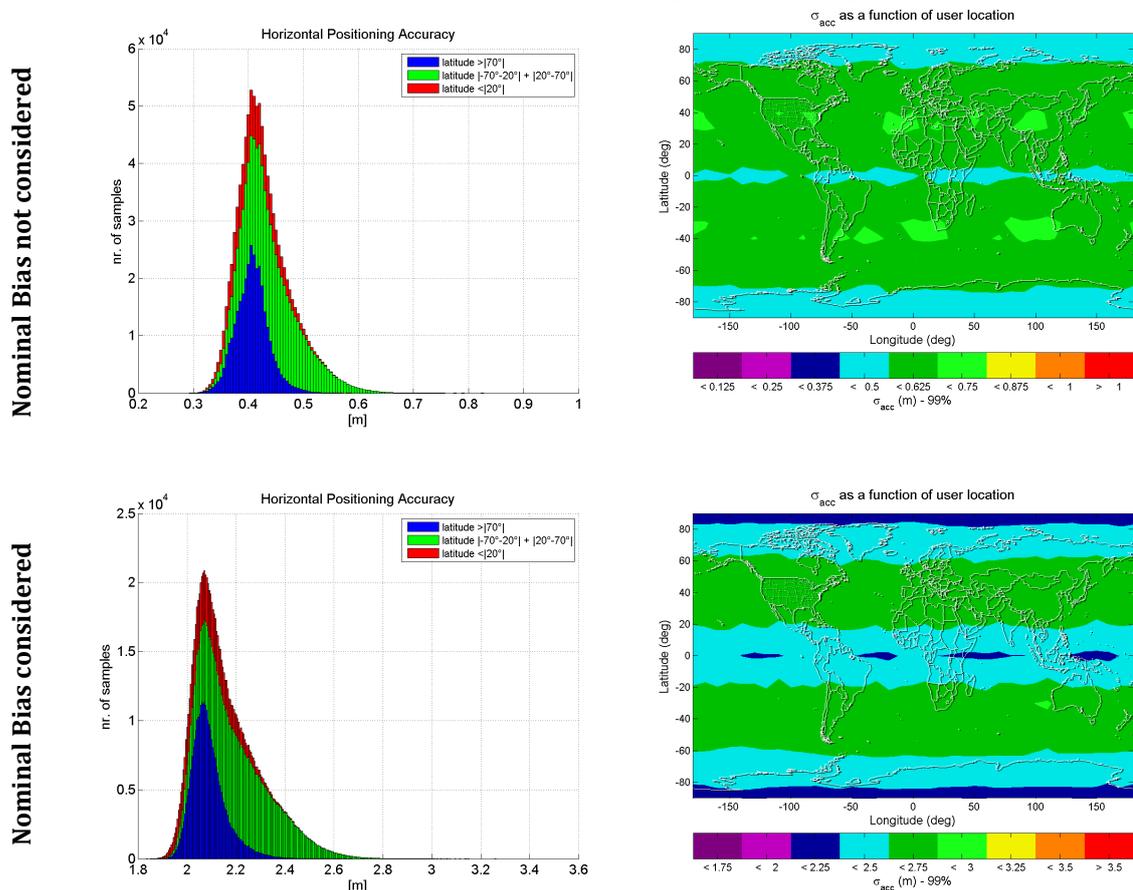
Figure 8-3: Horizontal Position Accuracy (left: PDF over all grid points and epochs; right: Position Accuracy as function of User Location) – GPS+Gal+GLO

The results for the horizontal position accuracy based on the triple constellation (GPS+Gal+GLO) are depicted in Figure 8-3. The impact of considering nominal biases (0.75 m) on pseudorange

127

measurements is a shift of the mean value of the power density function in the order of 0.10 m. The global accuracy figures showing 99-percentile values per user location reveal a strong dependence on latitude as expected. Equatorial areas together with areas above 70°N and below 70°S, approximately, show better accuracy performance (~<0.50 m without considering nominal biases on the pseudorange measurements) compared to mid-latitude regions (~<0.65 m without considering nominal biases on the pseudorange measurements). The statistics for the horizontal position accuracy are summarized in Table 8-1 for both cases, neglecting and considering nominal biases on the pseudoranges respectively. Percentile values (67-percentile, 95-percentile and 99-percentile) are shown together with the mean values for each scenario. The statistics are computed from the samples obtained over all time steps and all user locations.

Table 8-1: Horizontal Position Accuracy Statistics

Horizontal Position Accuracy (over all time steps and user locations)							
	Nominal biases not considered [m]				Nominal biases Considered [m]		
	67-perc.	95-perc.	99-perc.	Mean	67-perc.	95-perc.	99-perc.	Mean
GPS only	0.78	1.03	1.22	0.74	2.59	3.16	3.58	2.53
GPS+Gal	0.57	0.70	0.77	0.55	2.36	2.67	2.87	2.30
GPS+Gal+GLO	0.44	0.52	0.58	0.43	2.20	2.43	2.57	2.16

It can be observed that the position accuracy improves with more available satellites. This is due to the higher robustness of the positioning and due to the geometry factor when more satellites are available. RAIM in general is a function of the geometry of the satellites and therefore its performance strongly depends on the number of satellites and their distribution over the sky (DOP). To assess the sensitivity on the position accuracy, the 95-precentile values over all user locations per time epoch is provided as a time series. Figure 8-4 shows time series of the 95-percentile value of the results over all grid points and per time instance. For every time step the horizontal position accuracy has been computed at each grid point respectively and in a following step based on these values the 95-percentile value has been derived. A global grid is used with a 10° sampling for latitude and longitude. The time series shown cover a period of 1 day where GPS only scenarios are simulated with a sampling rate of 60 seconds and the multi-constellation scenarios (GPS+Galileo and GPS+Galileo+ GLONASS) are based on a sampling rate of 600 seconds.
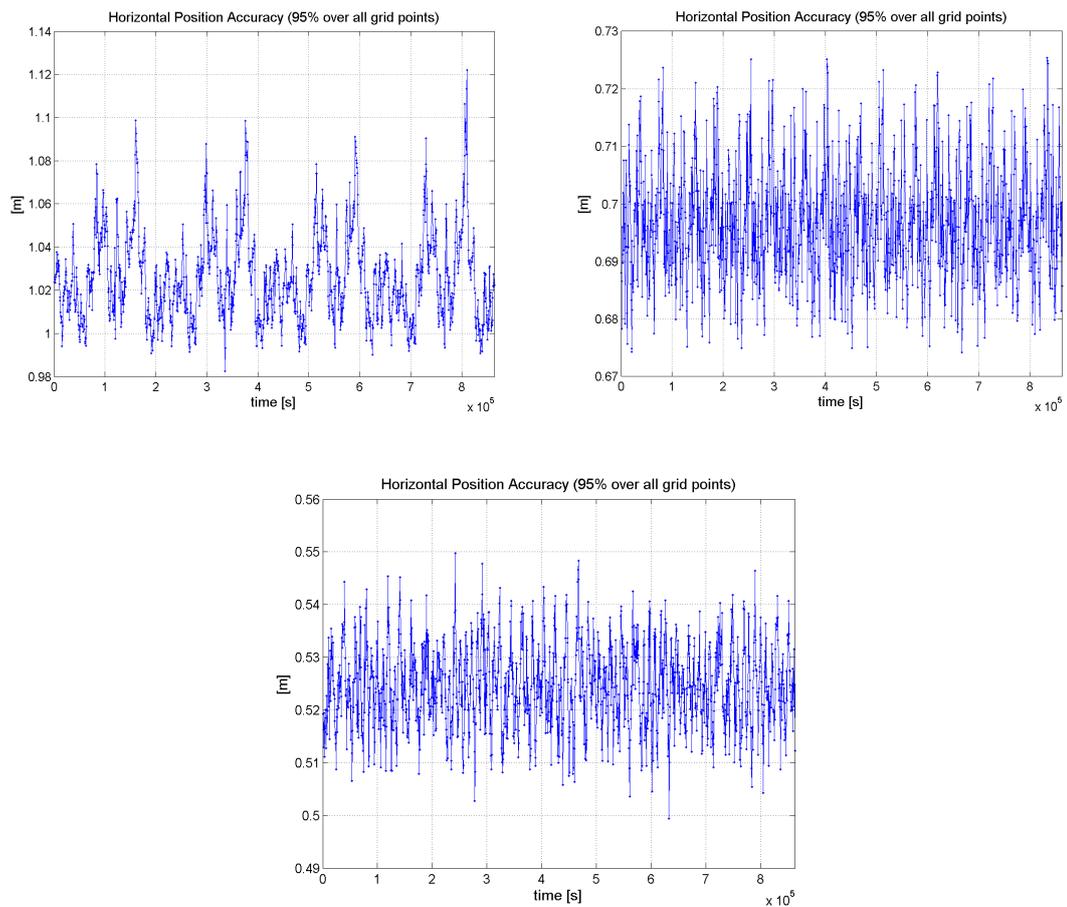
Figure 8-4: Horizontal Position Accuracy shown as 95-percentile over all grid points as function of time (nominal biases neglected); top left: GPS only, top right: GPS+Gal, bottom: GPS+Gal+GLO

The examples shown refer to the horizontal position accuracy neglecting the presence of nominal pseudorange biases. It can be seen, that for the single constellation case the sensitivity to the geometry is higher compared to the multiple constellation cases that show a quite more stable behavior over time. The values vary around 0.60 m for the GPS only case while the values range around the level of 0.38 m for the GPS+Gal case. For the triple constellation case (GPS+Gal+GLO) the results range in the order of 0.31 m. However, the main conclusion that can be drawn from this exercise is the fact that the dependency on the geometry of the satellites decreases if more satellites are available.

8.2   Integrity Performance Results

Integrity performance results in terms of HPL as function of the user location as well as the availability have been evaluated. For both aspects a dedicated plot is shown together with the corresponding statistics. The performance analyses have been performed for the single, dual and triple constellation case. For each grid point in the service area n HPLs have been computed where n is a function of the total evaluation period and the sampling rate. In the HPL plots the 99-percentile values of the n HPL samples per grid point are shown. For the integrity availability plots the percentage of samples with HPL<HAL is shown for each grid point. For an overview of the used key algorithm parameters it is referred to the Annex A.3.

8.2.1   LSR RAIM

Figure 8-5 and Figure 8-6 show HPL and integrity availability as function of the user location for the different constellation cases. Also the presence of nominal biases on the pseudoranges (0.75 m) has been considered. The analysis is based on the single failure detection capability. That means that the probability of having simultaneous multiple failures is considered in the total integrity risk. The applied masking angle is at 5°.
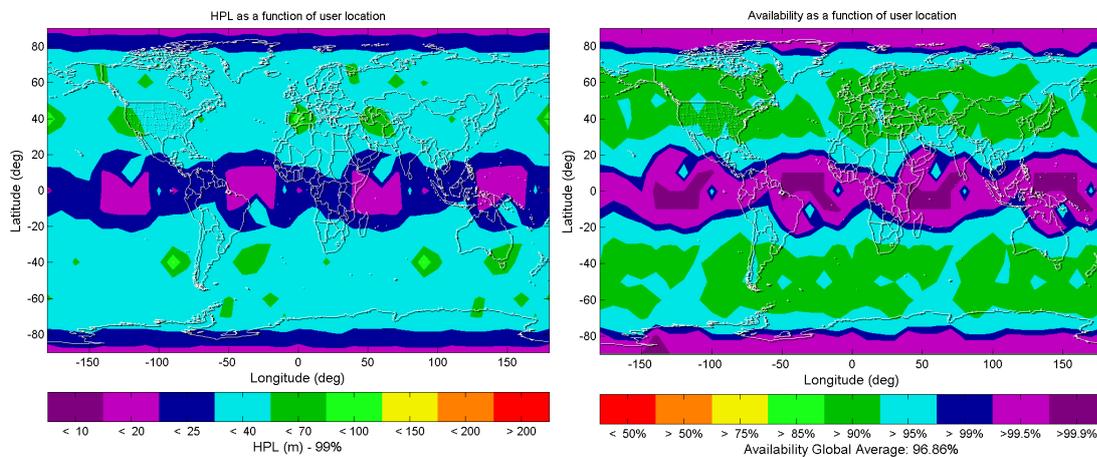

Figure 8-5: HPL (left) and Availability (right) as function of user location, nominal biases considered, GPS only
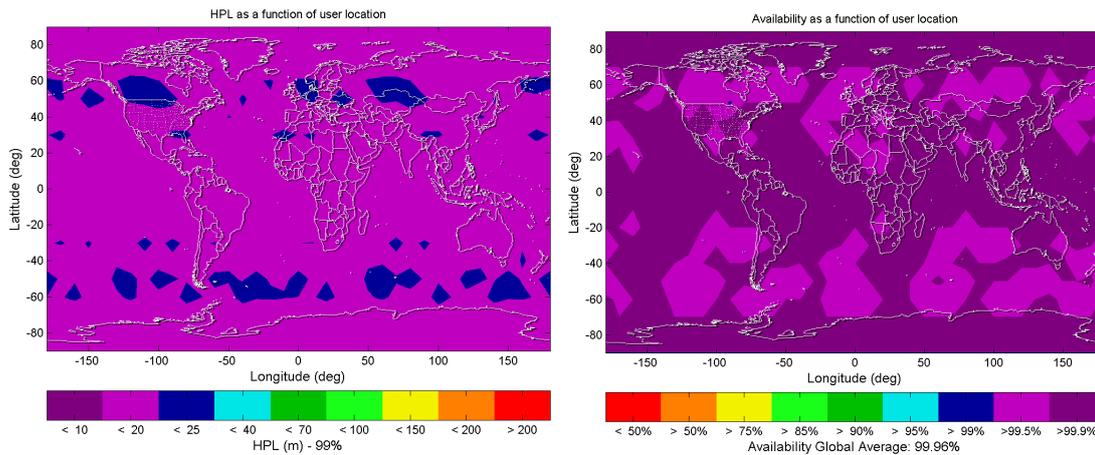
Figure 8-6: HPL (left) and Availability (right) as function of user location, nominal biases considered, GPS+Gal

Triple constellations are not considered for the LSR RAIM. The reason is that the probability of having multiple simultaneous satellite failures exceeds the requirement for the total integrity risk assuming three constellations. Due to the dis-ability of the algorithm to cope with multiple simultaneous satellite failures, a reliable integrity performance statement is not possible. The statistics of the integrity performance results are summarized in Table 8-2.

Table 8-2: Overview Integrity Performance (LSR RAIM)

Integrity Performance (LSR RAIM)							
	Availability global coverage [%]	**HPL**					
		mean [m]	**max [m]**	**min [m]**	**67-perc.**	**95-perc.**	**99-perc.**
GPS only	96.86	12.93	1735.51	4.54	13.92	22.76	30.86
GPS+Gal	99.96	7.96	33.65	2.71	8.77	14.10	17.90
GPS+Gal+GLO	N/A	N/A	N/A	N/A	N/A	N/A	N/A

8.2.2 Novel RAIM

The Novel RAIM is a new method that has been developed in the frame of this thesis. This method makes use of the specific environmental conditions that are valid exclusively for the maritime user. Namely the fact that the user moves horizontally along the sea surface is exploited. The method is described in detail in section 5.4. A HPL is computed per time step and per user location.

Figure 8-7 and Figure 8-8 show the integrity performance results for the single and dual constellation case. Also the presence of nominal biases on the pseudoranges (0.75 m) has been considered. The analysis is based on the multiple failure assumption. That means that due to dis-ability of the Novel RAIM to cope with multiple simultaneous satellite failures, this probability is considered by subtracting it from the total integrity risk respectively. The masking inclination angle for the Novel

RAIM is chosen to be 20° for the performance analyses. A dedicated sensitivity analysis is presented in section 8.4 that assesses the performance in dependency of the applied elevation mask.
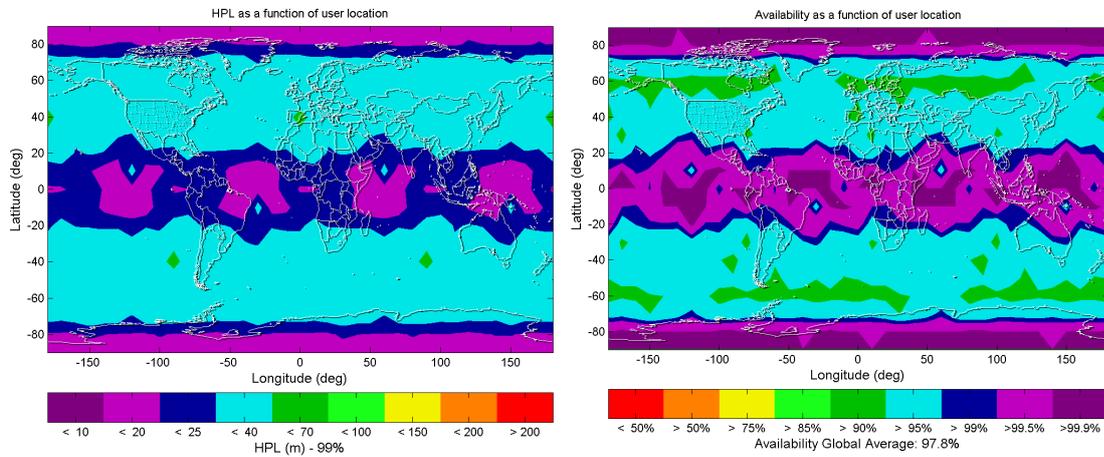
Figure 8-7: HPL (left) and Availability (right) as function of user location, nominal biases considered, GPS only (masking angle 20°)
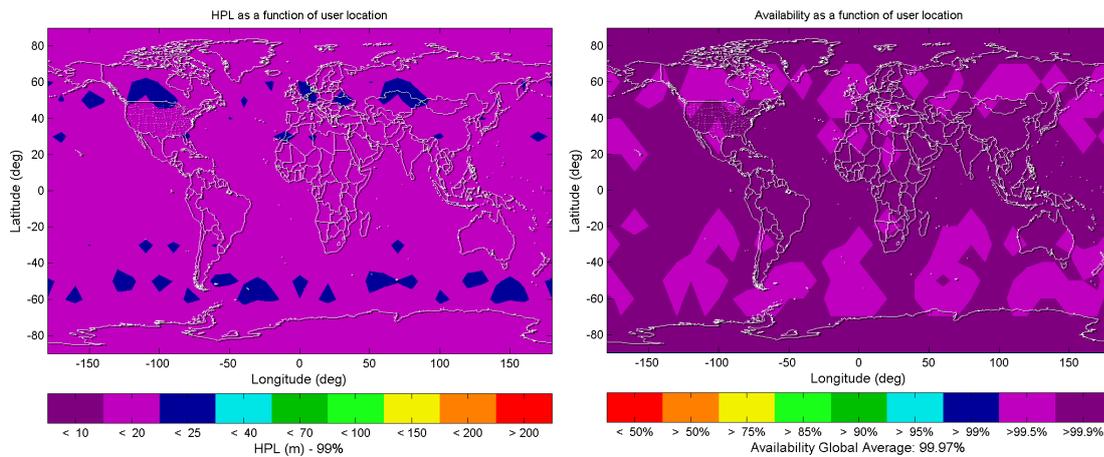
Figure 8-8: HPL (left) and Availability (right) as function of user location, nominal biases considered, GPS+Gal (masking angle 20°)

Triple constellations are not considered for the Novel RAIM. The reason is (as for the LSR RAIM) that the probability of having multiple simultaneous satellite failures exceeds the requirement for the total integrity risk assuming three constellations. Therefore, a reliable integrity performance statement is not possible. The statistics of the integrity performance results are summarized in Table 8-3.

Table 8-3: Overview Integrity Performance (Novel RAIM)

Integrity Performance (Novel RAIM, masking angle 20°)							
	Availability global coverage [%]	HPL					
		mean [m]	max [m]	min [m]	67-perc.	95-perc.	99-perc.
GPS only	97.80	12.55	962.66	4.54	13.64	21.60	28.57
GPS+Gal	99.97	7.96	33.65	2.71	8.77	14.08	17.80
GPS+Gal+GLO	N/A	N/A	N/A	N/A	N/A	N/A	N/A

8.2.3 MHSS RAIM

The MHSS RAIM approach is a development from Stanford University that has been originally developed for aviation purposes. However, this algorithm allows for flexible modelling of the threat space accordingly. This algorithm has the ability to consider multiple simultaneous satellite failures. That is the reason why for the triple constellation case, the integrity performance can be evaluated. The algorithm is described in detail in section 5.5.

Figure 8-9, Figure 8-10 and Figure 8-11 show HPL (left) and availability of integrity (right) as function of user location based on single, dual and triple constellation. The applied user masking angle is 5°.
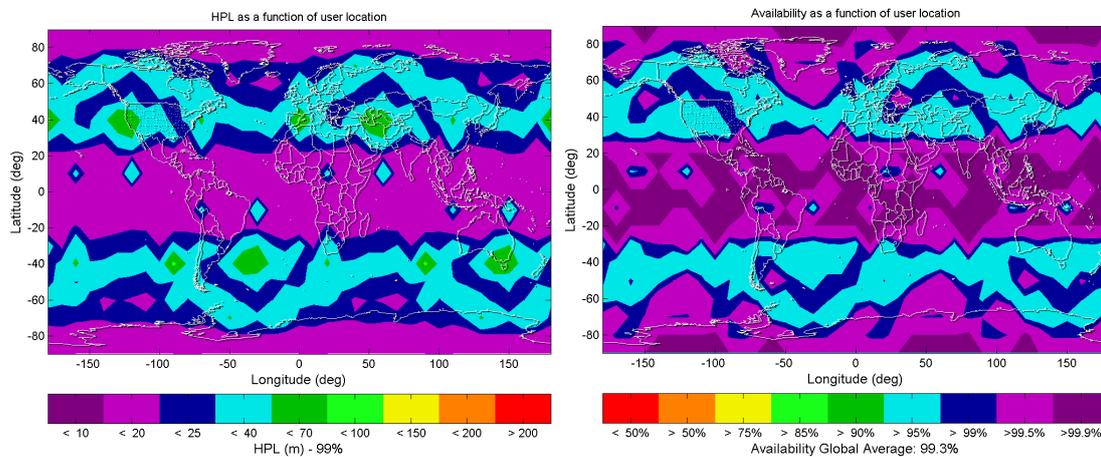


Figure 8-9: HPL (left) and Availability (right) as function of user location, nominal biases considered, GPS only
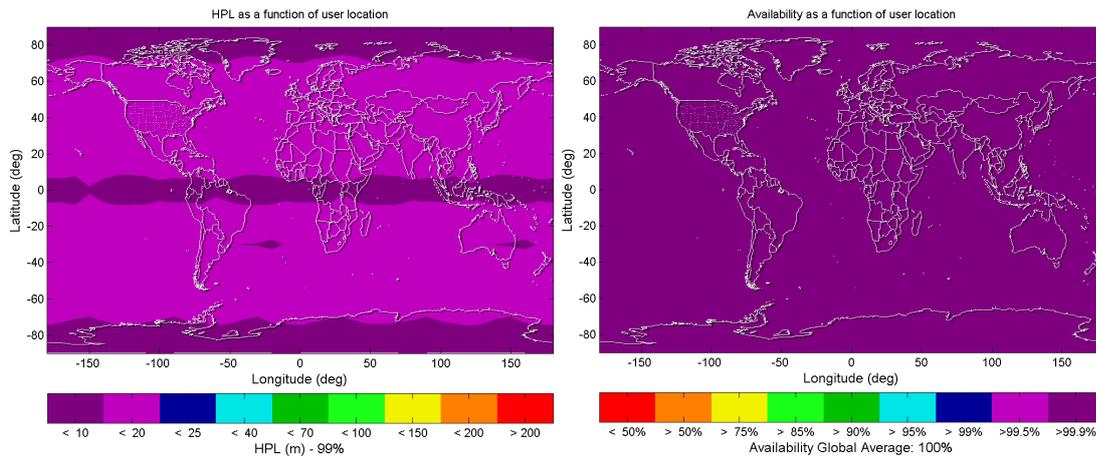
Figure 8-10: HPL (left) and Availability (right) as function of user location, nominal biases considered, GPS+Gal
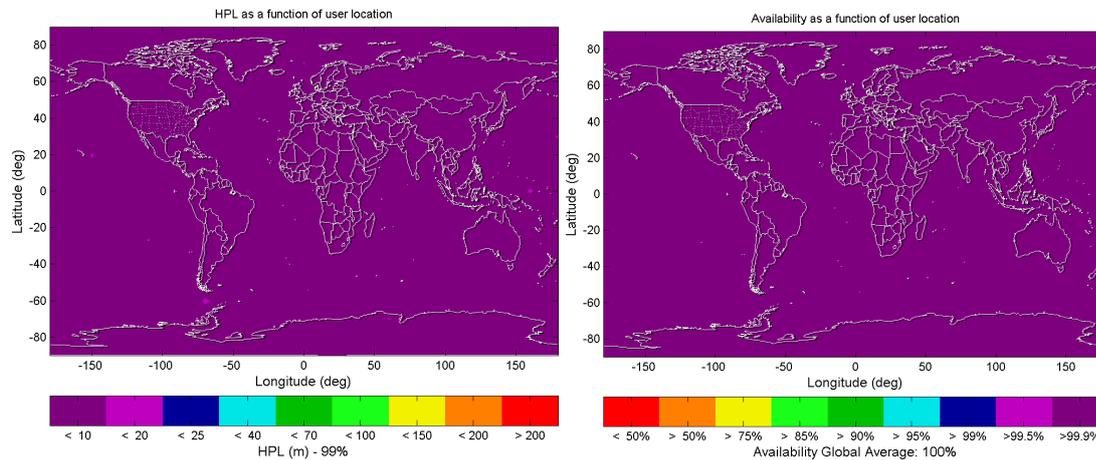

Figure 8-11: HPL (left) and Availability (right) as function of user location, nominal biases considered, GPS+Gal+GLO

The statistics of the integrity performance results are summarized in Table 8-4.

Table 8-4: Overview Integrity Performance (MHSS RAIM)

Integrity Performance (MHSS RAIM)							
	Availability global coverage [%]	HPL					
		mean [m]	max [m]	min [m]	67-perc.	95-perc.	99-perc.
GPS only	99.29	10.77	1682.85	6.59	11.14	16.55	23.12
GPS+Gal	100.00	7.61	15.74	5.69	7.97	9.74	10.99
GPS+Gal+GLO	100.00	5.55	10.51	4.47	5.74	6.63	7.20

A comparison of the integrity performance for all three algorithms is given in section 8.5.

8.3 Continuity Performance Results

Continuity performance results are given assuming a continuity time interval (CTI) of 15 minutes and 3 hours. The results are presented in a global map as function of user location showing the percentage of time where the requirement is met. Continuity is therefore a function of the number of continuity events that occurred, the CTI and the total evaluation period.

8.3.1 LSR RAIM

Two different cases using different exposure periods are investigated (15 minutes and 3 hours). It has to be noted that single and dual constellation scenarios are considered (Figure 8-12 and Figure 8-13). Due to the fact that the implemented algorithm does not account for multiple satellite failures, its probability is directly considered in the integrity risk allocation. However, when three constellations (GPS+Gal+GLO) are assumed, the probability of having multiple satellite outages exceeds the total allowable integrity risk (see Annex A.3). Continuity is assessed for each grid point on the global map using the method as described in section 7.5.2.3. The continuity results are based on the HPLs obtained in section 8.2.
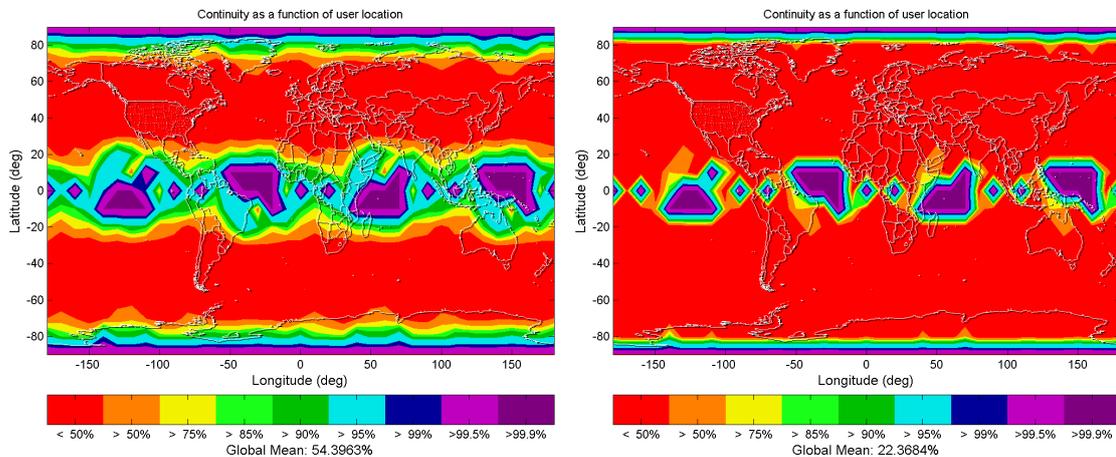
Figure 8-12: Continuity (LSR RAIM) as function of user location (left: 15 min CTI; right: 3 h CTI), GPS only
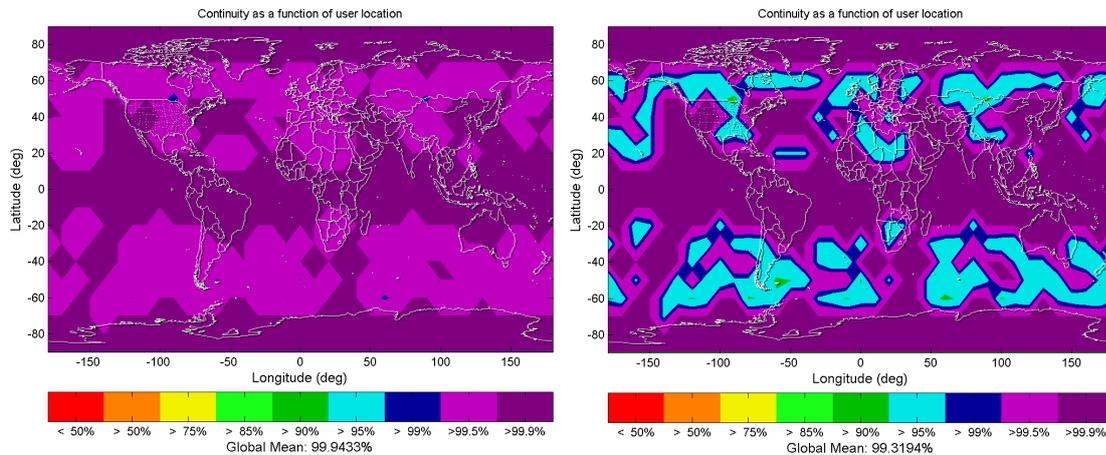
Figure 8-13: Continuity (LSR RAIM) as function of user location (left: 15 min CTI; right: 3 h CTI), GPS+Gal

The statistics of the continuity performance results are summarized in Table 8-5.

Table 8-5: Overview Continuity Performance (LSR RAIM)

Continuity Performance (LSR RAIM) Availability global coverage [%]		
	Exposure Period	
	15 min	3 hours
GPS only	54.40	22.37
GPS+Gal	99.94	99.32
GPS+Gal+GLO	N/A	N/A

8.3.2   Novel RAIM

Continuity performance is evaluated taking into account two different cases using different exposure periods (15 minutes and 3 hours). The consideration of a third constellation has been disregarded for the same reason as for the LSR RAIM. As the implemented algorithm does not account for multiple satellite failures, its probability is directly considered in the integrity risk allocation. This constitutes a hard constraint to two constellations as the probability of having multiple satellite outages exceeds the total allowable integrity risk (see Annex A.3). The results are presented in Figure 8-14 and Figure 8-15. For each scenario (GPS only and GPS+Gal), continuity performance is shown based on a CTI of 15 minutes (on the left) and on a CTI of 3 hours (on the right) respectively. Continuity is assessed for each grid point on the global map using the method as described in section 7.5.2.3. The continuity results are based on the HPLs obtained in section 8.2.
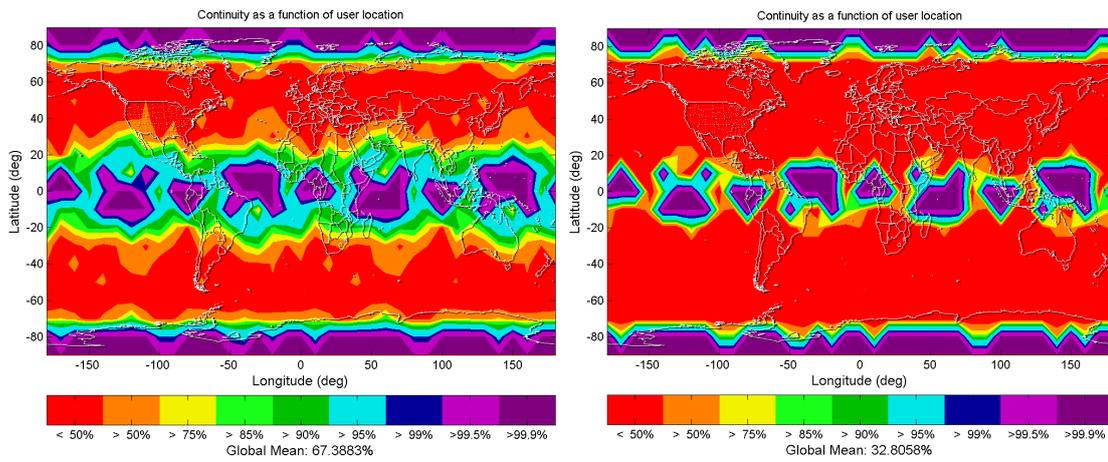
Figure 8-14: Continuity (Novel RAIM) as function of user location (left: 15 min CTI; right: 3 h CTI), GPS only
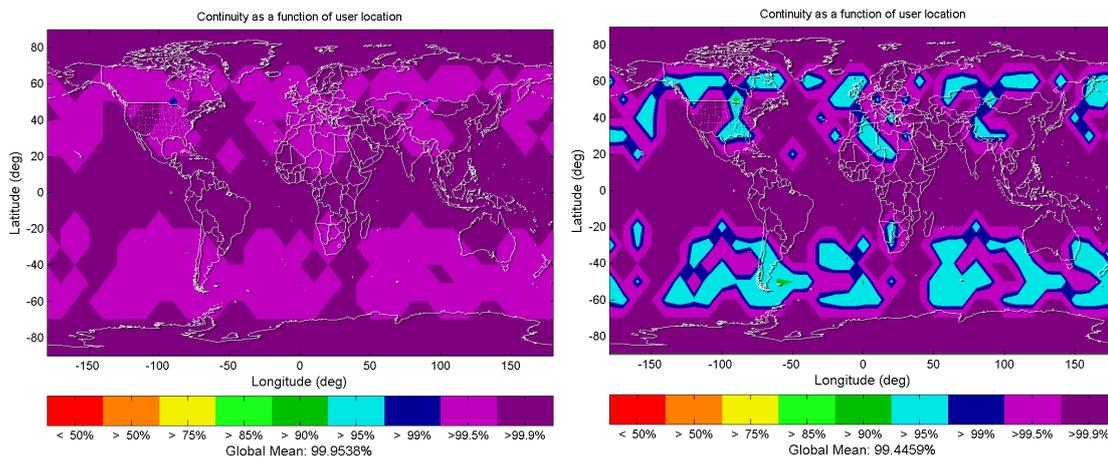
Figure 8-15: Continuity (Novel RAIM) as function of user location (left: 15 min CTI; right: 3 h CTI), GPS+Gal

The statistics of the continuity performance results are summarized in Table 8-6.

Table 8-6: Overview Continuity Performance (Novel RAIM)

Continuity Performance (Novel RAIM) Availability global coverage [%]		
	Exposure Period	
	15 min	3 hours
GPS only	67.39	32.81
GPS+Gal	99.95	99.45
GPS+Gal+GLO	N/A	N/A

8.3.3   MHSS RAIM

Two different cases using different exposure periods are investigated (15 minutes and 3 hours). It has to be noted that single, dual and triple constellation scenarios are considered (see Figure 8-16, Figure 8-17 and Figure 8-18). For each scenario (GPS only and GPS+Gal), continuity performance is shown based on a CTI of 15 minutes (on the left) and on a CTI of 3 hours (on the right) respectively. Continuity is assessed for each grid point on the global map using the method as described in section 7.5.2.3. The continuity results are based on the HPLs obtained in section 8.2.
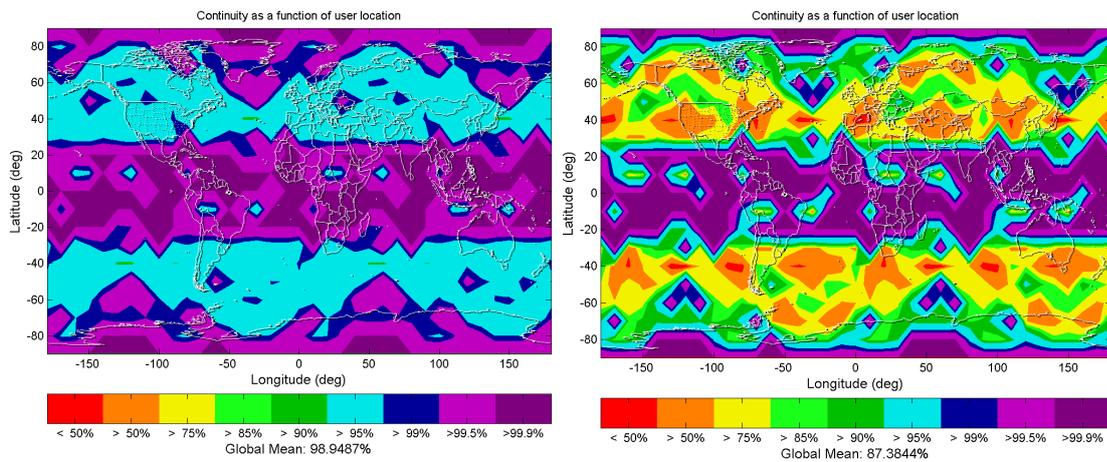

Figure 8-16: Continuity (MHSS RAIM) as function of user location (left: 15 min CTI; right: 3 h CTI), GPS only
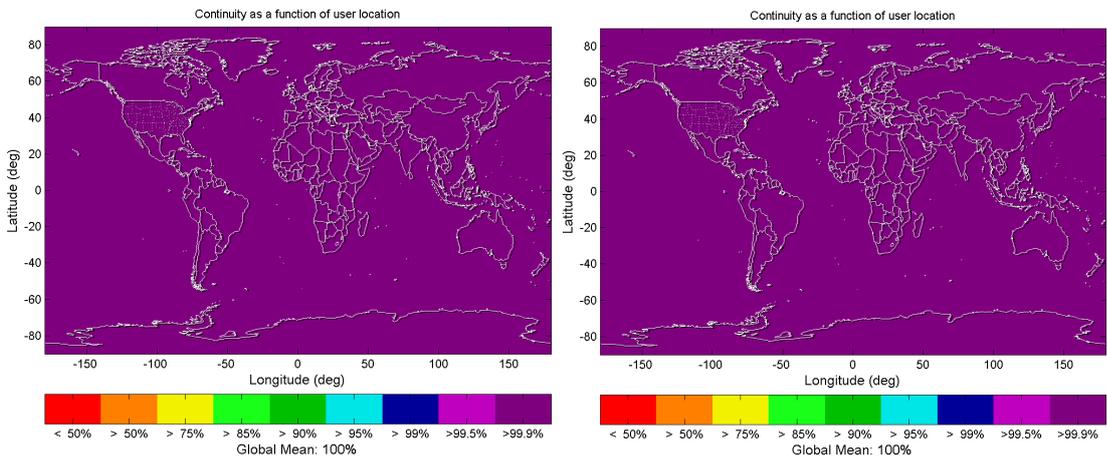

Figure 8-17: Continuity (MHSS RAIM) as function of user location (left: 15 min CTI; right: 3 h CTI), GPS+Gal
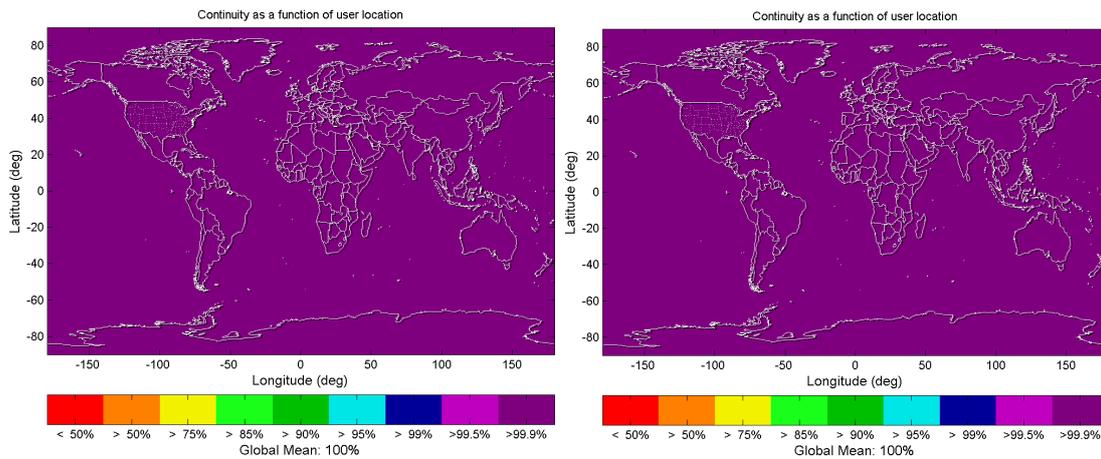
Figure 8-18: Continuity (MHSS RAIM) as function of user location (left: 15 min CTI; right: 3 h CTI), GPS+Gal+GLO

The statistics of the continuity performance results are summarized in Table 8-7.

Table 8-7: Overview Continuity Performance (MHSS RAIM)

Continuity Performance (MHSS RAIM) Availability global coverage [%]		
	Exposure Period	
	15 min	3 hours
GPS only	98.89	86.68
GPS+Gal	100.00	100.00
GPS+Gal+GLO	100.00	100.00

A comparison of the continuity performance for all three algorithms is given in section 8.5.

8.4   Elevation Dependency of Novel RAIM

One of the main drivers for the performance of RAIM is the number of available satellites and its geometry. Performance is usually defined by the worst case geometry case. This analysis evaluates the user performance based on different satellite geometries by choosing different elevation masks at user level. This approach has been chosen because – while looking at the horizontal component only – the very low satellites might introduce uncertainty to the vertical component while it usually is an advantage for the horizontal position component. Looking at the mapping factors which transforms the vertical into the horizontal domain a dependency of the elevation mask is obvious. In order to retrieve the optimum performance, a sensitivity analysis has been performed, investigating on the dependency of availability as a function of the applied elevation mask.
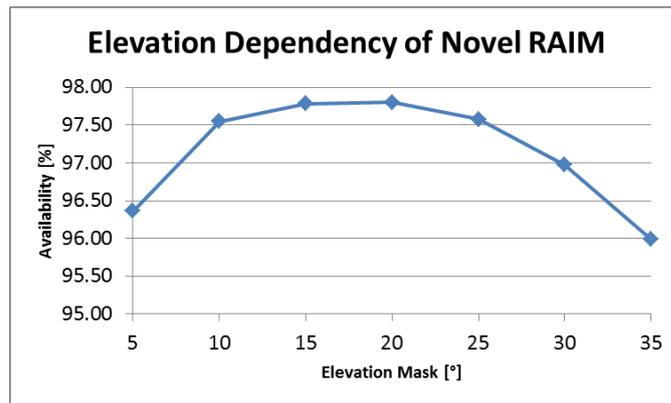
Figure 8-19: Availability of Integrity as function of Elevation Mask

For simplification reasons, availability is limited to integrity and thus neglecting continuity. A single constellation (GPS only) is assumed in this analysis. As can be seen from Figure 8-19, there exists a clear dependency on availability when choosing different elevation masks. At the lowest elevation mask of 5°, the corresponding availability is around 96%. Availability increases up to the level of 97.8% if also the elevation mask is increased up to 20°. If a higher elevation mask than 25° is chosen, then performance decreases again. This leads to the conclusion that optimal results can be achieved when choosing the elevation mask to be at the level of 20°. Although the conclusion is based on a single constellation (GPS only), the same conclusion is likewise drawn also for the dual constellation (GPS+Gal) scenario. The result from this analysis has been anticipated for the previous performance analyses.

Of course, this kind of analysis could have been performed for the other algorithms as well in order to assess the sensitivity against the elevation mask. However, this activity is not performed in the frame of this thesis but is instead identified as a potential future work.

8.5   Conclusion

Performance evaluation results are summarized based on the selected RAIM algorithms. First of all, it has to be noted that the accuracy is independent from the RAIM algorithm itself. Evaluations have been performed with and without the consideration of a consistent bias on pseudoranges on all satellites. The major outcome is that the accuracy requirement is fully met even assuming a single constellation. In addition, it has been demonstrated that – especially considering a single constellation – performance is a function of the geometry and can therefore vary quite significantly. To anticipate, this is also the main driver for the degraded performance for integrity and continuity.

Integrity performance is given with respect to its availability as well as the resulting HPLs. The availability of integrity is the percentage of available samples (over the evaluation period and with a defined sampling rate) for which the HPL complies with the HAL respectively. Continuity performance is evaluated taking into account an exposure period of 15 minutes respective 3 hours. The availability of continuity basically gives the ratio of events (HPL exceeding corresponding HAL) and the total evaluation period taking into account the sampling rate and the continuity exposure period.

The main results are summarized in Table 8-8 allowing for checking against the respective requirement values. As stated above, accuracy is not shown due its independency from the RAIM algorithms.

Table 8-8: Summary of Performance Results

Scenario	Algorithm	Avail. of Integrity [%]	Avail. of Continuity [%]	
			15 min	3 hours
Requirement		**99.8**	**99.8**	**99.8**
Single Const. (GPS only)	LSR RAIM	96.86	54.40	22.37
	Novel RAIM	97.80	67.39	32.81
	MHSS RAIM	99.29	98.89	86.68
Dual Const. (GPS+Gal)	LSR RAIM	99.96	99.94	99.32
	Novel RAIM	99.97	99.95	99.45
	MHSS RAIM	100.00	100.00	100.00
Triple Const. (GPS+Gal+GLO)	LSR RAIM	N/A	N/A	N/A
	Novel RAIM	N/A	N/A	N/A
	MHSS RAIM	100.00	100.00	100.00

The following conclusions can be drawn:

- Novel RAIM shows improved performance compared to LSR RAIM in any case. This is to be expected as Novel RAIM basically must be seen as an extension of the LSR RAIM. Hence, by design, the worst case performance cannot fall below the performance level of LSR RAIM. Especially for the single constellation scenario, a clear improvement can be observed due to more robustness of the Novel RAIM against weak satellite geometries.
- The performance of MHSS RAIM in general is higher than LSR and the Novel RAIM. This can be explained by the design of the algorithm that allows for a probabilistic weighting of the various threat cases and still fulfilling the integrity risk requirement. This is opposed to the other RAIM algorithms that solely are driven by the worst case performance.

- The LSR RAIM and Novel RAIM performance has been evaluated assuming a single constellation and dual constellation. In the Annex A.3 it is shown that the probability of having multiple simultaneous satellite failures exceeds the requirement for the total integrity risk assuming three constellations. For this reason, scenarios assuming a third constellation are neglected. The dis-ability of proper multiple fault detection capabilities of these two algorithms constitute clearly a limitation. However, the MHSS RAIM has the ability to properly cope with multiple simultaneous satellite failures and therefore results are presented up to the use of three constellations.

- The requirement in terms of integrity is met considering multiple constellations. Insufficient performance levels using a single constellation can be observed for all three RAIM algorithms. Using a single constellation reveals partly weak satellite geometries that cause outliers in the HPL time series. Thus, this perception underlines the fact that RAIM performance is strongly driven by the satellite geometry.

- The continuity requirement is met only if multiple constellations and an exposure period of 15 minutes are considered. It is clearly shown that the continuity requirement over 3 hours cannot be met by LSR RAIM and Novel RAIM. However, MHSS RAIM satisfies continuity requirements for both the 15 minutes and the 3 hours exposure period assuming multiple constellations.

Also, an additional analysis has been performed to complement and support the performance evaluation analyses. The dependency of the elevation mask of the Novel RAIM has been assessed. It is shown that performance is a function of the elevation mask applied at user level. Following the design of the Novel RAIM algorithm, it is shown that optimal performance is achieved if an elevation mask of 20° is used. This elevation mask has been used throughout the performance evaluations.

9 Advanced RAIM Related Considerations

The situation nowadays of the GNSS is such that no sufficient integrity parameters are provided to the user on a global basis. It is obvious that with the current GNSS design, integrity and continuity cannot be guaranteed to the user. To overcome this limitation, an Advanced RAIM (ARAIM) architecture is discussed in current literature [WG-C ARAIM 2015]. This architecture is supposed to complement current GNSS in order to provide integrity measures to the user. The architecture consists in principle of an additional independent monitoring network. A dedicated central processing facility collects the data from the network and computes an Integrity Support Message (ISM) in order to provide the user with the required integrity parameters. The parameters contained in the ISM shall then be used by the MHSS RAIM algorithm. ARAIM allows a ground system to provide updates regarding the nominal error characterization and fault rates for the multiplicity of contributing satellites and constellations. The infrastructure of ARAIM constitutes a third party that might take over considerable parts of the integrity burden. An important advantage of the ARAIM concept is the potentially reduced complexity of the system compared to already established systems like SBAS.

First, the ARAIM architecture and its design drivers are addressed and presented. System architecture aspects are identified and potential impacts due to the different requirements specified by ICAO and IMO are highlighted. Second, an overview of common overbounding concepts is presented together with their weaknesses and strengths taking into account maritime user environmental conditions. Third, from a user perspective, the assumption of the same model for the error contributions due to multipath and interference for the maritime user as for the aviation might be questioned. Therefore, the option of considering multipath and interference in the allocation of the integrity/continuity risk is still to be assessed. An assessment of the sensitivity of performance with respect to the contribution of multipath and interference is done and its results are outlined in this chapter.

9.1 Architecture and Design Drivers

The conventional RAIM algorithms are based on a set of fixed parameters regarding the nominal performance and fault probabilities of a GNSS. The concept of ARAIM however introduces the usage of an ISM allowing for flexibility to adapt to changing environmental conditions. The ISM is computed and disseminated by an independent ground network to the maritime user. This section indents to highlight the individual segments on a high-level basis. This allows for a better classifica-

tion and identification of the role of ARAIM dedicated infrastructure that aims at extending available and used infrastructure to allow for the provision of integrity to the user.

9.1.1 Overview of Segments

An overview of the high-level elements that will be part of the ARAIM architecture and their interactions among each other is provided. The overall architecture can be distinguished into four segments (user segment, space segment, GNSS ground segment and independent ground network). It is important to note that the first three segments that have been identified (user-, space- and GNSS ground segment) are added as part of a conventional GNSS as implemented as of today already. Thus, the ARAIM dedicated segment would be the independent reference network (IRN) together with an independent processing chain allowing deriving respective parameters as well as the capability of disseminating the derived set of parameters to the user. Thus, the interaction of the following elements allows for the provision of the needed information to allow for positioning with required integrity and continuity at user level. The following list highlights the four segments together with selected details to provide a better understanding:

- User Segment

  The maritime user is equipped with a GNSS receiver provided with multi-frequency and multi-constellation capabilities. The user positioning is based on carrier phase smoothed code measurements. Additionally, the user receiver is able to receive and introduce the content of the ISM into its internal processing.

- Space Segment

  The space segment consists of three independent constellations which will be GPS, Galileo and GLONASS. All satellites disseminate GNSS signals on multi frequencies.

- GNSS Ground Segment

  This segment comprises a global network of reference stations in charge of observing the GNSS satellites respectively on a continuous basis and providing them to a central processing facility. The processing facility will use this data to compute estimates of the satellite clock and ephemeris amongst others and to generate the navigation message which is then uplinked to the satellites. More details on the Orbit Determination and Time Synchronization (ODTS) processing can be found in [Dach et al 2007] and [Gonzalez 2013].

- Independent Reference Network (IRN)

  The IRN consists of independent GNSS sensor stations collecting all observation data from all satellites simultaneously. This observation data is collected in a central facility which is in charge of computing the parameters that go into the ISM. Furthermore the IRN has the capability to disseminate the ISM to the user [WG-C ARAIM 2012].

The relationship of these elements is depicted in Figure 9-1:
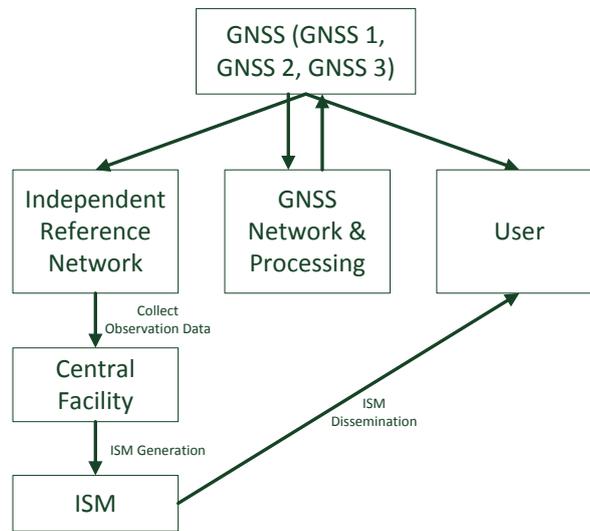
Figure 9-1: Relationship of Ground, Space and User Segment

To summarize, ARAIM architecture refers to s segment in addition to existing GNSS infrastructure comprising of an independent reference network as well as the capability of collecting and processing the data in a central facility and to disseminate the derived set of integrity related parameters to the user. Further details can be found in the next section.

9.1.2   Architectural Characteristics

This section gives an overview of the relevant characteristics and performance drivers for a potential ARAIM architecture. The following design drivers have been identified according to [WG-C ARAIM 2012]:

- Ground Monitoring Network

  The density of the ground system needed to support ARAIM can vary from sparse to dense. It can also span the globe or be confined to single sites. This reference network may be purpose-built for ARAIM or drawn from existing SBAS or GNSS networks.

- Bounding Methodology

  The bounding methodology is categorized by the amount of time that the monitors collect data before updating their estimates of the GNSS constellation health. The ground monitors may be allowed to collect data for one or more days before updating its estimates. On the other hand, the ground network may be responsible for much more rapid bounding of these parameters.

- Assertion Regarding Constellation Faults

The wide faults may be associated with a variety of assertions. These assertions range from "wide faults do not exist" to "wide faults can simultaneously effect more than one constellation".

- Content of ISM

  If present, the ISM may need only one bit per satellite to indicate whether that satellite is suitable for use. At the other extreme, it may broadcast a full set of replacement parameters for the ephemeris of every useable satellite.

- ISM Latency

  ISM latency describes the time between Integrity Support Messages (i.e. Time to ISM Alert, TIA). The TIA measures the end-to-end delay from the onset of an integrity fault to the alert in the aircraft. As such, it is strongly connected to the bounding methodology and the concept of ISM operation.

- ISM Dissemination

  The ISM may be broadcast continuously to the fleet (e.g. broadcast from SBAS or GNSS). Near the other extreme, it may only reach the aircraft at the time of dispatch. An overview of possible options on how to distribute the ISM to the user is summarized in the following [Blanch et al 2013]:

  - L-Band RNSS allocation (GNSS, SBAS),
  - VHF Aeronautical Mobile Route Services (AMRS) allocation,
  - ISM dissemination at gate dispatch.

The items listed above identify significant performance drivers in the ARAIM infrastructure that have an impact on the user performance. It is clear that for each of the identified items a wide range of implementations are possible. In total, a wide variety of different ARAIM implementations could be thought of and therefore this field constitutes a huge area of research and developments. For example [WG-C ARAIM 2015] contains analyses regarding expected ODTS performance as function of the reference network configuration. Further, it contains several analyses covering selected items above aiming at identifying an optimum architecture in terms of costs, performance and compatibility with existing GNSS and their infrastructure.

9.1.3   ISM Parameters

As indicated above, the ARAIM infrastructure is in charge of deriving integrity related parameters with which a user is able to make a statement of its integrity. Those parameters are contained in an ISM that is disseminated to the user and updated every pre-defined time intervals. A baseline set of ISM parameters has been proposed in [WG-C ARAIM 2012] and summarized for convenience in Table 9-1. The ISM baseline consists of five different parameters aiming at characterizing and describing the conditions for a user. Therefore, the nominal (i.e. fault-free) clock and ephemeris

performance, expressed as $\sigma_{URA,i}$ and $\sigma_{URE,i}$, is provided per satellite individually. These errors refer to contributions that are GNSS specific and therefore apply to all users in general. An additional parameter $b_{nom,i}$ characterizes nominal biases on the pseudorange to satellite i. Potential root causes of the presence of such biases have been summarized in section 6.7. Two further parameters are contained in the ISM that are related to a probabilistic characterization of failure rates per satellite I ($P_{sat,i}$) as well as per constellation j ($P_{const,j}$). These parameters are direct input to the MHSS RAIM algorithm and finally determine the number of potential threat cases that are to be considered and how the total integrity risk is allocated to these threat cases.

Table 9-1: ISM Baseline [WG-C ARAIM 2012]

ISM baseline	
$\sigma_{URA,i}$:	standard deviation of the clock and ephemeris error of satellite I used for integrity
$\sigma_{URE,i}$:	standard deviation of the clock and ephemeris error of satellite I used for accuracy and continuity
$b_{nom,i}$:	maximum nominal bias for satellite I used for integrity
$P_{sat,i}$:	prior probability of fault in satellite I per approach
$P_{const,j}$:	prior probability of a fault affecting more than one satellite in constellation j per approach

Various possibilities for an ISM implementation arise: for example, the validity period for each of the parameters does not necessarily need to be the same. Obviously, some parameters might change more frequently (for example $\sigma_{URE,i}$) than others (for example $P_{const,j}$). This allows for updating only a subset of all parameters at a time. Another aspect is the area of applicability of the ISM: a single ISM that is applicable on a global basis to all users is as opposed to regional areas of applicability. This of course depends also on the availability of required infrastructure to monitor the satellites respectively. The set of parameters constitutes a baseline which can be adapted in any case by removing or adding new parameters.

9.1.4 Conclusion

GNS systems as of today are not capable of satisfying integrity needs to the level of what is specified for vertical guidance in the aviation case [Blanch et al 2010a]. The desire to serve also flight operations with higher demands (i.e. LPV) justifies the ARAIM infrastructure. As has been shown regularly in the recent past, the benefit of ARAIM in terms of performance is undoubted [WG-C ARAIM 2015]. Of course, as such an infrastructure is in the development phase, it can be thought of how to widen its usage not only to aviation but also to maritime services.

Chapter 9 arranges the ARAIM infrastructure in the context of GNSS. It is highlighted that ARAIM aims at extending existing GNSS infrastructure in order to provide the required level of integrity to the user. Various architectural characteristics have been identified each with a wide band of implementation possibilities. This leads to a plethora of different options and alternatives for an ARAIM dedicated architecture.

Depending on the design of the ARAIM infrastructure, the fault monitoring burden can be split between the user and the supporting ARAIM ground system [Blanch et al 2010a]. An important aspect would be that parts of the integrity burden could be allocated to the ground infrastructure, therefore allowing relaxing the user requirements. Various fault detection techniques can be implemented on ground protecting the user against certain threats. The development of detection barriers constitutes a wide field of research. An example of a methodology for the design of integrity barriers can be found in [Soualle et al 2015].

In the following sub-sections, selected aspects regarding the ARAIM infrastructure are identified and worked out. As already mentioned, many aspects have already been investigated, such as the configuration of a potential monitoring network and its impact on various ISM parameters [WG-C ARAIM 2015]. The intention in the following is to cover selected aspects focusing on maritime services rather than aviation. An overview and review of overbounding techniques as well as selected sensitivity analyses related to the fault-free error assumptions and ISM latency are provided in the further sub-sections.

9.2 Overbounding Concepts

Protection Level equations are based on the assumption that the pseudorange error distributions are known and follow a Gaussian behavior. This assumption is very attackable and in many cases even proven to be not true [Rife et al 2004c]. So, a clear need is identified to describe any error distribution in a way to satisfy the protection level equations. The error overbounding techniques allow for describing error distributions without requiring the errors to follow exactly Gaussian behavior with known variance. An error overbound is a conservative representation of an underlying error distribution that represents the worst possible error distribution [Rife et al 2004b].

The error characteristics on the pseudoranges are not exactly known. Consequently, any construction of an error overbounding has to be based on partial information of these errors. The only information available may be measurements recorded in the past. Based on this information, estimators of the probability densities of the true errors can be determined. The common approach is that the estimators of the probability densities are constructed to be probability densities, too. Of most interest is the fact that the final position error is overbounded given the pseudorange errors

are overbounded. Therefore, it is important to understand how the estimations of the true probability densities based on data from the past propagate under convolution and scaling into the position domain.

This section gives an overview about common methods of how to overbound a given error distribution with all its advantages and disadvantages. Another aspect is the fact that the overbounding techniques lead to the impression that they act on the assumption of having sufficient statistical significance (e.g. number of samples) available. The concern, that this does not need to be necessarily the case under real life conditions, is also met in this section.

9.2.1   Overview

In real life, the errors on pseudoranges are not exactly known. It is very likely that the distribution of an error does not necessarily follow a well-characterized Gaussian distribution. This is the case when not sufficient data is available to demonstrate the characteristic of the distribution or simply when the error does not follow a known distribution (e.g. multipath). Further, the presence of an offset in a pseudorange error distribution must not be neglected and must be treated carefully. In [DeCleene 2000b] it is shown that there exist several error sources that potentially might be affected by a mean in the respective error distributions (for example multipath or mis-calibration of the antenna phase centre). However, the computation of protection levels is based on the assumption that the individual error components are following a Gaussian behavior. These assumptions about the error distributions following Gaussian behavior are not proven to be correct. In contrast, it is very likely that the tails of the probability functions are not necessarily characterized by a normal distribution [DeCleene 2000b].

Each error distribution follows certain characteristics which can be described by the following properties. Those properties do have an antagonism respectively representing basically two conditions. For example an error distribution is symmetric or not. Thus, the following characteristics of error distributions need to be considered and have direct impact on the overbounding strategy as will be discussed later.

Antagonisms

symmetry	↔	asymmetry
central	↔	non-central
unimodal	↔	multi-modal
overbound in range domain	↔	overbound in position domain

From these antagonisms, the following is assumed: the error distributions follow very conservative (however realistic) conditions about the characteristics of error contributors (asymmetric, non-zero mean and multimodal). And of course the error distribution that overbounds in the pseudor-

ange domain must also guarantee the position error to be overbounded. As will be highlighted further on, not every overbounding technique fulfils these requirements. In principle, there exist a wide range of error overbounding methods that are however based on different assumptions about the characteristics of the underlying error distributions.

The design of an error overbound can be very different: on the one hand, tight overbounds might suffer from the fact that not necessarily all errors are overbounded. In this case, a certain probability of having un-bounded errors is considerable but optimizes continuity. On the other hand, loose overbounds might have higher probabilities of overbounding the errors. This case optimizes integrity. Thus, the performance of an error overbound and its implications on integrity and continuity is closely related.

Each overbounding method has its advantages and disadvantages which will be discussed in the following. This section provides an overview of techniques used to overbound an error distribution. A further method is named the "moment bounding" which will not be further discussed within this thesis. However, for the interested reader the following reference is given [Rife et al 2004c].

9.2.1.1 Gaussian Overbounding

Pragmatically spoken, a distribution p_x can be said to be pdf overbounded by p_y if the following condition is met for all values of t [DeCleene 2000b]:

$$p_x(t) \le p_y(t)$$

9.1

This condition cannot be met for all values of t because every pdf integrates to one. In order to overcome this issue it has been proposed applying pdf bounding between specified intervals $t \le -L\sigma$ and $t \ge L\sigma$. Investigations were performed to define adequate values for L. These investigations consist of the analysis of the behavior of the error distributions after several numbers of convolutions. The result was that the tail probability is very sensitive to the shape and character of the core error distributions [DeCleene 2000b].

A proposed method in [Rife et al 2004c], [Ober et al 2001] suggests to introduce an overbound directly in the position domain. The tail bounding method complies with the PL requirement in the position domain. Its error distribution G_b has greater probability mass in the tails than the actual error distribution G_a. The following inequalities define a conservative position-domain bound when evaluated at the PL:

$$G_b(x = -PL) \ge G_a(x = -PL) \ \& \ \big(1 - G_b(x = PL)\big) \ge \big(1 - G_a(x = PL)\big)$$

9.2

However, transferring the tail bounding concept to the pseudorange error distributions does not guarantee tail bounding in the position domain. This fact clearly constitutes a constraint to this method which consequently is out of scope.

9.2.1.2   CDF Overbounding

A method called CDF overbounding has been proposed by [DeCleene 2000b] that defines an error overbound G_o provided with more tail probability mass than the actual distribution G_a for all values t [Rife et al 2004c]:

$$G_a(t) \leq G_o(t) \ for \ all \ t \leq 0$$

9.3

$$G_a(t) > G_o(t) \ for \ all \ t > 0$$

9.4

Figure 9-2 depicts an example of a CDF overbound assuming an actual error distribution G_a with a sigma of one. The red plane represents the possible area for the CDF overbound G_o.
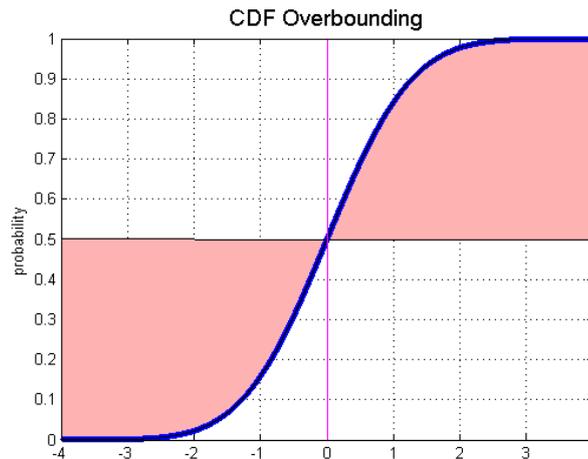
Figure 9-2: CDF Overbounding

This method reveals a true overbounding method in a sense that it has been shown in [DeCleene 2000b] that pseudorange error distributions overbounded with this method guarantee the position error to be overbounded, too. A mathematical proof for this is provided in [DeCleene 2000b]. However, it is also stated that the range-to-position conversion, the CDF overbound and the actual error distribution must obey certain shape restrictions. Namely, G_o and G_a must be symmetric, unimodal and zero-mean [Rife et al 2004c]. The fact that this bounding method is only valid under

the latter mentioned conditions marks a clear constraint for any GNSS user applications in a real environment where these conditions do not hold true anymore. The overbounding methods that will be introduced below overcome these limitations.

9.2.1.3 Paired Overbounding

In order to overcome the restrictions of an error distribution being necessarily symmetric, unimodal and zero-mean, another method has been introduced in [Rife et al 2004a]. The paired overbounding holds for arbitrary error distributions that are not necessarily required being zero-mean, symmetric and unimodal. The paired overbounding uses a set of two CDF overbounds. More precisely, the overbound is split into a pair of overbounds each for the left and right side of the error distribution (G_R and G_L) separately.

$$G_L(x) \geq G_a(x), for\ all\ x$$

9.5

$$G_R(x) \leq G_a(x), for\ all\ x$$

9.6

The overbounding CDF G_0 is constructed from the left (G_L) and right (G_R) bounds.

$$G_0 = \begin{cases} G_L(x)\ \forall G_L < \dfrac{1}{2} \\ \dfrac{1}{2}\ otherwise \\ G_R(x)\ \forall G_R > \dfrac{1}{2} \end{cases}$$

9.7

Figure 9-3 illustrates the principle of paired overbounding: an example error distribution following Gaussian behavior with a sigma of one is shown in blue. Furthermore, the possible areas in which the left bound of the distribution G_L (red) and the right bound G_R (blue) fulfill the condition for paired overbounding are depicted. In order to emphasize the compatibility of this method for non-zero mean condition, an offset in the error distribution is depicted in cyan.
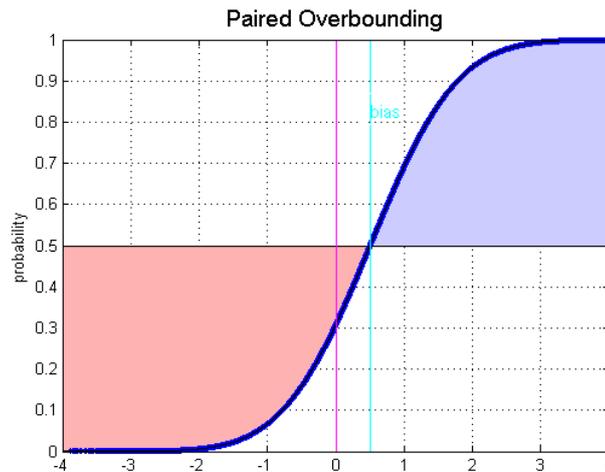
Figure 9-3: Paired Overbounding

In [Rife et al 2004a], it has been shown that paired overbounds are preserved through convolution for error distributions being not necessarily symmetric, unimodal and zero-mean. Hence, using this overbounding method, pseudorange error distribution overbounds guarantee overbounded error distributions in the position domain [Rife et al 2004b].

For paired overbounding, a restriction is mentioned in [Rife et al 2004c] that the intuitive note of a wider Gaussian distribution being be more conservative than a narrow one does not hold universally. Namely, the range of valid inflation values is limited by the shift parameter. To overcome this issue an increase of the total mass parameter K would be necessary. For further details, it is referred to [Rife et al 2004c].

9.2.1.4 Excess-Mass Overbounding

Excess mass functions are functions having all properties of probability densities but not being normalized, i.e. they can be considered as non-normalized pseudo-probability densities. Thus, the excess-mass overbounding method implies that the overbound is allowed to integrate to a probability mass higher than one. The PDF excess-mass overbound is defined as

$$K = \int_{-\infty}^{\infty} g_o(x)dx \geq 1$$

9.8

For further details on the PDF excess-mass overbound, it is referred to [Rife et al 2004c]. Likewise, the CDF excess-mass can be expressed as [Rife et al 2004c]

$$K = \lim_{x \to \infty} G_o(x) \geq 1$$

9.9

The parameter K represents the total probability mass of an error distribution and constitutes an additional degree of freedom for bounding actual error distributions. Both methods have no restrictions on distribution shape characteristics such as symmetry, local modes or non-zero means. The excess-mass overbound is defined by three parameters: total probability mass K, sigma-inflation parameter ξ and the unknown bias shift b:

$$G_L(x) = \int_{-\infty}^{x} K \cdot N(-b, \xi\sigma_a)dx$$

9.10

$$G_R(x) = \int_{-\infty}^{x} K \cdot N(b, \xi\sigma_a)dx + (1 - K)$$

9.11

Excess mass CDF bound is a generalized form of the paired overbounding. The parametrization permits the right-hand side of the overbound to take negative values and to guarantee a maximum value of 1 [Rife et al 2004c]. The same holds for the left side of the overbound but inverse. Figure 9-4 illustrates the principle of paired CDF overbounding with excess-mass. The red planes indicate the areas in which the overbound is valid on the respective side of the overbound. The probability is extended below 0 and above 1 to indicate the overbounds are allowed to exceed the total probability mass of 1 (grey areas). Additionally, for illustration an example pair of CDF overbounds is depicted (red curves).
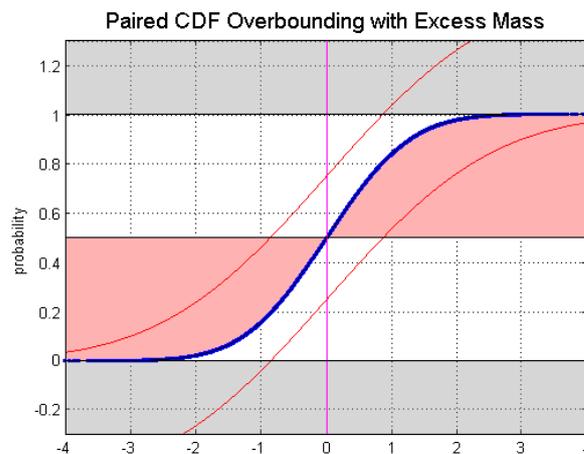
Figure 9-4: Paired Overbounding with Excess Mass

9.2.1.5   Core Overbounding

A core overbound decomposes the error distribution into two regions, a core and a tail. Each region is bounded separately. For this the theory is provided in [Rife et al 2004b] where it is shown that in principle an overbounding error distribution can be split into partial error distributions and still satisfy the overbounding condition for all values. This theory leads consequently to an error over-bound with the following form:

$$G_o(x) = (1 - P_{tail}) \cdot N(x; \sigma_n)$$

9.12

The error overbound is parameterized by two parameters: a width parameter σ and a tail probability P_{tail}. This tail probability enables the overbound to flatten itself. In doing so, no assumptions need to be made about the behavior of the underlying error distribution in its tails. This method allows for overbounding arbitrary error distributions especially with heavy tails. Based on a core overbound in the pseudorange domain, one can formulate the core overbound for the position domain [Rife et al 2004b]. The following equations shows the core overbound in the position domain after N convolutions (equal to having N satellites in view):

$$H_O(z) = (1 - P_{tail})^N \cdot N(z; \sigma_P) + \frac{1}{2} P_{im}$$

9.13

The relationship between the position error σ_P and the pseudorange variances σ_n^2 for satellite n can be found in section 5.3. The parameter P_{im} describes the total implicit tail probability and is bounded by the sum of the tail probabilities $P_{tail,n}$ in the pseudorange domain [Rife et al 2004b].

$$P_{im} \leq \sum_{n=1}^{N} P_{tail,n}$$

9.14

The position-domain bound associated with a set of core bounded pseudorange errors is itself a core bound. A mathematical proof is provided is [Rife et al 2004b]. The principle of core over-bounding is further illustrated in Figure 9-5.
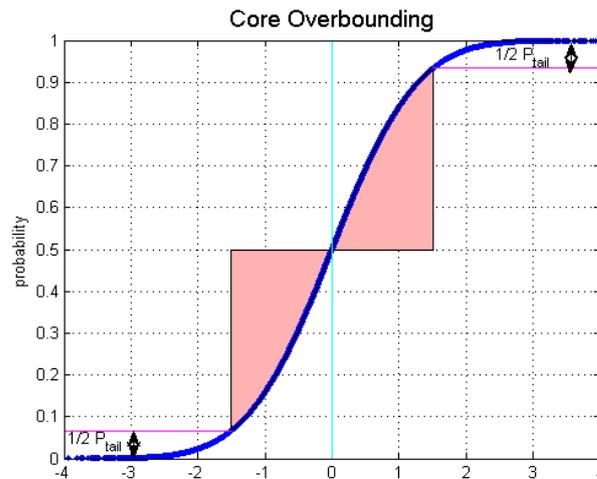
Figure 9-5: Core Overbounding

The idea that is developed in [Rife et al 2004b] is to allocate a fraction of the overall integrity risk budget to the probability that the position error exceeds its PL due to the fact that the pseudorange overbound does not overbound especially the tails of the error distributions:

$$\frac{P_{tail}}{2} = \frac{IR_{overbound}}{2N}$$

9.15

with $IR_{overbound}$ as the allocation of the IR due to overbounding, and N being the number of satellites. Here, the same value for P_{tail} is assumed for all satellite pseudorange error variances. This approach is extended to the Gaussian Core Gaussian Sidelobes (GCGS) bound that basically allows for more than one sidelobe in each tail. For the interested reader, the following reference is given: [Rife et al 2004b]. This paper [Rife et al 2004b] continues in describing the heavy tails of the error distribution by means of GCGS or Normal Inverse Gaussian distribution in order to mitigate by convolution. Heavy tails can be mitigated by convolution of non-Gaussian distributions (Central Limit Theorem). The Core Overbounding is deemed advantageous for real-time applications as it applies for arbitrary error distributions with heavy tail probabilities.

9.2.2 Impact of Reduced Number of Samples

One of the tasks of a potential ARAIM system is to state about current error characteristics in the system (for example URE or URA) [WG-C ARAIM 2015]. This task is based on an estimation process with a limited number of samples, and therefore limited statistical significance, leading to a constraint such that an overbound can only be estimated for a certain maximum percentile. The maxi-

mum percentile, that can be assessed with sufficient accuracy, is denoted as G. The probability that a sample x_i is within y is $1 - G$:

$$P(|x_i| < y) = 1 - G$$

9.16

Since not enough samples are available, the tails with smaller percentiles cannot be characterized. This approach has clearly an impact on the satellite failure probabilities. A certain probability called here overbounding risk G needs to be considered in the satellite failure probabilities for each satellite. This approach allows avoiding the use of overbounding methodologies which introduce conservative inflation factors, degrading significantly the continuity and availability performance and relying in any case on unverifiable assumptions. And at the same time, it can significantly relax the ground segment requirements, which does not need any more to guarantee bounding till small percentiles [Martini et al 2013].

The approach that is pointed out in the following is leaned on [Martini et al 2013]. It is based on the estimation of a so-called inflation factor that is used to inflate the error distribution and thus to compensate for the reduced number of available samples and its implied reduced statistical significance. The application of the inflation factor constructs the "real" distribution of the respective variate. This approach assumes that the underlying error distribution follows Gaussianity with a zero-mean. An unbiased estimator, used when the sample size is very large, is the standard deviation of the sample, denoted by S_N and defined as follows:

$$S_N = \sqrt{\frac{1}{N-1}\sum_{i=1}^{N}(x_i - \bar{x})^2}$$

9.17

with x_i being the observed values and $\bar{x}$ being the sample mean value of these observations over N samples. The ratio between S_N^2 and σ^2 is χ^2-distributed with $N - 1$ degrees of freedom:

$$\frac{(N-1)S_N^2}{\sigma^2} \sim \chi^2_{N-1,G}$$

9.18

Assuming a confidence level for which the probability of the ratio between S_N^2 and σ^2 is smaller than its corresponding value according to the χ^2-distribution is denoted as:

$$P\left(\frac{(N-1)S_N^2}{\sigma^2} \leq \chi_{N-1,G}^2\right) = G$$

9.19

The variance σ^2 is a (theoretical) variance which is assumed to be kown. From this equation the following formula can be derived by reposition:

$$P\left(S_N\sqrt{\frac{N-1}{\chi_{N-1,G}^2}} \leq \sigma\right) = G$$

9.20

It can be concluded that the inflation factor is derived as follows:

$$Inflation\ Factor = \sqrt{\frac{N-1}{\chi_{N-1,G}^2}}$$

9.21

Figure 9-6 (left) shows the sensitivity of the inflation factors as function of the number of available samples N based on different given value for the overbounding risk G. In addition, Figure 9-6 (right) shows the sensitivity of the inflation factors as function of the overbounding risk G based on different number of samples N. The inflation factors depend on the number of samples N and the overbounding risk G. The more samples N are available the smaller the inflation factors get. Also it can be observed that the smaller G gets, the higher the inflation factors become (because the tails of the distributions will be more exploited).
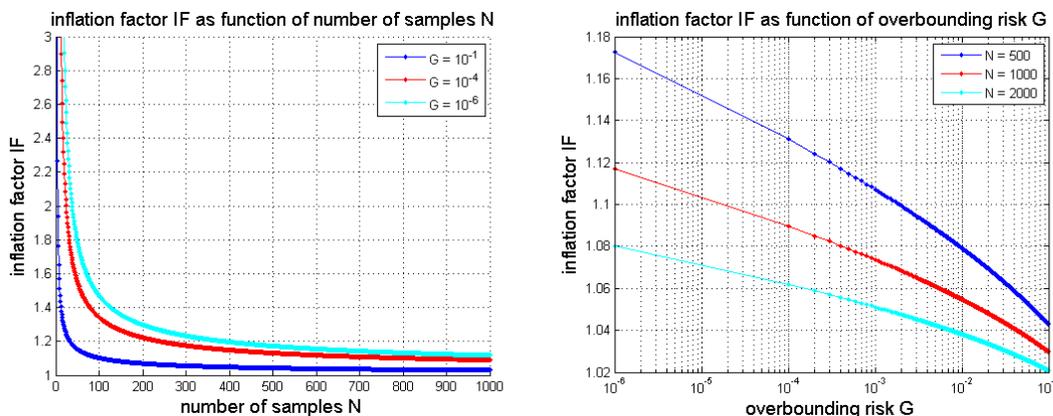
Figure 9-6: Inflation factors as function of number of samples N (left) and of overbounding risk G (right)

It has been shown that an error distribution that is based on a limited number of samples lacks of statistical significance. In order to compensate for this drawback, an inflation factor is derived that can be used to inflate the respective error distribution. Therefore, an additional parameter, namely an overbounding risk G is introduced. For a potential ARAIM design, the introduction of an overbounding risk parameter G in the ISM may be an option. This allows for reducing the integrity burden in the ground segment.

9.2.3   Conclusion

Different error overbounding techniques have been introduced and summarized. Each method enables overbounding of error distributions under certain conditions. An important point is that an error overbound in the pseudorange domain must guarantee an overbound of the position error as well. This requirement must be fulfilled. However, it turns out that there are overbounding techniques that guarantee this requirement only under certain conditions. Table 9-2 summarizes for each introduced overbounding method the conditions for an error distribution so that the requirement is fulfilled.

Table 9-2: Overview of Overbounding Methods

Method	Comment
Gaussian Overbounding	It allows for non-zero means, but still requires symmetry and unimodality.
CDF Overbounding	The real distributions must be zero-mean, symmetric and unimodal.
Paired Overbounding	It allows asymmetry, multiple modes and non-zero means.
Excess-Mass Overbounding	This method is similar to paired overbounding.
Core Overbounding	This method yields the same advantages as above, but also allows for uncertain tails.

DeCleene [Rife et al 2004b] has shown that in order to guarantee overbounding in the position domain, given overbound errors in the pseudorange domain, some pre-conditions must be fulfilled – namely that the error distributions must be symmetric, unimodal and zero-mean. Of course, these pre-conditions hardly correspond to reality. To overcome this limitation selected further methods are introduced in literature allowing for arbitrary error distributions to be overbounded (paired-, excess-mass- and core overbounding). All methods imply certain knowledge about the tails of the error distribution. However, the core bounding concept does not. Considering an unconsolidated multipath error model in the maritime context, this might be a favourable option. Applying core overbounding would potentially lead to an additional parameter in the ISM – namely a representative value for P_{tail}. It can be stated that the fact whether the error overbounding results in tighter or looser overbounds is strongly dependent upon the update rate of the error contribution parameters

contained in the ISM, and thus the number of available samples to estimate an error overbound. Moreover, the possibilities for parametrization of the error overbounds are limited due to bandwidth limitation.

Further, a method is highlighted that is leaned on [Martini et al 2013]. It is based on the estimation of a so-called inflation factor in order to compensate for a reduced number of available samples and its implied reduced statistical significance. The application of the inflation factor constructs the "real" distribution of the respective variate. This approach assumes that the underlying error distribution follow Gaussianity with a zero-mean. This aspect becomes relevant in case of high ISM update rates and a respective limited number of samples are available to estimate the respective ISM parameters. An intuitive way to increase the number of samples would be simply to take as many historical data as required. However, this approach is deemed not representative for the current state of the system respectively. Hence, the use of "newer" data should be targeted.

9.3   Sensitivity Analyses

The performed sensitivity analyses cover selected aspects regarding the assumptions that are made for ARAIM. Having pointed out an overview of the overbounding techniques and their challenges in the latter section, the first two aspects are related to the fault-free error models for multipath and interference. Fault-free error models – in particular for multipath– are well defined and commonly available for the aeronautic user which is agreed and documented accordingly in [RTCA 2006]. It is questionable, if these models are applicable for maritime users as well. The lack of a dedicated error model for multipath and interference for maritime applications drives the investigation on the question to which extent the existing models can be transferred to maritime applications. These analyses are based on the multi-constellation assumption. A third aspect is on the ISM latency and its impact on the ISM parameters. This aspect drives the ARAIM architecture design as for example a minimum required ISM latency presumes conditions that might exclude potential communication means beforehand. More details are provided below in this section.

9.3.1   Multipath

The impact of multipath –being an effect that depends on the user environment– is described with an empirical and elevation dependent model defined in [RTCA 2006]. One of the assumptions that is implied within this model is that the aviation user does not experience multipath contributions exceeding the model. As opposed to the aviation, the environmental conditions for a maritime user are different. Aa a maritime user moves along a sea surface the probability of the GNSS receiver receiving reflections of the GNSS signals is increased compared to relatively controlled conditions on an airplane. Two ways to overcome this issue have been identified: on the one hand, one could

define more stringent requirements on maritime GNSS hardware including antenna and increase the ability of the antenna mounted on a ship to protect from reflections of the GNSS signals. This could be done by either mounting adequate shields or implement software-based solutions (filters, etc.). On the other hand, one could adapt the multipath error model. However, no representative study has been performed over a sufficiently long period leading to an adequate error model for the maritime user with sufficient statistical significance.

The motivation for the following analysis is to assess the margin with respect to modelled multipath contribution and its impact on user performance. The impact of multipath on the GNSS signal is modelled as an additional bias in the error distribution on the pseudorange. Multipath might either impact one or more pseudorange measurements at user level. Therefore, two different scenarios are defined:

- The first scenario that is followed assumes a single pseudorange being impacted by multipath. That is to assess the maximum allowable bias on a specific pseudorange that is linked to the satellite – out of all satellites that are in view of the user – whose error contribution is most sensitive to positioning accuracy (critical satellite). In other words, assuming equal error contributions on all satellites being in view, the critical satellite is defined as the one whose contribution maps into horizontal position component to the largest extent. The multipath contribution will be modelled as a bias on the pseudorange measurement on a satellite I corresponding to the critical satellite.
- The second scenario is based on the assumption that all satellite measurements are affected with a bias simultaneously. There is no justification from a physical point of view that all pseudoranges at user level are afflicted with a bias of the same magnitude. The justificiation of this assumption is that all different multipath biases are overbounded by the maximum bias on a single pseudorange. This simplifies the analyses by abstracting the assumptions; however, this is deemed to be worst case scenario.

Both scenarios will be separately assessed with respect to the performance based on varying magnitudes of the additional bias on the respective pseudoranges. The strategy will be such that for each HPL that is computed per user location and time step, the bias on the critical satellite (and the bias on all pseudoranges respectively) will be incrementally increased as long as the following condition holds true:

$$HAL - HPL \leq TH$$

9.22

The respective threshold TH is a configurable parameter. In case the HPL exceeds already its HAL even if no bias is assumed on the respective pseudoranges for the satellites, the result for this

particular user location and time step is neglected. However, as demonstrated from previous performance evaluations, the multi-constellation scenarios provide full coverage of availability at any time. Consequently, there is a margin to be expected on all pseudoranges in view of the user.

9.3.1.1 Maximum Allowable Bias on Critical Satellite

This scenario assumes a single pseudorange being impacted by multipath. For that purpose, the critical satellite is chosen to be the one being affected by multipath. The critical satellite is defined as the satellite whose contribution to positioning accuracy (here horizontal component) is the most sensitive compared to the other satellites. That means that assuming n scenarios (with n satellites in view) with each the same bias on the pseudorange respectively, the positioning performance would be the most impacted if the bias is assumed for the critical satellite. The critical satellite can be identified using the projection matrix S (see section 5.3) describing the mapping from range into position domain (east and north position component):

$$critical\ satellite = max\left(\sqrt{S_{east}^2 + S_{north}^2}\right)$$

9.23

Selected statistics are summarized in Table 9-3. The simulation is based on a period of 10 days with a sampling rate of 600 seconds for both scenarios (dual and triple constellation). The constellation parameters are summarized in Annex A.2. A global grid with a sampling for latitude and longitude of 10° is used. For each grid point an elevation mask of 5° is applied. The derived statistics are based on the accumulated results over all time steps that have been evaluated per user location. For the derivation of the results, a threshold TH of 0.1 m is used reflecting the granularity of the values.

Table 9-3: Statistics for Maximum Allowable Bias on Critical Satellite

Maximum allowable bias on critical satellite [m]					
	mean	min	max	95-perc.	99-perc.
GPS+Gal	4.29	1.90	13.10	5.90	6.90
GPS+Gal+GLO	6.54	3.00	15.60	8.70	9.60

The results depict the maximum allowable bias on the critical satellite for which the condition from equation 9.22 is still met. That is the maximum being at 13.1 m for dual constellation and 15.6 m for triple constellation. A difference in the order of 2-3 m can be observed between the two or three constellation based scenarios. The more satellites are available, the higher the maximum allowable bias on a critical satellite can get. This can be explained by the robustness of the position solution with a higher number of satellites. This perception is underlined by the cumulative distribution functions (CDF) accordingly as shown in Figure 9-7.
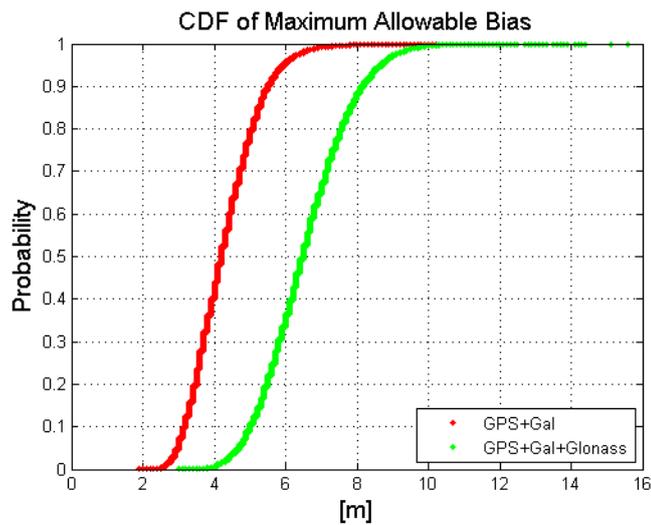
Figure 9-7: CDF of Maximum Allowable Bias (on Critical Satellite)

Another interesting aspect is the global distribution of the maximum allowable bias on a critical satellite. The maximum values per user location respectively are shown in Figure 9-8. A clear latitude dependency can be observed correlating with the typical geometry and number of satellites for the respective regions.
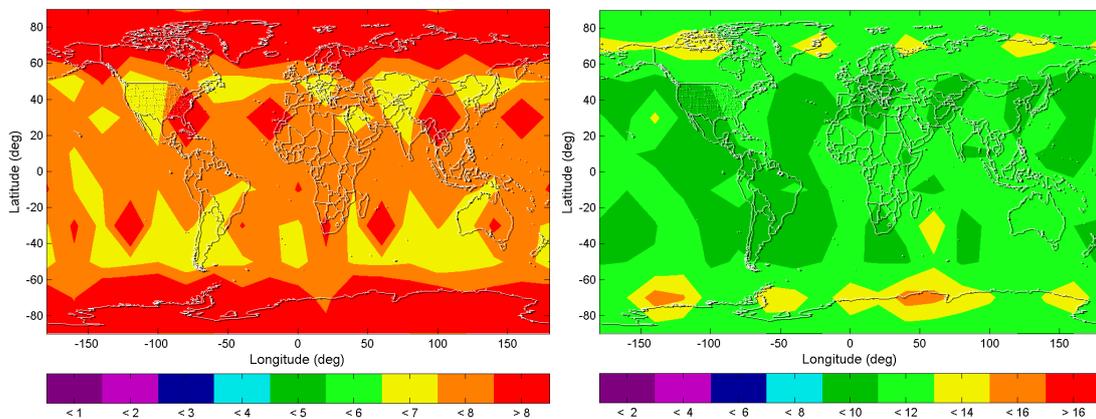
Figure 9-8: Maximum Allowable Bias on the Critical Satellite for dual (left) and triple (right) constellation scenarios (maximum values per user location)

An excerpt of the corresponding time series of the maximum allowable bias for two specific user locations is shown in Figure 9-9. The two user locations correspond to an equatorial location with latitude of 10 degrees (left) and a polar location with latitude 90 degrees (right). For both stations a longitude of 0 degrees has been chosen. The corresponding HPLs (in red) and the determined

maximum allowable bias on the corresponding critical satellite (in blue) are shown covering approximately a period of 2 days. The results below refer to a dual constellation scenario based on GPS and Galileo.
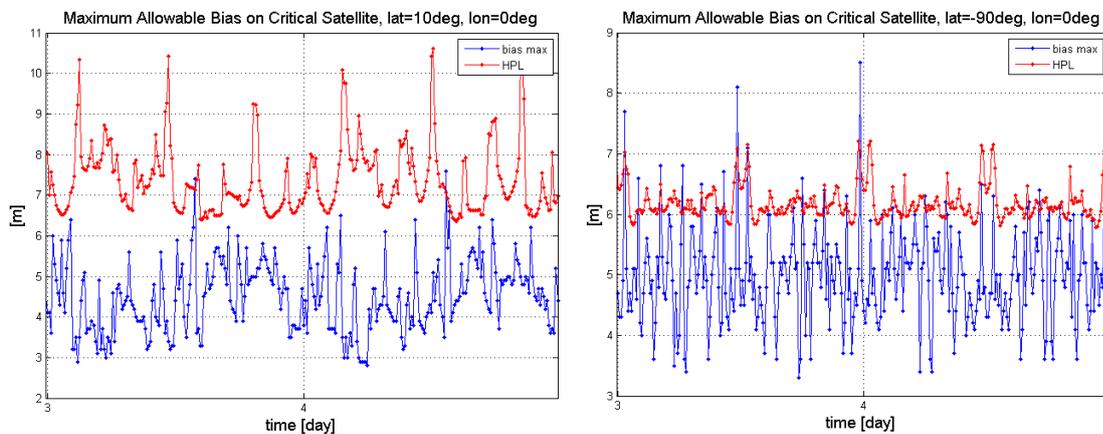
Figure 9-9: Maximum Allowable Bias versus its HPL over Time (GPS+GAL). Left: polar region; right: equatorial region

The HPLs shown in Figure 9-9 have been computed based on the assumption that every pseudorange is affected with a nominal bias of 0.75 m. It can be observed that both time series for the HPL as well as the maximum allowable biases on the critical satellite respectively show spurious outliers. In cases where the outliers from both time series coincide, it appears that there is an increased margin for a bias on the critical satellites range. Obviously these are cases in which the critical satellite is less sensitive to positioning compared to other periods because the biases reach here their maximum. On the other side, some HPL values show peaks where the maximum allowable biases on the critical satellite respectively do not or even reveal comparable low values. In those cases, the critical satellites show their highest sensitivity to positioning error. These events repeat at orbital period respectively.

9.3.1.2   Additional Biases on all Satellites

The second scenario aims at assessing the maximum allowable bias given that all available pseudorange measurements are affected by multipath simultaneously. It is deemed very unlikely that all pseudoranges at user level are afflicted with a bias of the same magnitude. The justificiation of this assumption is that all different multipath biases are overbounded by the maximum bias on a single pseudorange. This simplifies the analyses by abstracting the assumptions; however, this is deemed to be the worst case scenario.

Analogously to the latter scenario, the approach is such that the biases are increased incrementally as long as the condition from equation 9.22 is still met. The maximum bias that is applied to all pseudoranges fulfilling this condition is reported here as the maximum allowable bias on all satellites. Selected statistics of the accumulated values per user location over all time steps are summarized in Table 9-4 taking into account two and three constellations.

Table 9-4: Statistics for Maximum Allowable Bias on all Satellites

Maximum allowable bias on all satellites [m]					
	mean	min	max	95-perc.	99-perc.
GPS+Gal	1.15	0.70	1.30	1.30	1.30
GPS+Gal+GLO	1.25	0.90	1.40	1.30	1.40

Granularity of 0.1 m can be observed in the results (see Figure 9-10) due to a trade-off between computational effort and accuracy of results. This granularity corresponds to the applied TH respectively. The smaller TH is chosen, the more iterations are required thus leading to higher computational effort and vice versa. However, it is ensured that these results are to be interpreted as conservative because the HPLs are compared to a "reduced" HAL: $HPL \leq HAL - TH$ (see equation 9.22). There is no significant difference between the two scenarios in the percentile values (95-percentile and 99-percentile).
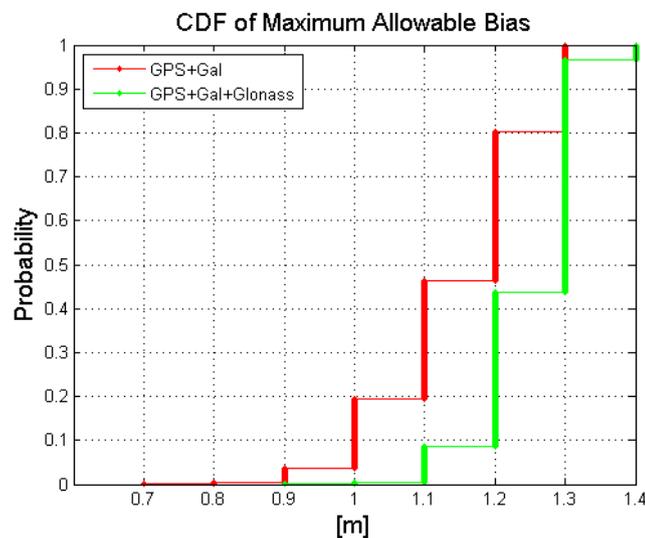
Figure 9-10: CDF of Maximum Allowable Bias (on All Satellites)

Also the global distribution as shown in Figure 9-11 of the maximum allowable bias that affects all satellites in view simultaneously reveals more latitude dependency for the dual constellation scenario compared to the triple constellation scenario. The results for the triple constellation case

are globally more homogenously distributed compared to the dual constellation case. That is mainly explained due to the fact that the geometries are more stable over time with more satellites available.
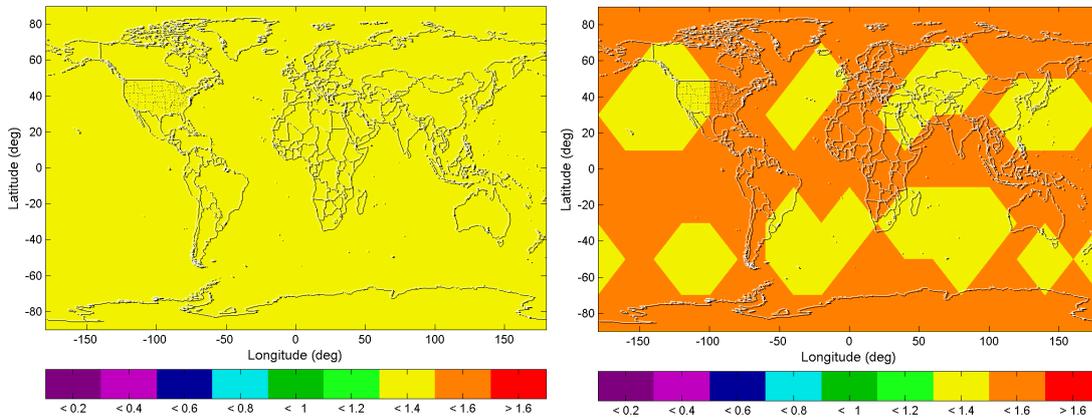

Figure 9-11: Maximum Allowable Bias on All Satellites for dual (left) and triple (right) constellation scenario (maximum values per user location)

The common offsets on all observed pseudoranges are not absorbed into the contributions of the receiver clock in the PL computation algorithm. The MHSS RAIM considers the biases on the pseudoranges in an absolute matter; meaning that the mapping factors from range to position domain are treated absolutely. Therefore, the results constitute the worst case. The presented results lead to the conclusion that the more satellites are available, the less sensitive a user becomes against multipath on one or more pseudoranges. That means that a user is more robust to multipath the more satellites are available.

9.3.2 Interference

Interference can be defined as a superposition of any undesired signal that interferes with the reception of radio waves. The usage of low power levels in GNSS might lead to unintentional interference in their frequency bands [Hofmann-Wellenhof et al 2001]. Although a large number of mitigation techniques have been investigated to improve the performance of the GNSS receivers, there is no guarantee that interference can be fully mitigated [Trinkle et al 2001]. Interference of the GNSS signals might occur during maritime operations. For example, a ship in the vicinity of a coast or another ship might experience signal interference. For that reason, another sensitivity analysis has been performed assessing the vulnerability due to interference at user level. When some interfering signal is superimposed to the received signal, this may have the following three impacts on the pseudorange measurements [Martineau et al 2009]:

- The measurements are affected by some additional noise.
- One or several measurements are affected by a bias (divergence of measurements).
- Some or all of the measurements are no longer available (loss of tracking).

In the following analysis, the impact of interference on the GNSS signal is modelled as an inflation of the error distribution on the pseudorange. The impact on performance in terms of integrity and continuity as function of the inflation of the pseudorange errors is demonstrated. The approach followed is that the error distribution on each satellite pseudorange will be incrementally inflated until the HPL equals the HAL. The following model is assumed for multipath [RTCA 2006] that will be used:

$$\sigma_{mp}(elev) = a[m] + 0.53[m]e^{\frac{-elev}{10[deg]}}$$

9.24

The strategy that is followed is the inflation of the standard deviation of the pseudorange error by increasing the parameter a. The multipath error is a contributor – amongst others – to the fault-free error budget. Other options are available to simulate an artificial inflation of the pseudorange noise, however this one is deemed straight-forward. As a starting point, parameter "a" is defined being 0.13 m according to [RTCA 2006]. The impact on performance is analysed while increasing the parameter a. Performance in terms of availability is assessed separately to account for the different maritime applications for which some of them require continuity. Figure 9-12 (left) shows the availability of integrity as function of the parameter a neglecting continuity over the defined expo-sure periods. In contrast, Figure 9-12 (right) highlights availability taking into account continuity both over the exposure period of 15 minutes and 3 hours. The horizontal line (in red) corresponds to the requirement value for the availability on the left (99.8 %) and the continuity on the right (99.97 %).
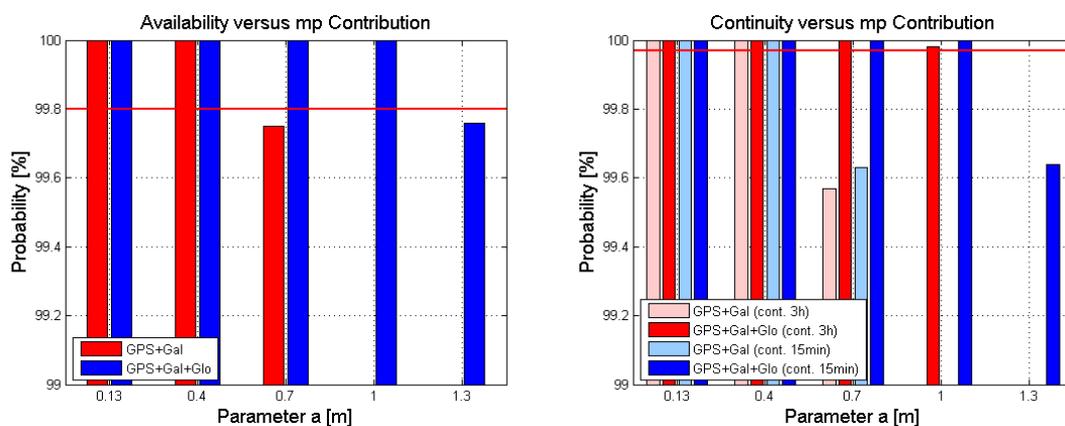
Figure 9-12: Availability (left) and Continuity (right) vs. Multipath Contribution

The perception is that there is a margin in the fault-free error budget that could be allocated to the contribution of signal interference. For dual constellation (GPS+Gal), a margin of around 0.30 m and for the scenario considering three constellations (GPS+Gal+ GLONASS) a margin of around 0.90 m is identified. These numbers are indicative as the granularity of the parameter a is 0.30 m. However, an interesting point that comes out of this analysis is that the conclusion holds the same for continuity regardless of the exposure period. Finally, it can be concluded that the presence of interference does not necessarily lead to an immediate unavailability of a maritime user. There is a certain margin, for which the maritime user is still able to cope with his overall availability demands.

9.3.3   ISM Latency

ISM latency is the period of time between two updates of one or more parameters contained in the ISM. The ISM latency which is denoted as τ_{lat} and the contents of the ISM are interdependent [Blanch et al 2013]. That means that, based on the assumed τ_{lat}, the content of the ISM needs to be adapted accordingly. ISM latency has an impact on how the ARAIM system is designed with respect to the way the ISM is distributed to the user [WG-C ARAIM 2015]:

- The dissemination of the ISM at dispatch for example is only suitable if the validity period of the ISM content is sufficiently long. A maritime user is very likely in transit for several days or even weeks.

- The dissemination via L-Band RNSS either from GNSS themselves or from SBAS is deemed a more complex solution. For such an approach the GNSS and the IRN need an interface for data exchange. The ISM content and latency are constrained by the bandwidth of such an L-Band RNSS link. Furthermore, this would imply an adaption of the applicable signal in space standards for the RNSS respectively.

- The VHF Aeronautical Mobile Route Services (AMRS) allocation is considered to be out of scope for maritime services as it is using instrastructure related to the aeronautics applications only [Eurocontrol 2010].

Another aspect is the capabilitiy to advise the user of any potential threats (for example GNSS signals that must not be used) through the ISM. Having the requirement of a Time-to-Alert (TTA) of 10 seconds, a distinction is made between threats which require the TTA to be detected and those who do not. To be consistent with the nomenclature from [Blanch et al 2013] the threats will be classified as High Dynamics Threats (HDT) and Low Dynamics Threats (LDT) respectively. The LDT refers to anomalies with higher latency than the TTA while the HDT are assumed to occur within the TTA. Two monitoring approaches are identified:

- The task of the monitoring of LDT failures (long-term monitoring) is allocated to the ground segment. This monitoring covers the fault-free integrity risk [Martini et al 2013].

- The task of the monitoring of HDT failures is allocated to the user segment (short- term monitoring). This monitoring covers the faulty case integrity risk. In the frame of ARAIM, this class of failures has been allocated to RAIM FD/FDE techniques [Martini et al 2013].

The ISM latency is therefore a relevant parameter when it comes to notifying the user of failures in the system. The shorter the ISM latency is defined, the higher the ability of the system reacting on failures and advising the user respectively. This again reduces the probabilities of failures that a user would experience. This could be done for example by integrating a flag that can be set to "use" or "do not use" per satellite into the ISM. However, this would again have an impact on the bandwidth of the ISM. The ISM latency is therefore a trade-off between several aspects to be considered.

As already stated above, the ISM parameters and latency are interdependent. A higher τ_{lat} yields more conservative ISM parameters due to compensative reasons. This property holds basically for all ISM parameters: the error characterization parameters (URE, URA and bias) as well as the failure probabilities (P_{sat}, P_{const}). The latter are assumed to grow linearly with τ_{lat}. Denoting the onset probability of a fault per time unit as P_{onset}, then the probability of a satellite fault P_{sat} should meet the following condition:

$$P_{sat} \geq \tau_{lat} \cdot P_{onset}$$

9.25

Figure 9-13 depicts the impact on P_{sat} as function of the ISM latency τ_{lat}. In this example, a P_{onset} probability of 8E-5 is assumed. This value corresponds to the satellite failure probability as derived in section 7.3. This graph shows the minimum required values for P_{sat} as conservative values are allowed according to equation 9.25.
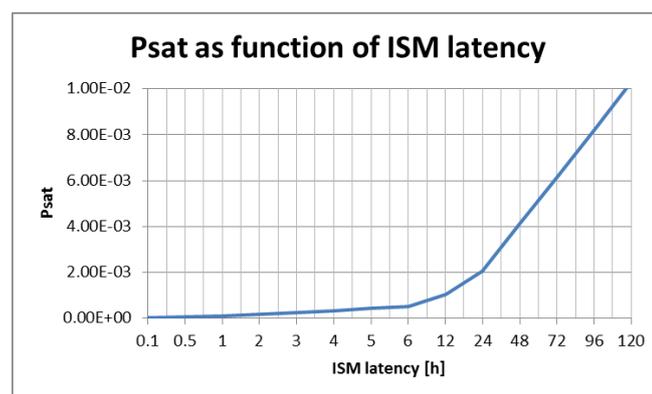
Figure 9-13: P_{sat} as function of ISM latency, based on $P_{onset} = 8 \cdot 10^{-5}$

The validation of probabilities in the order of 1E-5 would certainly require several years of uncorrelated data. Such numbers are always based on assumptions, e.g. decorrelation time or number of samples. The probability of failure for each satellite is a sum of all fractional probabilities of various pre-defined so-called Feared Events (see section 7.2). All these aspects would need to be characterized separately and summed up together to an overall P_{sat} per satellite. This is deemed a constant effort and as GNSS matures, more consolidated probabilities can be derived for P_{sat} as well as P_{const}.

Table 9-5 summarizes the performance in terms of availability based on several scenarios with different assumptions for each P_{sat}. For all the scenarios, two constellations (GPS+Gal) have been consistently assumed. The use of a single constellation does not allow the MHSS RAIM to meet the requirements (see section 8). Therefore, the dual constellation case has been defined as the worst case compared to the use of a third constellation. The aim of this analysis is to derive potential constraints on P_{sat} for which the requirement is still met. Results are depicted in Table 9-5 where the availability for integrity and continuity is shown over the various values for P_{sat} and P_{const}.

Table 9-5: Availability versus ISM Parameters

Const	ISM Parameters		Availability [%]		
	Psat	Pconst	Integrity	Continuity (15 minutes)	Continuity (3 hours)
GPS+Gal	1E-3	1E-4	100	100	100
GPS+Gal	1E-2 *)	1E-4	100	100	100
GPS+Gal	1E-3	1E-3	100	100	100
GPS+Gal	1E-4	1E-3	100	100	100

*) 20°x20° grid sampling has been used due to high computational effort.

As can be seen from Table 9-5, even for a P_{sat} up to 1E-2 the performance demands are still satisfied. On the other side, such a high value for P_{sat} yields also disadvantages: as it is shown in Figure 9-14, the number of subsets to be considered is a function of the number of available satellites and P_{sat}. The increase of the values for P_{sat} comes along with an increase of satellite subsets to be considered in the MHSS RAIM. This implies an increase of the computational effort as well.
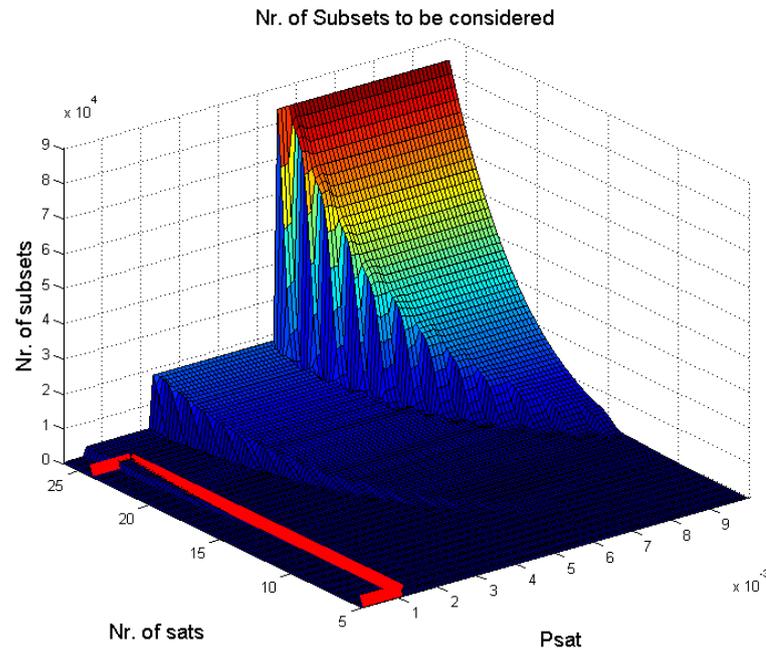
Figure 9-14: Number of subsets as function of P~sat~ and number of satellites

A threshold of $P_{sat,threshold} = \left(IR_{hor}/2\right)/10$ has been applied (see section 5.5). It can be seen that under extreme conditions (high P_{sat} and high number of satellites) the number of subsets is in the order of 9E4. From the author's experience, it can be stated that the computational effort taking into account such high numbers of subsets increases massively and its feasibility in a maritime user receiver needs to be demonstrated. In order to keep the number of subsets in a reasonable order of magnitude, the value for P_{sat} should not exceed 1E-3 (see red box in Figure 9-14). Within this range, the maximum number of subsets to be considered would be in an acceptable order of magnitude.

The original aim of this section is the derivation of a reasonable assumption for the ISM latency for maritime services. P_{sat} is assumed to be the only parameter in the ISM being interdependent with its latency. Therefore, the performance level as function of different values for P_{sat} has been assessed, motivated by identifying a reasonable maximum value for P_{sat} still satisfying the demands for a maritime user. However, P_{sat} turned out to be not a major driver for the achievable performance which has been investigated in more depth. This finding is valid for the horizontal position component but not necessarily for the vertical one. Nevertheless, another limitation has been identified that is the number of subsets to be considered in the MHSS RAIM algorithm. As shown above, if P_{sat} is higher than 1E-2, the number of subsets increases to the level of several ten thousands for which the computational load is deemed critical for real-time operations. Of course, as the

GNSS systems will mature with time, more adequate and reliable values for P_{sat} (and P_{const}) will be derived. It is shown that performance demands are still satisfied under given assumptions and together with the limitation on the number of subsets to be considered, a reasonable maximum value for P_{sat} of 1E-3 has been identified. This value would correspond to a maximum ISM latency in the order of 12 hours.

9.4   Conclusion

The performance evaluation results that are summarized in chapter 8 reveal that the MHSS RAIM method complies with the integrity and continuity requirement under the multi-constellation assumption. Thus, this method is the most promising one with respect to performance compared to the LSR RAIM and the Novel RAIM. The MHSS RAIM method is attaining attraction as it is supposed to be used as part of recent considerations towards an Advanced RAIM architecture. Those considerations are about the usage of a dedicated infrastructure that supports the user with integrity related input. The main segments consist of an independent ground reference network, a central facility that collects the data collected from the network and computes integrity related parameters. Those parameters are sent via an integrity support message to the user which applies the MHSS RAIM method. The overall architecture together with the potential design aspects are pointed out in this section.

As being one of the design drivers, an overview of the error overbounding concepts is provided in order to provide an understanding that different methodologies are available and might impact the design of a potential Advanced RAIM architecture. An error overbound in the pseudorange domain must guarantee an overbound of the position error as well. For this, it is highlighted that several pre-conditions need to be fulfilled: symmetry, unimodality and zero-mean centraility of the distribution. However, methods are introduced allowing for arbitrary error distributions to be overbounded (paired-, excess-mass- and core overbounding). Against the background of an unconsolidated multipath error model in the maritime context, the core-overbounding method is found to be a favourable option. Applying this method implies the use of an additional parameter in the ISM. Also the impact to the estimation uncertainty of an (Gaussian) error distribution against the number of available samples is assessed. To compensate for this uncertainty, an inflation factor might be introduced. This might become relevant in case the ISM update rate is so short that the number of available samples is limited in order to estimate parameters (such as URE for example) with sufficient statistical significance.

The fault-free error model (detailed in section 6) is more aviation related and thus might have inconsistencies with the environmental conditions for maritime users. This uncertainty drives the sensitivity analyses with respect to the multipath and interference error contributions. Perfor-

mance impact has been assessed in the presence of non-nominal multipath and interference. Hereby, multipath is modelled as a bias on one or more pseudoranges whereas interference is assumed to inflate the error variance on all satellites simultaneously. This analysis aims at assessing the order of magnitude for which the user is just compliance to its requirements: assuming multipath on a single pseudorange, the order of magnitude of the additional modelled biases can be up to several meters. However, in case of biases on all pseudoranges simultaneously, the additional modelled bias is still in the order of one meter. The presence of interference does not necessarily lead to an immediate unavailability of a maritime user. There is a certain margin in the order of decimeters of additional inflation of the pseudorange error variances, for which the maritime user is still able to cope with its overall availability demands. These results underline the robustness and the flexibility in the error modelling for the maritime user.

Also the aspect of ISM latency is highlighted in this section: different means of distributing the ISM to the user have been identified that directly imply constraints on ISM latencies. For example, if an ISM is distributed at gate dispatch, the design needs to account very likely long latency periods. The content of the ISM are interdependent: this is highlighted at the example of P_{sat}. This parameter scales linearly with the ISM latency. The MHSS RAIM method shows limitations if a too high value for P_{sat} is chosen. It is shown that this constraints the ISM latency to the order of approximately 12 hours.

10   Summary and Outlook

The main subject of this thesis is the performance evaluation of a maritime GNSS user. Hereby, the major focus is on the service parameters such as accuracy, integrity, continuity and availability. On the background of current developments in the field of GNSS, this thesis accommodates a multi-frequency and multi-constellation user environment. The International Maritime Organization has published service requirements for maritime services. Different sets of requirements have been identified within this thesis: ocean- and coastal operation as the operation referring to ships being not in direct vicinity of any land masses as opposed to port approach and restricted waters inland waterways. Both user operations differ mainly with respect to the continuity requirement. The first user group is not afflicted with a requirement for continuity and has therefore relaxed requirements compared to the second user group.

As discussed in detail in this thesis, the continuity requirement, being specified over an exposure period of 3 hours, does have certain implications on the threat modelling for a maritime GNSS user. The gained awareness is the fact that for integrity, a possible extension of the exposure period does not result in a higher or different number of events to be considered and their probability is assumed to grow linearly with the specified interval. Instead, for continuity, the number or type of events to be considered is different depending on the exposure period. While for the aeronautic user much shorter continuity exposure periods are applicable, certain assumptions can be formulated that are no longer valid for a maritime user. For example, the dynamics of a satellite constellation is required to be considered for a maritime user while the aeronautic user can safely assume static conditions. It is also a fact that a user has to deal with frequently updated navigation message content that might lead to discontinuity of service. Without the considerations of such threats, the consequence would be the complete unavailability of service. A detailed discussion of the latter is provided in this thesis.

The main driver for past and present developments in the field of GNSS integrity is the aviation community. Established integrity systems such as EGNOS for example are certified by the ICAO since 2011. For that reason, the conditions are far more understood for aeronautic users than for maritime users. Hereby, the fault-free error models and the threat model are of major relevance. This lack of reliability in the models drives the need for deep investigations on the question whether these models can be directly transferred for maritime users. The approach that is followed in this thesis is that the margin in those error models is assessed via a dedicated sensitivity analysis. The perception from these analyses is that there is a significant margin that can be exploited in order to relax the error models to more conservativism and still being able to cope with the service requirements.

A dedicated section summarizes the outcome of an extensive literature survey on integrity algorithms in general. Also, integrity algorithms that set themselves apart are depicted such as carrier phase based RAIM and hybridized RAIM together with INS. From this point on, a selection of RAIM algorithms is chosen that are used for further analysis within this thesis. The Least-Squares Residual Approach exploits measurement redundancy and is closely connected to the navigation solution in the receiver. On the background of multi-frequency and multi-constellation perspective, the usage of LSR RAIM gains high attraction also due to the fact that the GNSS performance is further improving. In the past, RAIM in general was only used for operations with less stringent requirements. This thesis accounts for the current and future GNSS developments and therefore the LSR RAIM has been chosen in order to assess its possibilities and limitations for maritime users. On top to the latter RAIM approach, a Novel RAIM has been developed in this thesis: it exploits the fact that maritime users move exclusively along the sea surface which is approximated by the geoid model and thus brings in an opportunity of using additional height information. The idea is to use the additional height information in order to perform a cross-check with the GNSS derived height. The possibility of performing fault detection based on a test statistic, expressed as the difference between the height derived from the geoid and the one based on GNSS, is assessed and the finding is that fault detection can be performed to a certain extent. Furthermore, a scheme is proposed in order to derive a horizontal protection level based on this test statistic. The MHSS RAIM is also introduced in this thesis: it is deemed being the algorithm used in the frame of a potential future Advanced RAIM system. A possible implementation of this system is making use of an independent reference network that is in charge of characterizing fault-free errors, satellite and constellation fault probabilities in near real-time and to provide these parameters via an Integrity Support Message to the user.

A major aspect in this thesis is the performance evaluation based on the introduced selection of RAIM algorithms. Performance is evaluated with respect to accuracy, integrity, continuity and availability. The outcome is that the usage of a single constellation is not an option to provide full service to ocean, coastal and port approach and restricted waters. The satellite geometry as being one of the main drivers for user performance gets affirmed within these analyses. Performance increases significantly if two or three constellations are used. However, LSR RAIM and Novel RAIM still struggle to satisfy the requirements. MHSS RAIM reveals full compliance for the multi-constellation scenarios and is thus the most promising approach from the selection.

A chapter is dedicated to design aspects of a potential Advanced RAIM architecture. Hereby, attention is given to identify and work out the differences in the architecture designs in general between maritime dedicated services and aviation services. Selected aspects are pointed out such as error overbounding. Also, a sensitivity analysis is provided aiming at assessing the impact on user performance based on ISM latency. A finding is that ISM latency has an impact on Advanced RAIM

system design with respect to the ISM dissemination strategy. The dissemination strategy is surely depending on the rate with which the ISM content needs to be updated. A maritime user is very likely in transit for several days or even weeks. The dissemination via L-Band RNSS either from GNSS themselves or from SBAS is identified as an option but is constrained by bandwidth and message content respectively.

This thesis aims at providing increasing awareness of the need for reliable integrity statements for the maritime user. The maritime sector is a fast growing user community heavily relying on GNSS. Therefore, the maritime user requirements need to be considered in present and future developments in the field of GNSS integrity. Future work would be required in assessing and characterizing fault-free error models, in particular with respect to local errors such as multipath and interference. Further investigations would also be required in characterizing feared events for maritime users taking into account dedicated integrity and continuity events.

Bibliography

[Abramowitz and Stegun 1972]   Abramowitz M., Stegun I.A.: "Handbook of Mathematical Functions with Formulas, Graphs and Mathematical Tables", National Bureau of Standards Applied Mathematics Series 55, tenth printing, Dec. 1972

[Baarda 1968]   Baarda, W.: "A testing procedure for use in geodetic networks". Publication on Geodesy, Niederlande, 1968, ISSN 0165-1706

[Bauer 2003]   Bauer, M.: "Vermessung und Ortung mit Satelliten; GPS und andere satellitengestützte Navigationssysteme", 5. Auflage, Wichmann Verlag, 2003

[Beattie 1988]   Beattie, J.: "The European Radionavigation Mix in the Year 2000", AV'88, Conference of the RIN, London, March 1988

[BeiDou System 2013]   BeiDou System: "Open Service Performance Standard", China Satellite Navigation Office, Version 1.0, Dec. 2013

[Betz et al 2000]   Betz J., Kolodziejski K.: "Extended Theory of Early-Late Code-Tracking for a Band limited GPS Receiver", Journal of the Institute of Navigation, Vol. 47, N°3, Fall 2000, p. 211-226

[Bilich et al 2012]   Bilich A., Schmitz M., Görres B., Zeimetz P., Mader G., Wübbena G., "Three-Method Absolute Antenna Calibration Comparison", IGS Workshop, 2012

[Blanch et al 2007]   Blanch, J. et al: "An Optimized Multiple Hypothesis RAIM Algorithm for Vertical Guidance", Stanford University, ION GNSS 20th International Technical Meeting of the Satellite Division, 25-28 September 2007, Fort Worth, TX, p. 2924-2933

[Blanch et al 2009]   Blanch, J., Mayer, C. et al: "Hysteresis in RAIM", Stanford University and German Aerospace Center, 22nd International Meeting of the Satellite Division of the Institute of Navigation, Savannah, GA, September 22-25, 2009, p. 2818-2823

[Blanch et al 2010a]   Blanch, J., Suzuki, K. et al: "Prototyping Advanced RAIM for Vertical Guidance", Stanford University and NEC Corporation, 23rd International Technical Meeting of the Satellite Division of the Institute of Navigation, Portland, OR, September 21-24, 2010, p. 285-291

[Blanch et al 2010b]	Blanch, J., Walter, T., Enge, P.: „RAIM with Optimal Integrity and Continuity Allocations Under Multiple Failures", Stanford University, IEEE Transactions on Aerospace and Electronic Systems, Vol. 46, No. 3, July 2010, p. 1235-1247
[Blanch et al 2010c]	Blanch, J., Walter, T., Enge, P.: „Status of US ARAIM Activity", Stanford University, EU/US Working Group C, Technical Meeting on ARAIM, Madrid Spain, 1 December 2010
[Blanch et al 2012]	Blanch J., Walter T., Enge P. et al: "Advanced RAIM User Algorithm Description: Integrity Support Message Processing, Fault Detection, Exclusion, and Protection Level Calculation", IONGNSS, 2012, p. 2828-2849
[Blanch et al 2013]	Blanch J., Walter T., Enge P.: "Critical Elements for a Multi-Constellation Advanced RAIM", Navigation: Journal of the Institute of Navigation, Vol. 60, No. 1, Spring 2013, p. 53-69
[Blanch et al 2014]	Blanch J., Walter T., Enge P.: „Exclusion for Advanced RAIM: Requirements and a baseline Algorithm", Stanford University, 2014
[Brenner 1990]	Brenner, M.: "Implementation of a RAIM Monitor in a GPS Receiver and an integrated GPS/IRS", Proceedings of the ION Third International Technical Meeting, Colorado Springs 1990, p. 397-414
[Brenner 1996]	Brenner, M.: „Integrated GPS/Inertial Fault Detection Availability", Navigation", Journal of The Institute of Navigation, Vol. 43, No. 2, Summer 1996, pp. 111-130.
[Brown 1988]	Brown, G., McBurney, P.: "Self Contained GPS Integrity Check Using Maximum Solution Separation", Iowa State University, Ames, Iowa, Navigation Journal of the Institute of Navigation, Vol. 35, No. 1, Spring 1988, p. 41-54
[Brown 1992]	Brown G.: "A Baseline RAIM Scheme and a Note on the equivalence of the three RAIM methods", Proceedings of the 1992 National Technical Meeting of The Institute of Navigation, January 27-29, 1992, Catamaran Resort Hotel, San Diego, CA, p. 127-137
[Brown 1997]	Brown R. G.: "Solution of the Two-Failure GPS RAIM Problem Under Worst-Case Bias Conditions: Parity Space Approach", Navigation, Journal of the Institute of Navigation, Vol. 44, No. 4, Winter 1997-1998, p. 425-432
[Chen 2011]	Chen, J.: "Analysis of the GNSS Augmentation Technology Architecture", Bejing Global Information Center of Application and Exploitation, Sep. 2011, ION GNSS 2011, p. 247-266

[China Daily Europe 2011]   China Daily Europe : "Satellite navigation system launched", De-cemeber 2011

[Dach et al 2007]   Dach R., Hugentobler U., Fridez P., Meindl M.: „Bernese GPS Software Version 5.0", Astronomical Institute, University of Bern, January 2007

[Datta-Barua et al 2006]   Datta-Barua S., Walter T., Blanch J., Enge P.: "Bounding Higher Order Ionospheric Errors for the Dual Frequency GPS User", Proceedings of the 19th International Technical Meeting of the Satellite Division of the Institute of Navigation (ION GNSS 2006), Fort Worth, TX, September 2006, pp. 1377-1392

[Davies 1990]   Davies K.: "Ionospheric Radio.", Peter Peregrinus Ltd., London, England, 1990

[DECCA 1979]   DECCA: "The DECCA Navigator. Principles and Performance of the System", DECCA Nav. Co., August 1979

[DeCleene 2000a]   DeCleene, B.: "Proof for ICAO Overbounding Requirement", Attachment B to ICAO GNSSP/WG-B Working Paper 24, January 2000

[DeCleene 2000b]   DeCleene, B.: „Defining Pseudorange Integrity – Overbounding," Proceedings of the 13th International Technical Meeting of the Satellite Division of The Institute of Navigation (ION GPS 2000), Salt Lake City, UT, September 2000, pp. 1916-1924.

[DeCleene 2001]   DeCleene B.: "Requirements" FAA WAAS Training Symposium, Ft. Belvoir, MD., Jan. 2001.

[De Heus 1982]   De Heus, H.:" Data-Snooping in Control Networks", International Federation of Surveyors – FIG – Proceedings Survey Control Networks, Meeting of Study Group 5B, 7th-9th July, 1982, Aalborg University Centre, Denmark. Schriftenreihe des Wissenschaftlichen Studiengangs Vermessungswesen der Hochschule der Bundeswehr München, Heft 7, S. 211-224, ISSN: 0173-1009

[Divis 2015]   Divis, D.: "GNSS Vulnerability Drives Proposal: U.S. Nears eLoran Decision with Broad International Implications", Inside GNSS 03/04 2015, p. 24-31

[EC 2008]   European GNSS Programmes, "Galileo Mission Requirements Document", Issue 7.0, 15.12.2008

[EC 2010]   European GNSS (Galileo): "Open Service, Signal In Space Interface Control Document", issue 1.1, Sept. 2010

[EC 2015]   European Union: "European GNSS (Galileo) Open Service; Ionospheric Correction Algorithm for Galileo Single Frequency Users", 2015

[EGM08 2008]   EGM08 (2008) Spherical Harmonic Coefficients of EGM08 (http://earthinfo.nga.mil/GandG/wgs84/gravitymod/egm2008/, last visited: 24.03.2015)

[El-Hattab 2013]   El-Hattab A.: "Influence of GPS antenna phase center variation on precise positioning", NRIAG Journal of Astronomy and Geophysics, Vol.2(2): 272-277, December 2013

[Ene et al 2008]   Ene, A., Blanch, J. et al: "Validation of Multiple Hypothesis RAIM Algorithm Using Dual-frequency GNSS Signals", Stanford University, ENC GNSS, 2008

[Erikson 2011]   Erikson, Lt Col Robert: "Global Positioning System Status", Sixth Meeting of the International Comitee on GNSS, 5.09.2011

[ESA 2014]   ESA, Navipedia, http://navipedia.org/, last visited: 6.10.2014

[Eurocae 2006]   EUROCAE WG 62, "Interim Minimum Operational Performance Specification for Airborne Galileo Satellite Receiver Equipment", White paper, May 2006.

[Eurocontrol 2010]   Eurocontrol: „Guidance on the use of ICAO Aeronautical Mobile (Route) Service VHF band (118 MHz – 137 MHz) by the Military", Ref.-Nr.: 10/06/04-63, Edition-Nr.: 1.0, 08.04.2010.

[European Union 2015]   European Union: "European GNSS (Galileo) Open Service Signal in Space Interface Control Document", Issue 1.2, November 2015

[European Union 2016]   European Union: "European GNSS (Galileo) Open Service Signal in Space Operational Status Definition", Issue 1.1, July 2016

[Forssell 2008]   Forssell, B.: "Radionavigation Systems", Artech House, 2008

[GEAS 2010]   GEAS Panel: "Phase II of the GNSS Evolutionary Architecture Study", February 2010

[Geodesy, Trends and   "Geodesy, Trends and Prospects" (book), National Research Council
Prospects 1978]   (U.S.) Committee on Geodesy, National Geodetic Information Center, 1978

[GLONASS 1998]   ICD-GLONASS (1998). "GLONASS Interface Control Document" (Version 4.0). Coordinational Scientific Information Center Russian Space Forces, Moscow. English Translation of Russian Document.

[GMV 2011]   GMV, "BeiDou General Introduction", http://www.navipedia.net/index.php/BeiDou_General_Introductio, 2011, last visited: 22.02.2016

[Gonzalez 2013]   Gonzalez, F.: "Performance of new GNSS satellite clocks", Dissertation, Karlsruhe Institute of Technology, KIT Scientific Publishing ISBN 978-3-7315-0112-1, 2013

[GPS 2016]   http://www.gps.gov/policy/legislation/loran-c/   (last   visited: 9.02.2016)

[GPS Navstar 2008]   GPS Navstar, Department of Defense: "GLOBAL POSITIONING SYS-TEM STANDARD POSITIONING SERVICE PERFORMANCE STAND-ARD", 4th Edition, September 2008

[Gratton et al 2009]   Gratton L., Joerger M., Pervan B.: "Carrier Phase Relative RAIM Algorithms and Protection Level Derivation", Proceedings of the 2009 International Technical Meeting of The Institute of Navigation January 26 – 28, 2009, p. 256-264

[GSA 2015]   European Global Navigation Satellite Systems Agency, "GNSS Market Report", Issue 4, March 2015

[Hammer 2010]   Hammer, J.: David E., "Stochastic Analysis of ADS-B Integrity Re-quirements", the MITRE Corporation, Digital Avionics Systems Conference (DASC), 2010 IEEE/AIAA 29th, 3-7 Oct. 2010, DOI: 10.1109/DASC.2010.5655473

[Hansen 1989]   Hansen, E.: „Integrated Use of of GPS and Intertial Navigation for Flight Inspections", MSc Thesis, Norw. Inst. Of Technology, Div. Of Telecomm., Trondheim, 1989

[Heck 1981]   Heck, B.: „Der Einfluß einzelner Beobachtungen auf das Ergebnis einer Ausgleichung und die Suche nach Ausreißern in den Beobach-tungen", 1981, AVN 88, Heft 1, 17-34.

[Heck 1983]   Heck B.: „Das Analyseverfahren des geodätischen Instituts der Universität Karlsruhe Stand 1983", in WELSCH, Walter (Hrsg.): „Deformationsanalysen '83 Geometrische Analyse und Interpretati-on von Deformationen Geodätischer Netze", Beiträge zum Geodäti-schen Seminar 22. April 1983 Schriftenreihe des Wissenschaftlichen Studiengangs Vermessungswesen der Hochschule der Bundeswehr München, Heft 9, S. 153-182 ISSN: 0173-1009

[Hegarty 1996]   Hegarty C.J.: "Analytical Derivation of Maximum Tolerable In-Band Interference Levels for Aviation Applications of GNSS", Proceedings of the 9th International Technical Meeting of the Satellite Division of The Institute of Navigation, Sept. 17-20, 1996, p. 439-448

[Helmert 2006]   Helmert, F.R.: „Die Ausgleichsrechnung nach der Methode der kleins-ten Quadrate", VDM Verlag Dr. Müller; Auflage: 1 (27. Dezember 2006), ISBN-10: 383640219X

[Hewitson 2003]	Hewitson, S.: "GNSS Receiver Autonomous Integrity Monitoring: A Separability Analysis", Proceedings of the 16th International Technical Meeting of the Satellite Division of The Institute of Navigation (ION GPS/GNSS 2003) September 9 – 12, 2003, p. 1502-1509
[Hofmann-Wellenhof et al 2001]	Hofmann-Wellenhof B., Lichtenegger H., Collins J.: "GPS – theory and practice". 5., Springer Verlag, Wien, 2001
[Hofmann-Wellenhof et al 2008]	Hofmann-Wellenhof B., Lichtenegger H., Wasle E.: „GNSS – Global Navigation Satellite Systems", Springer-Verlag Wien, Austria, 2008
[Hopfield 1969]	Hopfield, H.S.: "Two-quartic tropospheric refractivity profile for orrecting satellite data". Journal of Geophysical Research (74) 18/1969, S. 4487-4499
[Hopfield 1978]	Hopfield, H.S.: "Tropospheric correction of electro-magnetic ranging signals to a satellite: Study of parameters". In: RICHARDUS, P. (Hrsg.): Proceedings of International Symposium on Electromagnetic Distance Measurement and the Influence of Atmospheric Refraction. Wageningen, Niederlande, 23.-28. Mai 1978, Netherlands Geodetic Commission, Delft, Niederlande, S. 205-215
[Hoque et al 2012]	M. Mainul Hoque and Norbert Jakowski: "Ionospheric Propagation Effects on GNSS Signals and New Correction Approaches", Global Navigation Satellite Systems: Signal, Theory and Applications, Prof. Shuanggen Jin (Ed.), ISBN: 978-953-307-843-4, 2012
[Hwang 2005]	Hwang, P., Brown, R.: "RAIM FDE Revisited: A New Breakthrough In Availability Performance With NIORAIM (Novel Integrity-Optimized RAIM), Rockwell Collins Inc., Iowa State University, ION NTM 2005, 24-26 January 2005, San Diego, CA, p. 654-665
[ICAO 2005]	International Civil Aviation Organization: "International Standards and Recommended Practices", Annex 2 to Convention on International Civil aviation, Rules of the Air, Tenth edition, July 2005
[ICAO 2006a]	Commercial Aviation Safety Team/ International Civil Aviation Organization, Common Taxonomy Team, "Phase of flight definitions and usage notes", February 2006.
[ICAO 2006b]	International Civil Aviation Organization: "International Standards and Recommended Practices", Annex 10 to Convention on International Civil aviation, Volume I, Radio Navigation Aids, Sixth edition, July 2006
[ICAO 2015]	International Civil Aviation Organization, http://www.icao.int/, last visited: 2.06.2015

[ICGEM 2016]	International Centre for Global Earth Models (ICGEM), GFZ Helmholtz Centre Potsdam, International Association of Geodesy, weblink: http://icgem.gfz-potsdam.de/ICGEM/, 2016
[IMO 1983]	IMO, "IMO Resolution A.529(13) – Accuracy Standards for Navigation", 17.11.1983
[IMO 1985]	IMO, "IMO Resolution A.577(14) – Operational Status of Electronic Position-Fixing Systems", 20.11.1985
[IMO 1989]	IMO, "IMO Resolution A.666(16) – World-Wide Radionavigation System", 19.10.1989
[IMO 1995]	IMO, "IMO Resolution A.815(19) – World-Wide Radionavigation System", 15.12.1995
[IMO 1997]	IMO, "IMO Resolution A.860(20) – Maritime Policy for a Future Global Navigation Satellite System (GNSS)", 27.11.1997
[IMO 1999]	IMO, "IMO Resolution A.880(21) – Implementation of the International Safety Management (ISM) Code by 1 July 2002", 25.11.1999
[IMO 2002]	IMO, "IMO Resolution A.915(22) – Revised Maritime Policy and Requirements for a Future Global Navigation Satellite System (GNSS)", 22.01.2002
[IMO 2003]	IMO, "IMO Resolution A.953(23) – World-Wide Radionavigation System", 5.12.2003
[IMO 2011]	IMO, "IMO Resolution A.1046(27) – Worldwide Radionavigation System", 20.12.2011
[International Loran Association 2007]	International Loran Association: "Enhanced Loran Definition Document", Report Version: 0.1, 12. January 2007
[Isshiki 2008]	Isshiki, H.: "A New Method for Detection, Identification and Mitigation of Outliers in Receiver Autonomous Integrity Monitoring (RAIM), School of Naval Architecture and Ocean Engineering, University of Ulsan, ION GNSS 21st. International Technical Meeting of the Satellite Division, 16-19, September 2008, Savannah, GA, p. 151-158
[Julien 2005]	Julien O.: "Design of Galileo L1F tracking loops", Ph.D. thesis, University of Calgary, Department of Geomatics Engineering, 2005.
[Kaplan 2006]	Kaplan, E.D., Hegarty C.J.: "Understanding GPS: Principles and Applications", Artech House, Second Edition, 2006
[Kayton et al 1997]	Kayton, M., Walter, F.: „Avionics Navigation Systems", Second Edition, a wiley-interscience publication, 1997

[Klepsvik et al 2007]	Klepsvik, J. O., Ober, P. B., Baldauf M.: "A Critical Look at the IMO Requirements for GNSS", ION GNSS 20th International Technical Meeting of the Satellite Division, 25-28, September 2007, Fort Worth, TX, p. 1931-1942
[Laurel 1999]	Laurel, MD.: "GPS Risk Assessment Study: Final Report". The Johns Hopkins University Applied Physics Laboratory, VS-99-007, January 1999
[Lechner 2003]	Lechner, W.: „LORAN-C – Current Performance in Europe and Future Interoperability with GNSS", Paper No 296, Reelektronika, GNSS 2003 – The European Navigation Conference, Graz
[Lee 1986]	Lee Y. C.: "Analysis of Range and Position Comparison Methods as a Means to Provide GPS Integrity in the User Receiver", Proceedings of the Annual Meeting of the Institute of Navigation, Seattle, WA, June 24-26, 1986, pp. 1-4
[Lee 1988]	Lee Y. C.: "New Concept for Independent GPS Integrity Monitoring", Navigation, Journal of the Institute of Navigation, Vol. 35, No. 2, Summer 1988, p. 239-254
[Lee 2008]	Lee, Y., McLaughlin, M.: "A Position Domain Relative RAIM Method", The MITRE Corporation, Center for Advanced Aviation System Development (CAASD), IEEE, 2008, p. 271-284, DOI: 10.1109/PLANS.2008.4570016
[Lee 2013]	Lee Y. C.: "New Advanced RAIM with Improved Availability for Detecting Constellation-wide Faults, Using Two Independent Constellations", NAVIGATION, Journal of The Institute of Navigation, Vol. 60, No. 1, Spring 2013, pp. 71-83
[Lehmann et al 2006]	Lehmann R., Scheffler T.: "Zur Grobfehlererkennung in geodätischen Deformationsnetzen", Hochschule für Technik und Wirtschaft Dresden (FH), Hochschule Magdeburg-Stendal (FH), 7. Geokinematischer Tag, Freiberg, 2006
[Liu 1998]	Liu F., "Airborne Multipath Analysis", Presentation given to RTCA SC-159 WG-4, December 1998
[MAAST 2014]	MAAST – Matlab Algorithm Availability Simulation Tool (http://waas.stanford.edu/staff/maast/maast.html, last visited: 22.10.2014)
[Martineau 2008]	Martineau, A: „Performance of Receiver Autonomous Integrity Monitoring (RAIM) for Vertically Guided Approaches", PhD thesis, Université de Toulouse, 2008

[Martineau et al 2009]   Martineau, A., Macabiau, C.: "GNSS RAIM Assumptions for Vertically Guided Approaches", ENAC, 22nd International Meeting of the Satellite Division of The Institute of Navigation, Savannah, GA, September 22-25, 2009, p. 2791-2803

[Martini et al 2013]   Martini I., Rippl M., Meurer M.: „Integrity Support Message Architecture Design for Advanced Receiver Autonomous Integrity Monitoring", Proceedings of ENC 2013, Mai

[Mayer 2006]   Mayer, M.: "Modellbildung für die Auswertung von GPS-Messungen im Bereich der Antarktischen Halbinsel", Dissertation, Deutsche Geodätische Kommission bei der Bayerischen Akademie der Wissenschaften, Reihe C, Heft Nr. 597, 2006

[Miaoyan 2008]   Miaoyan, Z. et al: "Multi-Constellation RAIM for Simultaneous Double-Fault Satellite Scenarios", Beihang University, Beijing, China, ION GNSS 21st. International Technical Meeting of the Satellite Division, 16-19, September 2008, Savannah, CA, p. 123-131

[Milner et al 2011]   Milner, C, Feng, S. et al: "A Holistic Approach to Carrier-Phase Receiver Autonomous Integrity Monitoring (CRAIM)", Proceedings of the 24th International Technical Meeting of The Satellite Division of the Institute of Navigation (ION GNSS 2011), September 20 – 23, 2011, Oregon Convention Center, Portland, Oregon, Portland, OR, p. 2689-2695

[Mink et al 2013]   Mink M, Daubrawa J.: "Do More Satellites Really Lead to A Better Integrity Performance? A Demonstration for SBAS", Proceedings of ENC 2013, May

[Mink et al 2015]   Mink M., Heck B.: "Performance of a Novel RAIM Considering the IMO Requirements", MTE-ISIS Conference 10.-14.10.2015

[Montenbruck et al 2000]   Montenbruck, O., Gill E.: „Satellite orbits – models, methods, and applications", Springer Verlag, Berlin, 2000

[Murphy et al 1999]   Murphy T., J. Booth: "GBAS SARPs Review and Validation of Airborne Multipath Requirements", GNSSP WG B Toulouse, October 1999 WP43

[Murphy et al 2008]   Murphy, T., Harris, M.: "RAIM Performance in the Post SA Era", ION GNSS 21st. International Technical Meeting of the Satellite Division, 16-19, September 2008, Savannah, CA, p. 139-150

[Napier 1989]   Napier, M.: "The integration of satellite and inertial positioning systems", The NAV 89 Conf. of the Royal Inst. Of Nav., London, September 1989

[Navstar GPS 2012]   Navstar: "Global Positioning Systems Directorate Systems Engineer-
                        ing & Integration Interface Specification IS-GPS-200G", 5. Sept. 2012

[Navstar GPS 2013]   Global Positioning Systems Directorate Systems Engineering &
                        Integration: "Interface Specification IS-GPS-200", Navstar GPS Space
                        Segment/Navigation User Interface, IS-GPS-200H, 24. September
                        2013

[Navstar GPS 2006]   Navstar Global Positioning System: "Interface Specification IS-GPS-
                        200", Revision D, IRN-200D-001, March 2006

[Niemeier 2008]   Niemeier W.: „Ausgleichungsrechnung: Statistische Auswertemtho-
                        den", De Gruyter Lehrbuch, Auflage: 2, ISBN-10: 3110190559, 2008

[Ober et al 2001]   Ober PB., Farnsworth R., Breeuwer E., van Willigen D.: „SBAS Integri-
                        ty Verification", Proceedings of ION GPS 2001, 1805-1812

[Parkinson et al 1988a] Parkinson B.W. and Axelrad P.: "A Basis for the Development of
                        Operational Algorithms for Simplified GPS Integrity Checking",
                        Proceedings of the Satellite Division First Technical Meeting, The
                        Institute of Navigation, Colorado Springs, CO, 1987, pp. 269-276 (A
                        revised version also appeared later under the title, "Autonomous
                        GPS Integrity Monitoring Using the Pseudorange Residual", Naviga-
                        tion, Journal of the Institute of Navigation, v.35, No.2, Summer 1988,
                        pp. 255-274.)

[Parkinson et al 1988b] Parkinson, B.W., Axelrad P.: "Autonomous GPS Integrity Monitoring
                        Using the Pseudorange Residual", NAVIGATION: Journal of the
                        Institute of Navigation Vol. 35, No. 2, Summer 1988, p. 255-274

[Parkinson et al 1996]   Parkinson B.W., Spilker Jr. J.J., Axlrad P., Enge P.: "Global Positioning
                        System: Theory and applications". Vol. 2, American Institute of
                        Aeronautics and Astronautics, Washington, Washington DC, USA,
                        1996

[Pelzer 1980]   Pelzer, H.: „Geodätische Netze in Landes- und Ingenieurvermessung",
                        Konrad Wittwer, Stuttgart, 1980

[Petovello 2006]   Petovello M., Lachapelle G.: „How can dual frequency code and
                        carrier measurements be optimally combined to enhance position
                        solution accuracy?", Inside GNSS, July/August 2006, p.17

[Petovello 2013]   Petovello M.: "Multipath vs. NLOS signals", Article in Inside GNSS,
                        Nov/Dec 2013, link: „http://www.insidegnss.com/auto/novdec13-
                        Solutions.pdf"

[Powell 1982]   Powell C.: "Performance of the DECCA Navigator on Land", IEE Proc.,

	Vol. 129, Pt. F, No. 4, 1982, p. 241-248, DOI; 10.1049/ip-f-1.1982.0036
[Pullen et al 1998]	Pullen S., et al.: "Aviation Requirements and LAAS Performance Prediction", LAAS Tutorial, Holloman AFB, N.M., Dec. 15, 1998.
[Pullen et al 2002]	Pullen S. et al, "System Overview, Recent Developments, and Future Outlook for WAAS and LAAS", Department of Aeronautics and Astronautics, Stanford University, 2002
[Rapp 1993]	Rapp R.H.: "Geoid undulation accuracy," in IEEE Transactions on Geoscience and Remote Sensing, vol. 31, no. 2, pp. 365-370, Mar 1993
[Rife et al 2004a]	Rife J., Pullen S. et al: "Paired Overbounding and Application to GPS Augmentation", Position Location and Navigation Symposium, IEEE, 2004, p. 439-446, DOI: 10.1109/PLANS.2004.1309027
[Rife et al 2004b]	Rife J., Pullen S., Pervan B., and Enge P.: "Core Overbounding and its Implications for LAAS Integrity", Proceedings of the Institute of Navigation's ION-GNSS 2004, pp. 2810-2821
[Rife et al 2004c]	Rife J., Walter T., Blanch J.: "Overbounding SBAS and GBAS Error Distributions with Excess-Mass Functions", The 2004 International Symposium on GNSS/GPS, Sydney, Australia, 6-8 December 2004
[Rife et al 2008]	Rife, J., Phelts, R.: "Formulation of a Time-Varying Maximum Allowable Error for Ground-Based Augmentation Systems", Stanford University, 2008
[Roberts et al]	Roberts, W. et al: "Analysis of the Performance of RAIM Algorithms for Civil Aviation Approach Operations Using GPS and Galileo", Nottingham Scientific Ltd
[Rotourier 2004]	Roturier B.: "APV EGNOS procedures, an efficient and reliable answer to the need for vertical guidance for approaches", Technical revue n°67, Service Technique de la Navigation Aérienne, November 2004
[RTCA 2006]	RTCA/ DO 229D, "Minimum Operational Performance Standards for Global Positioning Systems / Wide Area Augmentation System Airborne Equipment", RTCA, Inc., Washington D.C., USA, 2006
[Saastamoinen 1972]	Saastamoinen, J. (1972): "Atmospheric correction for the troposphere and stratosphere in radio ranging of satellites". In: HENRIKSEN, S.W., A. MANCINI UND B.H. CHOVITZ (Hrsg.): 3rd International Symposium on the use of artificial satellites for geodesy. AGU, 15.-17. April 1971, Washington, Washington DC, USA, S. 247-251

[Saastamoinen 1973]   Saastamoinen, J. (1973): "Contributions to the theory of atmospheric refraction", Bulletin Geodesique (48) 105, S. 279-298, (48) 106, S. 383-397, (49) 107, S. 13-34

[Schempp et al 2002]   Schempp, T. R. and Rubin, A. L.: "An Application of Gaussian Bounding for the WAAS Fault-Free Error Analysis", Proceedings of the ION GPS meeting, Portland, OR, 24-27 Sept. 2002, p. 766-772

[Schroth et al 2008]   Schroth, G., Ene, A., Blanch, J., Walter, T., Enge, P.: "Failure Detection and Exclusion via Range Consensus". In: European Navigation Conference 2008. ENC GNSS 2008, 2008-04-22 – 2008-04-25, Toulouse, France

[Schuch 2012]   Schuch, H.: "GPS Accuracy", GeoCounsel, Inc, 22.09.2012

[Seeber 1989]   Seeber, G.: „Satellitengeodäsie: Grundlagen, Methoden und Anwendungen", Verlag: De Gruyter; Auflage: 1. Januar 1989, ISBN-10: 3110100827

[Shen 2009]   Shen, J.: "Compass/BeiDou Status", BNStar Navigation Technology & System, Inc., Rome (Italy), June 2009

[Sherman 2003]   Sherman, L.: Loran for Required Navigation Performance 0.3: The Current Work of Loran Integrity Performance Panel (LORIPP), Stanford University and US Coast Guard Loran Support unit, ENC GNSS, 2003

[Shively 1999]   Shively, C.: "Derivation of Acceptable Error Limits For Satellite Signal Faults in LAAS", Center for Advanced Aviation System Development, The MITRE Corporation, McLean VA, ION GPS 1999, 14-17 September 1999, Nashville, TN, p. 761-770

[Soualle et al 2015]   Soualle F., Mink M., Braun. R., Carcanague S., Boyer M.: "Methodology for the Design of Integrity Barriers in a Regional Augmentation Satellite System", Proceedings of the 28th International Technical Meeting of The Satellite Division of the Institute of Navigation (ION GNSS+ 2015) September 14 – 18, 2015, p. 1551-1564

[Sturza 1988]   Sturza M. A.: "Navigation System Integrity Monitoring Using Redundant Measurements", Navigation, Journal of the Institute of Navigation, v.35, No. 4, Winter 1988-89, pp. 483-501

[Sturza et al 1990]   Sturza M. A., and Brown A. K.: "Comparison of Fixed and Variable Threshold RAIM Algorithms", Proceedings of the Third International Technical Meeting of the Satellite Division of the Institute of Navigation (ION GPS-90), September 19-21, 1990, Colorado Springs, CO, pp. 437-443

[Trinkle et al 2001]   Trinkle M., Gray D.: „GPS Interference Mitigation; Overview and Experimental Results", University of Adelaide, South Australia 5001, Proceedings of the 5th International Symposium on Satellite Navigation Technology & Applications, 2001

[Van Etten 1976]   Van Etten, J.P.: "Medium accuracy, low cost navigation: Loran-C versus the alternatives." AGARD Conference Proceedings, No. 176, pp. 25/1-12, 1976

[Walter et al 1995]   Walter, T, Enge P.: "Weighted RAIM for Precision Approach", Proceedings of the 8th International Technical Meeting of the Satellite Division of The Institute of Navigation (ION GPS 1995), September 12 – 15, 1995, Palm Springs, CA, p. 1995-2004

[Walter et al 2004]   Walter, T., Blanch, J., and Rife, J.: "Treatment of Biased error distributions in SBAS," Proceedings of the 2004 International Symposium on GPS/GNSS, Sydney, Australia, 6-8 December, 2004

[Walter et al 2005]   Walter, T., DeCleene B.: "Integrity Overview", Presentation held at Stanford University, 2005

[Weblink 2014a]   Weblink: http://en.wikipedia.org/wiki/Dynamic_trimming,   last visited: 21.10.2014

[Weblink 2014b]   Weblink: http://en.wikipedia.org/wiki/Sailing#Heeling, last visited: 21.10.2014

[Weblink 2014c]   Weblink: http://en.wikipedia.org/wiki/Squat_effect,   last   visited: 21.10.2014

[Weblink 2014d]   Wikipedia (Suchbegriff „Loran", last visited 3.12.2014).

[Weblink 2015a]   Weblink: http://igs.org/mgex/, last visited: 27.04.2015

[Weblink 2015b]   Weblink: http://www.cospas-sarsat.int/en/, last visited: 7.04.2015

[Weblink 2015c]   Wikipedia, http://en.wikipedia.org/wiki/International_Maritime_Organization, last visited: 2.06.2015

[Weblink 2016a]   BeiDou   Navigation   Satellite   System   in   Wikipedia, https://de.wikipedia.org/wiki/Beidou_(Satellitennavigation),   last visited: 22.02.2016

[Wendel 2011]   Wendel, J.: „Integrierte Navigationssysteme, Sensordatenfusion, GPS und Inertiale Navigation", 2. Auflage, Oldenbourg Verlag, 2011, ISBN: 978-3-486-70439-6

[Wendel et al 2008]   Wendel, J., Meister, O., Mönikes, R.: „GPS/INS Integrity Monitoring using a Modified GPB1 Filter Bank", MBDA, University of Karlsruhe, ION GNSS 21st. International Technical Meeting of the Satellite

	Division, 16-19 September 2008, Savannah, GA, p. 1589-1595
[WG-C ARAIM 2012]	GPS-Galileo Working Group C ARAIM Technical Subgroup Interim Report, Issue 1.0, December 19th, 2012
[WG-C ARAIM 2015]	EU-U.S. Cooperation on Satellite Navigation; Working Group C-ARAIM Technical Subgroup, Milestone 2 Report Final Version, February 11th, 2015
[Wicki 1989]	Wicki, F.: Arbeit im Rahmen eines ETH Projekts "Zuverlässigkeit in der amtlichen Vermessung", (weblink: https://www.ethz.ch/content/dam/ethz/special-interest/baug/igp/igp-dam/documents/Reports/176.pdf), 1989
[Wonnacott 2010]	Wonnacott R.: "A 10 cm geoid for South Africa", published in Articles PositionIT, May 17th, 2010, weblink: http://www.ee.co.za/article/a-10-cm-geoid-for-south-africa.html, last visited: 01.09.2016
[Wouter]	Wouter, J.: Loran-C Challenges GNSS: From a Quarter Nautical Mile Down to Meter-Level Accuracy, Delft University of Technology
[Zaugg 2002]	Zaugg, T.: "A New Evaluation of Maximum Allowable Errors and Missed Detection Probabilities for LAAS Ranging Source Monitors", Raytheon Company, Navigation and Landing Systems, ION 58h Annual Meeting/CIGTF 21st Guidance Test Symposium, 24-26 June 2002, Albuquerque, NM, p. 187-194
[Zeimetz and Kuhlmann 2001]	Zeimetz P.H., Kuhlmann H.: "Validation of the Laboratory Calibration of Geodetic Antennas based on GPS Measurements", FIG article of the month, February 2011

Annex

A.1 MAAST

The Wide Area Differential GPS (WADGPS) Laboratory of Stanford University has developed the Matlab Algorithm Availability Simulation Tool (MAAST). Its original intention was to provide a tool for availability simulation of the Wide Area Augmentation System. However, in the further stages of development of the tool also the MHSS algorithm implementation can be found. This software is available as public domain for users wishing to simulate the impact on availability as a result of proposed changes in the system in the context of WAAS and MHSS. It is a public for which the MAAST Software Developer's Guide is provided to assist those wishing to use, modify or tailor MAAST for their own specific purposes [MAAST 2014]. The purposes of this guide are provided below:

- Identify the key features of the MAAST program that allow users to customize and modify the code for their own application.
- Provide necessary information to the user to simplify the code and subroutine customizations.
- Provide detailed reference information of files, functions and data matrices to facilitate end-user software modifications.

MAAST was designed for easy modification and changes of the code for user specific customization. Modified algorithms can be integrated quickly into MAAST by modifying only a few lines of code. To facilitate flexibility, MAAST is organized into the following functional areas:

- Graphical User Interface (GUI): user specified inputs.
- SVM directory files containing WAAS reference stations (WRS), satellite, ionosphere grid point (IGP) and other data files.
- Algorithm and Simulation: primary error algorithm processing
  - o Satellite/User computations: computed at each time interval
  - o WMS processing: code noise and multipath error (CNMP), troposphere delay (TROPO), user differential range error (UDRE) and grid ionosphere vertical error (GIVE) computations [MAAST 2014]
  - o User processing: user error computations
  - o Output processing: availability, HPL and VPL processing as requested
- Output display: color displays of availability, HPL and VPL contour plots.

A top level view of the MAAST architecture is depicted in Figure A-1.
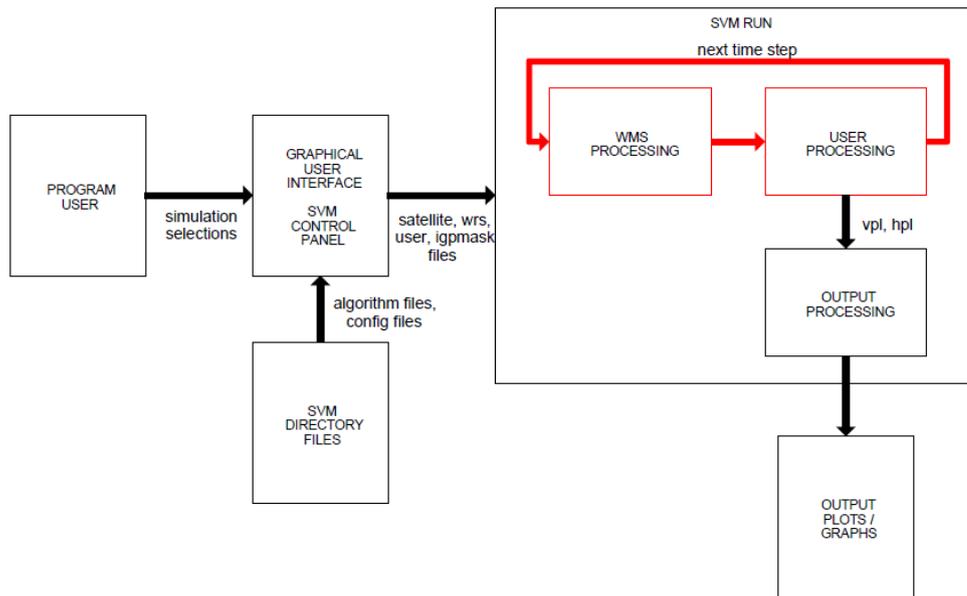
Figure A-1: Service Volume Model (SVM) Analysis Block Diagram (Top Level View)

The Matlab Algorithm Availability Simulation Tool (MAAST) is a free to use Matlab based tool and can be used as a System Volume Simulator (SVS). The tool kit can be downloaded from the following link [MAAST 2014]. Also further details on the tool can are summarized in [MAAST 2014].

Adaptions

MAAST is an open source development kit which has been adapted for the work in the frame of this work. The following main adaptions and implementations have been made:

- Novel RAIM,
- LSR RAIM,
- Adapted Integrity risk allocation for MHSS RAIM,
- Adaptions to perform sensitivity analyses.

These activities led to a considerable set of additional functions that are embedded in existing MAAST code.

A.2 Simulation Parameters

This section summarizes the relevant parameters that have been used in the performed simulations.

Constellation Parameters

The constellation parameters are shown for GPS (Figure A-2), Galileo (Figure A-3) and GLONASS (Figure A-4).

ID	Eccentricity	Time of Applicability [s]	Orbital Inclination [rad]	Rate of Right Ascen [r/s]	SQRT(A) [m^0.5]	Right Asc at TOA [rad]	Argument of Perigee [rad]	Mean Anom [rad]	Af0 [s]	Af1 [s/s]	week
1	0	344063	0.96	0	5153.62	4.76	0	4.68	0	0	703
2	0	344063	0.96	0	5153.62	4.76	0	2.82	0	0	703
3	0	344063	0.96	0	5153.62	4.76	0	0.20	0	0	703
4	0	344063	0.96	0	5153.62	4.76	0	0.73	0	0	703
5	0	344063	0.96	0	5153.62	5.81	0	1.41	0	0	703
6	0	344063	0.96	0	5153.62	5.81	0	3.03	0	0	703
7	0	344063	0.96	0	5153.62	5.81	0	5.41	0	0	703
8	0	344063	0.96	0	5153.62	5.81	0	3.57	0	0	703
9	0	344063	0.96	0	5153.62	0.57	0	1.95	0	0	703
10	0	344063	0.96	0	5153.62	0.57	0	0.21	0	0	703
11	0	344063	0.96	0	5153.62	0.57	0	5.93	0	0	703
12	0	344063	0.96	0	5153.62	0.57	0	4.22	0	0	703
13	0	344063	0.96	0	5153.62	1.62	0	2.36	0	0	703
14	0	344063	0.96	0	5153.62	1.62	0	4.63	0	0	703
15	0	344063	0.96	0	5153.62	1.62	0	0.61	0	0	703
16	0	344063	0.96	0	5153.62	1.62	0	2.92	0	0	703
17	0	344063	0.96	0	5153.62	2.67	0	3.44	0	0	703
18	0	344063	0.96	0	5153.62	2.67	0	5.28	0	0	703
19	0	344063	0.96	0	5153.62	2.67	0	5.82	0	0	703
20	0	344063	0.96	0	5153.62	2.67	0	1.15	0	0	703
21	0	344063	0.96	0	5153.62	3.71	0	4.17	0	0	703
22	0	344063	0.96	0	5153.62	3.71	0	6.03	0	0	703
23	0	344063	0.96	0	5153.62	3.71	0	1.84	0	0	703
24	0	344063	0.96	0	5153.62	3.71	0	2.36	0	0	703

Figure A-2: Constellation Parameters for GPS

ID	Eccentricity	Time of Applicability [s]	Orbital Inclination [rad]	Rate of Right Ascen [r/s]	SQRT(A) [m^0.5]	Right Asc at TOA [rad]	Argument of Perigee [rad]	Mean Anom [rad]	Af0 [s]	Af1 [s/s]	week
75	0.0001	15	0.98	0	5440.57	0.44	0	-0.38	0	0	1576
76	0.0001	15	0.98	0	5440.57	0.44	0	0.41	0	0	1576
77	0.0001	15	0.98	0	5440.57	0.44	0	1.19	0	0	1576
78	0.0001	15	0.98	0	5440.57	0.44	0	1.98	0	0	1576
79	0.0001	15	0.98	0	5440.57	0.44	0	2.76	0	0	1576
80	0.0001	15	0.98	0	5440.57	0.44	0	-2.73	0	0	1576
81	0.0001	15	0.98	0	5440.57	0.44	0	-1.95	0	0	1576
82	0.0001	15	0.98	0	5440.57	0.44	0	-1.16	0	0	1576
83	0.0001	15	0.98	0	5440.57	2.53	0	-0.12	0	0	1576
84	0.0001	15	0.98	0	5440.57	2.53	0	0.67	0	0	1576
85	0.0001	15	0.98	0	5440.57	2.53	0	1.45	0	0	1576
86	0.0001	15	0.98	0	5440.57	2.53	0	2.24	0	0	1576
87	0.0001	15	0.98	0	5440.57	2.53	0	3.03	0	0	1576
88	0.0001	15	0.98	0	5440.57	2.53	0	-2.47	0	0	1576
89	0.0001	15	0.98	0	5440.57	2.53	0	-1.69	0	0	1576
90	0.0001	15	0.98	0	5440.57	2.53	0	-0.90	0	0	1576
91	0.0001	15	0.98	0	5440.57	4.63	0	0.15	0	0	1576
92	0.0001	15	0.98	0	5440.57	4.63	0	0.93	0	0	1576
93	0.0001	15	0.98	0	5440.57	4.63	0	1.72	0	0	1576
94	0.0001	15	0.98	0	5440.57	4.63	0	2.50	0	0	1576
95	0.0001	15	0.98	0	5440.57	4.63	0	-3.00	0	0	1576
96	0.0001	15	0.98	0	5440.57	4.63	0	-2.21	0	0	1576
97	0.0001	15	0.98	0	5440.57	4.63	0	-1.43	0	0	1576
98	0.0001	15	0.98	0	5440.57	4.63	0	-0.64	0	0	1576

Figure A-3: Constellation Parameters for Galileo

ID	Eccentricity	Time of Applicability [s]	Orbital Inclination [rad]	Rate of Right Ascen [r/s]	SQRT(A) [m^0.5]	Right Asc at TOA [rad]	Argument of Perigee [rad]	Mean Anom [rad]	Af0 [s]	Af1 [s/s]	week
38	0.0016	101153	1.15	0	5050.54	10.58	3.04	2.33	0	0	703
39	0.0023	125740	1.15	0	5050.52	10.58	5.94	2.38	0	0	703
40	0.0017	184459	1.15	0	5050.54	16.87	3.06	5.80	0	0	703
41	0.0012	130606	1.13	0	5050.58	6.41	5.97	5.70	0	0	703
42	0.0002	147425	1.13	0	5050.59	12.70	3.96	4.83	0	0	703
43	0.0002	95235	1.14	0	5050.54	10.58	2.64	2.57	0	0	703
44	0.0017	95626	1.14	0	5050.54	10.58	6.03	0.85	0	0	703
45	0.0023	100028	1.13	0	5050.53	6.41	5.83	2.75	0	0	703
46	0.0021	188648	1.13	0	5050.55	12.69	3.17	4.21	0	0	703
47	0.0005	186377	1.12	0	5050.55	14.77	5.77	3.04	0	0	703
48	0.0005	183155	1.12	0	5050.55	14.77	5.93	3.20	0	0	703
49	0.0030	180230	1.13	0	5050.54	12.68	6.20	5.40	0	0	703
50	0.0002	95070	1.13	0	5050.55	6.40	2.79	1.10	0	0	703
51	0.0006	120928	1.12	0	5050.55	8.49	2.49	5.63	0	0	703
52	0.0003	122163	1.12	0	5050.55	8.49	0.67	2.16	0	0	703
53	0.0006	164892	1.13	0	5050.54	12.68	1.69	5.96	0	0	703
54	0.0020	176994	1.14	0	5050.54	16.88	0.12	2.05	0	0	703
55	0.0035	108022	1.14	0	5050.54	10.60	3.00	4.98	0	0	703
56	0.0020	176719	1.14	0	5050.54	16.88	2.80	0.10	0	0	703
57	0.0006	187560	1.13	0	5050.55	14.77	4.80	2.66	0	0	703
58	0.0015	187587	1.13	0	5050.55	14.77	4.60	3.66	0	0	703
59	0.0013	180159	1.13	0	5050.55	14.77	4.64	5.60	0	0	703
60	0.0012	186542	1.13	0	5050.54	12.69	4.10	6.10	0	0	703

Figure A-4: Constellation Parameters for GLONASS

The used elevation mask is 5° in all simulation runs (except for Novel RAIM). Note that the given time of applicability is used to reference the respective sets of ephemeris data to their validity periods. The current time starts for each simulation with 0. The given constellation parameters are used during the simiulation for the respective simulation periods (see section A.3). More details on the computation from the Kepler elements to the satellite positions can be found in [Navstar GPS 2006].

A.3 Algorithm Key Parameter Values

This section summarizes the key parameter values for each algorithm that have been used in the performance evaluations.

A.3.1 LSR RAIM

Recalling the equation for the integrity risk

$$IR = P_{occ,single\ failure} \cdot P_{md,i} \cdot P(P_E > PL)_i + P_{occ,multiple\ failure} \cdot P_{md,j} \cdot P(P_E > PL)_j$$

10.1

where i refers to the single failure case and j to the multiple failure case respectively. There is no mechanism implemented for detecting multiple simultaneous failures which leads to a $P_{md,j}$ of 1. Assuming $P(P_E > PL)_j$ equal to 1 leads to the following equation:

$$P_{md} = \frac{IR - P_{occ,multiple\ failure}}{P_{occ,single\ failure} \cdot P(P_E > PL)}$$

10.2

The two "unknowns" in this equation are P_{md} and $P(P_E > PL)$. The following algorithm key parameters are assumed in the performance evaluations (Table A-1):

Table A-1: Probabilities of Satellite Failure

Probability of multiple simultaneous failures	
GPS only	2E-6 per 3 hours
GPS+Gal	8E-6 per 3 hours
GPS+Gal+GLO	2E-5 per 3 hours (excess of Req.)
Probability of single failures	
GPS only	2E-3 per 3 hours
GPS+Gal	4E-3 per 3 hours
GPS+Gal+GLO	6E-3 per 3 hours

In the following, probabilities for P_{md} are computed assuming a $P(P_E > PL)$ of 0.5 thar corresponds to the mapping of the Pbias parameter from the test statistic domain into the position domain. This is done for the three different cases (GPS only, GPS+Gal and GPS+Gal+GLO) taking into account the different probabilities as summarized in Table A-1.

$$P_{md\,GPS\,only} = \frac{IR - P_{failure\ multiple\ SV,GPS\ only,3h}}{P_{failure\ single\ SV,GPS\ only,3h} \cdot P(P_E > PL)} = \frac{1E-5/_{3h} - 2E-6/_{3h}}{2E-3/_{3h} \cdot 0.5} = 8E-3$$

10.3

$$P_{md\,GPS+Gal} = \frac{IR - P_{failure\ multiple\ SV,GPS+Gal,3h}}{P_{failure\ single\ SV,GPS+Gal,3h} \cdot P(P_E > PL)} = \frac{1E-5/_{3h} - 8E-6/_{3h}}{4E-3/_{3h} \cdot 0.5} = 1E-3$$

10.4

Table A-2: Probabilities under Single Failure Assumption

P$_{md}$	Single failure assumption
GPS only	8E-3
GPS+Gal	1E-3
GPS+Gal+GLO	-

Table A-2 shows the satellite failure probabilities under the single failure assumption. The single failure assumption corresponds to the case where RAIM is considering only single failures. That means that the probability of multiple satellite failures is considered in the total integrity risk budget.

The P_{fa} is a function of the continuity requirement. The continuity risk is directly allocated to the P_{fa} (3E-4).

The following overall parameters are assumed (Table A-3):

Table A-3: Overall Key Parameters (LSR RAIM)

	GPS only	GPS+Gal	GPS+Gal+GLO
period	86400s	862200s	862200s
sampling	60	600s	600s
Grid stepsize	10x10	10x10	10x10
URE/URA (all const.)	0.5 / 1.0	0.5 / 1.0	0.5 / 1.0
Bias (int/cont) (all const.)	0.75 / 0	0.75 / 0	0.75 / 0

A.3.2 Novel Maritime RAIM

Analogously to LSR RAIM the probability of multiple faults needs to be considered. Hence the available IR* is

$$IR^* = IR - P_{occ,multiple\ failure}$$

10.5

This leads to the following values in dependency of the number of constellation in use (using the values from above):

$$IR^*_{GPS\ only} = 8E - 6/3h$$

10.6

$$IR^*_{GPS+Gal} = 2E - 6/3h$$

10.7

IR* is equally allocated to two different cases:

$$p_{1,GPS\ only} = \frac{IR^*}{2} = 4E - 6$$

<div align="right">**10.8**</div>

$$p_{1,GPS+Gal} = \frac{IR^*}{2} = 1E - 6$$

<div align="right">**10.9**</div>

$$P(P_E > PL)_{2,GPS\ only} = \frac{\frac{IR^*}{2}}{P_{failure\ single\ SV,GPS\ only} \cdot P_{md}} = 4E - 3$$

<div align="right">**10.10**</div>

$$P(P_E > PL)_{2,GPS+Gal} = \frac{\frac{IR^*}{2}}{P_{failure\ single\ SV,GPS+Gal} \cdot P_{md}} = 2E - 3$$

<div align="right">**10.11**</div>

An overview of the algorithm key parameter values is provided in Table A-4.

Table A-4: Algorithm Key Parameter Values (Novel Maritime RAIM)

Parameter	Value
Novel Maritime RAIM	
$\sigma_{hsea\ surface}$	1m
Masking angle	20°
K(P$_{fa}$)	4.21
K(p1)GPS only	4.61
K(p1)GPS+Gal	4.89
K(PE>PL)2,GPS only	2.89
K(PE>PL)2,GPS+Gal	3.09

The following overall parameters are assumed (Table A-5):

Table A-5: Overall Key Parameters (Novel RAIM)

	GPS only	**GPS+Gal**	**GPS+Gal+GLO**
Period	86400s	862200s	862200s
Sampling	60	600s	600s
Grid stepsize	10x10	10x10	10x10
URE/URA (all const.)	0.5 / 1.0	0.5 / 1.0	0.5 / 1.0
Bias (int/cont) (all const.)	0.75 / 0	0.75 / 0	0.75 / 0

A.3.3 MHSS RAIM

The key parameters that have been in the MHSS RAIM algorithm in the simulations are presented in Table A-6 (GPS only), Table A-7 (GPS+Gal) and Table A-8 (GPS+Gal+GLO).

Table A-6: Algorithm Key Parameter Values (MHSS RAIM) GPS only scenario

Parameter (MHSS RAIM)	Value
Psat_thres	PHMIhor/2=5E-6
IR$_{hor}$	1E-5
PL$_{tol}$	1E-2
Pconst,GPS	0
Pconst,thres	2E-8
Psat (all const.)	2.57E-4
P$_{fa,hor}$	1.67E-6
period	86400s
sampling	60
Grid stepsize	10x10
URE/URA (all const.)	0.5 / 1.0
Bias (int/cont) (all const.)	0.75 / 0

Table A-7: Algorithm Key Parameter Values (MHSS RAIM) GPS+Gal scenario

Parameter (MHSS RAIM)	Value
Psat_thres	PHMIhor/2=5E-6
IR$_{hor}$	1E-5
PL$_{tol}$	1E-2
Pconst,GPS	1E-4
Pconst,Gal	1E-4
Pconst,thres	2E-8
P$_{fa,hor}$	1.67E-5
Psat (all const.)	2.57E-4
period	862200s
sampling	600s
Grid stepsize	10°x10°
URE/URA (all const.)	0.5 / 1.0
Bias (int/cont) (all const.)	0.75 / 0

Table A-8: Algorithm Key Parameter Values (MHSS RAIM) GPS+Gal+GLO scenario

Parameter (MHSS RAIM)	Value
Psat_thres	PHMIhor/2=5E-6
IR_{hor}	1E-5
PL_{tol}	1E-2
Pconst,GPS	1E-4
Pconst,Gal	1E-4
Pconst,GLO	1E-4
Pconst,thres	2E-8
$P_{fa,hor}$	1.67E-5
Psat (all const.)	2.57E-4
period	862200s
sampling	600s
Grid stepsize	10°x10°
URE/URA (all const.)	0.5 / 1.0
Bias (int/cont) (all const.)	0.75 / 0

Acknowledgements